National Library of Canada
Acquisitions and Bibliographic Services Branch
395 Wellington Street
Ottawa, Ontario
K1A 0N4

Bibliothèque nationale du Canada
Direction des acquisitions et des services bibliographiques
395, rue Wellington
Ottawa (Ontario)
K1A 0N4

Your file Votre référence

Our file Notre référence

NOTICE

The quality of this microform is heavily dependent upon the quality of the original thesis submitted for microfilming. Every effort has been made to ensure the highest quality of reproduction possible.

If pages are missing, contact the university which granted the degree.

Some pages may have indistinct print especially if the original pages were typed with a poor typewriter ribbon or if the university sent us an inferior photocopy.

AVIS

La qualité de cette microforme dépend grandement de la qualité de la thèse soumise au microfilmage. Nous avons tout fait pour assurer une qualité supérieure de reproduction.

S'il manque des pages, veuillez communiquer avec l'université qui a conféré le grade.

La qualité d'impression de certaines pages peut laisser à désirer, surtout si les pages originales ont été dactylographiées à l'aide d'un ruban usé ou si l'université nous a fait parvenir une photocopie de qualité inférieure.

Canada

Behaviour and Design of Earthquake Resistant Low-Rise Shear Walls

by

Hossein Mohammadi-Doostdar

A thesis submitted to
the Faculty of Graduate Studies and Research
in partial fulfillment of the requirements
for the degree of

Doctor of Philosophy

in Civil Engineering *

Department of Civil Engineering
University of Ottawa
Ottawa, Canada

October, 1994

* The Ph.D. Program in Civil Engineering
is a joint program with Carleton University
administered by the Ottawa-Carleton
Institute for Civil Engineering

ISBN 0-612-00589-5

Canada

UNIVERSITÉ D'OTTAWA
UNIVERSITY OF OTTAWA

Abstract

A combined experimental and analytical research was conducted to investigate behaviour of low-rise concrete shear walls under simulated seismic loading. The experimental part of the research program includes tests of two large-scale shear wall specimens under inelastic load reversals. The walls were 1500 mm high and 100 mm thick, and had either 2000 mm or 1500 mm lengths, producing aspect ratios of 0.75 and 1.0. The effect of aspect ratio on shear sliding and failure modes was one of the major test parameters. The results indicated that both walls were able to develop flexural yielding and failed in crushing of diagonal struts. Little or no strength decay was observed up to approximately 0.92 % and 1.83 % lateral drift in walls with aspect ratios of 0.75 and 1.0, respectively. Shear sliding was limited to approximately 10 % of total lateral displacement, prior to the onset of strength degradation, indicating no premature failure caused by this mechanism. The deformation components indicate that flexure and shear were equally important in these walls, and formed approximately 80 % of total lateral displacement.

A new analysis procedure was developed as part of the analytical investigation. The procedure can be used for strength and deformation computations for low-rise shear walls with aspect ratios of 1.0 or less. It is based on equilibrium, compatibility, and material models. Potential failure planes are first identified and analyses of wall sections are carried out. One of the potential failure planes is the horizontal wall section at the base, and is critical against flexure. A standard plane section analysis is conducted at this section. The compression region determined from the plane section analysis is used to establish the second failure plane, which is inclined towards the loading corner. An inclined section analysis is conducted along this section based on experimentally observed strain variation. Diagonal compression in inclined concrete strut is checked against crushing. The strain condition computed from the inclined section analysis provide sufficient information to

establish shear force-shear deformation relationship. The analysis procedure has been verified extensively against available test data.

The analytical approach was simplified for use in design. A design procedure is recommended for low-rise shear walls with aspect ratios of 1.0 or less.

IN THE NAME OF GOD THE COMPASSIONATE AND THE MERCIFUL

Acknowledgement

Thank Almighty God for giving me the opportunity, courage, strength and support throughout this research. My deepest appreciation goes to my thesis supervisor, professor Saatcioglu for his guidance and encouragement throughout the project and his financial support at times when it was most needed. Thanks are also due to professor Gardner for his suggestions during the construction of test walls. I would also like to thank my fellow graduate students who helped me during the construction of test walls. The technical support given by Mr. Claude Lavigne and Mr. Brent Cotter from the machine shop of the Department of Civil Engineering for the construction of test setup and test specimens is gratefully acknowledged. Especial thanks go to Mr. Mongi Grira for his continuous support, suggestions and help during construction and testing of the specimens, especially for the extra effort he put on my project beyond over and above his duties as the lab supervisor. The financial support given by the Ministry of Culture and Higher Education of the Islamic Republic of Iran is greatly appreciated.

Especial thanks are extended to my wife for her continuous support, patience and prayers and to my three sons for their encouragement and sacrifice. Their help during testing of the wall specimens, including many hours they spent in evenings, is greatly appreciated.

Contents

List of Figures

List of Tables

Notations

A_{cv}	Concrete section area resisting shear force
A_s	Area of reinforcing steel
A_{shi}	Cross-sectional area of i^{th} horizontal reinforcement
A_{svi}	Cross-sectional area of i^{th} vertical reinforcement
b_f	Flange width
C_c	Vertical compression force in compression concrete
d_b	Reinforcement diameter
E_c	Modulus of elasticity of concrete
E_{shi}	Elastic modulus of i^{th} horizontal reinforcement
E_{svi}	Elastic modulus of i^{th} vertical reinforcement
f_{2t}	Concrete compressive stress in the strut at the top
f_{c2}	Concrete stress along the length of the compression strut
f_{c2m}	Concrete strength along the length of the compression strut
f_{c1i}	Concrete tensile stress perpendicular to inclined section for each strip
f_{cr}	Cracking strength of concrete
F_{shi}	Axial force in i^{th} horizontal reinforcement
F_{svi}	Axial force in i^{th} vertical reinforcement
f_{shi}	Axial stress in i^{th} horizontal reinforcement
f_{svi}	Axial stress in i^{th} vertical reinforcement
f_y	Yield strength of reinforcing steel
f_{ybe}	Yield strength of vertical steel in the boundary element
f_{yh}	Yield strength of horizontal web steel
f_{yv}	Yield strength of vertical web steel
f_{ybi}	Yield strength of i^{th} horizontal reinforcement

f_{yvi}	Yield strength of i^{th} vertical reinforcement
h_f	flange thickness
h_i	Depth of the i^{th} strip
h_s	Height of each grid
h_{strip}	Depth of the each strip
h_w	Wall height
l_w	Wall length
t	Wall web thickness
V_{ACI}	Wall shear capacity based on the provisions of ACI 318-89 Building code
v_{av}	Average shearing stress in concrete strut
V_d	Shear force along the inclined section
V_{des}	Wall shear capacity based on the simplified approach
V_{dowel}	Shear force in the reinforcement resisted by dowel action
V_{exp}	Wall shear capacity measured by experiment
V_f	Shear force at concrete compression zone
V_n	Nominal shear strength of the wall per ACI 318-89
V_{prop}	Wall shear capacity based on the proposed analytical procedure
V_{strip}	Shear force in each strip
V_u	Ultimate shear load of the wall
v_u	Ultimate shear strength of the wall
w	Web width of the strip
f'_c	Cylinder crushing strength of concrete
β	Angle of inclination of strut force in simplified approach
Δ_{sh}	Shear deformation
Δ_{shear}	Total horizontal shear displacement
Δ_{xyi}	Horizontal shear displacement at each strip
ε_0	Strain in concrete at cylinder strength

ε_1	Strain in concrete perpendicular to inclined section
ε_{1b}	Strain perpendicular to inclined section at the base
ε_{1c}	Mid-height strain perpendicular to the inclined section
ε_{1hi}	Strain in i^{th} horizontal reinforcement perpendicular to inclined section
ε_{1i}	Concrete strain perpendicular to inclined section at i^{th} level
ε_{1t}	Strain perpendicular to inclined section at the top
ε_{1tv}	Vertical component of strain perpendicular to inclined section at the top
ε_{1vi}	Strain in i^{th} vertical reinforcement perpendicular to inclined section
ε_2	Strain in concrete parallel to inclined section
ε_{2b}	Strain parallel to inclined section at the base
ε_{2hi}	Strain in i^{th} horizontal reinforcement parallel to inclined section
ε_{2i}	Concrete strain parallel to inclined section at i^{th} level
ε_{2t}	Component of strain parallel to inclined section at the top
ε_{2vi}	Strain in i^{th} vertical reinforcement parallel to inclined section
ε_{cc}	Extreme compression fiber strain in concrete
ε_{hi}	Strain in i^{th} horizontal reinforcement
ε_{l1}	Concrete strain in diagonal direction (diagonal one)
ε_{l2}	Concrete strain in diagonal direction (diagonal two)
ε_{vi}	Strain in i^{th} vertical reinforcement
ε_x	Concrete strain in horizontal direction
ε_y	Concrete strain in vertical direction
ϕ	Angle of friction
γ_{strip}	Shear distortion for each strip
γ_{xy}	Shear distortion
γ_{xyi}	Shearing strain in i^{th} strip

θ	Inclination of the diagonal failure plane
ρ_a	Reinforcement ratio of the web steel in the wall (minimum value of horizontal and vertical web reinforcement ratios)
ρ_y	Reinforcement ratio
ρ_{be}	Reinforcement ratio in the boundary element
ρ_h	Reinforcement ratio of horizontal web steel
ρ_v	Reinforcement ratio of vertical web steel
τ	Shearing stress in concrete parallel to inclined section

Chapter 1

Introduction

1.1 General

Reinforced concrete shear walls are used in earthquake resistant structures to satisfy the requirements for lateral strengths and stiffness against seismic forces. These functions are served for buildings of any height, including low-rise and high-rise buildings. Reinforced concrete walls are also used in nonseismic areas. In this case their primary function becomes increasing lateral stiffness against wind loads. Shear walls also support gravity loads and provide partitioning. The use of a shear wall is generally considered to be the least expensive method of increasing overall rigidity of concrete buildings.

Shear walls in earthquake resistant buildings control lateral drift thereby reducing damage to non-structural elements. Structures possessing adequate stiffness, such as those with shear walls, satisfy the requirements of safety and damage control when they contain sufficient ductility and energy-absorption capacity. These walls are generally designed to resist a major portion of total lateral load due to wind or earthquake.

Structural walls designed for regions of low intensity earthquakes behave elastically. In regions of high intensity excitations, however, the structural response can no longer remain elastic, and some yielding of the walls is anticipated. The design force requirements for such buildings is reduced because of yielding and subsequent energy dissipation of the lateral load resisting system. If a structural wall can develop the required ductility, i.e., capacity for large energy dissipation in the postelastic range without a significant loss of strength, then the requirements for both strength and stiffness of the structure are satisfied. Therefore, structural walls are

designed for strength, stiffness, and ductility. Consequently, well designed shear walls can prevent structural collapse in the event of a major earthquake.

One of the governing parameters of structural response in shear walls is the ratio of applied moment-to-applied shear. For structural walls subjected to inertia forces at floor levels, this parameter is expressed in terms of wall aspect ratio. The aspect ratio of a wall is defined as the ratio of wall height to horizontal wall length.

Structural walls with high aspect ratios are called flexural walls as they behave predominantly in the flexure mode. Walls with low aspect ratios are called squat or low-rise walls. Response of these walls is predominantly in the shear mode. Low-rise walls may develop premature shear failure which may reduce ductility of these walls. Therefore shear failures are generally considered undesirable.

Design of tall flexural walls is similar to that of beams. They can be designed to behave in a ductile manner by promoting flexural yielding of vertical reinforcement. This can be achieved if design shear capacity of the wall is larger than the shear load corresponding to flexural strength. In low-rise walls, however, shear and flexure are closely related. Presence of high intensity shear forces may lead to premature diagonal tension or diagonal compression failures prior to the attainment of ductile flexural response. In some cases a continuous crack may form at the base of the wall after several inelastic cycles of deformation, causing sliding shear failure. Shear sliding along the base prevents further increase in load carrying capacity of a wall. Furthermore, the method of load application, nature of loading, and type of shear reinforcement are different for low-rise shear walls than those for ordinary beams. Therefore, analysis of low-rise structural walls can not be based on procedures applicable to tall flexural walls. One of the objectives of the current research program includes development of a rational analytical procedure for evaluation of low-rise shear walls under combined flexure, shear and

axial load. The research work also includes an experimental component in which hysteretic response of earthquake resistant shear walls was investigated under simulated seismic loading.

1.2 Previous Research

The majority of previous research on low-rise shear walls involves experimental research. Therefore, most of the conclusions have limitations dictated by the test parameters such as wall dimensions, cross-sectional shape, vertical and horizontal reinforcement, material properties, and other geometric and loading conditions considered. These Experimental models, although provide invaluable insight into the behaviour of shear walls, cannot be used as general analysis and design tools.

A summary of literature on low-rise shear walls is presented in this section. The determination of ultimate strength of walls has been the primary objective of previous research. Very few researchers have concentrated on analytical prediction of overall behaviour, including inelastic stiffness and deformation characteristics. In general it was concluded that the prediction of inelastic ultimate strength and inelastic deformations in low-rise shear walls are only possible by means of empirical relationships.

J. R. Benjamin and H. A. Williams, 1957

Benjamin and Willimas reported the results of an experimental investigation conducted at Stanford university during the period of 1951 to 1956. The experimental program involved tests of one-story plain and reinforced concrete shear walls subjected to in plane loading. The effects of panel proportions, reinforcement arrangement and the characteristics of end column regions were investigated.

The specimens were designed and constructed as either Type B small scale models or Type C large scale models. Type B specimens were tested in a 200,000 lb Reihle testing machine, whereas Type C specimens were tested in a specially constructed shear jig.

Several different modes of failure were observed during the tests. These include:

1. Tension column failure.
2. Diagonal cracking of panel in tension zone.
3. Panel cracking and bending of compression column.
4. Failure of tension column steel after the cracking of panel and overstressing of column steel.
5. Composite failure involving tension column yielding, panel cracking and compression column shearing.

The main objective of the research investigation was to develop data on shear walls to be used for the design of structures resisting atomic blast loads. It was concluded that ultimate load and deflection were highly statistical quantities, and the ultimate strength and corresponding deflections can be predicted only by means of empirical relationships.

F. Barda, J. M. Hanson, and W. G. Corley, 1973 and 1977

Results of tests on eight one third scale low-rise shear wall specimens with boundary elements were reported and analysed. The test variables included amount of flexural reinforcement, amount of horizontal and vertical web reinforcement, and wall aspect ratio. Test walls had a flanged type cross section with 4.0 in (100 mm) thick web and flanges. The flange width was 24.0 in (600 mm). All walls had a constant wall length of 75.0 in (1875 mm), and three different wall heights of 17.5 in (437.5 mm), 37.5 in (937.5 mm), and 75.0 in (1875 mm). Two specimens were subjected to monotonic loading, while the others were subjected to reversed cyclic load. The walls were over designed for flexure. Consequently they all failed due to shear.

Two of the walls developed sliding shear distress along the top construction joint during the final stages of loading.

The main objective of the research program was to obtain data on strength, energy absorption and performance of low-rise cast-in-place shear walls with boundary elements under reversed cyclic loading.

Some of the findings and conclusions obtained are listed below:

1. Vertical and horizontal web reinforcement were both effective in producing a distributed crack pattern with reduced crack widths.
2. Vertical and horizontal web reinforcement both contributed to wall strength. The contributions varied, however, depending on the wall aspect ratio.
3. Horizontal web reinforcement did not contribute to shear strength of walls with aspect ratios of 1/2 or less.
3. The presence of top tie beam had a pronounced effect on shear strength of walls with aspect ratios of 1/4 and 1/2.
4. Shear force was transmitted to the base through diagonal compression struts formed between successive cracks.
5. Load reversals resulted in a nearly orthogonal pattern of cracking. However, the behaviour of the walls were not considerably affected by the crack pattern.
6. Load reversals resulted in 10 % reduction in shear strength as compared to monotonic loading.

A. E. Cardenas, H. G. Russel, and W. G. Corley, 1980

Behaviour of rectangular low-rise shear walls was investigated experimentally by Cardenas et. al. Total of seven walls with an aspect ratio of 1.0 were tested. All specimens were of rectangular cross section having 75.0 in (1875 mm) length, 75.0 in (1875 mm) height, and 3.0 in (75 mm) thickness. They were labelled as SW-7 through SW-13. Specimens SW-10,

SW-11, and SW-12 did not contain any vertical web reinforcement. Vertical reinforcement was either distributed uniformly or provided at the ends, forming boundary elements. Specimen SW-10 had no horizontal web reinforcement. Loading was monotonic for all specimens except specimen SW-13 which was subjected to ten cycles of load reversals. There was no vertical load applied to any of these specimens. The observed failure mode was shear for SW-7, SW-8 and SW-10, flexure-shear for SW-9 and SW-13, and shear-anchorage for SW-11 and SW-12.

The objective of the experimental investigation was to obtain basic information on strength and deformation of reinforced concrete walls under slowly-applied lateral forces, and to investigate the contribution of vertical and horizontal web reinforcement to shear capacity. The following conclusions were reported.

1. In low-rise shear walls the development of flexural capacity is possible if walls have relatively large shear capacity. Therefore, the amount and relative distribution of web vertical and horizontal reinforcement are major parameters affecting strength of walls.
2. Low-rise walls with boundary elements can carry an appreciable amount of shear load even after the destruction of web. However, a considerable reduction in load carrying capacity of the wall was observed due to severe damage to the web.
3. A decrease of seven percent in shear strength of a wall was recorded due to cyclic loading compared to a companion specimen under monotonic loading.
4. Both horizontal and vertical web reinforcement were effective in carrying shear in walls with an aspect ratio of 1.0. Relative contributions of web reinforcement for walls with different aspect ratios was not studied.

A. J. Synge, 1980

Synge conducted reversed cyclic load tests on four reinforced concrete shear walls with an aspect ratios of 1/2. The test wall specimens were half size models; 3.0 meters long, 1.5 meters high and 100 mm thick. Two of the specimens were flanged walls and the other two had

rectangular cross-sections. One wall in each group contained diagonal shear reinforcement. Loading was cyclic (displacement reversals). The following were reported to be the objectives of the test program:

1. To confirm that brittle shear failure of low-rise walls with aspect ratios of 1/2 can be suppressed, and these walls, if properly designed, can behave in ductile flexural mode.
2. To investigate the effectiveness of diagonal reinforcement in limiting sliding shear displacements, and in improving energy absorption of low-rise shear walls.
3. To explain the load resisting mechanism of low-rise walls, and to define the role of horizontal reinforcement in response.
4. To qualitatively study the parameters liable of the rapid stiffness degradation of low-rise walls caused by sliding shear.

Some of the main conclusions obtained are listed below:

1. The walls resisted applied loads in flexural mode, and diagonal tension failure was suppressed by using proper amount of horizontal reinforcement.
2. With the increase in imposed cumulative lateral drift the role of horizontal reinforcement in resisting shear was increased.
3. The use of diagonal reinforcement continuous into the footing, decreased the magnitude of shear sliding and substantially improved hysteretic performance.

It was proposed that vertical reinforcement is to be designed for flexure while horizontal and diagonal web reinforcements are to be designed for diagonal tension and sliding shear. Expressions were proposed for the design of horizontal and diagonal reinforcement.

K. Ogata and T. Kabeyasawa, 1984

Ogata and Kabeyasawa tested reinforced concrete shear walls with different moment-to-shear ratios (M/QD) under reversed cyclic loading. Six two-fifth scale shear walls with boundary

columns were tested with different ratios and details of reinforcement. Test walls were representative of the first story walls of a seven story building tested as part of the U.S.-Japan co-operative research program. The specimens had the same dimensions. The length, height and thickness were 2000 mm, 1500 mm and 80 mm respectively. Boundary columns were 200 by 200 mm in cross section. Two of the specimens (K5 and K6) had diagonal reinforcement in addition to conventional reinforcement. The loading apparatus used was designed to apply variable moment to shear ratio, constant amplitude gravity load, and cyclic lateral shear force. Three specimens, K2, K3, and K4 failed in sliding shear at M/QD of 1.0, whereas the remaining three failed in diagonal compression at M/QD of 0.75.

The objective of the research project was stated as follows:

1. To determine the role of the moment-to-shear ratio of loading, M/QD, on the failure modes of walls.
2. To assess roles of shear and flexural reinforcement on hysteretic behaviour of walls.
3. To compare the response of diagonally reinforced specimens with that of conventionally reinforced specimens.
4. To evaluate the contributions of flexural and shear deformations to overall wall deflection.

The following observations were reported as part of their conclusions:

1. Ductile flexural yielding was observed in walls with M/QD ratios between 1.25 and 2.0. Brittle shear failure was observed in specimens with M/QD ratios of 1.0 and 0.75.
2. The flexural theory can be used to evaluate flexural strength of walls.
3. A larger portion of the total energy input was dissipated by flexural deformations of walls with higher M/QD ratios.

4. Specimens with diagonal reinforcement had higher shear strength and energy dissipation capacity than those reinforced with conventional orthogonal reinforcement of equal steel ratio.

T. T. C. Hsu and Y. L. Mo, 1985

An analytical model was developed by Hsu and Mo to predict strength and Behaviour of low-rise reinforced concrete shear walls with boundary elements. The model was based on equilibrium and compatibility conditions as well as a softened stress-strain relationship for concrete in diagonal compression struts and truss analogy. The load deformation history is determined by solving a set of simultaneous equations iteratively. This model is applicable to low-rise shear walls with aspect ratio less than unity where predominant behaviour is shear. Shear walls are assumed to have boundary elements strong enough to resist applied bending moment and shear force without premature failure. Therefore, it is assumed that the walls fail in shear without the possibility of premature failure of boundary elements in bending or sliding shear.

The analytical model was verified against 24 low-rise wall tests. It was shown that the model was capable of predicting shear strength, shear distortions, steel strains, and concrete strains with acceptable accuracy throughout the loading history. This model accounts for shear deformations only. Therefore, it is only intended for low-rise shear walls. For medium and high-rise shear walls where flexural deformation plays a dominant role, the model is not applicable.

S. Wiradinata, 1985

Two rectangular low-rise shear walls with aspect ratios of 1/2 and 1/4 were tested by Wiradinata. Both walls were 2000 mm long and 100 mm thick. Wall 1 was 1000 mm high and wall 2 was 500 mm high. The amount of reinforcement and the loading history used in both specimens were identical. Loading was cyclic (displacement reversals). The main variable was

the wall aspect ratio. Wall 1 failed by diagonal tension followed by excessive crushing of concrete at the compression toe and the top corner of the wall, and Wall 2 failed in sliding shear.

The followings were the objectives of the study:

1. To determine the effect of aspect ratio on wall behaviour.
2. To define the role of horizontal reinforcement in resisting shear forces.
3. To understand better the load resisting mechanism of low-rise shear walls.
4. To identify roles of vertical and horizontal reinforcement in resisting applied loads.

The following conclusions were reported:

1. Shear strength of low-rise walls increases with decrease in aspect ratio.
2. Sliding shear governs the failure mode for walls with an aspect ratio of 1/4.
3. It is possible to achieve a ductile flexural response in walls with aspect ratio of 1/2 with minimum horizontal reinforcement ratio of 0.25 %, where the applied shear stress is limited to $0.65\sqrt{f_c'}$ Mpa.
4. Repeated load reversals are the cause of stiffness degradation in low-rise walls.

S. T. Mau and T. T. C. Hsu, 1986

Mau and Hsu proposed a direct solution for load-deflection history of low-rise shear walls. Their work was based on equilibrium and compatibility conditions, and softened stress-strain relationship for concrete in diagonal compressive struts. Three possible modes of failure were introduced depending on the amount of longitudinal reinforcement in walls. The three modes corresponded to under-reinforced, balanced, and over-reinforced walls. Simple equations were derived for each of the three failure modes expressing shear strength. Design recommendations were also made for low-rise shear walls with boundary elements. The proposed theory is only applicable to low-rise shear

walls with boundary elements with aspect ratio less than unity and without external vertical loads. Design recommendations were further limited to static loads.

R.G. Oesterle, 1986

An analytical procedure was developed by Oesterle to determine strength, inelastic deformation capacity and failure modes for hinging regions of shear walls. Vertical and horizontal equilibrium of the truss system within the hinging region and across the base of the wall were considered. The analytical study was based on the results of experimental investigation, also conducted by Oesterle et. al. (Oesterle et. al, 1976, 1979 and 1986). These experimental investigations involved testing of large-scale isolated structural walls, with aspect ratios of 2.4, subjected to in-plane lateral load reversals. The primary objective of the experimental investigation was to determine mechanisms limiting strength and deformation capacities of walls, and to identify parameters influencing wall behaviour. The test variables included loading history, cross-sectional shape, amount of vertical and horizontal reinforcement, amount of confinement reinforcement in boundary elements, moment to shear ratio, axial compressive stress, and concrete strength. Results of the experimental program indicated that properly designed shear walls do possess inelastic deformability required during response to seismic loading. It was also concluded that the web crushing mode of failure is related to both the applied level of shear stress and the amount of inelastic deformations sustained by the hinging region.

The objective of the analytical research was to develop procedures for an integrated analysis of significant behavioural mechanisms within the hinging region of reinforced concrete structural walls capable of predicting strength, deformation capacity, and failure modes for earthquake resistant shear walls. The failure modes included web crushing and shear compression failures associated with walls subjected to high nominal shear stresses.

It was concluded that the analysis procedure developed in this study provided a reasonable estimate of shear wall strength, deformation capacity and failure modes. The results of analysis were in good agreement with experimental data in terms of crack width and spacing, tensile and compressive strains, inelastic deformations, strength, and failure modes for the hinging regions.

C. F. Pilette, 1987

Pilette examined behaviour of low-rise shear walls under cyclic load reversals. He tested two rectangular walls with aspect ratios of 1/2. Both walls were 1/3 scale, and had 2000 mm length, 100 mm thickness and 1000 mm height. The main variables were the amount of horizontal and vertical reinforcement. Both walls failed in sliding shear. The objective of the test program was to identify failure modes of low-rise shear walls under reversed cyclic loading.

The following conclusions were reported:

1. Ductility in low-rise walls with aspect ratios of 1/2 can be attained if diagonal tension capacity of the wall is limited to shear force causing sliding shear.
2. Walls with an aspect ratio of 1/2 perform with limited but acceptable ductility when reinforced with minimum horizontal reinforcement ratio of 0.25 %.
3. The continuous horizontal crack which forms at the base of a wall, due to cyclic loading, triggers the sliding shear failure mechanism.
4. Sliding shear failure may take place before the attainment of ultimate shear or ultimate flexural capacity calculated according to the ACI Building Code.
5. Degree of base fixity during testing significantly affects wall response.

Z. F. Wasiewicz, 1988

Two low-rise shear walls with aspect ratios of 0.25 and 0.5, were tested by Wasiewicz under cyclic loading. Both walls were of rectangular cross section, 2000 mm long and 100 mm thick, and were provided with specially detailed reinforcement at the construction joint to prevent

shear sliding in addition to conventional orthogonal web reinforcement. Test specimens were labelled as wall 3 and wall 6. Wall 3 was 500 mm high, whereas wall 6 was 1000 mm high. Vertical reinforcement ratios were the same in both walls but horizontal reinforcement ratios were different. Both walls failed in diagonal compression due to degradation of concrete strength in the web under reversed cyclic loading.

The objective of the research project was to investigate sliding shear phenomenon in low-rise shear walls, and to develop design information for prevention of sliding shear failure in seismic resistant shear walls. Some of the conclusions, which resulted from this investigation, are listed below:

1. Sliding shear failure can be suppressed by the use of specially detailed reinforcement along the construction joint.
2. Sliding shear failure in low-rise walls occurs at a shear force approximately equal to 70.0% of that associated with flexural capacity.
3. Low-rise walls subjected to cyclic load reversals behave in shear mode.

I. D. Lefas, M. D. Kotsovos, and N. N. Ambraseys, 1990

Thirteen structural walls were tested under a constant axial load and a monotonically increasing horizontal load. The specimens consisted of 750 mm square walls with 70 mm thickness, and 650 mm long and 1300 mm high rectangular walls with 65 mm wall thickness.

The objective of the research project was to investigate effects of wall aspect ratio, axial load, concrete strength, and the amount of horizontal web reinforcement on strength, stiffness, and deformation characteristics of walls. The following conclusions were drawn from this experimental investigation:

1. Axial compression reduces vertical and horizontal displacements.

2. The presence of axial compression results in a wider band of crushing due to increased depth of neutral axis, but reduced web crushing.
2. Horizontal load capacity is increased by axial compression.
3. Horizontal web reinforcement does not have a significant effect on shear capacity, which cannot be described by the truss analogy.
4. Concrete strength does not significantly affect the strength and deformational characteristics of walls.
5. Shear resistance was associated with triaxial compressive stress conditions in the compression zone at the base.
6. The collapse of the specimens occurred due to the failure of concrete compression zone.
7. In spite of its small depth, the compression zone appears to be the main contributor to shear resistance, since neither the horizontal reinforcement nor aggregate interlock were found to significantly affect the maximum load-carrying capacity of the walls tested.

S. L. Wood, 1990

The results of 143 laboratory tests of one and two story reinforced concrete walls were reviewed to evaluate the validity of current design provisions for nominal shear strength. The review also provided information on the sensitivity of measured shear strength to experimental parameters, such as loading history and the amount of web reinforcement.

Applicability of modified truss analogy to low-rise structural walls under earthquake induced loads was also evaluated. The walls had three cross-sectional geometry; barbell, (105 specimens), flanged (20 specimens), and rectangular (18 specimens). Sixteen specimens were two stories high. Shear span to depth ratios (i.e., aspect ratios) ranged between 0.5 and 1.0 for most specimens. Three types of lateral loading was applied statically in the plane of the wall. These consisted of monotonic loading up to failure (90 specimens), cyclic loading in one

direction (50 specimens), and reversed cyclic loading (3 specimens). Axial compression was applied to 18 specimens with an average concentric stress varying from 7% to 18% of concrete cylinder strength. For the remaining 125 specimens the average axial compressive stress was less than 0.5% of concrete cylinder strength.

Test specimens considered in this study had four common characteristics:

1. Specimens were all isolated walls.
2. In plane static lateral load was applied to all walls.
3. All walls failed in shear mode.
4. Wall web was reinforced uniformly with vertical and horizontal reinforcement.

The following conclusions were reported as a result of this investigation:

1. Shear strength of reinforced concrete is not linearly related to the amount of web reinforcement.
2. Equation 6 from Appendix A of ACI 318-83 (Eq. 21-6 of ACI 318-89) underestimates nominal shear strength of walls with low reinforcement ratios, and may overestimate nominal shear strength if the wall is reinforced with more than 1.5 times the minimum web reinforcement ratio of 0.25%.
3. For test specimens with uniformly distributed orthogonal web reinforcement a reasonable lower bound for average shear strength is in the order of $6\sqrt{f_c'}$ Psi.
4. Maximum average shear strength increases with increase in vertical (boundary and web) reinforcement.

C. R. Farrar, W.E. Baker, and R. C. Dove, 1990

Farrar et. al, conducted different types of experiments to investigate post-cracking stiffness of low-rise shear walls. The research work included experimental modal analysis, and tests under cyclic-static loading, and simulated seismic base excitations. Different size

walls were used, including one of the largest reinforced concrete shear walls ever tested in a laboratory setting. Wall response beyond cracking was shown to be a function of the maximum load imposed on the structure. It was reported that postcracking stiffness of structures dropped significantly as compared to their stiffness prior to cracking.

N. Onozato and M. Mochizuki, 1991

Analytical research was conducted by Onozato and Mochizuki to evaluate strength and deformation of multistory framed shear walls. The study focused on single story single span framed shear walls. Both flexure and shear modes of failure were considered. An analytical model was proposed to analyze framed shear walls. The analytical model was shown to be in good agreement with experimental data.

F. Y. Cheng, G. E. Mertz, M. S. Sheu, and J. F. Ger, 1993

Fifteen rectangular low-rise walls with 1000 mm width and 100 mm thickness were tested under different types of loading. Wall height varied between 500 mm and 750 mm, resulting in aspect ratios of 0.50 to 0.75. All walls were reinforced with horizontal and vertical web reinforcement, distributed evenly in the web. Four different loading patterns were used. These were; one-sided cyclic loading, simulated seismic loading, monotonic loading, and two sided cyclic loading. An analytical approach was developed for calculating shear and bending deformations, as well as shear and bending hysteretic models. A good agreement was obtained between analytical and experimental results. It was also concluded that horizontal reinforcing bars have little effect on the shear deformation of low-rise shear walls.

W.B. Siao, 1994.

Refined strut-and-tie model was employed by Siao to predict the Behaviour of low-rise shear walls with aspect ratios equal to or less than one. An attempt was made to introduce a unified method of analysis for deep beams, corbels, and low-rise shear walls. The shear

capacity of selected reinforced concrete wall specimens were predicted using formulas established for top-loaded deep beams and corbels. The results compared well against experimental data.

1.3 Research Needs

It is clear from the limited research reported in the literature that the behaviour and design of low-rise walls under monotonic and seismic loading are not well understood. While the state of knowledge has advanced significantly for tall flexure dominant structural walls, many questions remain to be answered for analysis and design of shear dominant low-rise walls.

One area that lacks procedures and analytical tools is inelastic analysis of shear dominant concrete walls where diagonal tension and diagonal compression due to shear play significant roles. Sliding shear that was observed in walls with low aspect ratios and the interaction of shear with flexure adds further to the complexity of the problem. There is need for an analytical procedure to establish inelastic shear force-shear deformation relationship and the limiting material strengths for low-rise walls. This relationship is essential for establishing hysteretic relationships for shear walls subjected to seismic excitations. Most hysteretic models used for dynamic inelastic analysis of reinforced concrete structures require elastic and inelastic rigidities as input. This information can only be provided if the force-deformation characteristics of members can be computed. Furthermore, analysis of walls and understanding of the limiting conditions of materials lead to more rational design procedures.

The current design approach for low-rise shear walls is based on empirical test data. Since the test data is extremely limited, the applicability of the empirical design expressions remain to be questionable. In fact it has been shown by some researchers that the code provisions may provide unsafe designs when sliding shear is the governing mode of behaviour, and over

conservative results when diagonal tension governs. There appears to be a need for a rational design procedure for seismic resistant low-rise shear walls.

1.4 Objective and Scope

The overall objective of the research program is to investigate inelastic behaviour of low-rise shear walls experimentally and analytically, and to develop design and analysis procedures for earthquake resistant shear walls. The objective is achieved through the following scope:

- Review of previous research and state of the art on behaviour and design of low-rise shear walls.
- Design and construction of two large scale shear walls for testing under simulated seismic loading.
- Preparation of a laboratory test set-up, and instrumentation of specimens for testing under slowly applied lateral load reversals.
- Testing of wall specimens, and evaluation of test data.
- Review of available analytical approaches on inelastic shear behaviour of reinforced concrete structural elements.
- Development of a new analytical approach for computation of inelastic shear force-shear deformation relationship.
- Preparation of a computer software incorporating the analytical procedure developed.
- Verification of the analytical procedure by comparing against test data obtained from the experimental part of the current research program, as well as those reported previously in the literature.
- Comparisons of analytical wall capacities obtained by the proposed procedure with those based on the current ACI 318-89 Building Code provisions and those recorded experimentally.

- Development of a shear design procedure for low-rise shear walls.
- Comparisons and verification of the proposed design procedure with behaviour observed in tests.
- Presentations of experimental and analytical findings, and preparation of a thesis.

Chapter 2

Behaviour of Low-Rise Walls

2.1 General

Low-rise shear walls under monotonic or cyclic lateral loading exhibit behaviour that is different than those observed for beams, columns, and flexure dominant structural walls. The difference stems from geometry, boundary conditions, and the way transverse loads are applied to these structural members. An in depth study of low-rise wall behaviour requires identification of the parameters that influence wall behaviour, understanding of the effects of these parameters on mechanism of load resistance, and investigation of failure modes involved. These issues will be discussed in this chapter based on the state-of-the-art. Furthermore, current analytical models that attempt to describe wall behaviour, and practical design provisions that are recommended by current building codes are discussed. A review of relevant aspects of beam behaviour is also made as it relates to wall response.

2.2 Parameters that Affect Strength of Low-Rise Walls

Wall Aspect Ratio

One of the governing parameters of structural response in low-rise walls is aspect ratio. High shear forces associated with low aspect ratios may result in diagonal tension, compression or sliding shear failures prior to the development of flexural capacity (Wiradinata and Saatcioglu 1986, and Saatcioglu 1991). Shear failure is regarded as a brittle failure mode and may reduce inelastic deformability of low-rise walls, essential for

dissipation of earthquake induced seismic energy. Therefore, the aspect ratio is an important geometric parameter that may alter the wall behaviour from a flexure dominant ductile response to a shear dominant brittle response.

Presence of Top Beam or Floor Slab

Lateral loads on buildings due to seismic induced inertia forces are applied at floor levels where concentration of mass is present. In a typical shear wall, the load is introduced along the joint between the floor slab or top tie beam and the wall, as a line load. Transfer of this load to the floor below or foundation occurs through diagonal compressive struts, kinking of vertical bars at diagonal crack planes, tension in horizontal shear reinforcement, and aggregate interlock across crack surfaces. The top tie beam or floor slab affects the distribution and inclination of diagonal cracks. These elements are usually stronger and stiffer than the wall panel itself, and may change the angle of the failure plane to diagonal corner-to-corner plane in walls with aspect ratios less than 1.0. In this case, the top tie beam works as a gigantic stirrup and limits the advancement of diagonal cracks reaching the beam, preventing diagonal tension failures along these planes. Therefore the presence of a top beam and a floor slab may change the mode of behaviour in low-rise walls.

Boundary Elements

The behaviour of a short flanged shear wall is more complex than that of a rectangular wall. Even a small amount of vertical reinforcement in flanges results in a high flexural capacity, and hence an excessive shear load on the web. Low-rise walls with boundary elements can support significant horizontal loads even after the web has been destroyed. However, the load carrying capacity is considerably reduced after severe damage to the wall (Barda et. al, 1977). Cantilever shear walls with boundary elements are different from the framed shear walls in which the wall essentially acts as an infill for the reinforced concrete frame surrounding the web. In framed shear walls, the boundary columns will resist applied moment and the web of the wall will resist a majority of the shear load. In general, walls with barbell or flanged cross-

sections resist significantly higher shear forces than a rectangular wall with the same amount and arrangement of web reinforcement (Lefas, et. al, 1990a).

Construction Joints

Construction joints in low-rise shear walls under inelastic load reversals may deteriorate under cyclic loading, and may become the weak link in the chain. These walls may experience shear sliding along the construction joint prior to the attainment of the capacity of the wall panel. The energy dissipation capacity of the horizontal construction joint is generally poor because the interfaces along the construction joint are destroyed due to the sliding movements, resulting in dramatic strength degradation (Paulay, 1977). Therefore, the behaviour of construction joints may affect failure modes of shear walls and may play a dominant role in walls with low aspect ratios.

Types of Loading

Gravity loads on walls increase strength and decrease deformations of walls. Low-rise walls generally carry small gravity loads, and therefore, the beneficial effect of this type of loading may be ignored (Park and Paulay, 1975).

Cyclic lateral loading results in criss-crossing of diagonal cracks and may reduce diagonal compression strength of the web concrete. This leads to a reduction in the capacity of diagonal compressive struts. Cyclic loading also aggravates sliding shear along the construction joint. Therefore, although monotonic force-deformation relationships may be taken as representatives of the envelopes of hysteresis loops in flexure dominant members, the same may not be true at later stages of loading for low-rise walls where cyclic loading effects may result in strength degradation.

Amount and Relative Distribution of Horizontal and Vertical Web Reinforcement

The horizontal and vertical web reinforcement crossing inclined cracks contribute significantly to shear resistance of walls. The horizontal bars resist shear forces along their longitudinal axis, whereas, the vertical bars resist shear by kinking action at inclined cracks. Low-rise walls need to have relatively large shear capacity to be able to develop their flexural capacity. Therefore, the amount and distribution of horizontal and vertical web reinforcement are major parameters affecting strength. Careful arrangement of horizontal and vertical web reinforcement can control width, spacing and distribution of cracks. As the wall aspect ratio decreases, vertical web reinforcement becomes more effective in controlling diagonal cracks. An increase in the amount of vertical reinforcement will increase the overall capacity of the wall regardless of the type of failure, but may trigger sliding shear failure. On the other hand, wall aspect ratio has a pronounced effect on the extent to which the amount and arrangement of vertical and horizontal web reinforcement will affect the capacity and failure mode. For walls with very low aspect ratios (i.e, approximately 0.25) sliding shear is the governing mode of failure, and the amount and arrangement of web reinforcement will not alter this failure mode. For walls with aspect ratios between 0.5 and 1.0, an increase in the amount of horizontal reinforcement may result in a shift from diagonal tension failure to a diagonal compression or sliding shear failure. This is because there is more yielding of horizontal reinforcement when lower ratios of steel are used. For walls in this range of aspect ratio, the sliding shear always forms part of the total lateral displacement, and an increase in the horizontal web reinforcement ratio increases the percentage of displacement due to shear sliding. Although it has been shown that horizontal web reinforcement does not affect the shear capacity of walls with low aspect ratios significantly (Lefas et. al, 1990), it does affect inelastic shear deformations.

2.3 Mechanism of Shear Resistance in Low-Rise Walls

The mechanism of shear resistance in low-rise walls differs significantly from that for beams, including shear dominant deep beams. Major differences come from relative dimensions, boundary conditions, and imposed loading. Therefore, the extensive research conducted for beams can not be used directly to explain the mechanism of shear resistance in low-rise walls.

Low-rise walls provide resistance to applied shear stresses through diagonal tension and compression. Since the direct shear capacity of concrete along a horizontal plane is much higher than the diagonal tension capacity of concrete, shear failure along a plane parallel to the applied shear force does not precede formation of an inclined crack due to diagonal tension. Concrete alone can be held 100% responsible in providing shear resistance until cracking. Beyond the formation of diagonal cracks, however, the mechanism of shear resistance depends on a number of variables. A significant portion of horizontal shear continues to be transmitted to the foundation or storey below through diagonal compression. Diagonal compression is resisted by diagonal concrete struts that are formed between inclined tension cracks. The diagonal struts can only be maintained if sufficient diagonal tension resistance is provided by web reinforcement, especially under inelastic load reversals. Presence of web reinforcement controls the width of cracks, which help maintain additional shear resistance along the cracked surfaces through aggregate interlock. Low-rise walls also resist flexural stresses caused by horizontal shear forces, and may develop significant horizontal cracking at the critical section for flexure. Initially, some horizontal shear resistance also develops along these cracks through aggregate interlock. Under reversed cyclic loading, however, these cracks become continuous, and opening and closing of the cracks result in crushing of the concrete along the crack interface. This promotes direct shear action as a potentially critical mode of behaviour, producing shear sliding along the horizontal crack. The vertical reinforcement crossing inclined and horizontal cracks provide additional shear resistance through dowel action. Different

mechanisms of resistance are activated in cracked low-rise shear walls. The following sections provide highlight of the various mechanisms involved in low-rise shear walls.

2.3.1 Diagonal Compression Struts

Figure 2.1 illustrates a typical low-rise wall subjected to a horizontal shear force at the floor level. The shear force is transmitted to the foundation through diagonal compression struts between the inclined cracks. If the wall is over-designed against flexure and diagonal tension, by means of excessive vertical and horizontal reinforcement, these modes of failures are prevented, and the wall is forced to resist high compressive stresses in struts until the compression capacity of concrete is exhausted.

Diagonal struts can only be developed if a truss mechanism is formed, and the vertical and horizontal components of the diagonal force are equilibrated. Walls with aspect ratios of 1.0 or less require vertical tie element to equilibrate the vertical component of the strut. This is provided by vertical tension reinforcement. The inclination of diagonal struts in this case is dictated by the wall aspect ratio. Tests have demonstrated that diagonal struts usually develop between the diagonal corners of wall panels. Walls with aspect ratios grater than 1.0 may require additional tie elements, this time in the horizontal direction, to equilibrate the horizontal component of the diagonal force. The behaviour in this case is similar to that for beams, where transverse reinforcement is essential to develop the truss mechanism.

2.3.2 Aggregate Interlock Along Inclined Cracks

The surfaces of the cracks formed in the reinforced concrete elements are usually rough and irregular. Each of the cracked faces contain coarse aggregate particles. If the cracked surfaces form a continuous plane, under the action of the external load, the two faces of the cracked surfaces will move relative to one another and result in a contact of the coarse aggregates. Bearing and friction of aggregate particles resist and restrict the further movement of the two surfaces. This action is referred to as the "Aggregate Interlock", and may account for

significant shear resistance. If the crack width is controlled by sufficient reinforcement, or externally applied normal load, a significant amount of shear forces can be transmitted across the crack interface. Therefore, the significance of aggregate interlock depends on the width of the crack, the existence of external compressive force, and the web reinforcement crossing the crack.

Cyclic loading is another factor that influences aggregate interlock. Under inelastic load cycles the cracked surfaces slide against each other, deteriorating the mechanism of aggregate interlock. Beyond this stage shear friction mechanism is activated as discussed in the next section.

2.3.3 Shear Friction Hypothesis

Shear friction is a shear force developed along a cracked surface of concrete due to friction. Shear friction is based on the roughness and associated coefficient of friction between the cracked surfaces, as well as normal force acting on this surface. The mechanism of shear friction was originally derived from studies conducted on composite beams. This mechanism may be improved by providing reinforcement across the crack. If any externally applied tension exists across the crack, reinforcement must be provided to resist this tension in addition to that required to enhance the mechanism of shear friction. If, on the other hand, a cracked reinforced concrete element is subjected to a normal compressive force across the crack, and a shearing force along the crack, then the shearing force may be resisted by increased friction caused by the compression force along the crack. The friction force may be quite high due to the roughness and irregularity of cracked surfaces. However, this roughness, in the presence of slip along the crack, may cause the two pieces of concrete to separate slightly. If reinforcement is present normal to the crack, slippage and the subsequent separation along the crack will impose tension in the reinforcing steel. Therefore, there will exist a balancing compressive force normal to the crack as illustrated in Figure 2.2. This enhances the shear resistance provided by friction. The magnitude of this shearing resistance is equal to the compressive stress multiplied

by the tangent of the angle of friction. At ultimate, the shear resistance provided by friction can be written as:

$$V_u = A_s f_y \tan\varphi \qquad (2.1)$$

or

$$v_u = \rho_s f_y \tan\varphi \qquad (2.2)$$

The equation for shear friction is intended for an interface crack in a monolithic concrete construction. For the cases of artificially roughened or smooth construction joints, and for concrete to steel interfaces the same concept can be employed. However, smaller values of coefficient of friction should be used for these cases.

The above equations were later revised by F. Shaikh (Shaikh, 1978) through the introduction of effective coefficient of friction. Recommended values of coefficient of friction and effective coefficient of friction are available in the literature (Birkeland and Birkeland, 1967, Mast, 1968, Shaikh, 1978 and ACI 318-89).

Experiments reveal that in initially cracked concrete element, a limiting value for reinforcement parameter $\rho_s f_y$ exists, which clearly defines the effect of concrete strength on shear transfer strength. Below this value of reinforcement parameter the relationship between shear transfer strength and reinforcement parameter is independent of concrete strength. Above this value of reinforcement parameter, the rate of increase of shear transfer strength reduces by reduction in concrete strength, and behaviour is comparable with similarly reinforced, initially un-cracked concrete element (Mattock and Hawkins, 1972).

2.3.4 Web Reinforcement

Horizontal and vertical reinforcement used in low-rise walls form web reinforcement. The web reinforcement contributes to the mechanism of shear resistance by crossing inclined cracks caused by diagonal tension. It also controls crack widths, enabling continuation of aggregate interlock at high levels of shear stress. The relative contribution of horizontal and vertical web reinforcement is a function of wall aspect ratio and the amount and distribution of reinforcement in each direction. This also has a bearing on the inclination of diagonal tension cracks.

A major contribution of web reinforcement is to help develop the truss mechanism necessary for the formation of diagonal struts. In the majority of walls with rectangular cross-sections the web reinforcement may be the only source of tension element in the walls. Tensile forces in vertical and horizontal bars equilibrate the corresponding components of diagonal compressive struts, thereby sustaining the mechanism of shear resistance in walls.

2.3.5 Dowel Action, or Shear Transfer Through Reinforcement Crossing Shear Transfer Plane

A portion of the total applied shear is resisted by reinforcement crossing shear transfer planes. In general, the magnitude of this force is dependent on the crack width and shear displacement. Shear resistance of bars across a shear plane can be developed by one of the following three mechanisms (Park and Paulay, 1975):

1. Flexural deformation of reinforcement
2. Kinking of reinforcement
3. Shear stress across bars

2.3.5.1 Flexural Deformation of Reinforcement

Vertical reinforcement crossing a shear transfer plane deforms under horizontal shear as illustrated in Figure 2.3a. This deflected shape is associated with bending moments imposed on reinforcement. The equilibrium of forces leads to the following expression for shear resistance provided by this mechanism, at yield.

$$V_{dowel} = \frac{2M}{l} = \frac{4d_b A_s f_y}{3l\pi} \qquad (2.3)$$

This mechanism is utilized when full bearing exists between the vertical bars and the surrounding concrete. Under cyclic loading, concrete surrounding the vertical bars will be crushed at the interface leading to the loss of required bearing. To restore the bearing, the reinforcement is forced to deform excessively. This in turn activates another mechanism, called kinking of reinforcement.

2.3.5.2 Kinking of Reinforcement

This mechanism is likely to be the major source of dowel resistance in low-rise wall subjected to load reversals, particularly when small size bars are used. Shear resistance provided by kinking of vertical reinforcement is illustrated in Figure 2.3b, and accounts for the horizontal component of longitudinal tension force developed in vertical reinforcement.

$$V_{dowel} = A_s f_y \cos\alpha \qquad (2.4)$$

2.3.5.3 Shear Resistance Across Bars

This type of dowel action is less likely to be significant as compared to the previous two types. Some shear resistance is provided through shear area of reinforcement, perpendicular to the applied shear (Figure 2.3c). If the bars crossing the shear transfer plane are small in size, they

may fail in shear prior to developing the other modes of dowel action. The following empirical expression may be used to compute shear capacity of reinforcement.

$$V_{dowel} = \frac{A_s f_y}{\sqrt{3}} \tag{2.5}$$

2.4 Failure Modes for Low-Rise Walls

Low-rise shear walls with well designed foundations against overturning and uplift may develop inelastic behaviour when subjected to strong earthquakes. These walls may eventually fail in one of the following three failure modes:

1. Diagonal tension failure
2. Diagonal compression failure
3. Sliding shear failure

2.4.1 Diagonal Tension Failure

This type of failure is typical of low-rise walls with insufficient shear reinforcement. Upon formation of diagonal cracks, reinforcement crossing the cracks provides resistance against diagonal tension. If the reinforcement provided is not sufficient to sustain diagonal tension and the resulting truss mechanism it yields, resulting in diagonal tension failure. Walls with low aspect ratios, however, may have beams and floor slabs crossing diagonal tension cracks. In this case the walls continue resisting higher shear forces with little reinforcement, as the top and bottom structural elements control diagonal cracking. Eventually, these walls develop corner-to-corner diagonal cracks, and may still fail due to diagonal tension if insufficient reinforcement is present. However, this time the failure occurs at an increased load level (Figure 2.4).

2.4.2 Diagonal Compression Failure

When adequate shear reinforcement is provided to prevent diagonal tension failure, the wall continues resisting higher shear forces. This results in an increase in compressive stresses in diagonal struts. Under increasing compressive stresses, diagonal struts may exceed the compression capacity of concrete, leading to the crushing of concrete. This causes diagonal compression failure (Figure 2.5). Cyclic load reversals reduce the compressive capacity of cracked concrete in struts, and may result in reduced strength. This type of failure is highly undesirable, since diagonal compression failure causes dramatic and irrecoverable loss of strength.

2.4.3 Sliding Shear Failure

If diagonal tension and diagonal compression failures are suppressed by providing enough shear reinforcement, and by limiting nominal shear stress, sliding shear failure may occur, especially in walls with low aspect ratios. This type of failure is triggered after a few cycles of reversed loading and resulting continuous cracking along the base of the wall. Opening and closing of the flexural crack at the base reduce the mechanism of shear friction especially if significant yielding of vertical reinforcement occurs. Sliding shear results in sliding displacement along the construction joint at their base (Figure 2.6). Such displacement is responsible for a considerable reduction in stiffness and pinching of hysteresis loops, reducing energy dissipation capacity of the wall. Unless designed to prevent shear sliding or subjected to high axial compression, most low-rise shear walls are likely to develop significant shear sliding. These walls may eventually fail in the sliding shear mode, especially if their aspect ratios are low.

Tests have indicated that the shear transfer strength along the construction joint is significantly higher than diagonal tension and compression capacities of walls if the longitudinal reinforcement crossing the construction joint remain elastic. Therefore, for the design of elastic walls, sliding shear failure is not critical (Paulay et. al, 1982).

2.5 Methods of Analysis and Design for Low-Rise Shear Walls

Methods of analysis and design for low-rise shear walls are commonly based on truss models. The truss model in its original form was first introduced by Ritter in 1899 and Morch in 1902 for the analysis of reinforced concrete beams subjected to shear and bending. In this model cracked reinforced concrete member is idealized as a parallel chord truss. Bending moment is resisted as a couple by concrete forming a compression chord and longitudinal reinforcement forming a tension chord. Diagonal compression struts are formed between diagonal cracks, at an angle θ with the longitudinal reinforcement. Shear is resisted by compression in diagonal compression struts and tension in web reinforcement.

Shear strength of reinforced concrete beams using the truss model introduced by Ritter and Morch was based on 45 degree angle of diagonal struts. Tests have shown that stresses developed in stirrups were considerably less than those predicted. This is because the angle of inclination of diagonal struts are generally lower than 45 degrees and the contribution of uncracked concrete in compression zone to shear strength is ignored. Modified truss model was later introduced in which part of the applied shear force was assumed to be resisted by the uncracked concrete in compression zone. In this model the angle of diagonal struts is still assumed as 45 degrees.

The concept of truss model was later used by other researchers to introduce methods of analysis and design for members subjected to shear, flexure, and axial loads. These methods are briefly discussed in the following sections. Among the methods discussed, struts and ties model, equilibrium truss model, ACI Building Code approach, and the simplified method of Canadian Standard, consider equilibrium conditions. Compression field theory, the softened truss model, and the general method of Canadian Standard

consider equilibrium, compatibility, and softened stress strain relationship for concrete in diagonal struts.

2.5.1 Struts and Ties Model

Struts and ties model is similar to the truss model introduced by Ritter and Morch with a variable angle of inclination of diagonal compression struts. When used in the analysis of members subjected to shear and flexure, the compression chord and tensile chord resist bending moment in the form of a couple. Pinned joints are assumed at the intersection of web reinforcement with the longitudinal axes of compression and tensile chords. Diagonal compression struts are assumed to form between two joints at the end of each diagonal. Forces in the truss members are calculated using equilibrium equations only. The concept of shear transfer and the contribution of reinforcement is well defined by struts and ties model, but other types of shear transfer mechanism such as aggregate interlock and dowel action are not addressed by this model. The ultimate load is determined as the load causing first yielding of stirrups or crushing of concrete in diagonal struts when compressive stresses exceed 0.6 f_c' (Marti, 1985a,b). An important parameter in the design of reinforced concrete members by struts and ties model is the width of the diagonal struts. This makes experience an essential parameter for appropriate design of members. Struts and ties model often yields to overestimation of the capacity for structural walls (Lefas et. al, 1990a).

2.5.2 Equilibrium (Plasticity) Truss Model

The equilibrium truss model considers equilibrium and theory of plasticity based on yielding of reinforcement. The model is used for the analysis of structures at ultimate load stage. This method can be used for analysis of structures under moment, shear, axial load, and torsion (Hsu, 1993). The model is based on the assumption that at failure either transverse bars or both longitudinal and transverse steel yield before concrete crushes in diagonal compression struts (Hsu, 1993, MacGregor, 1992). Moment is carried by a couple between compression and tension struts formed at top and bottom chords of the beam. Plane section analysis is used to

determine the strain and stress distribution along the depth of the cross-section and hence to determine the width of top compression strut and loads in both longitudinal tension and compression struts due to flexure. Shear load is assumed to be resisted by web bars and diagonal struts as in the case of struts and ties model. Forces in web bars and diagonal compression struts caused by shear are determined through equilibrium equations alone.

2.5.3 Compression Field Theory

Compression field theory is based on the concept of tension field theory, introduced by Wagner in 1929. Cracked concrete is assumed as a new material with its own stress strain relationship resulting from softening effect of existing normal strains on the compressive strength of the material. The complete response of reinforced concrete members can be determined using equilibrium equations of the truss, compatibility conditions, and softened stress strain relationships for cracked concrete. Biaxial state of strains is transformed into the principal strains in member by the use of Mohr's circle. Principal stresses resulted from these strains are balanced through compression carried by concrete in diagonal compression struts and tension in longitudinal and transverse reinforcements. Concrete is assumed not to carry any tension after the formation of diagonal cracks. Modified compression field theory was later introduced as a revision of compression field theory in which concrete between cracks is assumed capable of carrying limited amount of tensile stress. Details of the analysis method for the prediction of response of reinforced concrete beams subjected to shear and axial load and also the response under combined shear, axial load, and bending can be found in references; Collins, 1978, Vecchio and Collins, 1988 and Collins and Mitchell, 1991.

2.5.4 Softened Truss Model

Softened truss model is used for analysis of structures under shear at both the serviceability and ultimate load stages. The method considers equilibrium equations of the truss, compatibility conditions, and softened stress strain relationship for concrete. The load deformation history of the member is determined by solving a set of simultaneous equations iteratively. The complete

procedure to analyze membrane elements using Softened Truss Model is documented in the Unified Theory of Reinforced Concrete (Hsu, 1993). The method is also applicable to low-rise shear walls with boundary elements strong enough to resist bending moments (Mau and Hsu, 1986).

2.5.5 Building Code Approach

ACI 318-89

Nominal shear strength of shear walls in seismic regions as predicted by ACI 318-89 Building Code is based on the modified truss model in which part of the shear strength is provided by un-cracked concrete and the remaining by web reinforcement. The following equation is used to determine nominal shear strength for walls with aspect ratios less than 2.0.

$$V_n = A_{cv}(\alpha_c \sqrt{f_c'} + \rho_n f_y) \leq 8\sqrt{f_c'} \qquad (2.6)$$

α_c is the coefficient varying linearly from 3.0 for aspect ratio of 1.5, to 2.0 for aspect ratio of 2.0, and f_c' is expressed in psi. The walls are required to have distributed shear reinforcement providing resistance in two orthogonal directions in the plane of the wall. For walls with aspect ratios less than 2.0, vertical web reinforcement ratio shall not be less than horizontal web reinforcement ratio.

The upper bound of $8\sqrt{f_c'}$ psi for shear strength is used to avoid modes of failure governed by compressive crushing of concrete in struts.

CSA Standards, CAN3-A23.3-M84

Shear strength of reinforced concrete shear walls in CSA A23.3 can be determined by either the simplified or general method. The simplified method is based on modified truss model, and is basically similar to the ACI 318-93 approach. The general method is, on the other hand, a

simplification of the approximate modified compression field theory in which constant values for longitudinal flexural strains at middepth of the section and compressive diagonal strains in compression struts are assumed

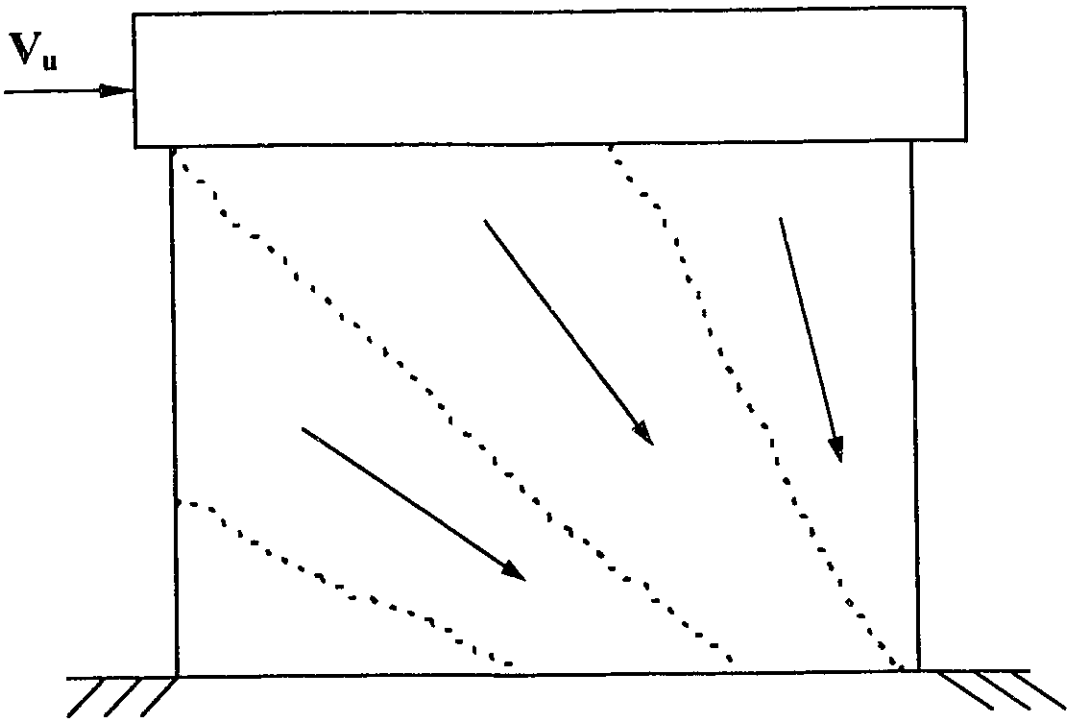

Figure 2.1 Typical Low-Rise Shear Wall Subjected to Lateral Load

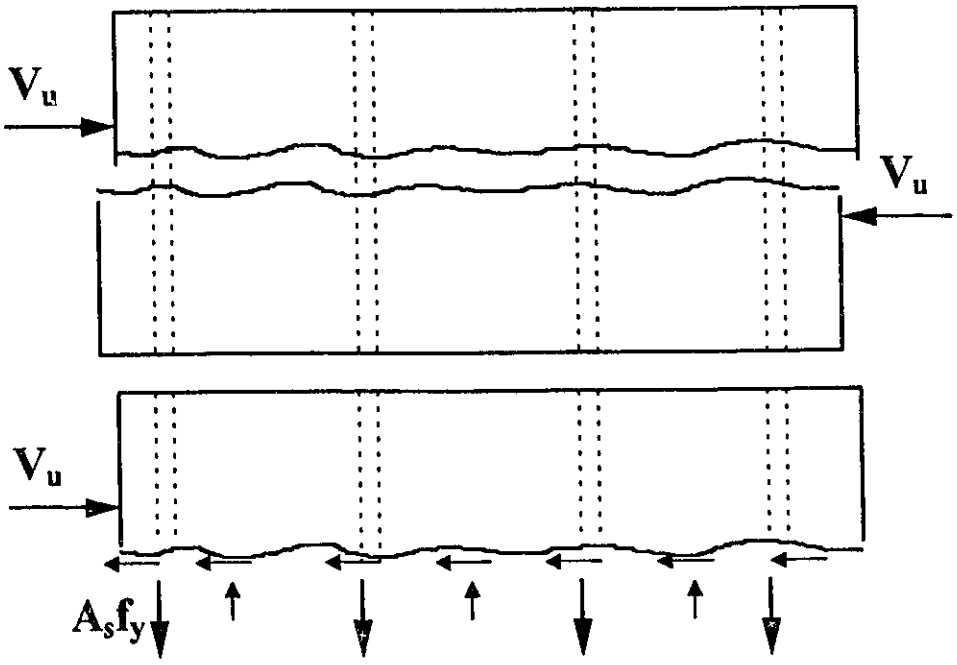

Figure 2.2 Shear Friction Principle

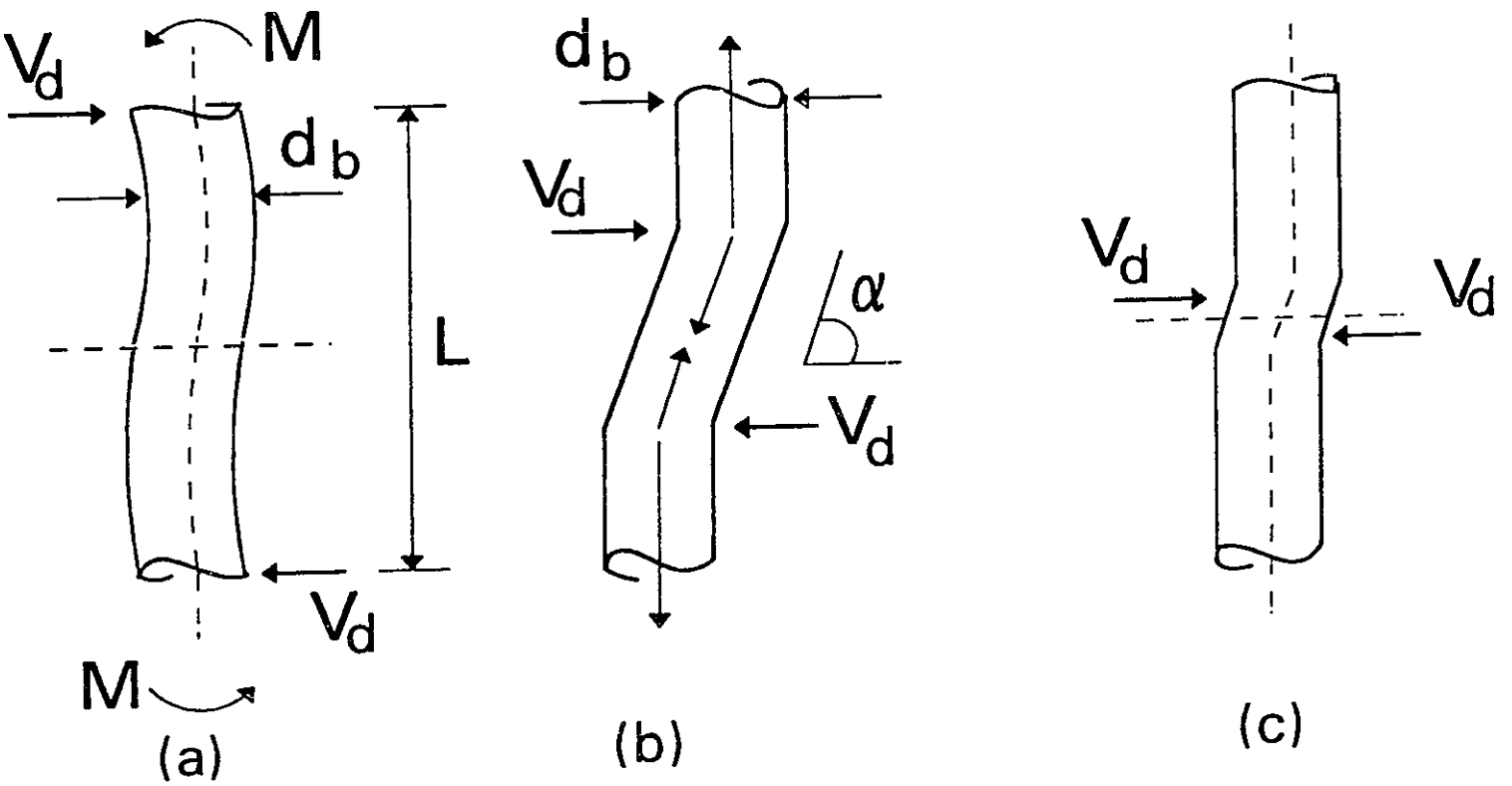

Figure 2.3 Dowel Action of Reinforcement, a) Flexural Deformation, b) Kinking, and c) Direct Shear

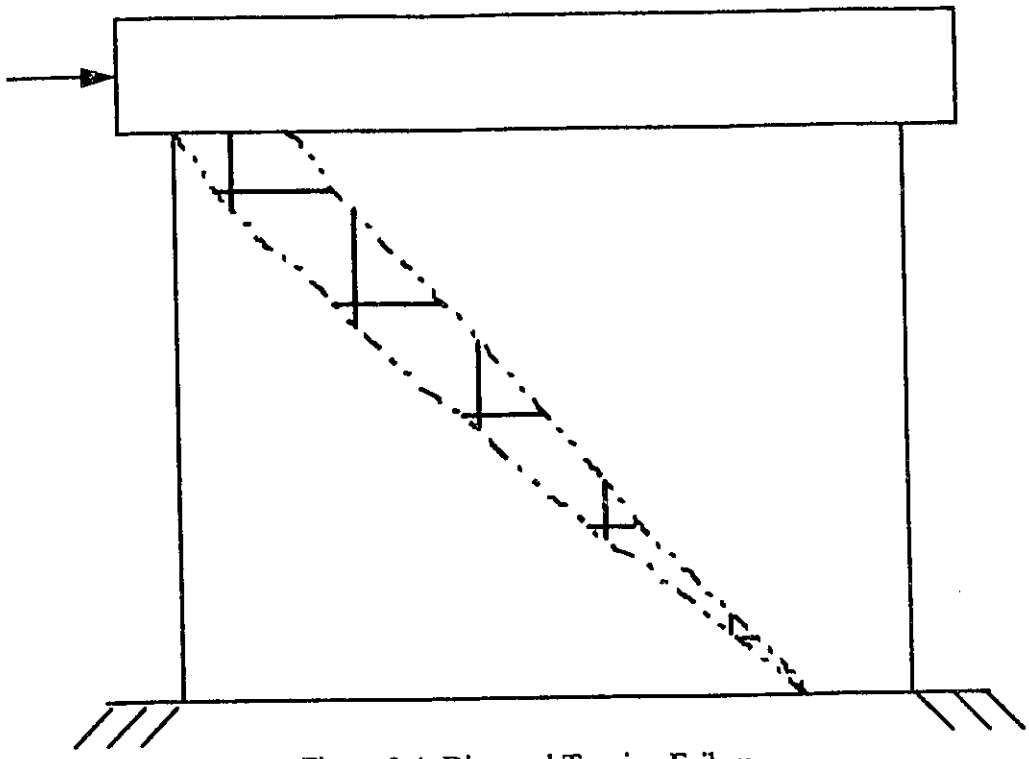

Figure 2.4 Diagonal Tension Failure

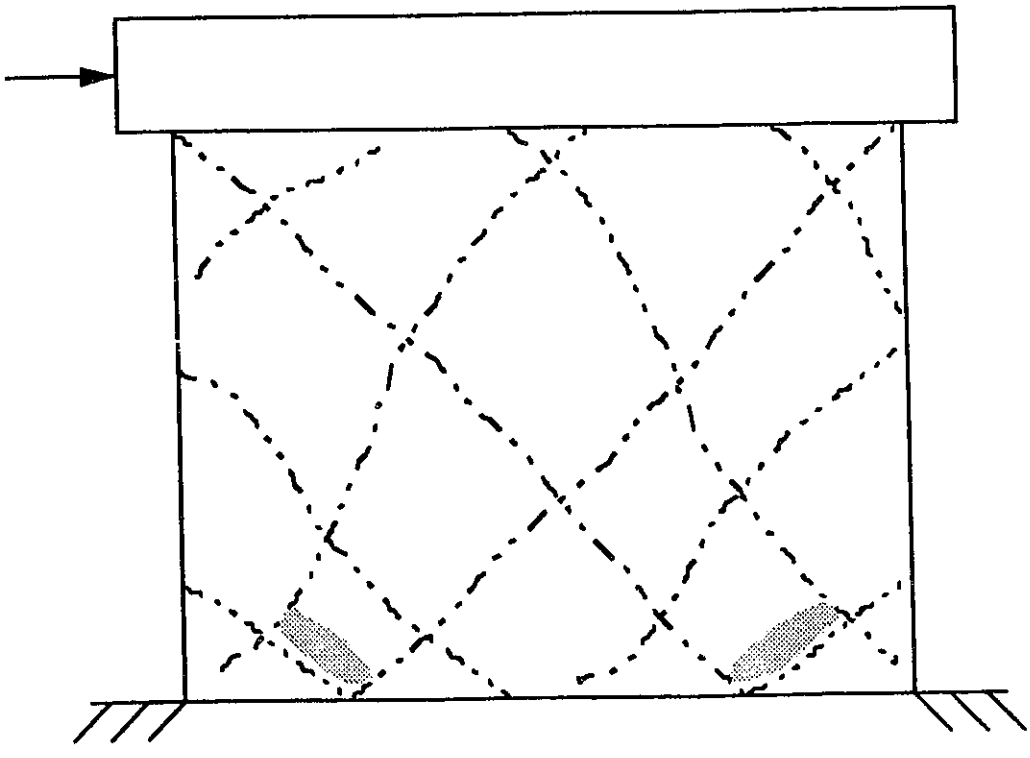

Figure 2.5 Diagonal Compression Failure

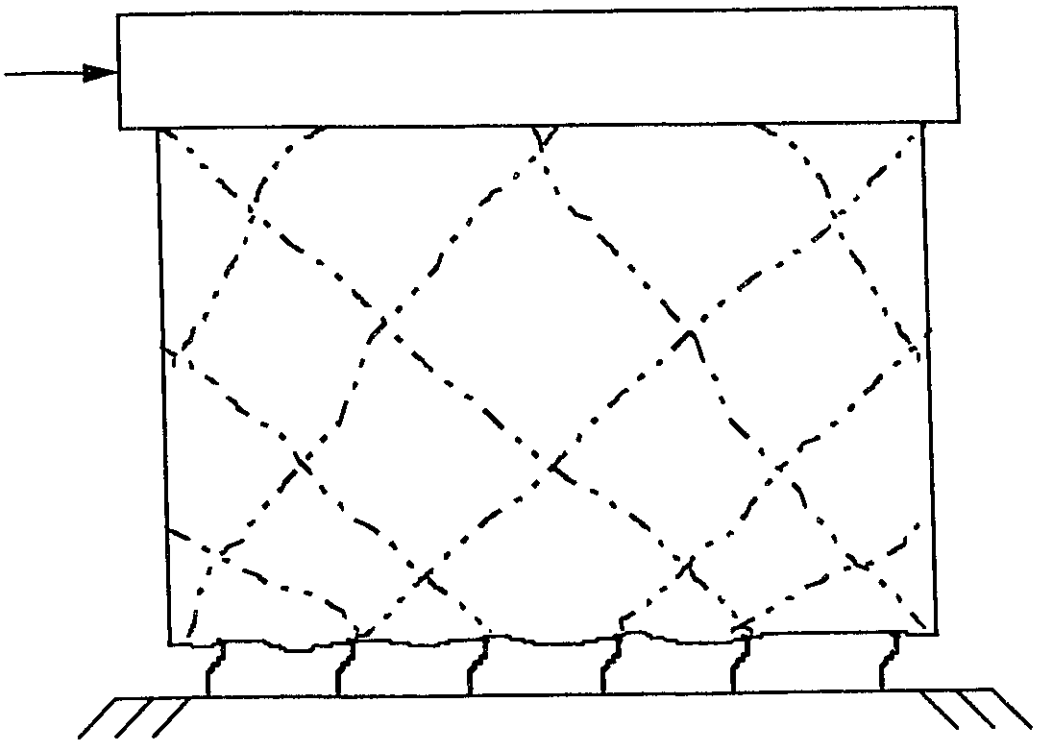

Figure 2.6 Sliding Shear Failure

Chapter 3

Experimental Program

3.1 General

An experimental investigation was carried out to study the effects of wall aspect ratio on performance, mechanism of shear resistance, and failure modes of shear walls. Wall aspect ratios were selected to complement the specimens previously tested by others as part of the same research program. The specimens were companion to those tested by Wiradinata (Wiradinata, 1985), Pilette (Pilette, 1987) and Wasiewicz (Wasiewicz, 1988). Two large scale low-rise walls with rectangular cross-sections were considered for testing. The specimens were labeled as Wall 7 and Wall 8, following the previously tested 6 low-rise walls. Both walls had a thickness of 100 mm and a height of 1500 mm. Wall 7 was 2000 mm long and Wall 8 was 1500 mm long, producing wall aspect ratios of 0.75 and 1.00 respectively. Both walls were reinforced with orthogonal horizontal and vertical reinforcement consisting of No. 10 deformed bars. Horizontal and vertical web reinforcement ratios for both walls were 0.8 %. The overall geometry and dimensions of the wall specimens and reinforcement details are shown in Figures 3.1 to 3.10. Details of test specimens, material properties, construction procedure, test set-up, and instrumentation are described in the following sections.

3.2 Design of Test Specimens

The specimens were cast with heavily reinforced base to provide full base fixity and heavily reinforced top beam to ensure uniform application of lateral load along the wall length at the top. The wall base was fixed to the laboratory strong floor during testing.

Design of Wall 7

Wall 7, with an aspect ratio of 0.75, was designed using 0.8 % horizontal and 0.8 % vertical web reinforcement ratios. Vertical reinforcement consisted of 8 pairs of No. 10 grade 400 deformed bars, uniformly placed in two layers. These bars were extended into the top beam and bottom slab by at least their development lengths. Two rows of vertical bars at each end of the wall were laterally supported against premature bucking by means of 6.4 mm plain hoops spaced at 80 mm along the full height of the wall. Horizontal web reinforcement consisted of 6 pairs of No. 10 grade 400 deformed bars, uniformly placed in two layers. Details of reinforcement arrangement are shown in Figures 3.1 and 3.2. The calculated flexural capacity of Wall 7, based on plane section analysis and measured material properties, was 720 kN.m. Strain hardening of reinforcement was considered in the analysis. The computed shear capacity, based on ACI 318-89 Building Code, was 884 kN.

Design of Wall 8

Wall 8 with an aspect ratio of 1.0 was designed using 0.8 % horizontal and 0.8 % vertical web reinforcement ratios. Vertical reinforcement consisted of 6 pairs of No. 10 grade 400 deformed bars, uniformly placed in two layers. These bars were extended into the top beam and bottom slab by at least their development lengths. Two rows of vertical bars at each end of the wall were laterally supported against premature bucking by means of 6.4 mm plain hoops spaced at 80 mm along the full height of the wall. Horizontal web reinforcement consisted of

6 pairs of No. 10 grade 400 deformed bars, uniformly placed in two layers. Details of reinforcement arrangement are shown in Figures 3.3 and 3.4. The calculated flexural capacity of Wall 8, based on plane section analysis and measured material properties, was 430 kN.m. Strain hardening of reinforcement was considered in the analysis. The computed shear capacity, based on ACI 318-89 Building Code, was 663 kN.

3.3 Fabrication of Specimens

The specimens were cast in wooden forms, built from 25 mm thick standard size plywood. Light coat of white paint was applied on the formwork to protect the wood and also to act as a bond breaker. Reinforcement cage for the bottom slab was placed in one piece. The base slab was constructed to have a rectangular shape. It was heavily reinforced with No. 20 deformed rebars as main reinforcement and No. 10 deformed bars as stirrups. The top beam cage was placed and supported by a wooden frame. The top beam was also heavily reinforced using No. 20 bars and No. 10 stirrups. The reinforcement detailing of top beams and bottom slabs for Wall 7 and Wall 8 are shown in Figures 3.7 to 3.10. Vertical and horizontal web reinforcements were assembled and anchored to the top and bottom reinforcement cages. Four 75 mm diameter plastic pipes were placed in designated locations in the bottom slab to allow for attachment of the base to the laboratory strong floor by means of 75 mm bolts. Four 40 mm diameter plastic pipes were also placed in designated locations in the top beam to secure the loading plates. The plates, one at each end of the top beam, were connected by strands passing through the 40 mm diameter holes.

Concrete was poured in two stages for each wall. The first stage involved casting of the bottom slab with reinforcement cage of the wall and top beam in place. High early strength concrete was supplied by a local ready mix company with a specified strength of 35 MPa. High slump concrete with 10 mm maximum aggregate size was ordered for easy workability. The proper roughness of the construction joint was achieved by leaving the area of the joint concrete

without trawling. This provided rough surface of the joint with a relief depth of about 10 mm consistent with current practice. Concrete surface was cured for a few days until the second stage of casting was done.

The second stage consisted of casting the wall and the top beam together. The formwork for the wall was laterally supported by threaded rods and wooden struts to prevent bulging during construction. The same threaded rods were also used to provide supports for attachments of the LVDT's required for testing. Concrete was carefully placed and vibrated using a 25 mm vibrator. Vibration of concrete was carefully done to prevent damage to strain gauges mounted on reinforcing bars. Control cylinders were cast from each batch of concrete. Figures 3.11 and 3.12 show pictures of Wall 8 and Wall 7 during construction.

The forms were stripped two days after casting. A light steel frame was constructed around the wall for the attachment of measuring devices. This frame was fixed to the base slab. Therefore the displacements measured using this frame were relative to the wall foundation. LVDT's and potentiometers were calibrated and mounted on the wall on predetermined locations using rods and plates and angles installed prior to and immediately after casting of concrete at each stage. Strain gauges and LVDT's were connected to a data acquisition system. Applied load was measured using pressure transducers mounted on the loading jack. All of the gauges and LVTD's and pressure transducers were tested for proper functioning prior to testing.

3.4 Test Setup

The test setup employed is shown in Figure 3.13. A reaction frame was used to support the hydraulic jack for the application of horizontal force. This frame consisted of two 'A' frames, each bolted to two 457 mm deep supporting channels which in turn were mounted and attached to identical channels by means of bolted connections. The bottom channels were attached to the laboratory strong floor using four 75 mm diameter high capacity bolts. These

two 'A' frames were connected by vertically placed 50 mm thick plate, which also provided support for the jack. A two way action hydraulic jack with a maximum capacity of 1500 kN was used to apply lateral load reversals. The jack was controlled by an electric oil pump. A 900 mm long shaft with swivel ends was placed between the hydraulic jack and the top of the specimen to transmit the load. Out of plane movement and associated twisting moment during the test was eliminated using a specially designed frame which prevented lateral wall movement. This frame guided the top beam during testing, and did not allow any out-of-plane movement.

Positive loading was applied by extending the jack shaft against the test specimen, while negative loading was applied by pulling the wall towards the jack by means of four post-tensioned strands mounted to a steel end plate. These strands were post-tensioned to 60 kN using a hydraulic jack. The strands were fixed in place using a 25 mm thick steel plate on the west side and specially designed steel box at the east side consisting of 100 mm thick plates. The steel box was attached to a 90 mm diameter shaft at the other end. The shaft of the jack could be extended 6.0 inches (152.4 mm). Therefore, the test setup was designed such that the zero horizontal deflection at the center of the top beam corresponded to 3.0 inches (76.2 mm) extension of the shaft, and hence the maximum possible horizontal top displacement in each direction was 3.0 inches (76.2 mm).

3.5 Instrumentation

3.5.1 General

The specimens were well instrumented for strain and displacement measurements. A Seimetric 200 Data Acquisition System (with 64 channels) was used to record the data. The strain measurements were taken both on reinforcement, by means of electrical strain gauges (type UN-120 with the coefficient factor of 2.085 and maximum strain of 0.5 %), and on concrete, by means of a Demec Gauge. The displacement readings were taken by Linear Variable

Differential Transducers (LVDT's) and potentiometers. The applied load was recorded through a pressure transducer installed on the hydraulic line of the jack. Details of instrumentation and locations of gauges are discussed in the following sections.

3.5.2 Strain Measurements on Horizontal and Vertical Reinforcement

Electrical resistant strain gauges were mounted on horizontal and vertical reinforcement near the intersection of steel bars with anticipated major diagonal cracks under positive and negative loadings. Two strain gauges were installed at each location 100 mm apart. Strains on vertical reinforcement along the construction joint were also measured by means of strain gauges.

Total of 59 and 50 strain gauges were used in Wall 7 and Wall 8 respectively. The locations and codings of strain gauges are shown in Figures 3.14 to 3.21. The bars were first smoothened using a grinder and a sand paper at strain gauge locations. The reduction of cross sectional area of the rebars was in the range of 1.5 %. The steel was then cleaned from dirt and grease using acidic solution and gauges were glued by an adhesive agent. A layer of wax was used to cover the gauges and terminals to prevent the penetration of moisture into the gauges. The gauges were then covered by a layer of stay soft putty and a tape to prevent an accidental damage during construction.

3.5.3 Strain Measurements on Concrete

Concrete strains on the walls were measured in vertical, horizontal and diagonal directions using a Demec gauge. Targets were placed on the walls, consisting of 12 mm diameter hard plastic chips, glued on the north faces of the walls, forming 200 by 200 mm grids covering the whole wall surface (see Figure 3.22). The Demec gauge was modified to measure strains in vertical and horizontal directions with a gauge length of 200 mm and in diagonal directions with a gauge length of 282.8 mm.

3.5.4 Displacement Measurements

The walls were prepared with steel brackets cast in the concrete base for building a light steel frame for instrumentation. Most of the displacement measurements were done through LVDT's and potentiometers attached to the steel reference frame. Top horizontal displacements were measured by two 150 mm stroke potentiometers positioned at the top, with tips secured to the top beam near the east and west ends. A 50 mm LVDT was positioned near mid-height, also for horizontal displacement measurement. Three other 50 mm LVDT's were placed along the construction joint for measurements of shear sliding. Vertical movements of the walls were also recorded by means of 150 mm stroke potentiometers. Two recordings were made on the top beam near the east and west ends. Additional vertical displacement readings were taken near the base to measure the extension and/or slippage of vertical reinforcement within the footing. The locations of LVDT's and potentiometers are illustrated in Figure 3.23.

3.5.5 Force Measurements

The horizontal force was measured by means of pressure transducers. Two pressure transducers (with 0.5 % precession) were mounted on the hydraulic line of the jack to measure the pressure for positive and negative loadings. They were connected to the data acquisition system and recorded through a personal computer. The pressure readings were later converted to loads using shaft areas for both positive and negative loading.

3.6 Loading Program

The specimens were tested under slowly applied lateral load reversals. The intended loading program for both walls is shown in Figure 3.24. Loading consisted of two parts. The first part included elastic loading and was applied in load control mode. The walls were cycled elastically three times at approximately one half the calculated ultimate load capacity. The elastic load used for the first three cycles of loading was 190 and 120 kN for Wall 7 and Wall 8

respectively. The second part was in deflection control mode and the walls were cycled three times at each of the incrementally increasing deflection level until failure. The deflection increments were based on yield deflection. The yield deflection, Δ_y, for Wall 7 was determined by drawing a straight line from the origin through the first yield load and its intersection with a horizontal line drawn at calculated ultimate load level. The first yield load was obtained experimentally when the strain gauge on the extreme tension reinforcement at the construction joint yielded. The yield displacement was determined as 5.0 mm for Wall 7. The strain gauge on extreme tension reinforcement was damaged in Wall 8. Therefore, the yield displacement Δ_y, was determined experimentally as the load at which the rate of change in displacement showed a sharp increase. This load level was marked as 7.5 mm.

3.7 Material Properties

Concrete

Ready mix concrete, obtained from a local supplier was used for both walls. High early strength concrete with a 28 day target strength of 35 MPa, 75 mm slump, and 10 mm maximum aggregate size was requested for both walls. Casting was done in two stages. Wall base was cast first for both specimens. Wall panels and top beams were cast in the second stage, about two weeks later. Control cylinders were taken from each of the two batches and were tested at different ages to determine strength gain.

Concrete was vibrated using 15 mm vibrators and steel rods. Due to the small wall thickness and presence of two layers of No. 10 bars in both horizontal and vertical direction, some casting problems were encountered. Small gaps formed in the wall at couple of locations which were later repaired with concrete of similar properties. Wall 7 and Wall 8 were tested three months and five months after casting, respectively. The final concrete strength during the test period was determined as 45 MPa.

Reinforcing Steel

Grade 400, No. 10 reinforcing bars were used as horizontal and vertical reinforcement. The reinforcement was ordered and obtained from the same batch. Coupon tests were performed to establish stress-strain characteristics of bars. Representative stress-strain relationship is shown in Figure 3.25.

3.8 Observed Behaviour and Test Data

3.8.1 General

This section presents observed behaviour of specimens during testing. Displacements and deformation components obtained from potentiometers, LVDT's, and Demec gauges are plotted as recorded during testing. The data are presented in the form of force deformation relationships for top horizontal and vertical deflections, mid-height horizontal deflection, anchorage slip, sliding shear, and web shear distortion. Strain gauge data are also plotted to show variation in steel strain. While this section presents the data as recorded during testing, evaluation and discussion of test results are presented in Chapter 4.

3.8.2 Wall 7

3.8.2.1 Observed Behaviour

Wall 7, with an aspect ratio of 0.75, developed horizontal cracks in the lower half of the wall during the first elastic loading to 190 kN. A horizontal crack formed along the construction joint, starting at the extreme tension fiber and extending to the third row of vertical reinforcement. More horizontal cracks and diagonal cracks formed with approximately 45 degree inclination during loading to $1\Delta_y$. The extreme tension reinforcement yielded at the construction joint and began to strain hardening. The previous horizontal crack along the

construction joint was widened and extended to the center of the wall. Similar crack pattern was observed in the opposite direction when the load was reversed to $-1\Delta_y$.

Horizontal crack along the construction joint became continuous during the first cycle of deformation at $2\Delta_y$. No new cracks were observed when the wall was pushed to $2\Delta_y$. However, widening of existing cracks was observed during this load stage. When the wall was reversed to $-2\Delta_y$ few new cracks formed in the upper west side of the wall with a major diagonal crack extending from the top west corner to the central area of the wall. Widening of existing cracks was observed during the third cycle at $2\Delta_y$, although no new cracks were formed at this load stage.

New diagonal cracks formed at the upper side of the wall during loading to $3\Delta_y$. These cracks extended from the top of the wall to approximately the third row of horizontal reinforcement from the top. The concrete cover at the west end was badly damaged near the foundation and started to crush during the last cycle of $3\Delta_y$. The horizontal crack along the construction joint and some of the flexural cracks near the base opened up wide enough to clearly expose the reinforcement.

No new cracks were formed when the wall was loaded to $4\Delta_y$. However, the concrete cover along the construction joint started to spall off and kinking of vertical reinforcement was observed. More spalling of concrete and kinking of vertical reinforcement was observed during the third cycle at $4\Delta_y$. Extensive spalling of cover concrete was observed at the east and west ends of the web near the foundation.

Concrete crushing at the west end extended to the first row of horizontal reinforcement when the wall was pushed to the first cycle of $5\Delta_y$. Vertical bars at both east and west ends of the wall started to buckle. More kinking of vertical bars and more crushing of concrete near the

construction joint was observed. Some crushing of diagonal compression struts was observed in the area between the first and third rows of vertical reinforcement near the west end of the wall. Sliding of the wall could be observed visually at this stage of loading.

Cycles at $6\Delta_y$ increased the intensity of diagonal cracking near the base, and criss-crossing of cracks led to disintegration of concrete along the first and the second rows of horizontal reinforcement. During $7\Delta_y$ cycles one of the horizontal cracks at this level widened and extended to fifth row of vertical reinforcement and eventually joining the base crack. This crack eventually caused the separation of the wall into two separate blocks. A similar crack was observed at $7\Delta_y$ propagating from the west side of the wall.

The failure of the wall was categorized as web compression failure near the compression toe. There was also extensive sliding at the base and appreciable amount of vertical bar buckling in the boundary elements. Extensive deterioration of concrete and kinking of vertical reinforcement along the construction joint was observed at failure. Figures 3.26 to 3.29 show pictures of Wall 7 at different stages of loading.

3.8.2.2 Recorded Data for Wall 7

Top Horizontal Deflection

Top horizontal deflection of the wall was measured using two 150 mm stroke potentiometers mounted on a light steel frame with targets attached to the top beam (Figures 3.23a and b, Nos.8 and 10). The accuracy of these potentiometer was 0.07 mm. The end attachments were such that bending of the potentiometers was eliminated to avoid the possibility of damage. Hysteretic load-displacement relationships for top horizontal deflection recorded by the two potentiometers placed near the east and west ends of the wall are shown in Figures 3.30 and 3.31. These readings were taken at 322.5 mm above the centerline of the top beam, where the potentiometers were mounted.

Mid-height Horizontal Deflection

The mid-height horizontal deflection was measured using a 50 mm stroke LVDT mounted on the same light frame used for instrumentation. A plastic plate was glued on the east end of the wall at mid-height (Figures 3.23a and b, No.6). The LVDT was fixed to the light frame targeting to the plastic plate. This spring loaded LVDT was able to record displacement in both directions. The accuracy of measurements was 0.03 mm. The hysteretic load-deflection relationship at mid-height of the wall is shown in Figure 3.32.

Top Vertical Deflection

Hysteretic load-deflection diagrams for vertical displacements of the top beam are shown in Figures 3.33 and 3.34. The displacements were measured using 150 mm potentiometers with 0.07 mm accuracy. These potentiometers were mounted on the light steel frame which was fixed to the base (Figures 3.23a and b, Nos. 7 and 9). Therefore, any possible rotation of the base during loading would not affect the readings. These readings, on the other hand, include displacements due to anchorage slip in the base.

Anchorage Slip

The anchorage slip deformations at east and west ends of the wall were measured over a 30 mm gauge length using two 150 mm potentiometers with 0.07 mm accuracy. These potentiometers were mounted on the light steel frame and their tips were resting freely on the targets made of plastic plates glued to the wall near the construction joint. The locations of the potentiometers are shown in Figures 3.23a and b (Nos 1 and 5). Hysteretic load-displacement relationships for anchorage slip at the east and west ends of the wall are shown in Figures 3.35 and 3.36, respectively.

Sliding Shear Displacements

Sliding shear displacements were measured at the center, east end, and west end of the wall using three 50 mm stroke LVDTs with 0.03 mm accuracy. The LVDTs were mounted on the

wall near the base with plastic target plates glued on the foundation. The locations of these LVDT's are shown in Figures 3.23a and b (Nos. 2, 3, and 4). Initially all three LVDT's recorded similar values. However, at later stages of loading, the formation of a large crack in the lower part almost separated the wall into two pieces and resulted in significantly different sliding measurements in the three LVDT's. The average of the three sliding readings was used to quantify the base slip. The hysteretic load-shear sliding relationships are shown in Figures 3.37 to 3.39.

Shear Deformations

Shear deformations were determined using Demec readings described in section 3.5.3. The locations of targets on the wall are shown in Figure 3.22 Demec readings were recorded at peak displacements of the first and third cycles at each deformation level for both positive and negative directions. Each set of reading included readings for four sides and two diagonals of each subgrid. The measurements were terminated after the first cycle at $3\Delta_y$ for positive loading, and the third cycle at $2\Delta_y$ for negative loading due to the exhaustion of the limits of the Demec gauge. Figure 3.40 shows the variation of shear deformation along the height of the wall for different stages of loading.

Strains in Reinforcement

Strains in vertical and horizontal reinforcement were measured at selected locations using electrical resistance strain gauges. These locations include construction joint for vertical bars, extreme tension and compression vertical bars inside the foundation, and predicted diagonal failure plane for vertical and horizontal reinforcement. The exact locations of strain gauges and the coding used for these gauges are shown in Figures 3.14 to 3.17. Figures 3.41 to 3.48 show typical hysteretic diagrams for strains in vertical and horizontal reinforcements. Unfortunately a good number of gauges could not be monitored due to the malfunctioning of some channels of the data acquisition system during testing.

3.8.3 Wall 8

3.8.3.1 Observed Behaviour

Wall 8 with an aspect ratio of 1.0 developed horizontal cracks in the lower half of the wall during the first elastic loading to 125 kN. A horizontal crack formed along the construction joint, starting at the extreme tension fiber and extending to the middle of the wall. More horizontal cracks and diagonal cracks formed with approximately 45 degree inclination during loading to $1\Delta_y$. Similar crack pattern was observed in the opposite direction when the load was reversed to $-1\Delta_y$.

Horizontal crack along the construction joint became continuous during the first cycle of deformation at $2\Delta_y$. Only one or two new cracks formed in the lower half of the wall when the wall was pushed to $2\Delta_y$. However, widening of existing cracks was observed during this load stage. The horizontal crack along the construction joint and some of the flexural cracks near the base opened up wide enough to clearly expose the reinforcement.

No new cracks were formed when the wall was loaded to $3\Delta_y$. However, the concrete cover at the west end was badly damaged near the foundation and started to crush during the last cycle of $3\Delta_y$.

When the wall was loaded to $4\Delta_y$, the concrete cover along the construction joint started to spall off and kinking of extreme vertical reinforcement was observed. More spalling of concrete and kinking of vertical reinforcement was observed during the third cycle at $4\Delta_y$. Extensive spalling of cover concrete was observed at the east and west ends of the web near the foundation. The spalling of cover concrete extended to approximately 100 mm in the foundation.

Crushing of diagonal compression struts was observed at the west end when the wall was pushed to the first cycle of $5\Delta_y$. More kinking of vertical reinforcement and more crushing of concrete near the construction joint was observed. Extensive spalling of cover concrete was observed at the east and west ends of the web and foundation during the third cycle at $5\Delta_y$. Increased intensity of diagonal cracking near the base, and criss-crossing of cracks at this stage of loading led to disintegration of concrete along the first and second rows of horizontal reinforcement. One of the horizontal cracks at the level of the first row of horizontal reinforcement widened and extended to the third row of vertical reinforcement and joined the base crack. This crack eventually caused the separation of the wall into two separate blocks. Sliding of the wall could also be observed visually at this stage of loading.

Extensive bar buckling and rupture of one of the vertical bars at east end was observed at the end of test due to badly damaged concrete cover in the web and foundation. The failure of the wall was categorized as web compression failure near the compression toe. There was also appreciable amount of sliding at the base and extensive vertical bar buckling and rupture of one of the vertical reinforcement in boundary element. Extensive deterioration of concrete and kinking of vertical reinforcement along the construction joint was observed at failure. Figures 3.49 to 3.52 show pictures of Wall 8 at different stages of loading.

3.8.3.2 Recorded Data for Wall 8

Top Horizontal Deflection

Top horizontal deflection of the wall was measured using two 150 mm stroke potentiometers mounted on a light steel frame with targets attached to the top beam (Figures 3.23a and b, Nos. 8 and 10). The accuracy of these potentiometer was 0.07 mm. The end attachments were such that bending of the potentiometers was eliminated to avoid the possibility of damage. Hysteretic load-displacement relationships for top horizontal deflection recorded by the two potentiometers placed near the east and west ends of the wall are shown in Figures 3.53 and

3.54. These readings were taken at 322.5 mm above the centerline of the top beam, where the potentiometers were mounted.

Mid-height Horizontal Deflection

The mid-height horizontal deflection was measured using a 50 mm stroke LVDT mounted on the same light frame used for instrumentation. A plastic plate was glued on the east end of the wall at mid-height (Figures 3.23a and b, No. 6). The LVDT was fixed to the light frame targeting to the plastic plate. This spring loaded LVDT was able to record displacement in both directions. The accuracy of measurements was 0.03 mm. The hysteretic load-deflection relationship at mid-height of the wall is shown in Figure 3.55.

Top Vertical Deflection

Hysteretic load-deflection diagrams for vertical displacements of the top beam are shown in Figures 3.56 and 3.57. The displacements were measured using 150 mm potentiometers with 0.07 mm accuracy. These potentiometers were mounted on the light steel frame which was fixed to the base (Figures 3.23a and b, Nos. 7 and 9). Therefore, any possible rotation of the base during loading would not affect the readings. These readings, on the other hand, include displacements due to anchorage slip in the base.

Anchorage Slip

The anchorage slip deformations at east and west ends of the wall were measured using two 150 mm potentiometers with 0.07 mm accuracy. These potentiometers were mounted on the light steel frame and their tips were resting freely on the targets made of plastic plates glued to the wall near the construction joint. The locations of the potentiometers are shown in Figures 3.23a and b (Nos. 1 and 5). Hysteretic load-displacement relationships for anchorage slip at the east and west ends of the wall are shown in Figures 3.58 and 3.59, respectively.

Sliding Shear Displacements

Sliding shear displacements were measured at the center, east end, and west end of the wall using three 50 mm stroke LVDT's with 0.03 mm accuracy. The LVDT's were mounted on the wall near the base with plastic target plates glued on the foundation. The locations of these LVDT's are shown in Figures 3.23a and b (Nos. 2, 3, and 4). Initially all three LVDT's recorded similar values. However, at later stages of loading the formation of a large crack in the lower part almost separated the wall into two pieces and resulted in significantly different sliding measurements in the three LVDT's. The average of the three sliding readings was used to quantify the base slip. The hysteretic load-shear sliding relationships are shown in Figures 3.60 to 3.62.

Shear Deformations

Shear deformations were determined using Demec readings described in section 3.5.3. The locations of targets on the wall are shown in Figure 3.22. Demec readings were recorded at peak displacements of the first cycle at each deformation level for both positive and negative directions. Each set of reading included readings for four sides and two diagonals of each subgrid. The measurements were terminated after the first cycle at $4\Delta_y$ for positive loading, and the first cycle at $2\Delta_y$ for negative loading due to the exhaustion of the limits of the Demec gauge. Figure 3.63 shows the variation of shear deformation along the height of the wall for different stages of loading.

Strains in Reinforcement

Strains in vertical and horizontal reinforcement were measured at selected locations using electrical resistance strain gauges. These locations include construction joint for vertical bars, extreme tension and compression vertical bars inside the foundation, and predicted diagonal failure plane for vertical and horizontal reinforcement. The exact locations of strain gauges and the coding used for these gauges are shown in Figures 3.18 to 3.21. Figures 3.64 to 3.68 show typical hysteretic diagrams for strains in vertical and horizontal

reinforcements. Unfortunately a good number of gauges could not be monitored due to the malfunctioning of some channels of the data acquisition system during testing.

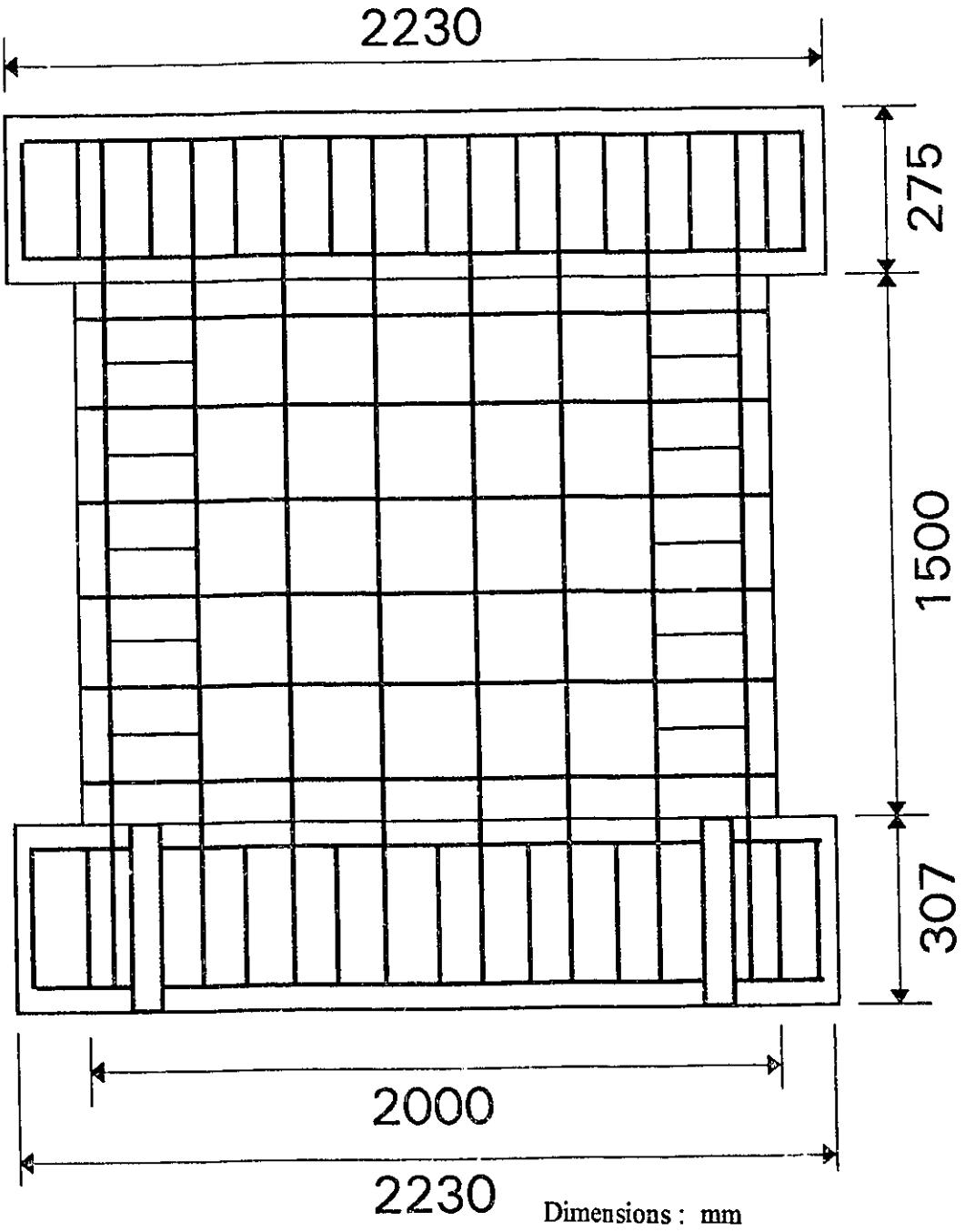

Figure 3.1 Geometry and Reinforcement Layout of Wall 7

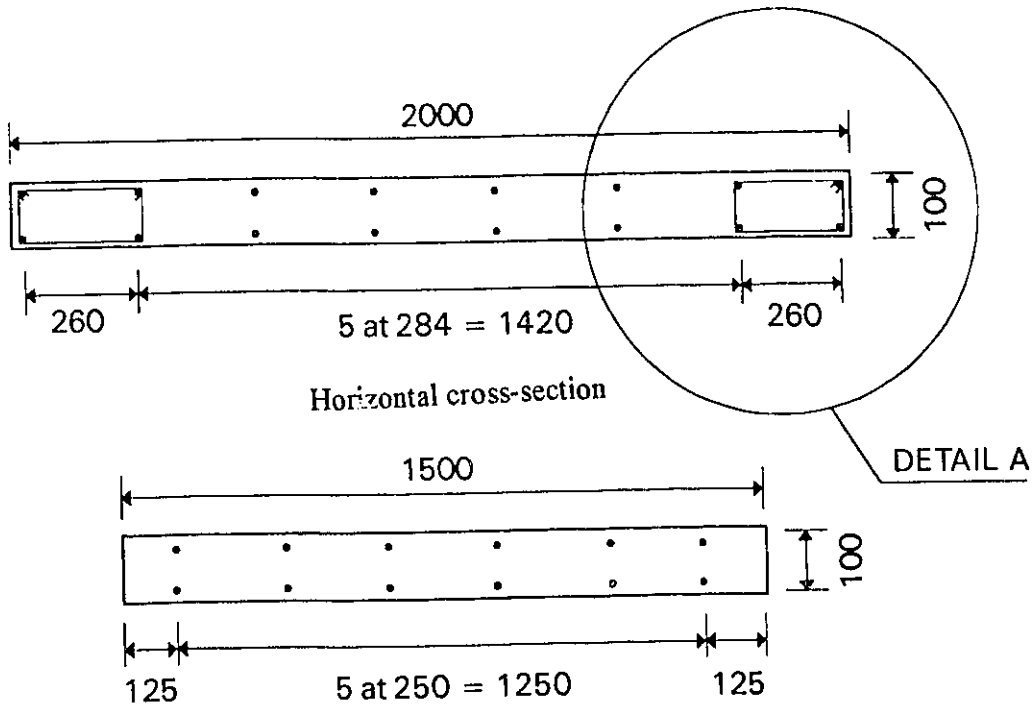

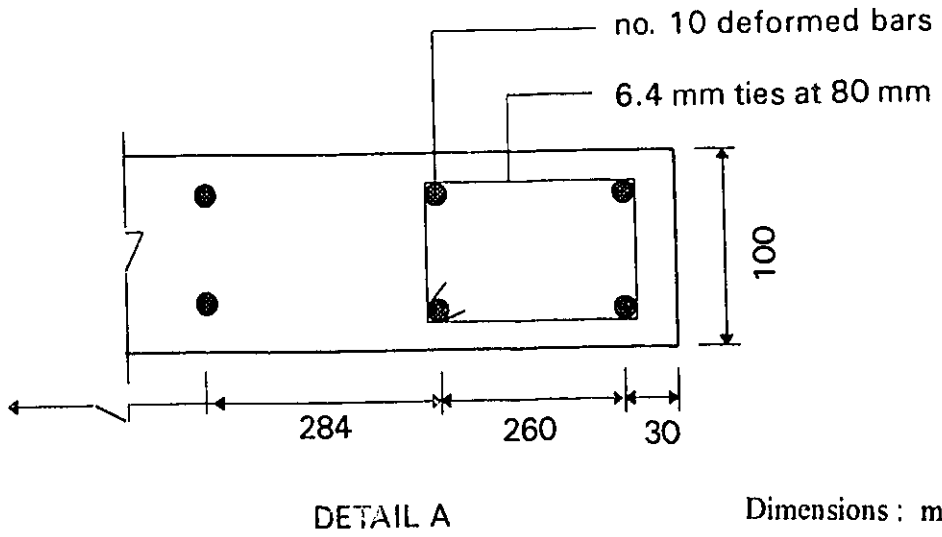

Figure 3.2 Horizontal (above) and Vertical (below) Cross-Sections of Wall 7

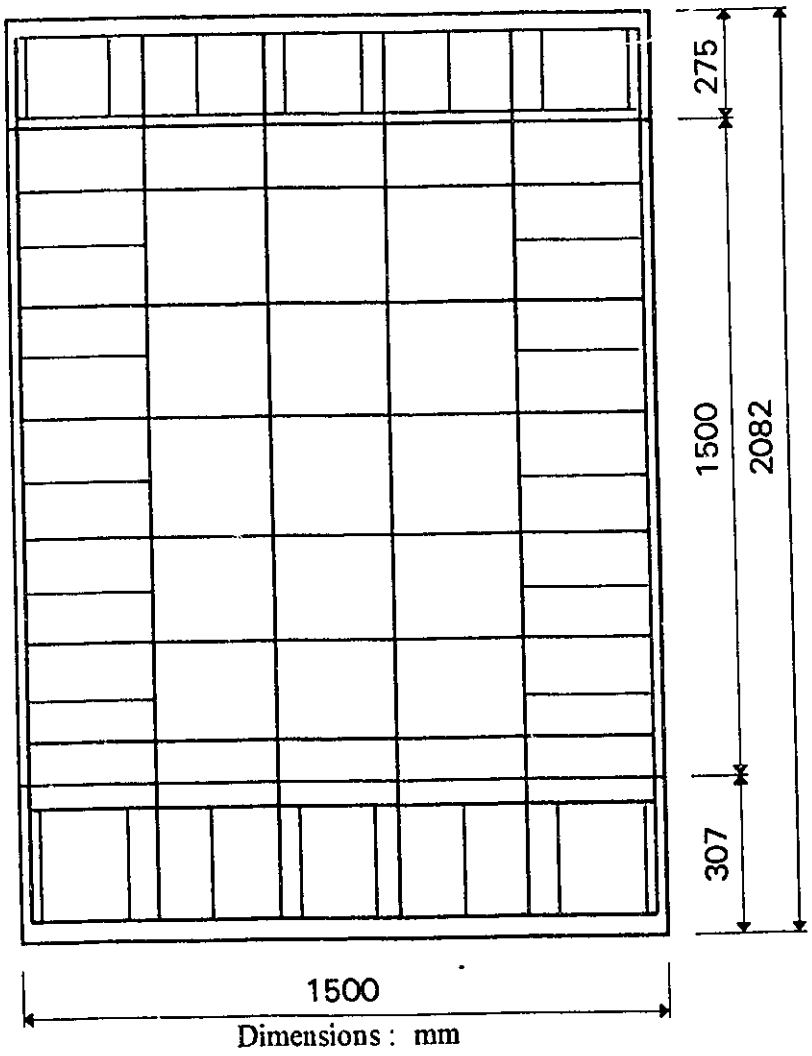

Figure 3.3 Geometry and Reinforcement Layout of Wall 8

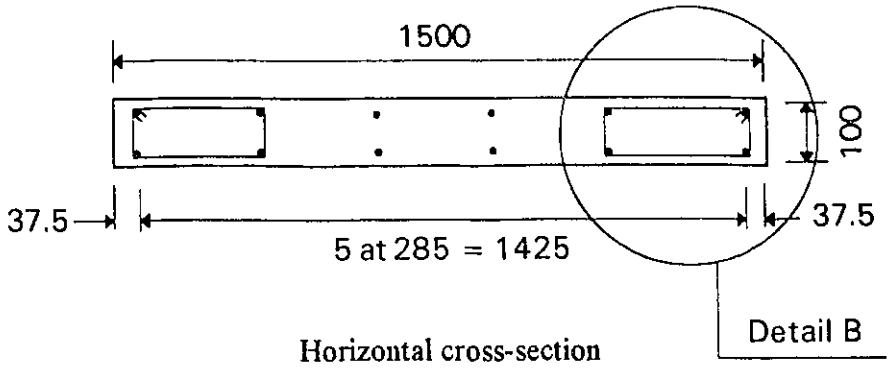

Horizontal cross-section

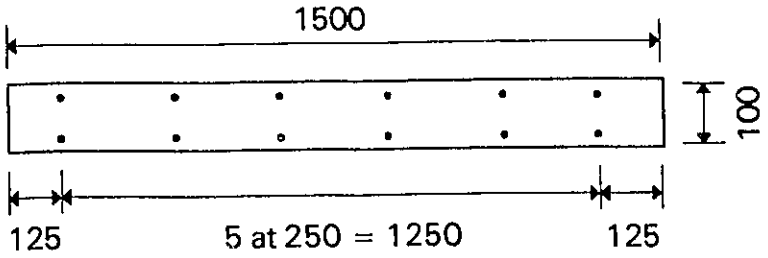

Vertical cross-section

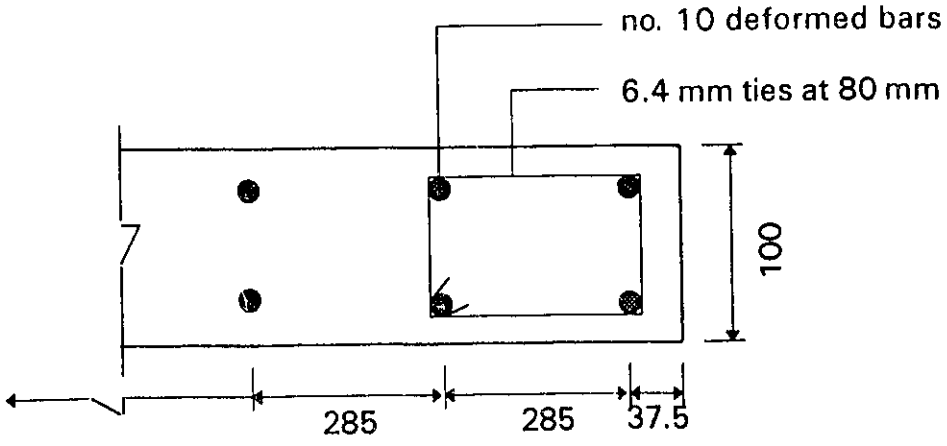

Dimensions : mm

DETAIL B

Figure 3.4 Horizontal (above) and Vertical (below) Cross-Sections of Wall 8

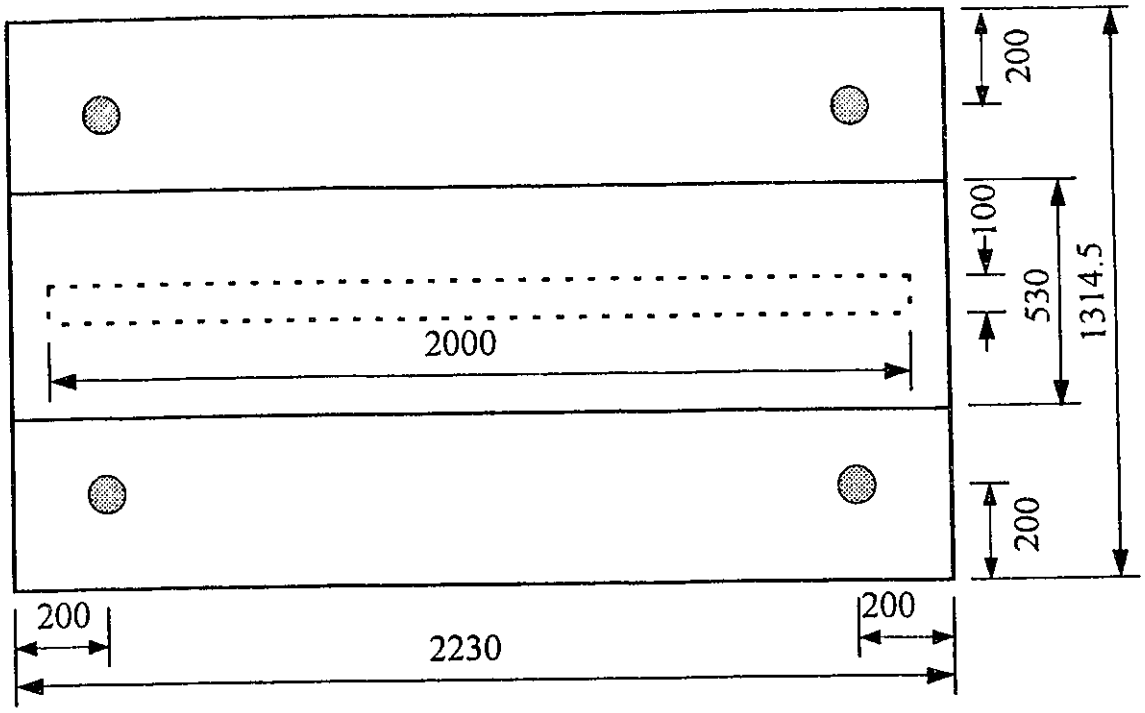

Figure 3.5 Plan View of Wall 7

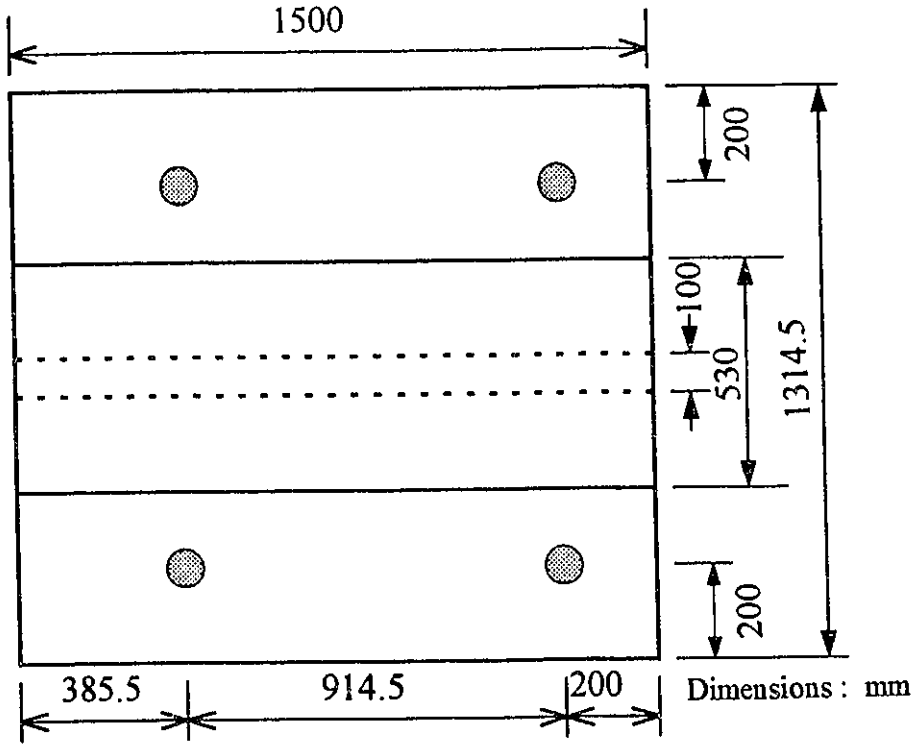

Figure 3.6 Plan View of Wall 8

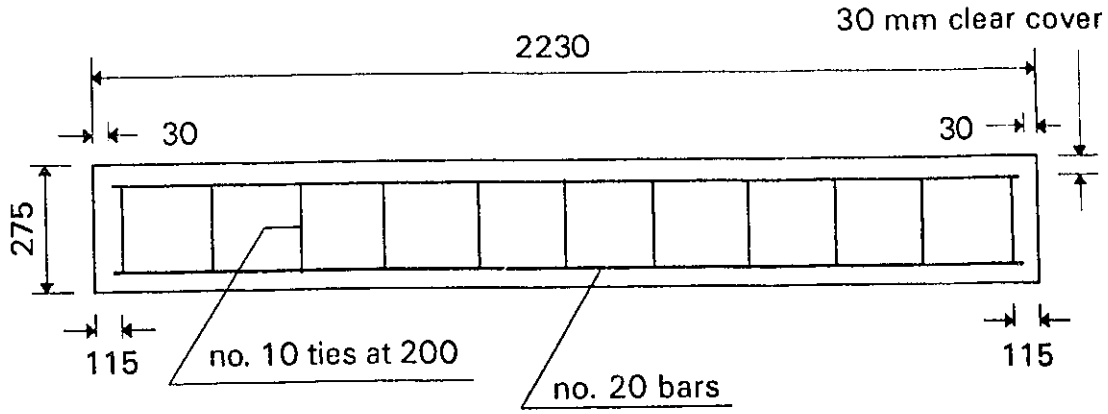

TOP BEAM

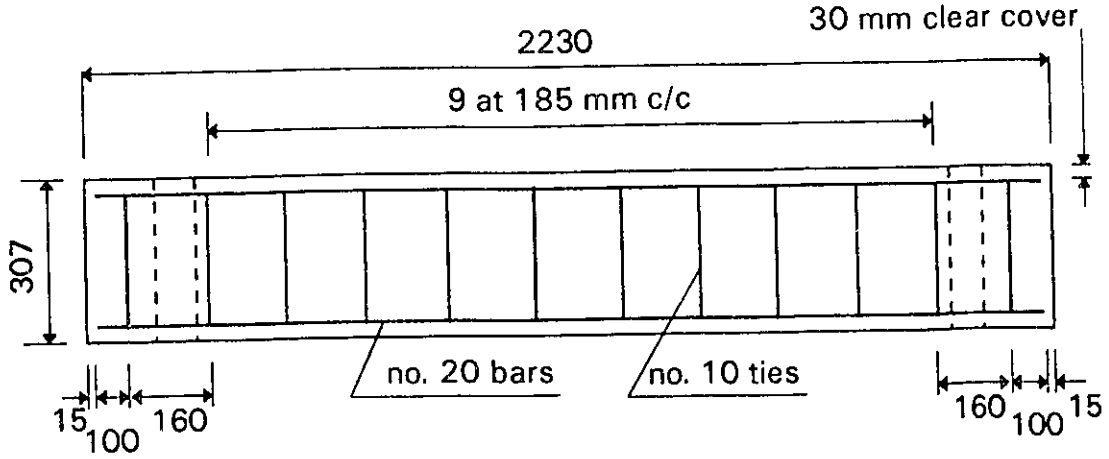

BOTTOM SLAB

Dimensions : mm

Figure 3.7 Sections of Top Beam (above) and Bottom Slab (below) of Wall 7

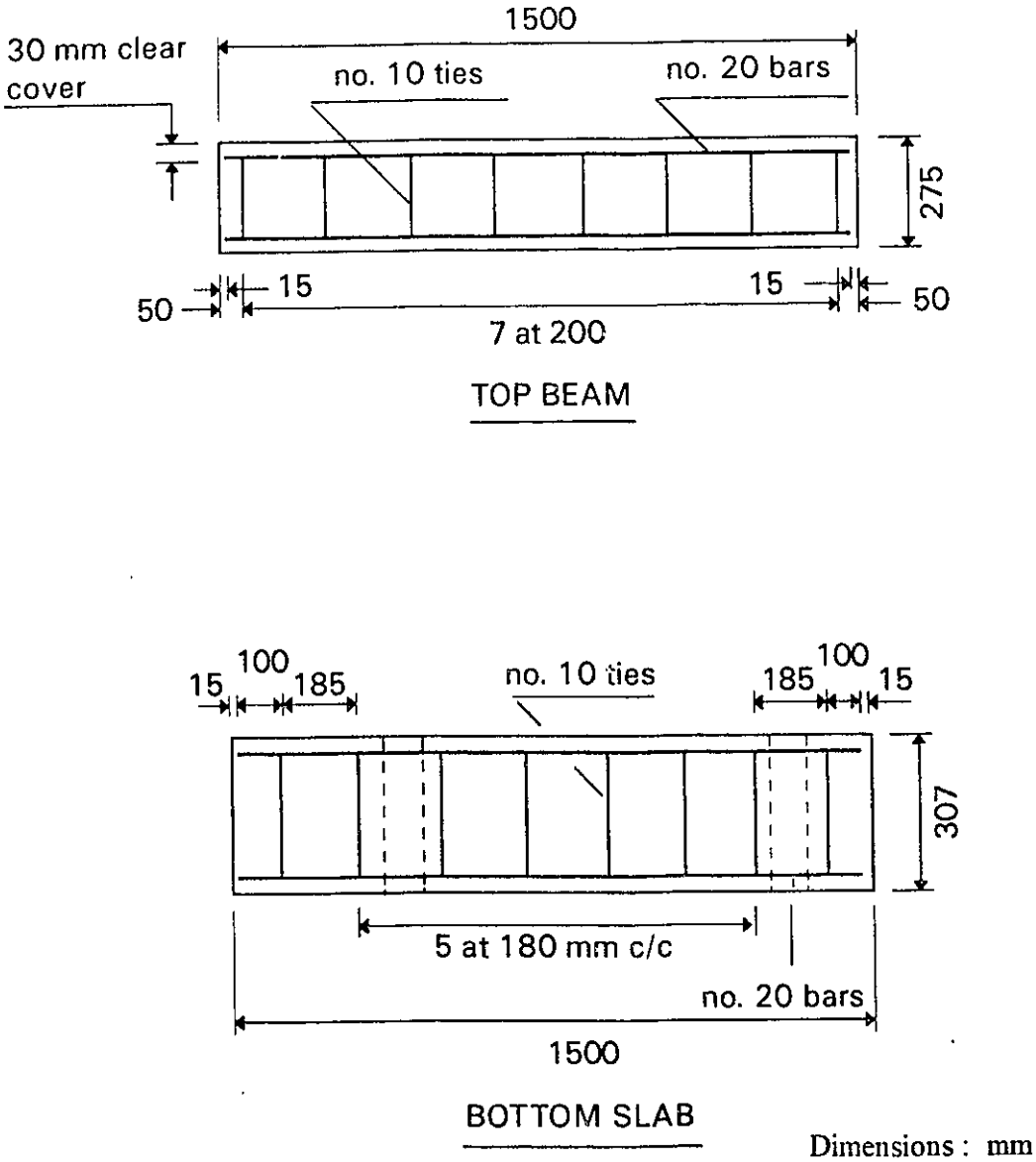

Figure 3.8 Sections of Top Beam (above) and Bottom Slab (below) of Wall 8

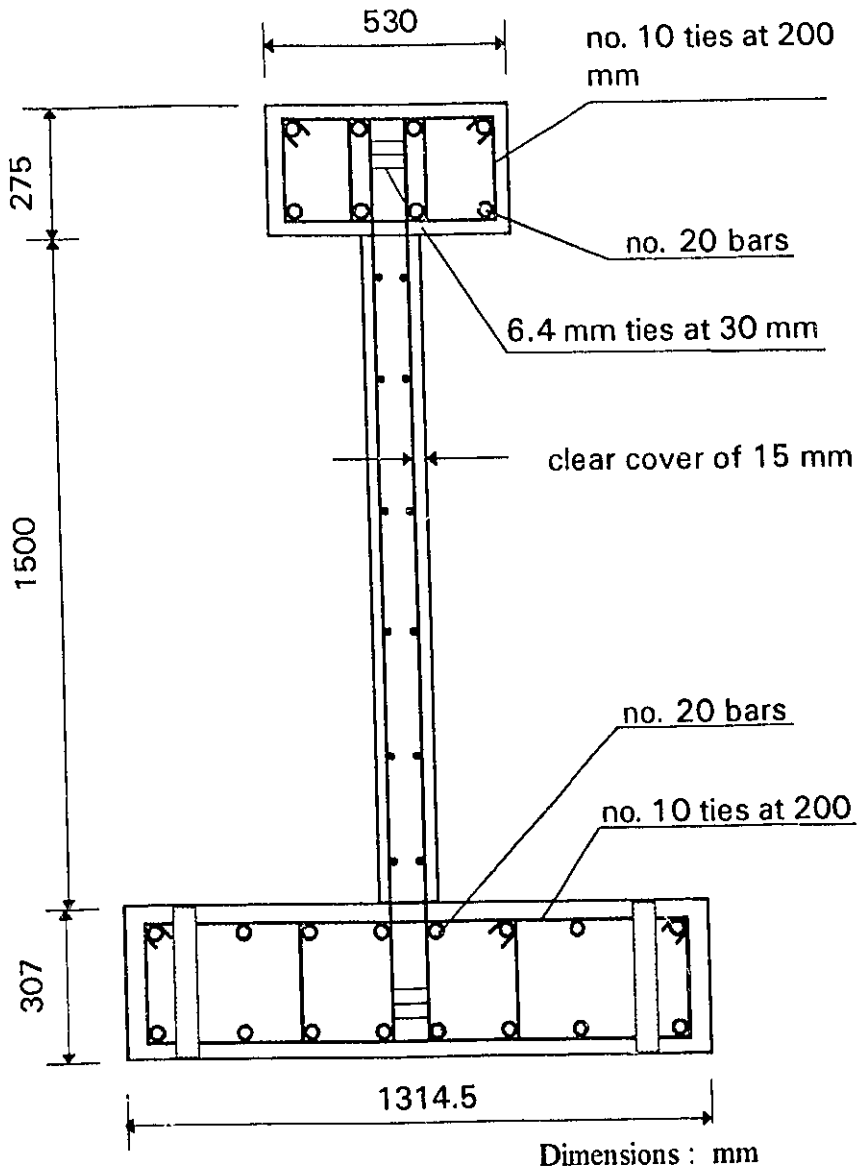

Figure 3.9 Side View of Wall 7 and Wall 8

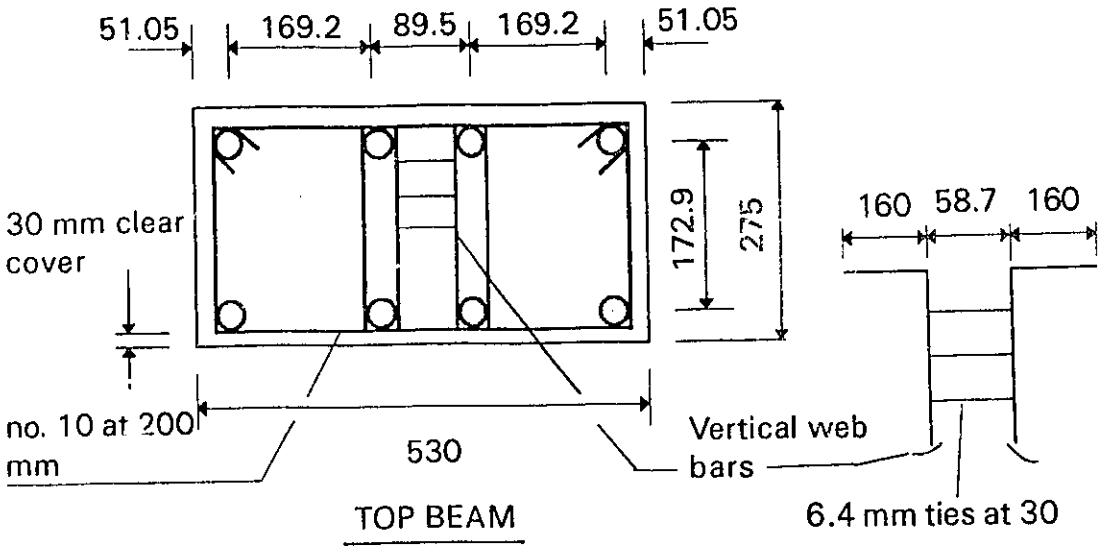

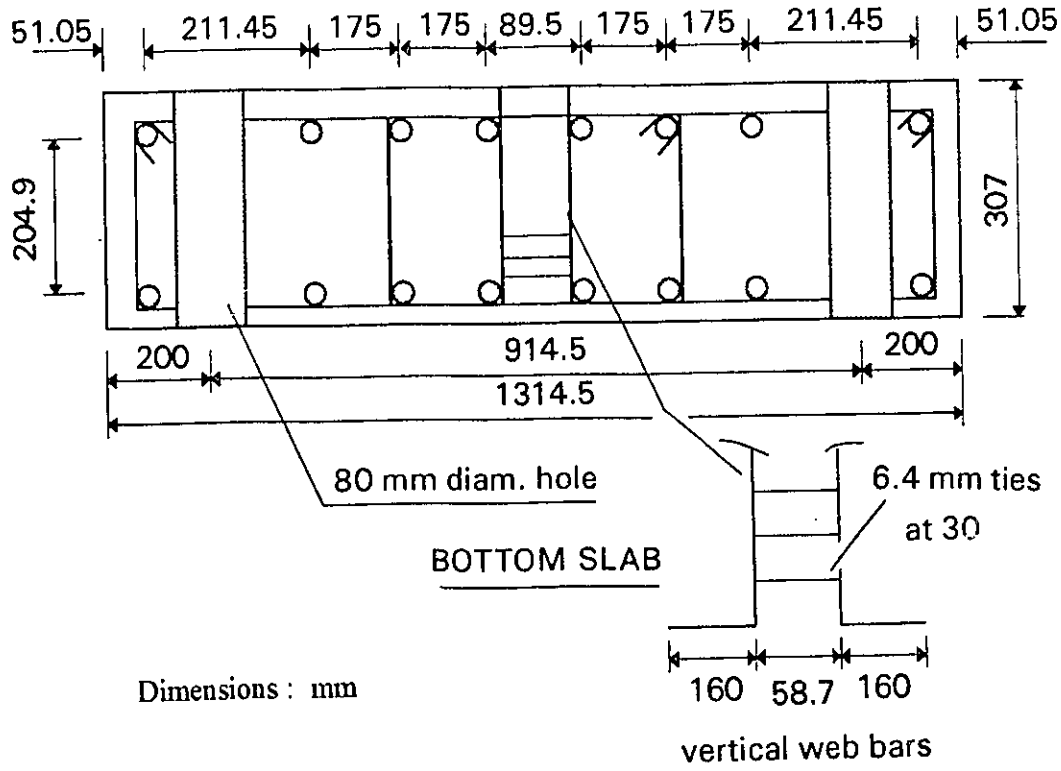

Figure 3.10 Reinforcement Layout of Top Beam (above) and Bottom Slab (below) for Wall 7 and Wall 8

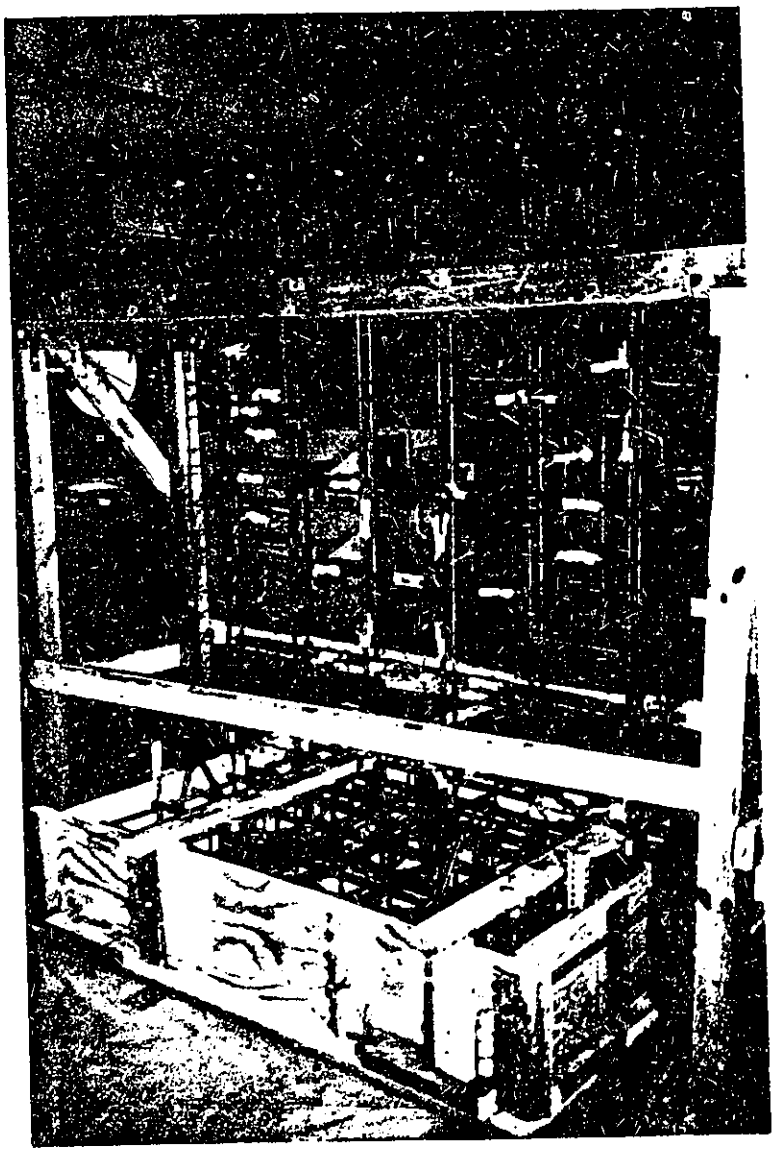

Figure 3.11 Wall 8 During Construction

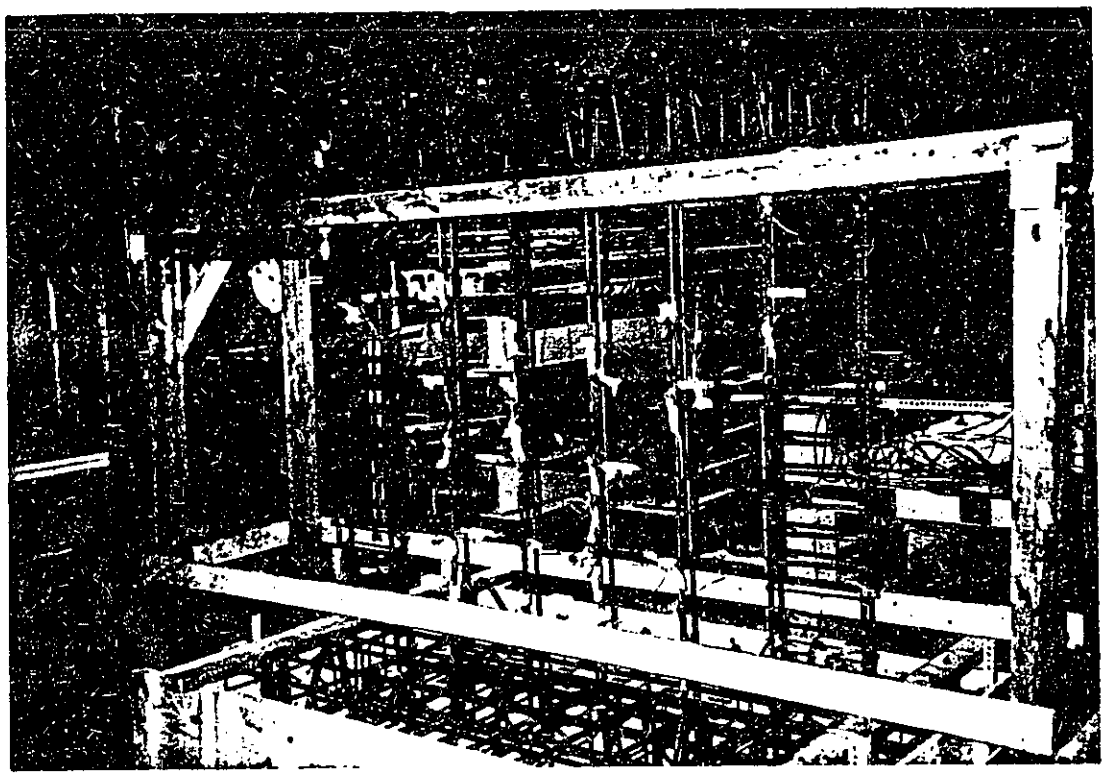

Figure 3.12 Wall 7 During Construction

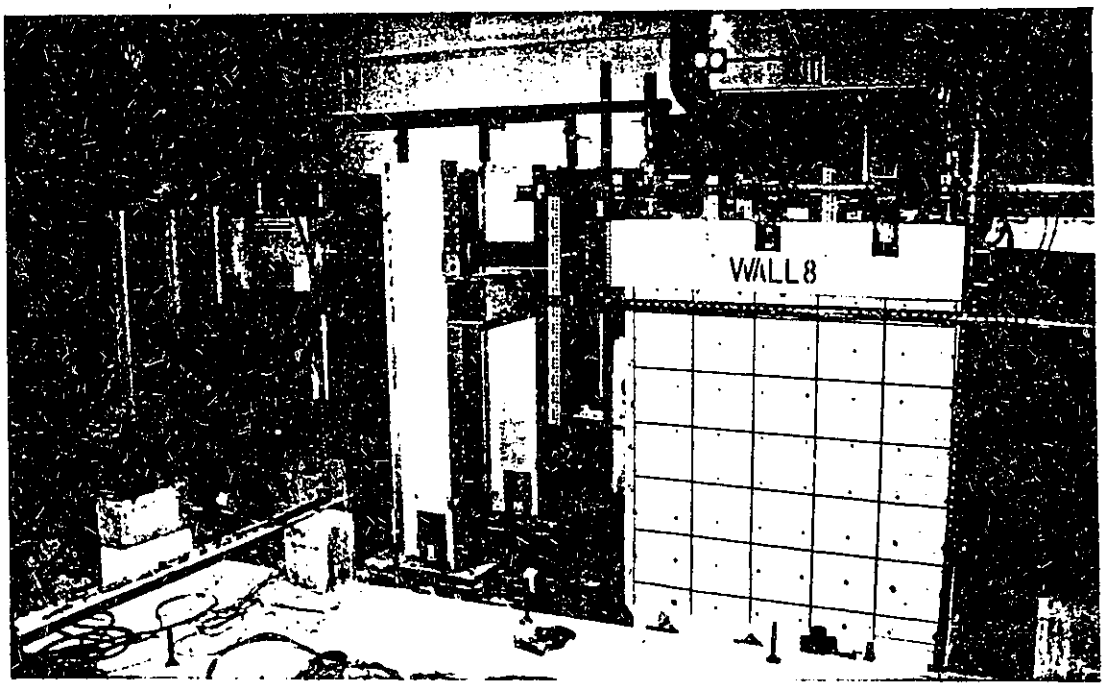

Figure 3.13 Overall View of the Test Set-Up

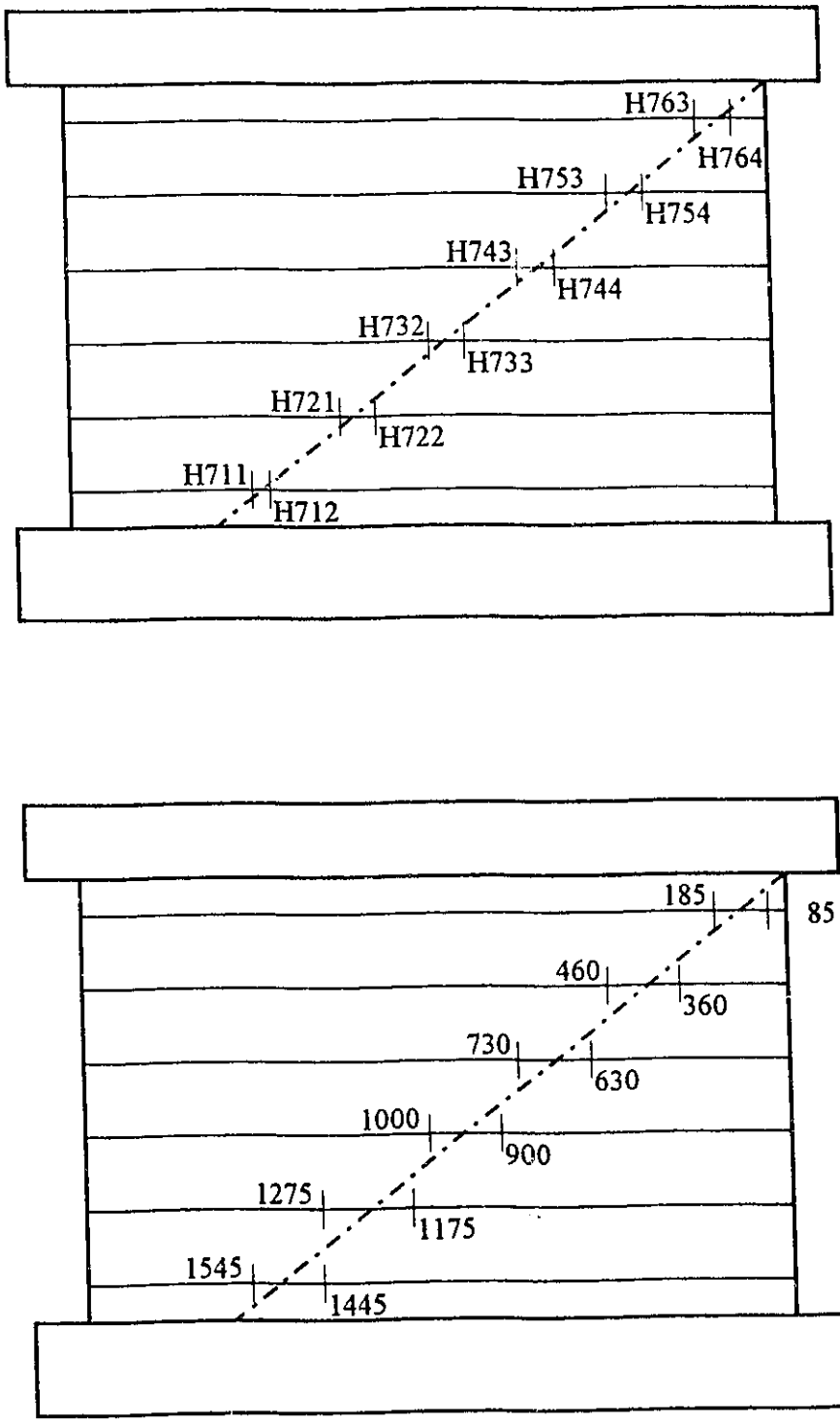

Figure 3.14 Strain Gauges on Horizontal Reinforcement for Wall 7 (Diagonal One) Codes (above) and Locations (in mm from right face), (below)

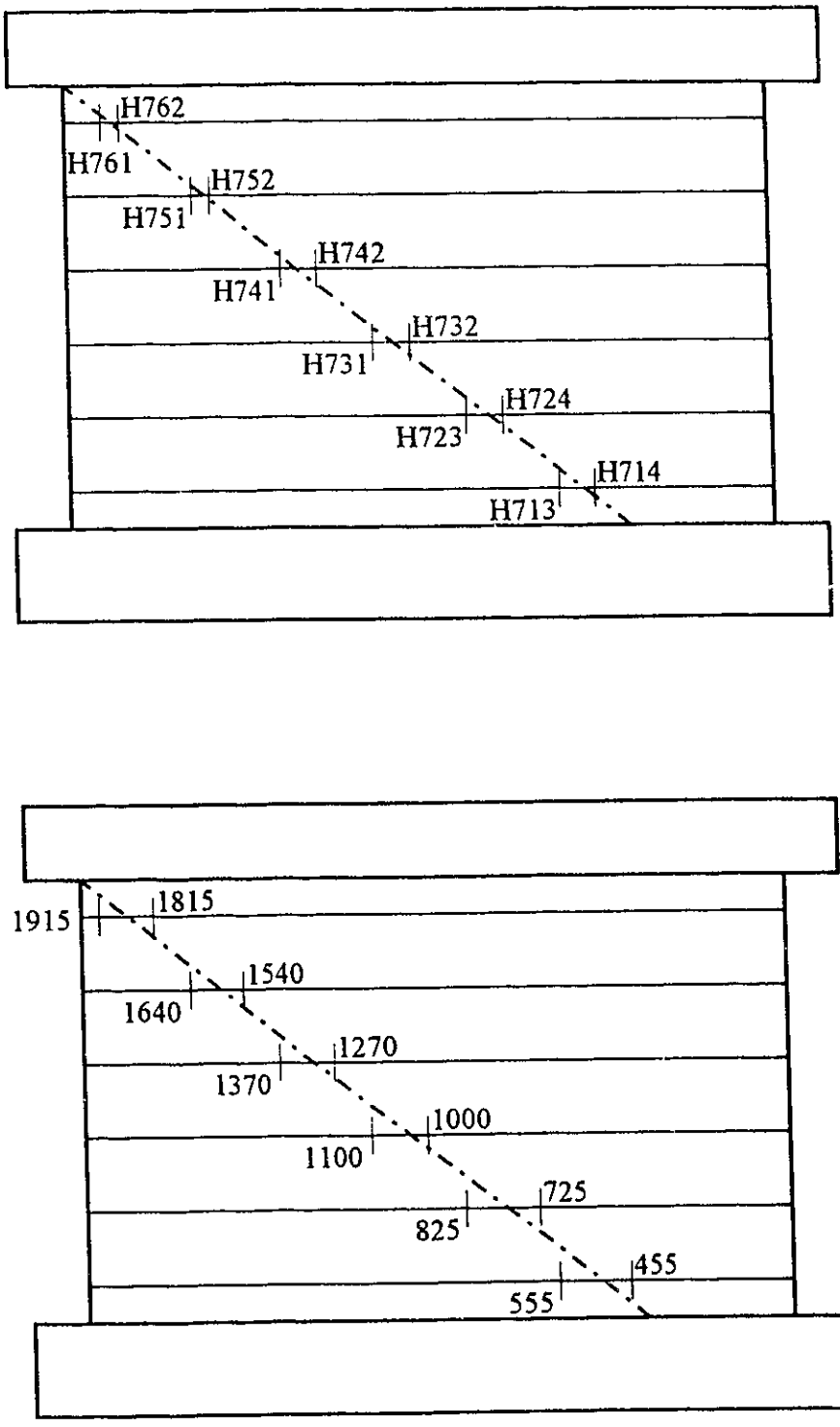

Figure 3.15 Strain Gauges on Horizontal Reinforcement for Wall 7 (Diagonal Two)
Codes (above) and Locations (in mm from right face), (below)

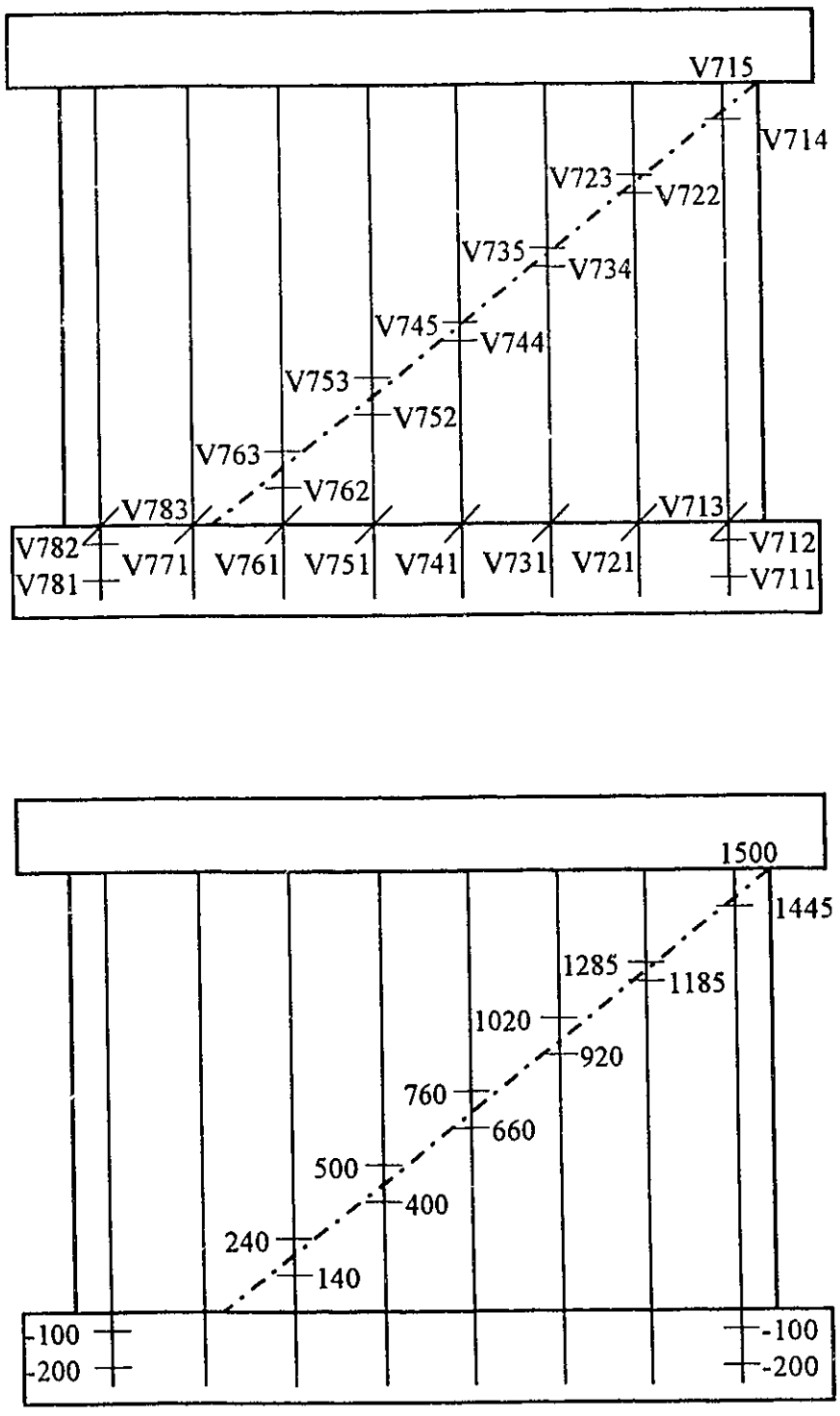

Figure 3.16 Strain Gauges on Vertical Reinforcement for Wall 7 (Diagonal One)
Codes (above) and Locations (in mm from base), (below)

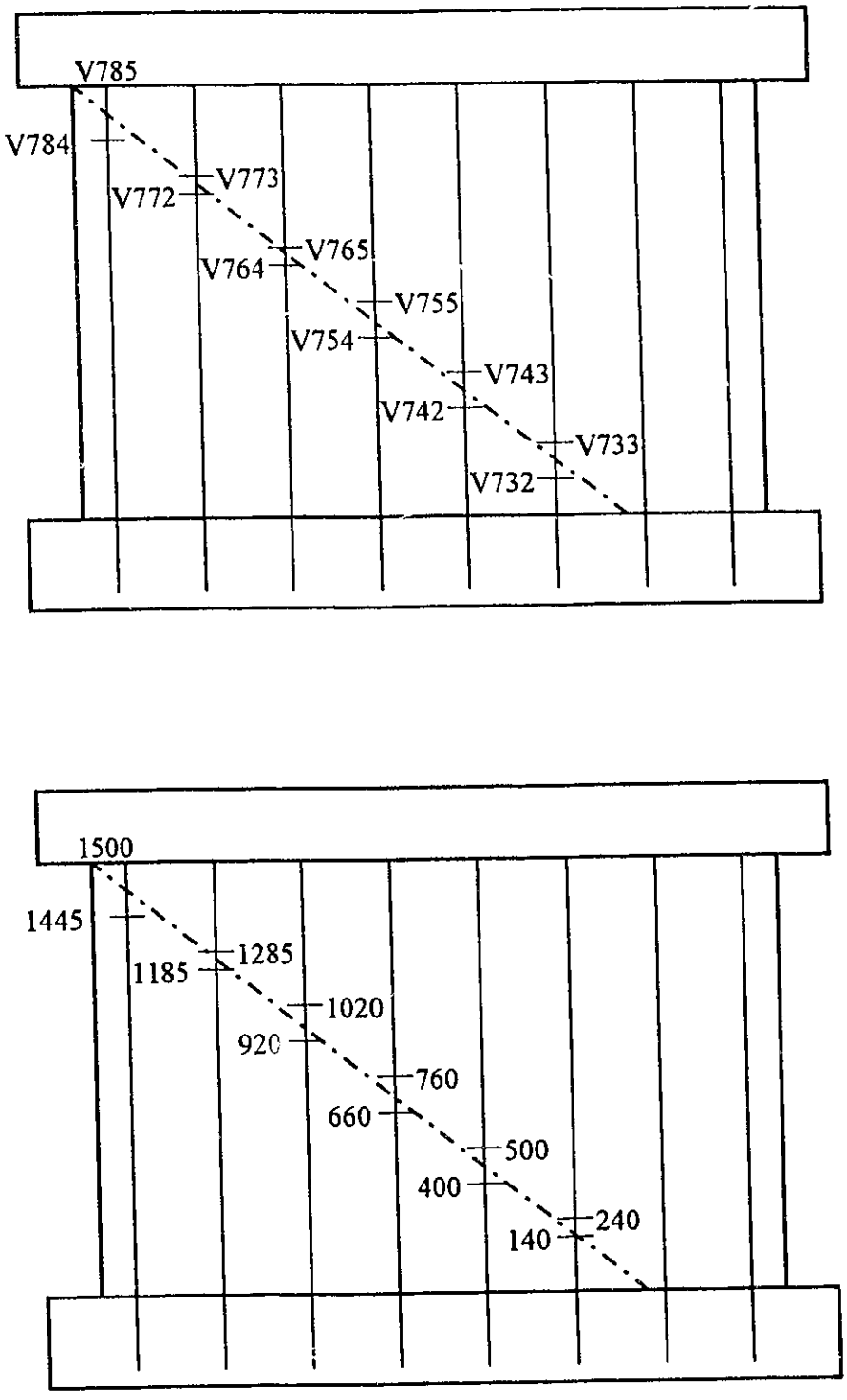

Figure 3.17 Strain Gauges on Vertical Reinforcement for Wall 7 (Diagonal Two)
Codes (above) and Locations (in mm from base), (below)

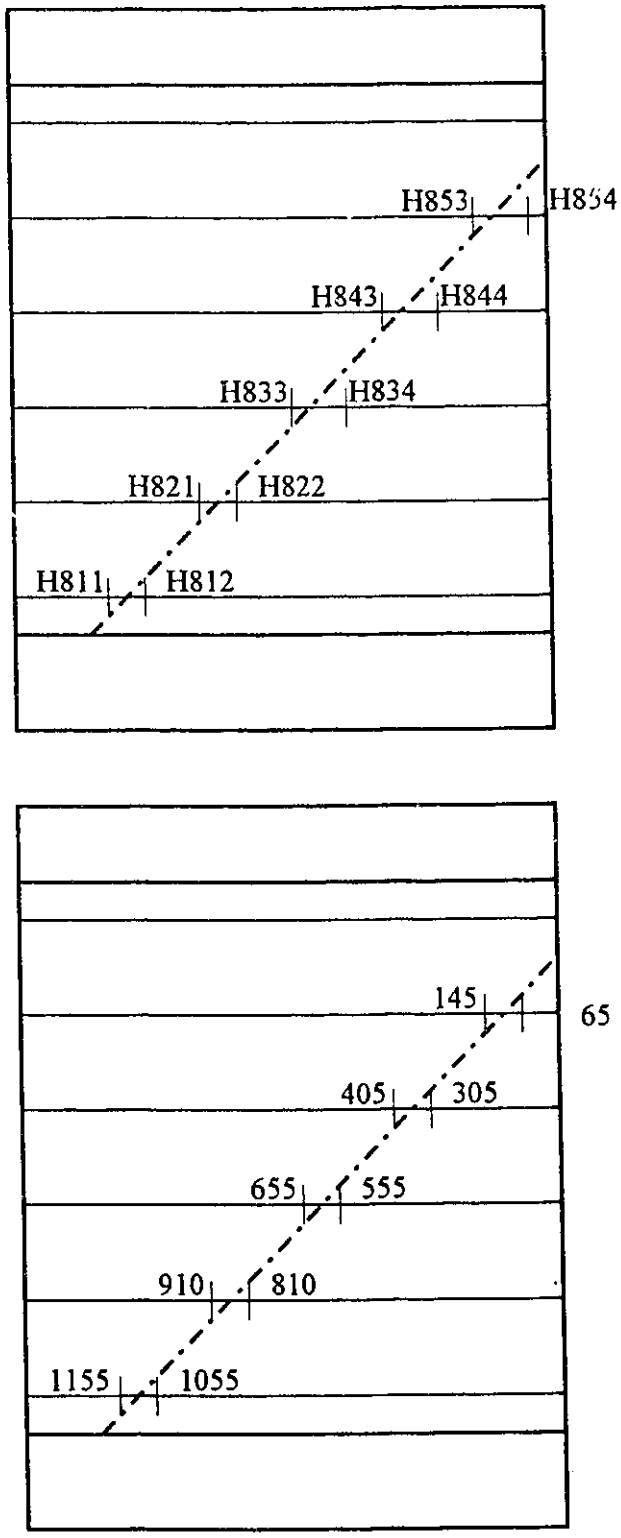

Figure 3.18 Strain Gauges on Horizontal Reinforcement for Wall 8 (Diagonal One)
Codes (above) and Locations (in mm from right face), (below)

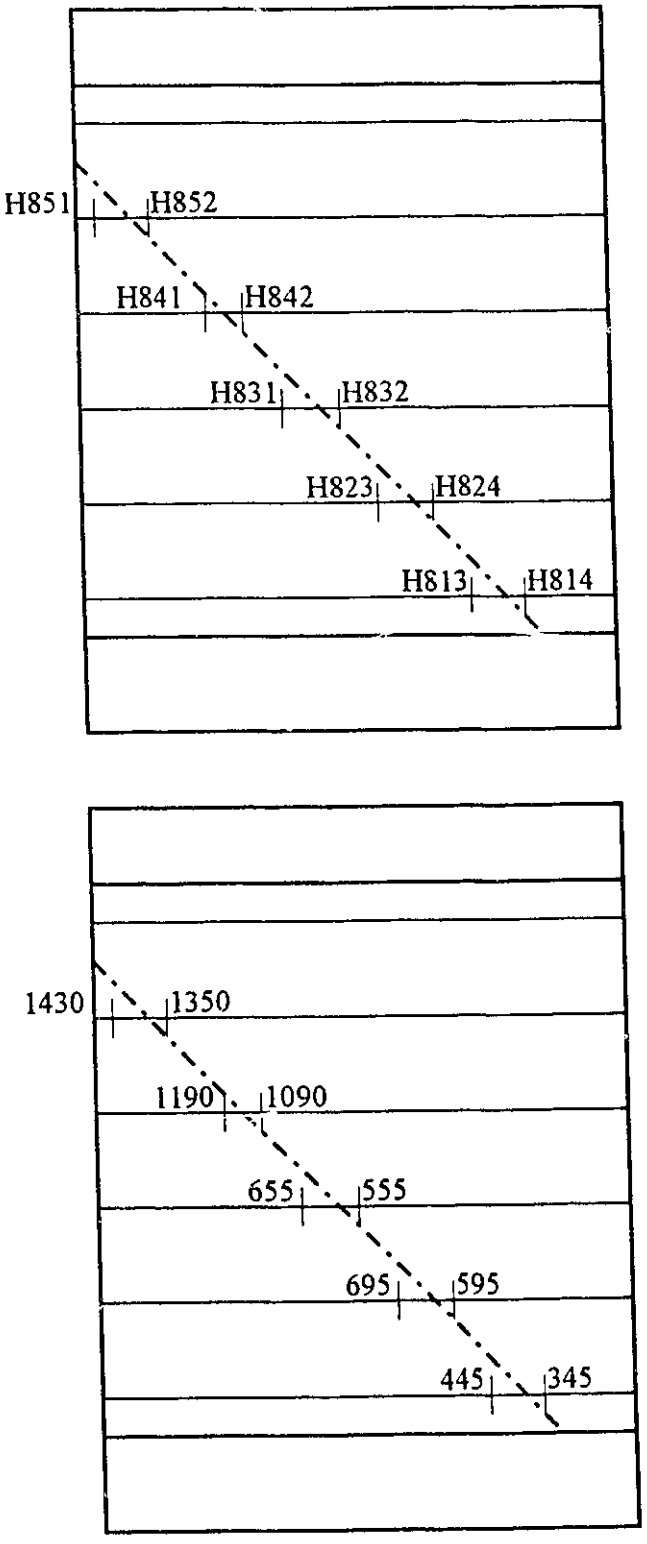

Figure 3.19 Strain Gauges on Horizontal Reinforcement for Wall 8 (Diagonal Two) Codes (above) and Locations (in mm from right face), (below)

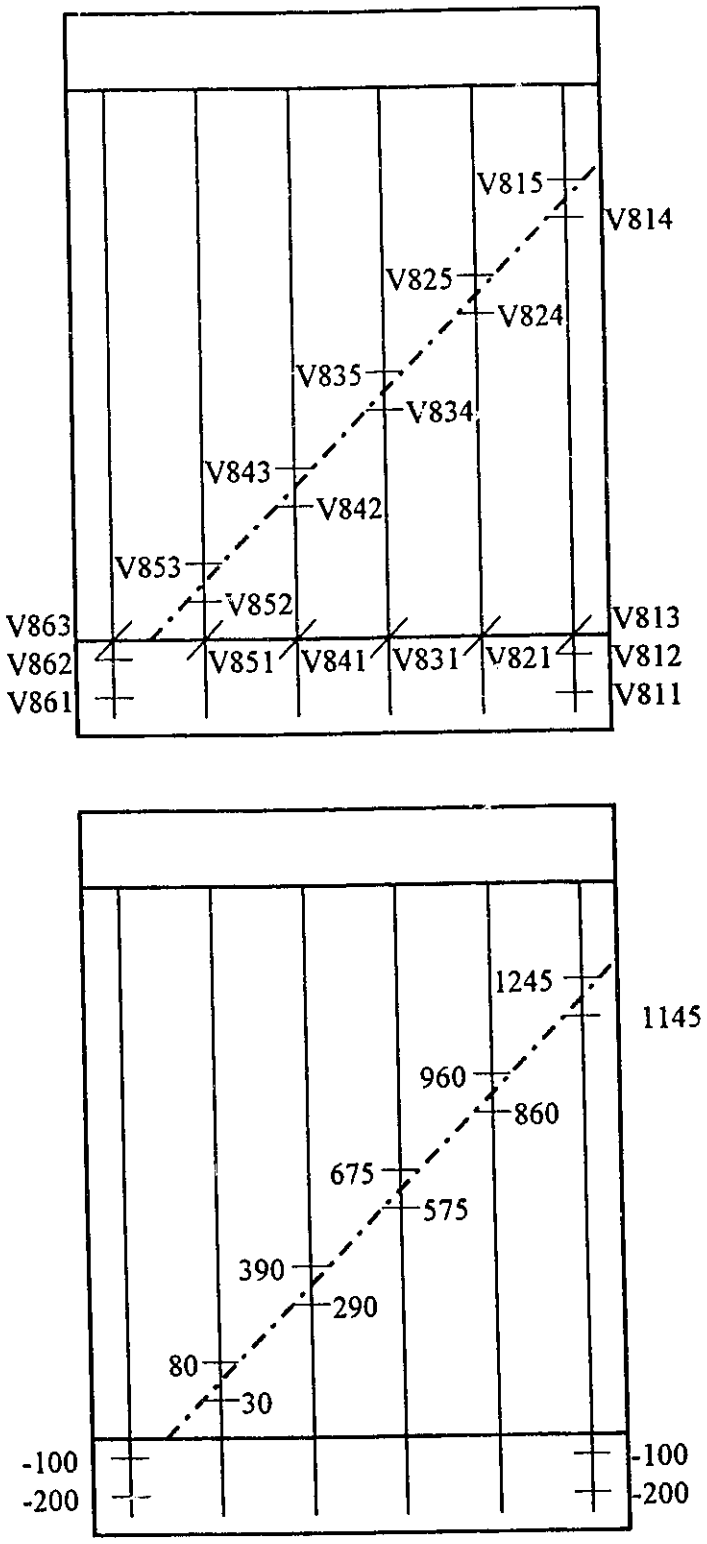

Figure 3.20 Strain Gauges on Vertical Reinforcement for Wall 8 (Diagonal One)
Codes (above) and Locations (in mm from base), (below)

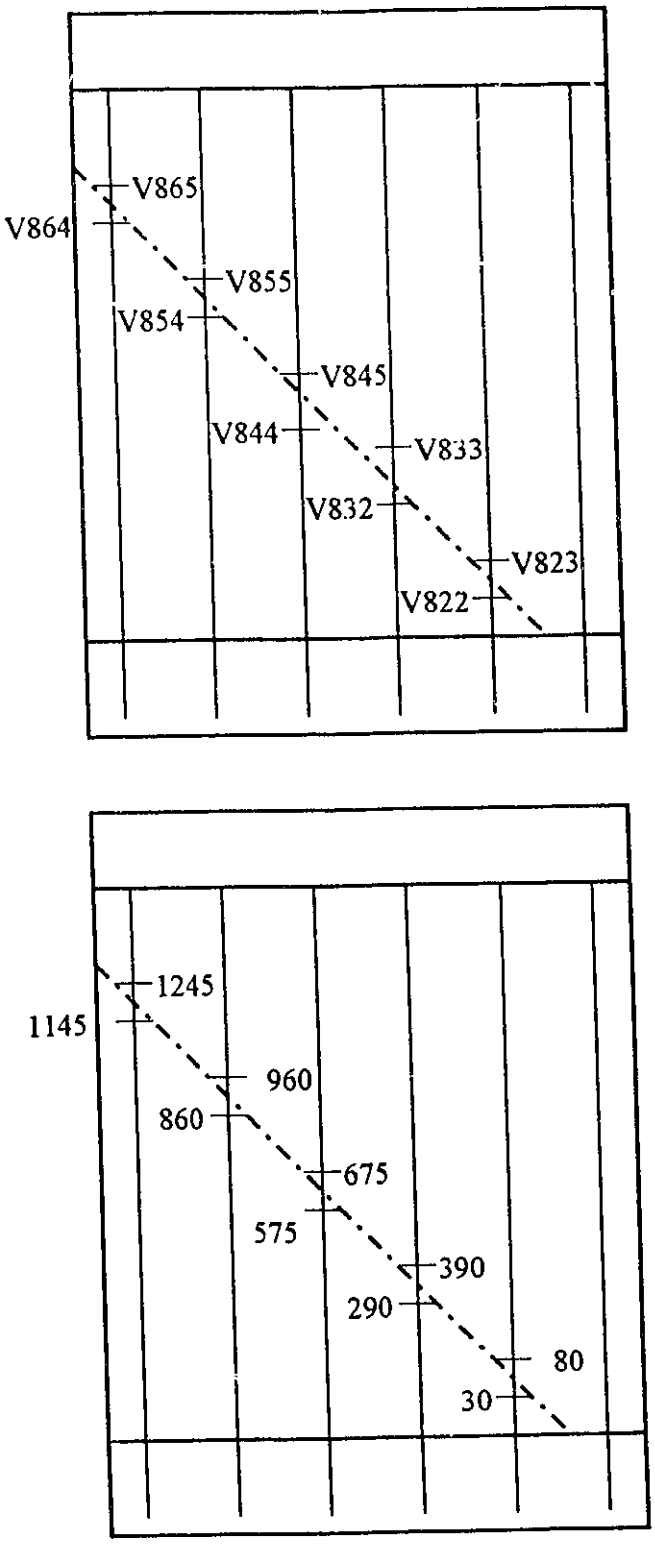

Figure 3.21 Strain Gauges on Vertical Reinforcement for Wall 8 (Diagonal Two)
Codes (above) and Locations (in mm from base), (below)

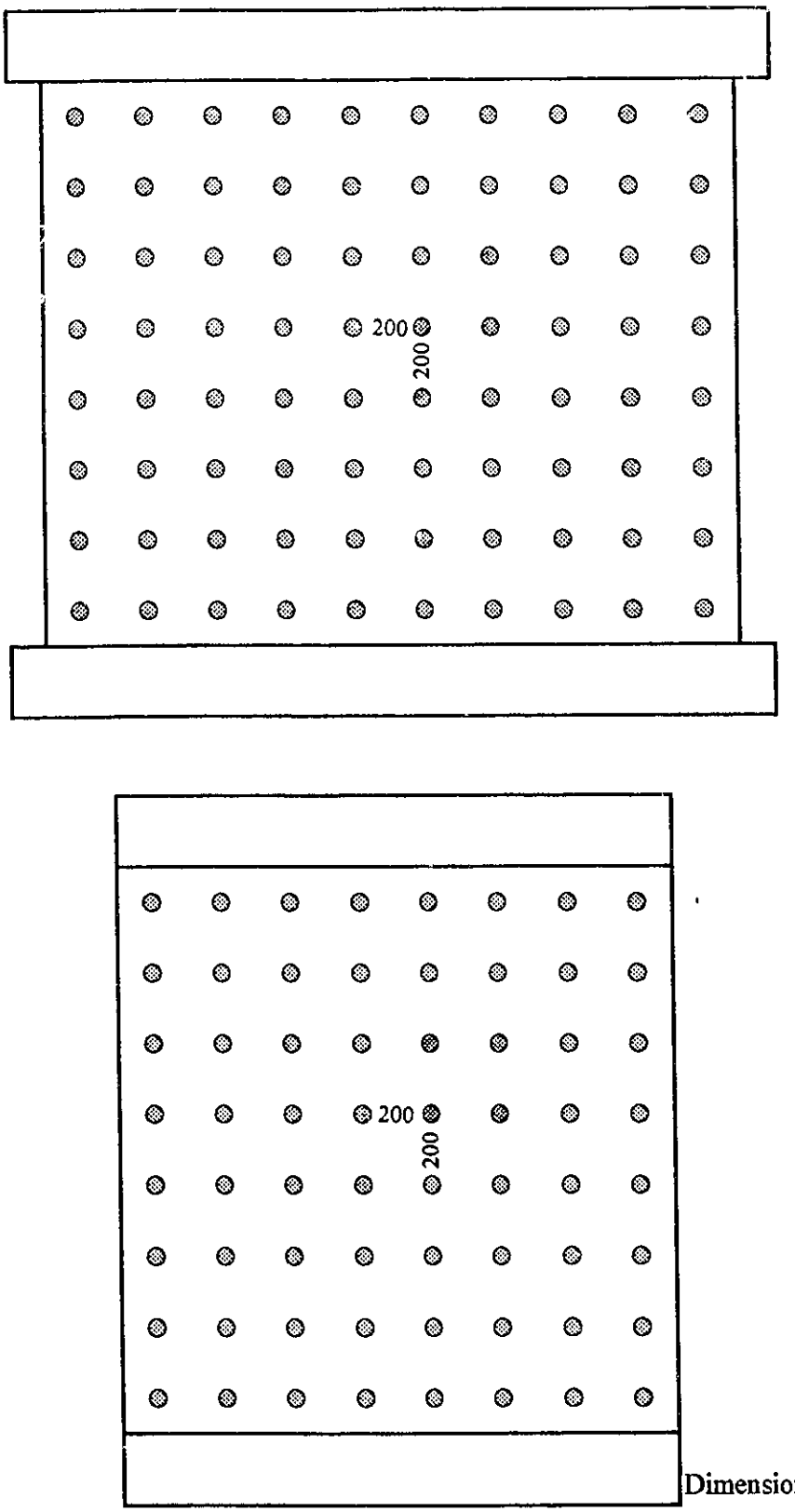

Figure 3.22 Arrangement of Demec Targets on Wall7 (above) and Wall 8 (below)

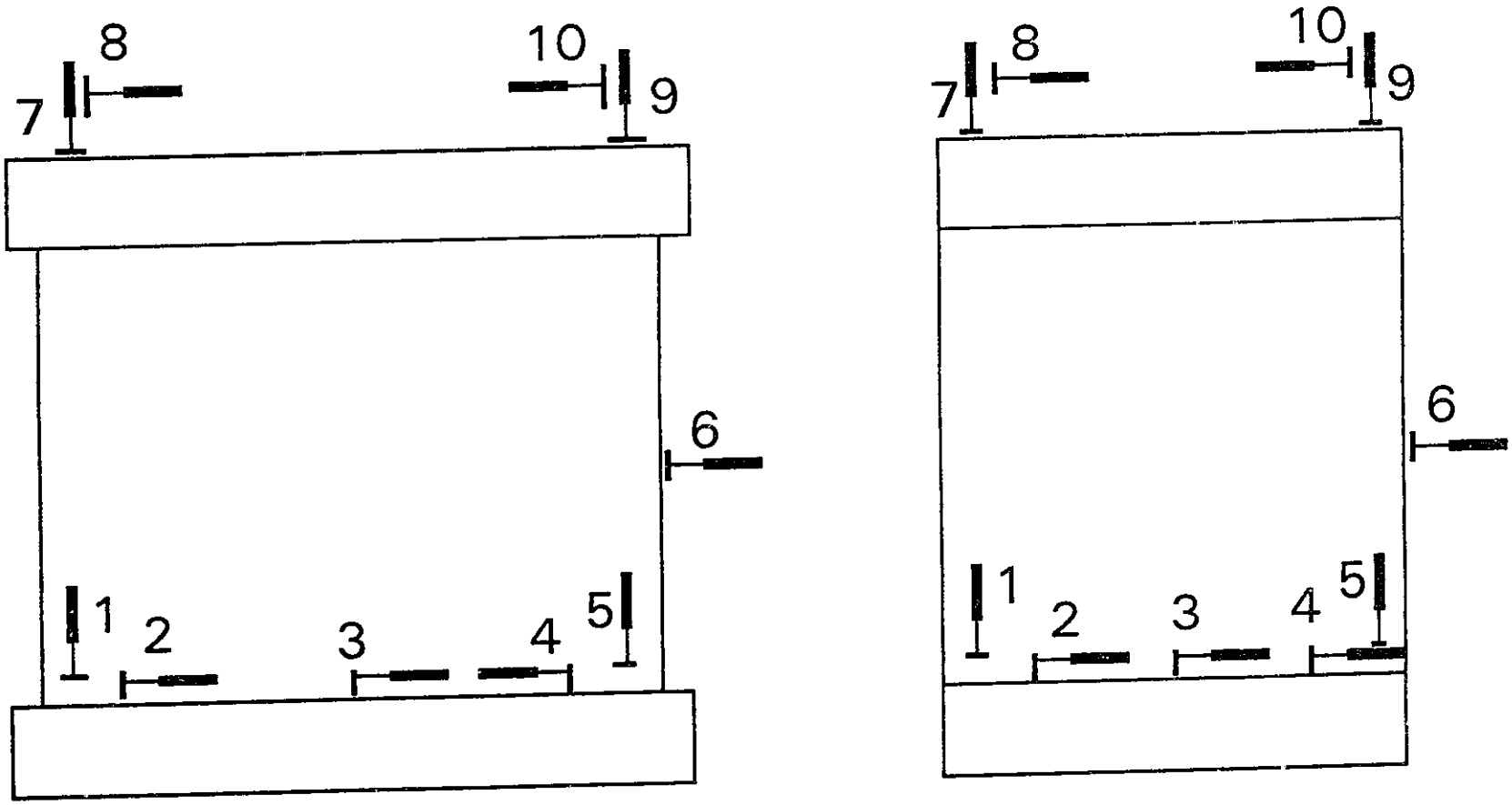

Figure 3.23a Potentiometers and LVDT's on Wall 7 (left) and on Wall 8 (right)

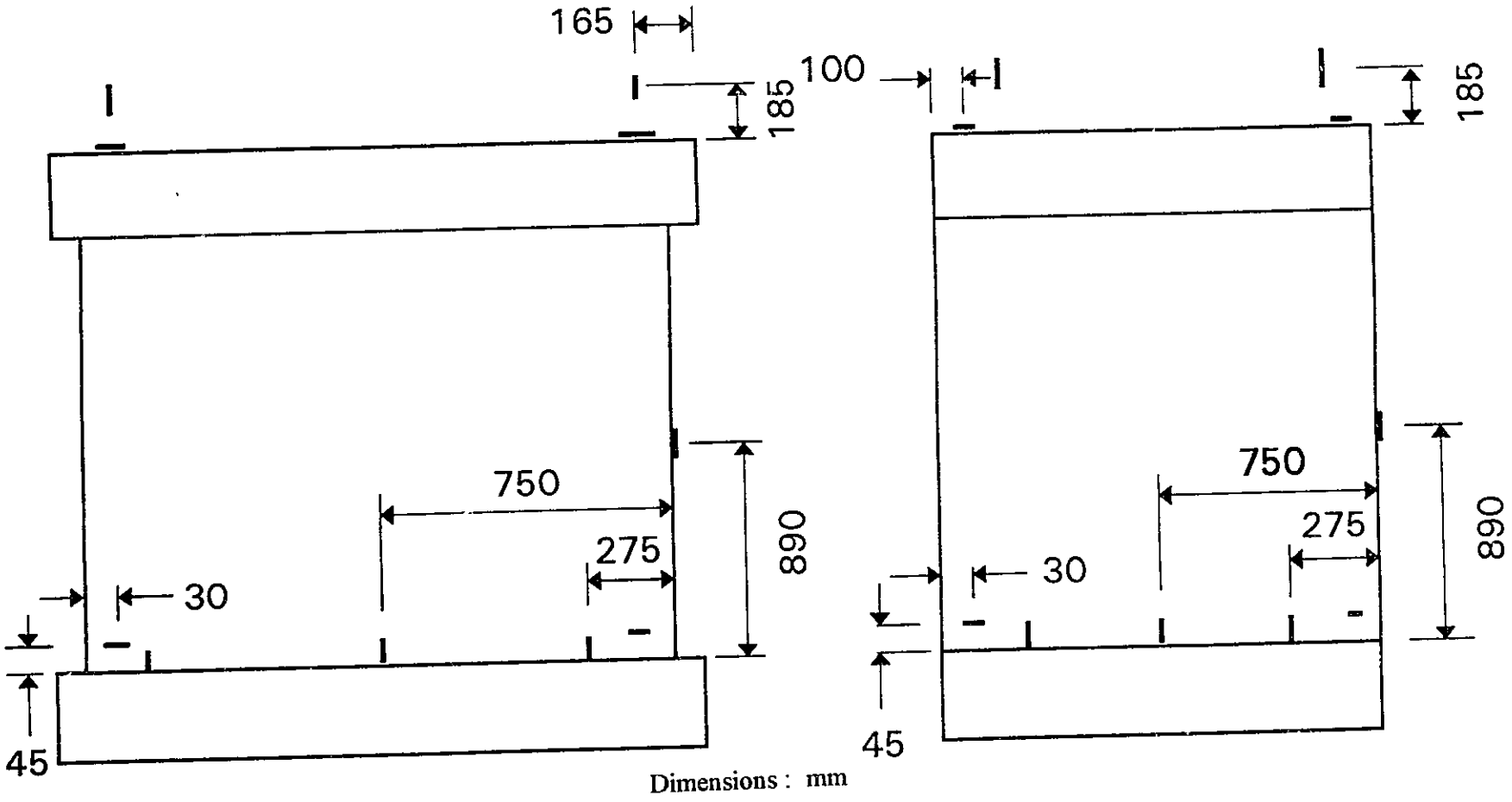

Figure 3.23b Locations of Targets for Potentiometers and LVDT's on Wall 7 (left) and on Wall 8 (right)

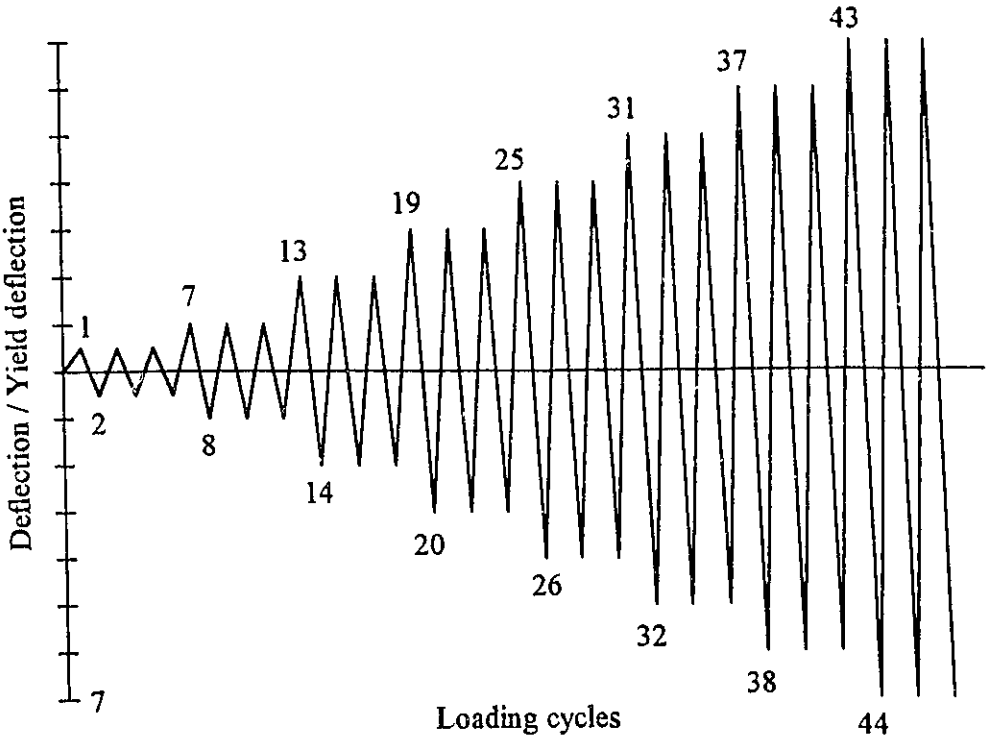

Figure 3.24 Lateral Load Program for Wall 7 and Wall 8

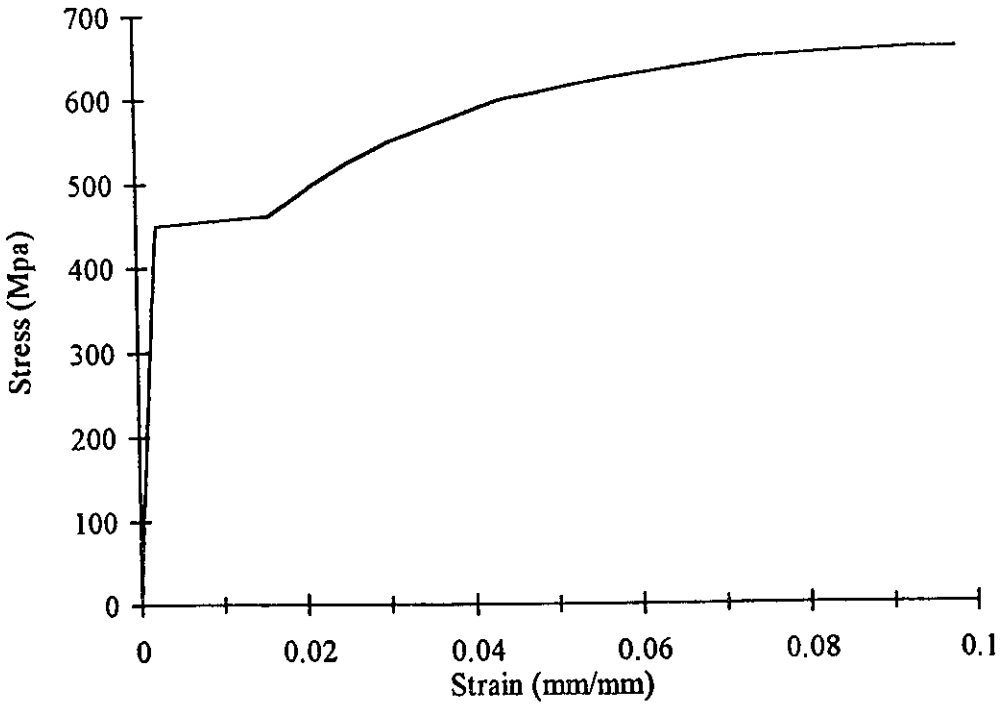

Figure 3.25 Stress-Strain Diagram for Reinforcing Steel

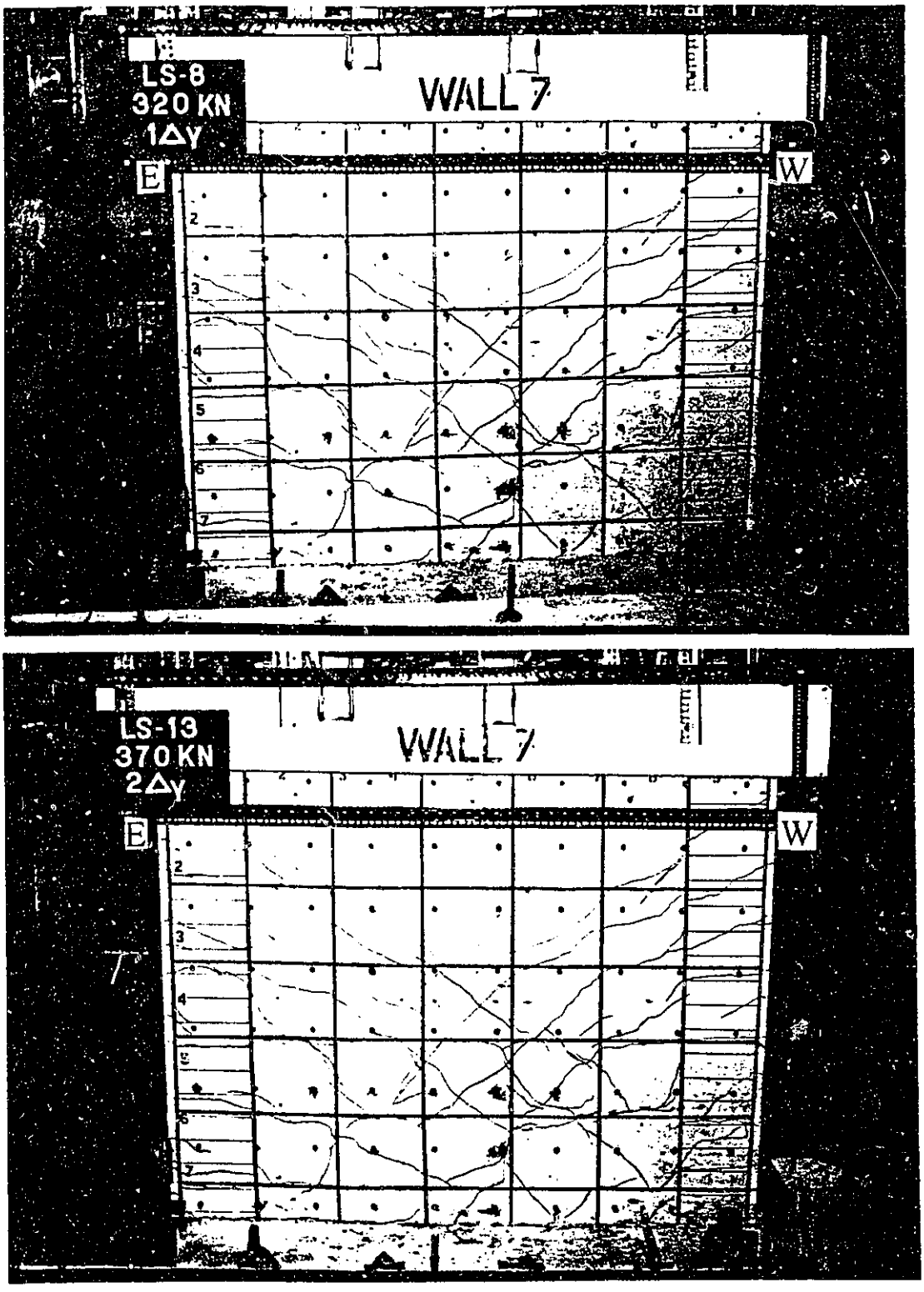

Figure 3.26 Wall 7 Crack Pattern, Cycle 1 (pulling) at 1 Δ_y (above) and Cycle 1 (pushing) at 2 Δ_y (below)

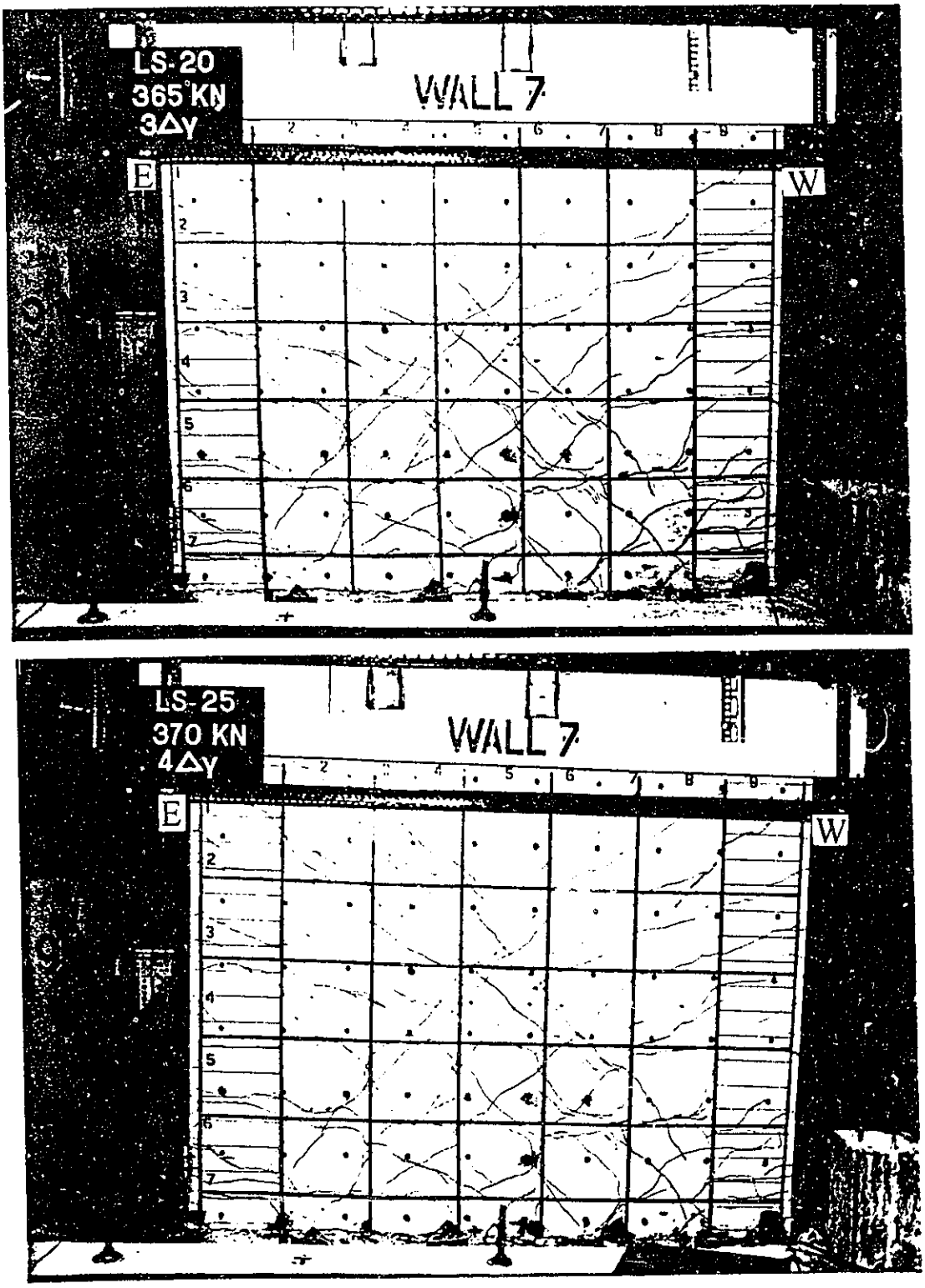

Figure 3.27 Wall 7 Crack Pattern, Cycle 1 (pulling) at $3\Delta_y$ (above) and Cycle 1 (pushing) at $4\Delta_y$ (below)

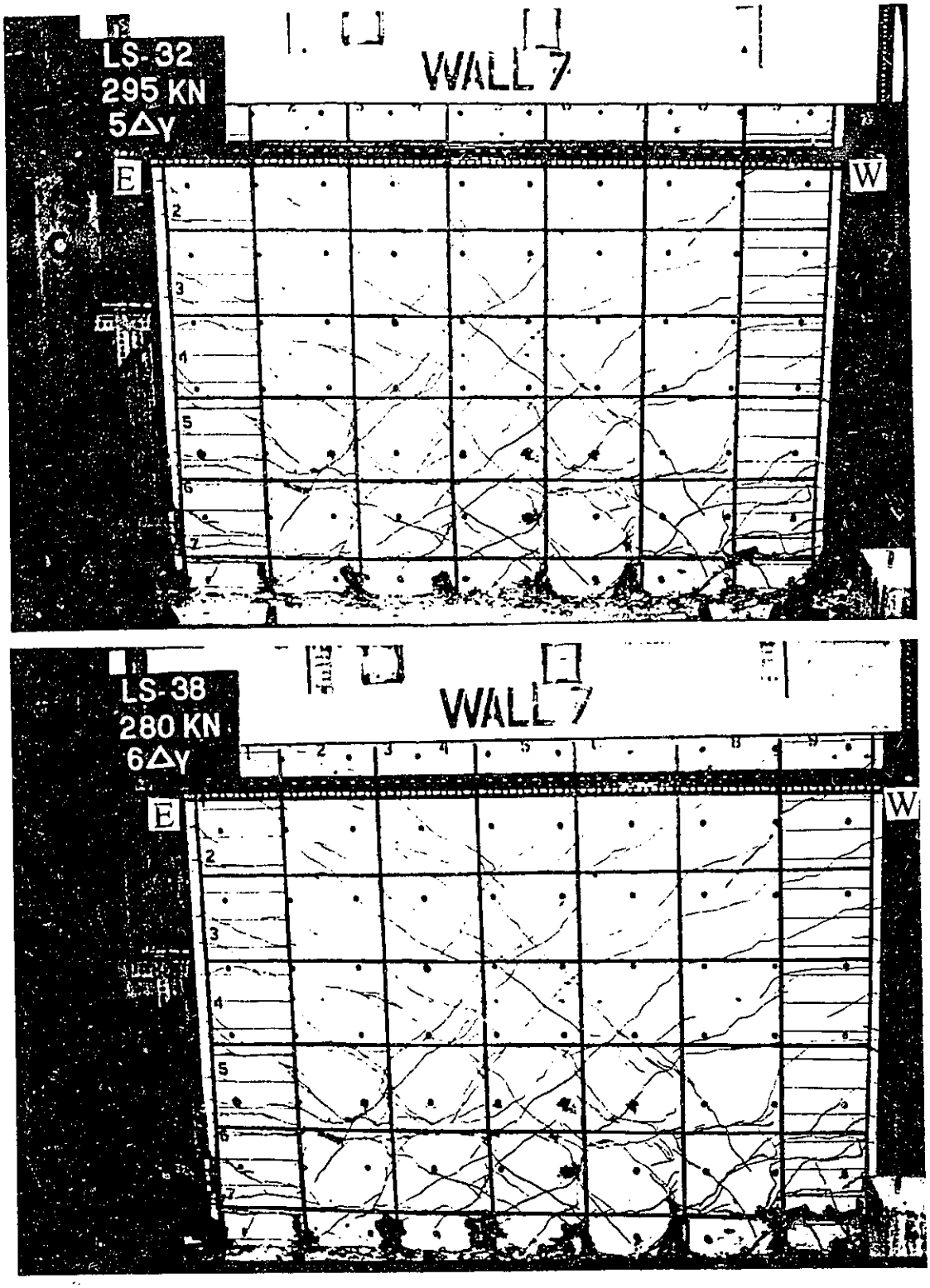

Figure 3.28 Wall 7 Crack Pattern, Cycle 1 (pulling) at $5\Delta_y$ (above) and Cycle 1 (pulling) at $6\Delta_y$ (below)

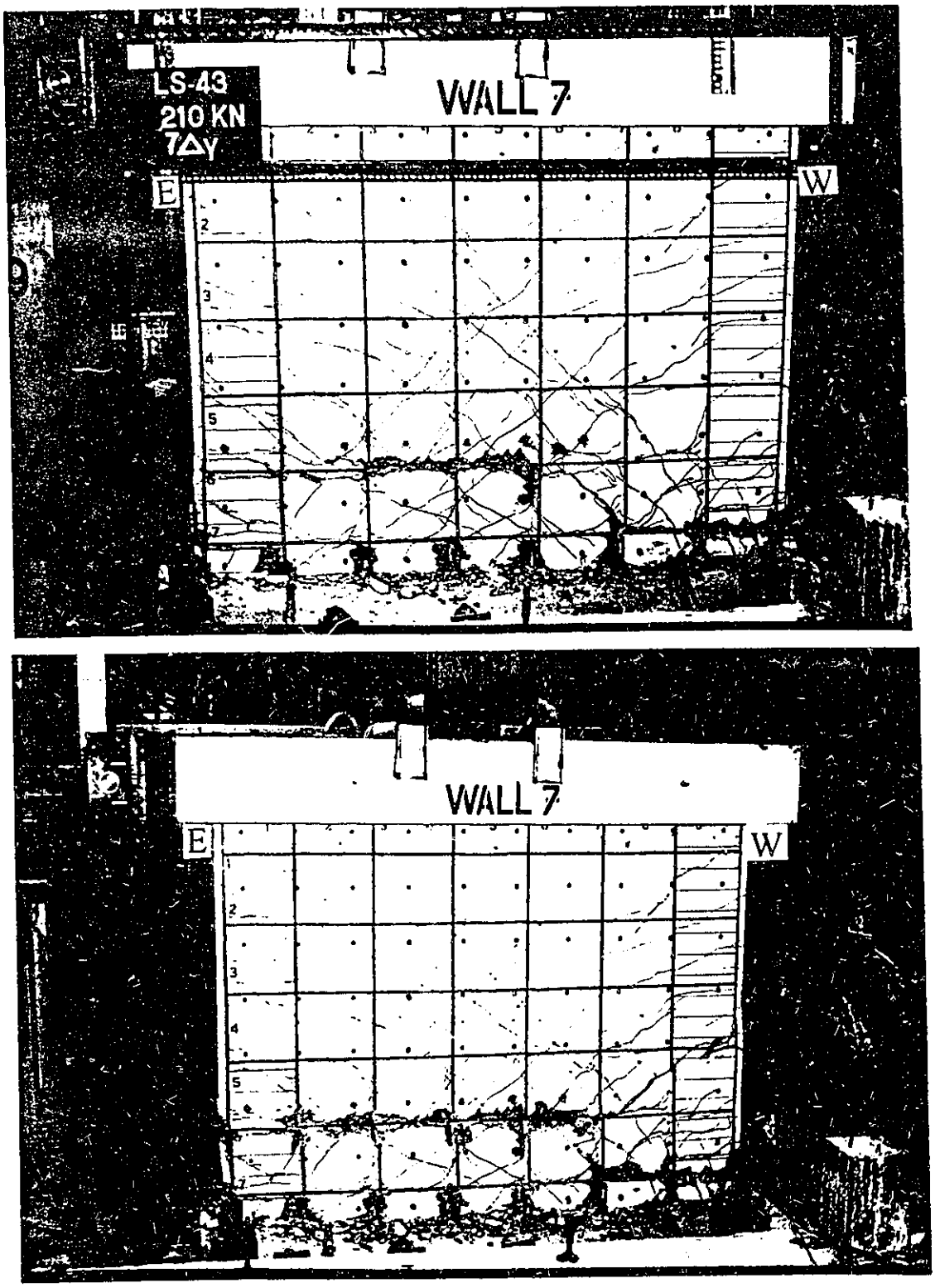

Figure 3.29 Wall 7 Crack Pattern, Cycle 1 (pulling) at $7\Delta_y$ (above) and at the End of Test (below)

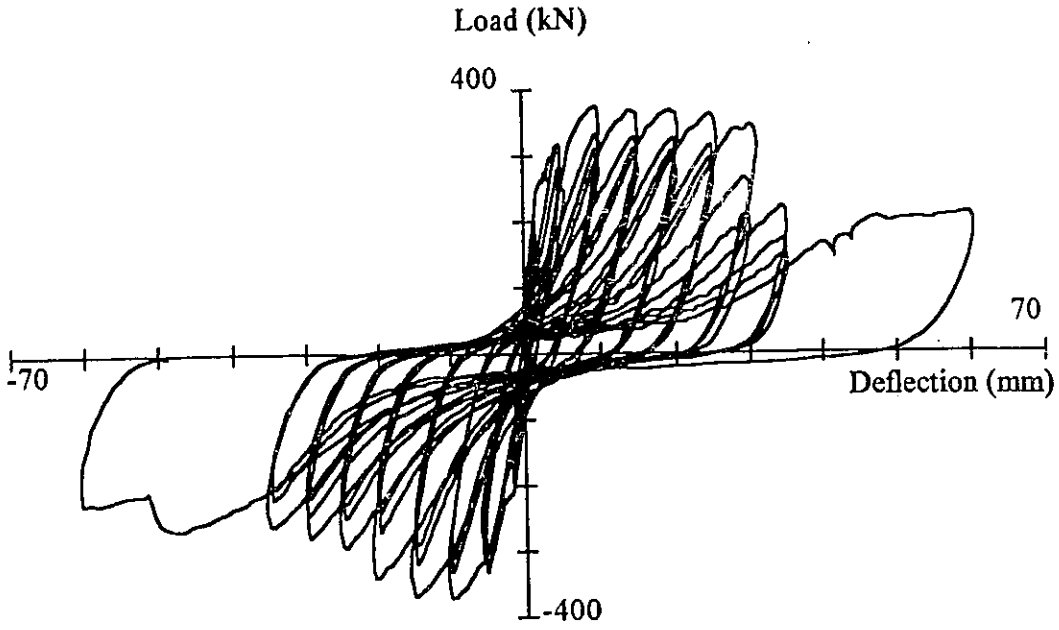

Figure 3.30 Load-East Top Horizontal Deflection for Wall 7
at the Level of Potentiometer

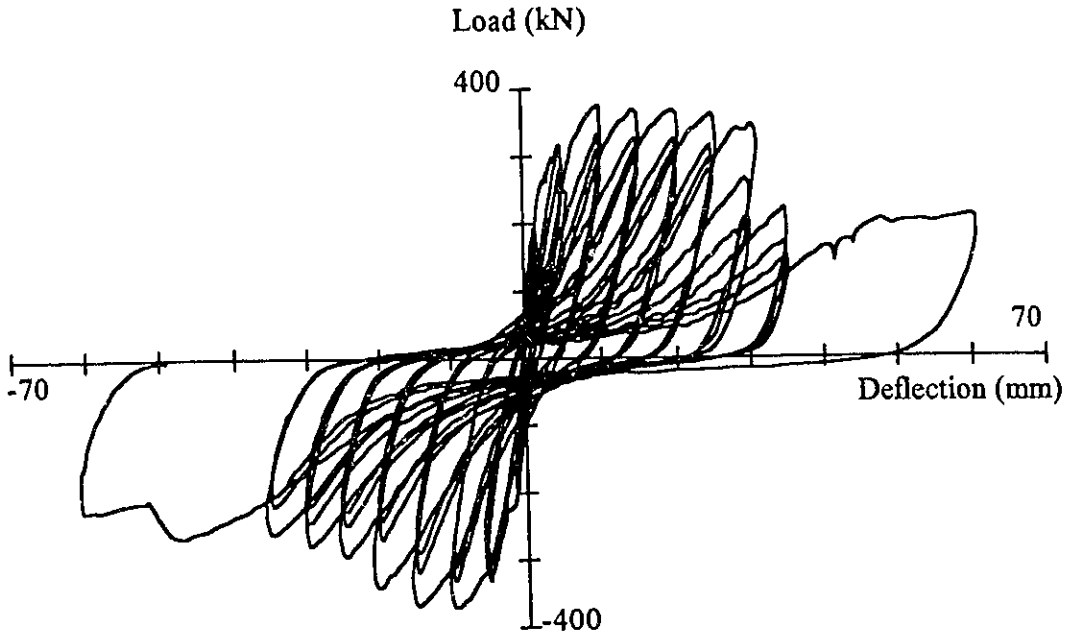

Figure 3.31 Load-West Top Horizontal Defection for Wall 7
at the Level of Potentiometer

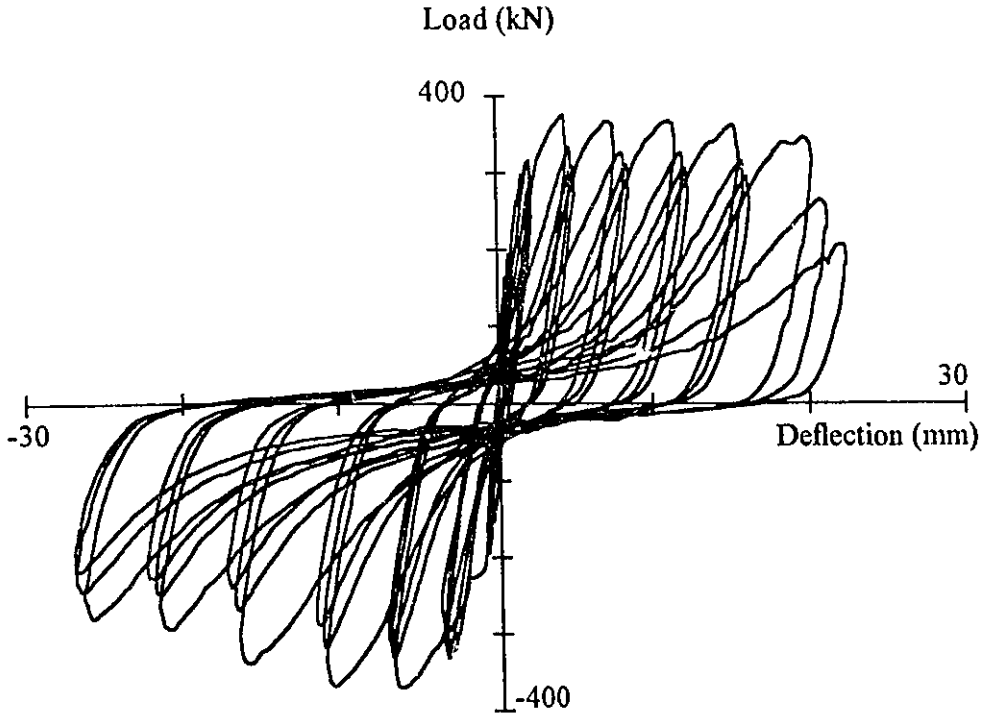

Figure 3.32 Load Mid-Height Horizontal Deflection for Wall 7

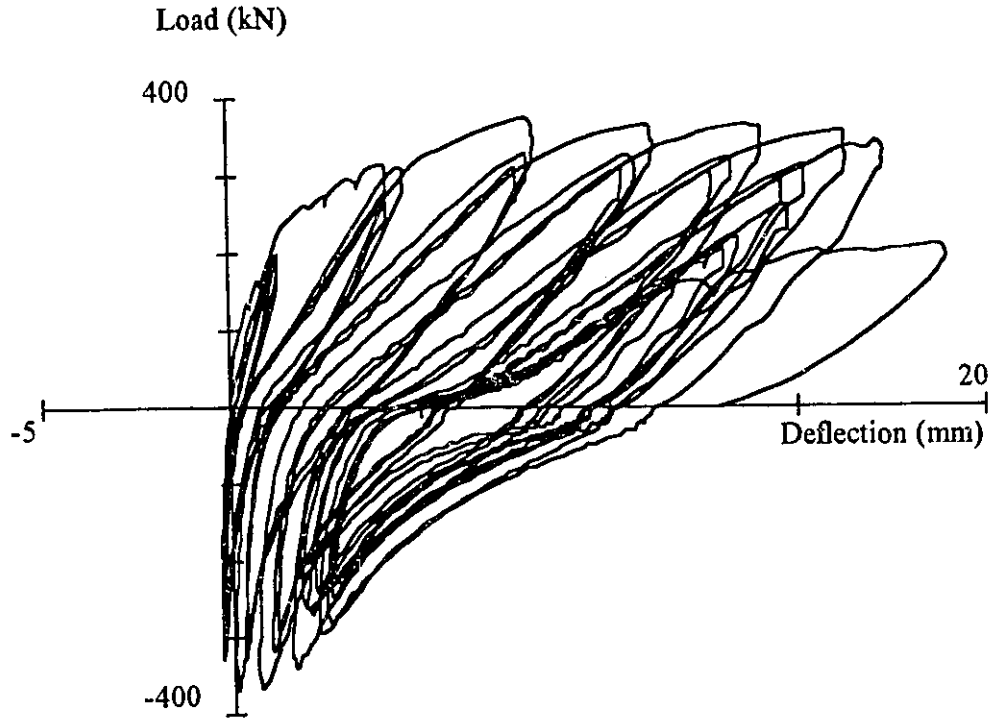

Figure 3.33 Load-East Top Vertical Deflection for Wall 7

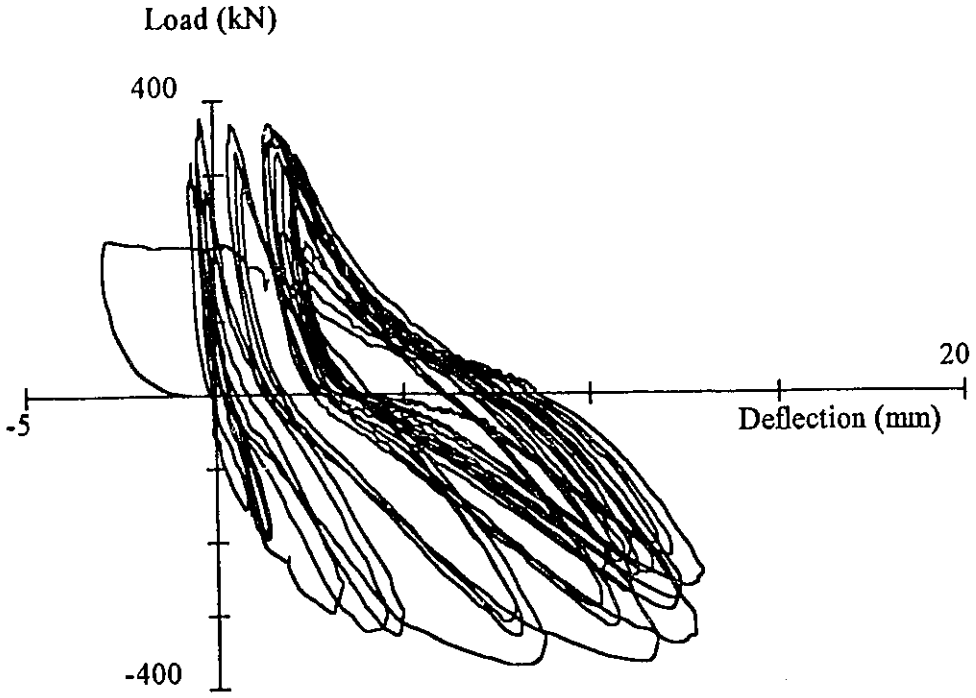

Figure 3.34 Load-West Top Vertical Deflection for Wall 7

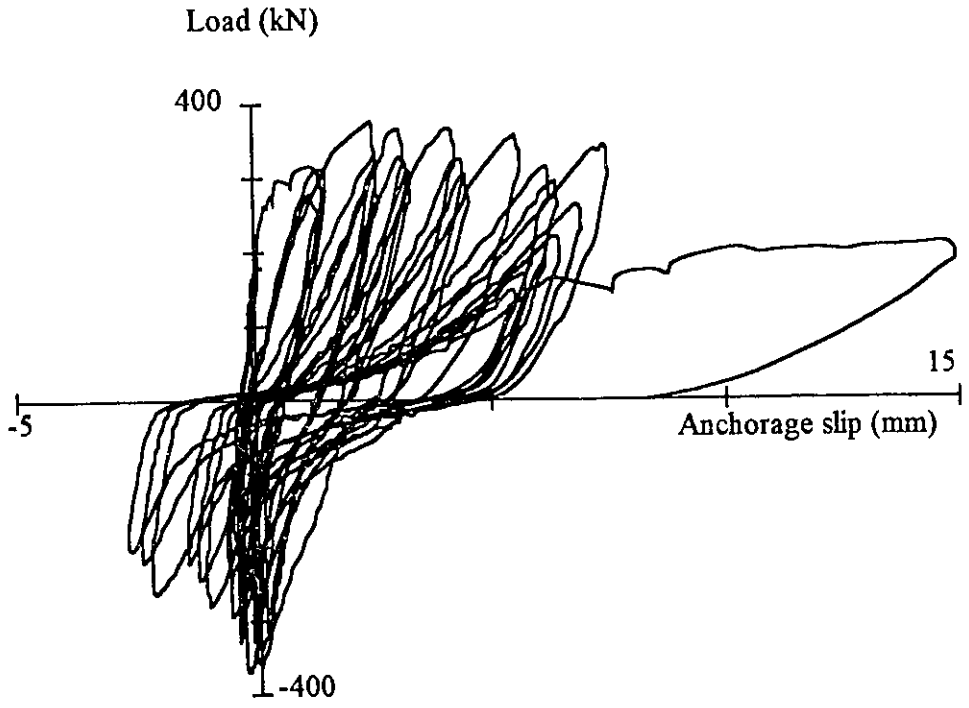

Figure 3.35 Load-East Anchorage Slip for Wall 7

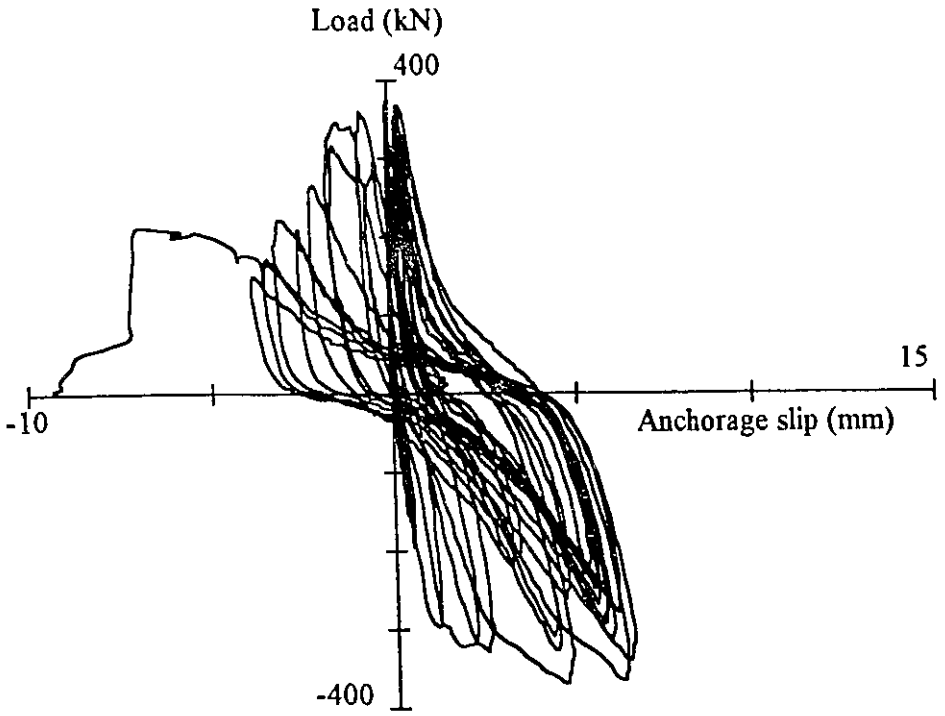

Figure 3.36 Load-West Anchorage Slip for Wall 7

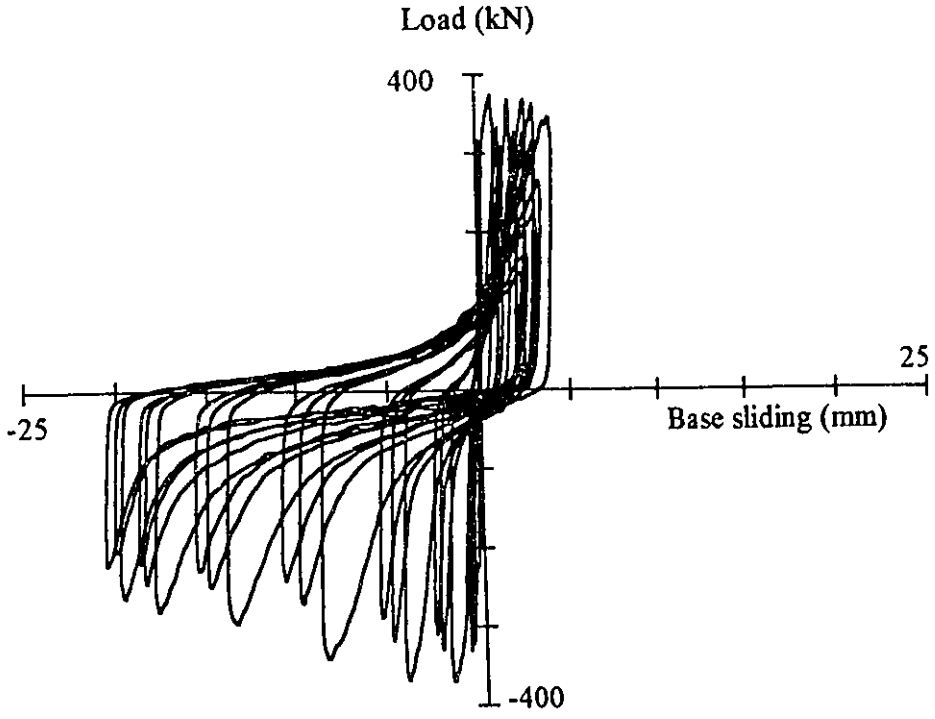

Figure 3.37 Load-East Base Sliding for Wall 7

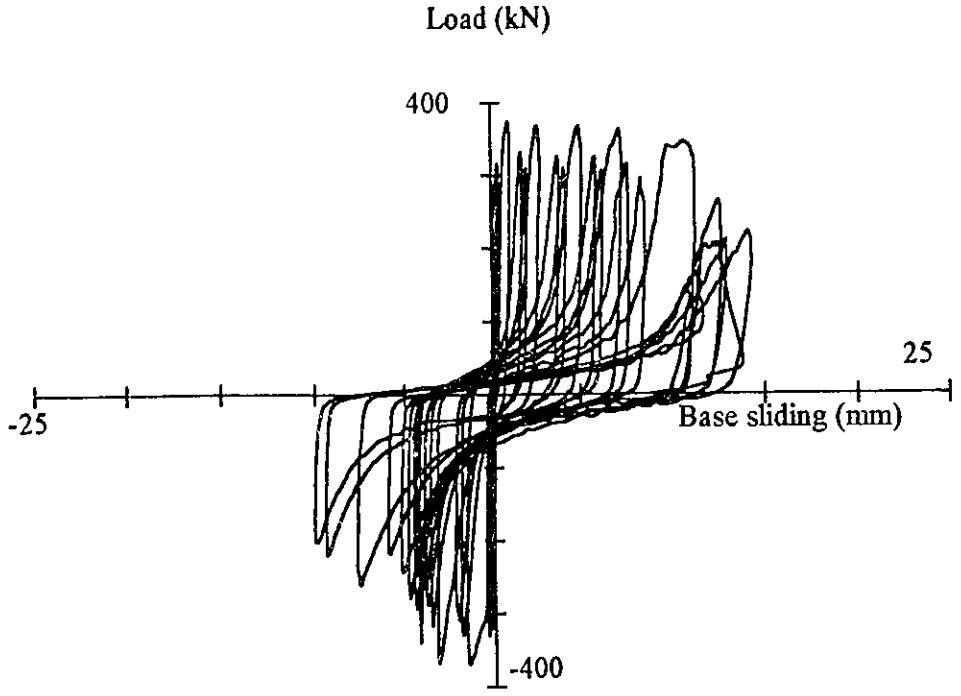

Figure 3.38 Load-West Base Sliding for Wall 7

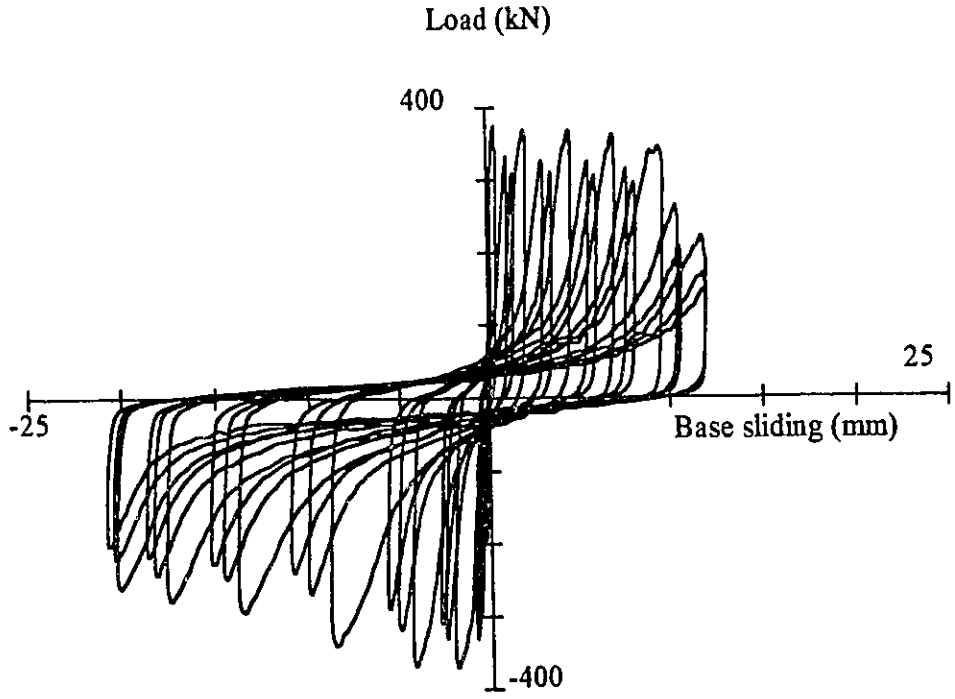

Figure 3.39 Load-Center Base Sliding for Wall 7

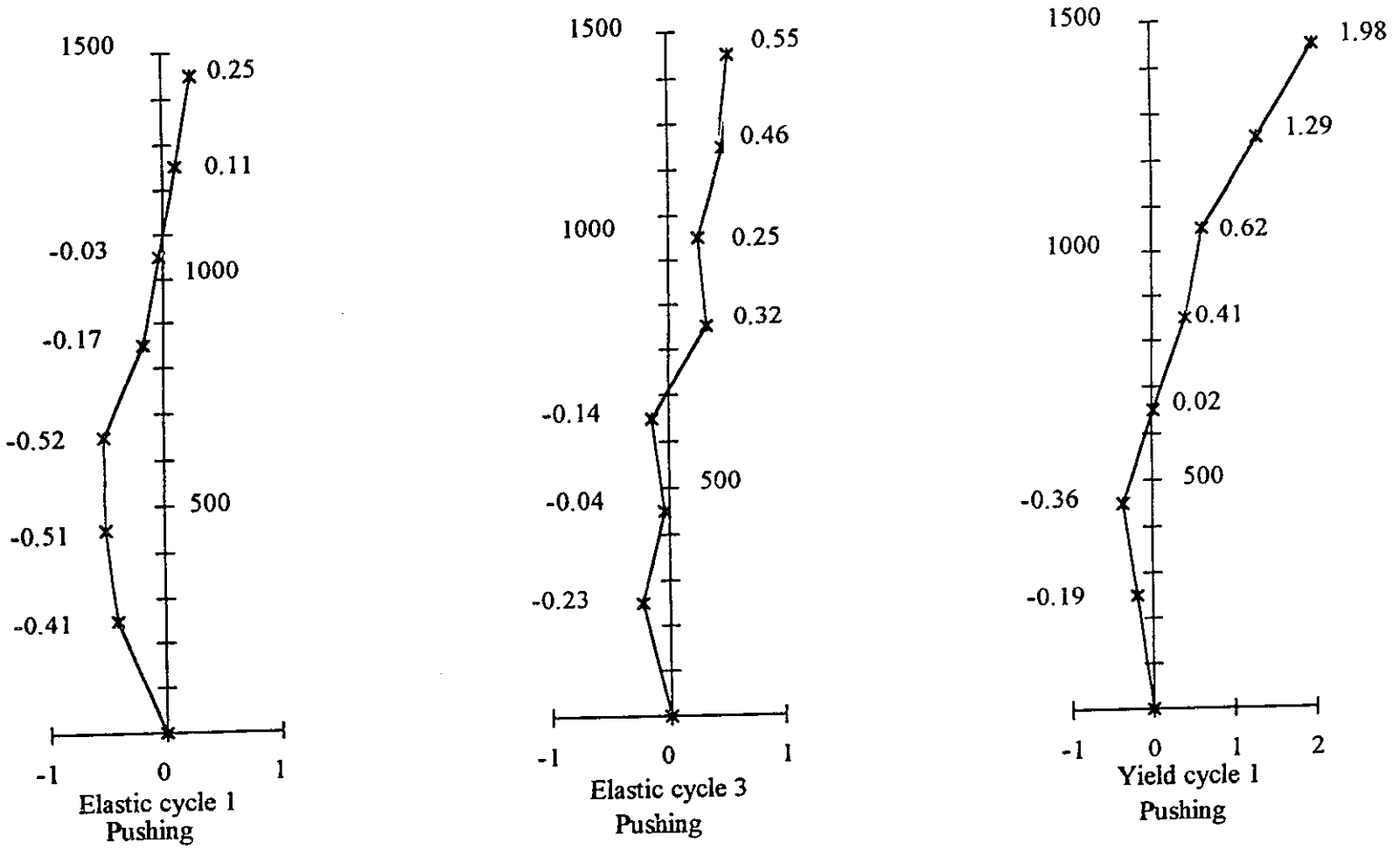

Figure 3.40a Shear Deformatrion Profile for Wall 7

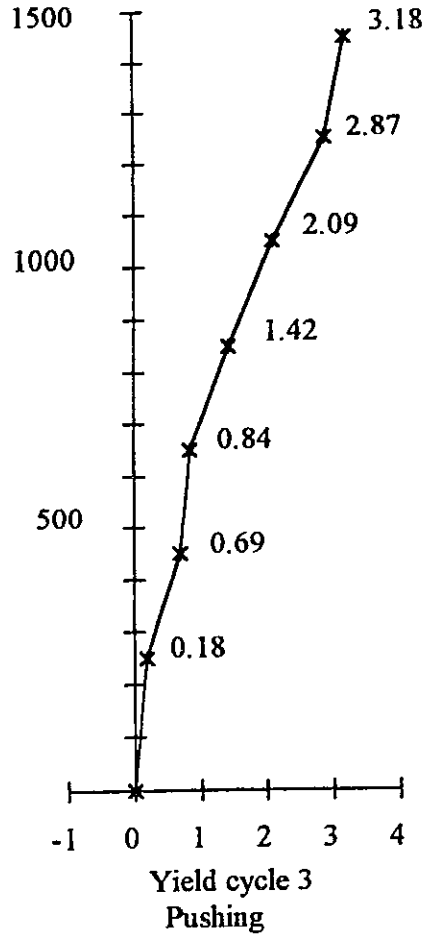

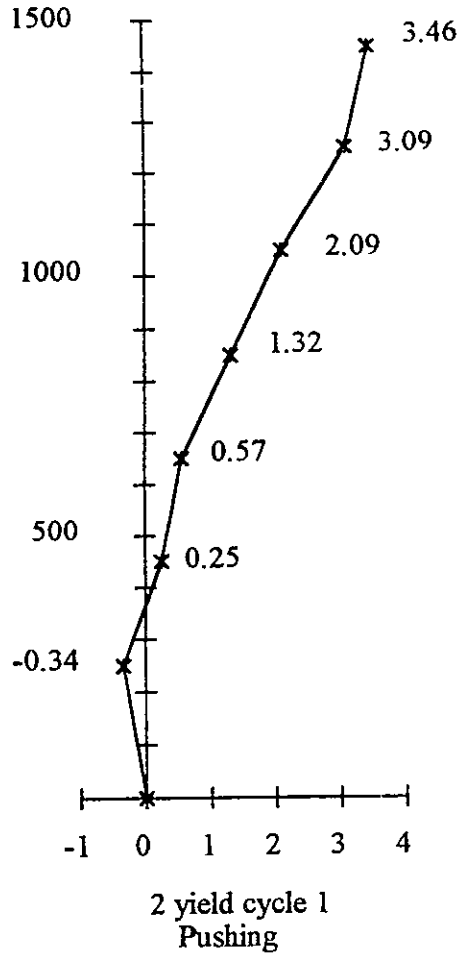

Figure 3.40b Shear Deformation Profile for Wall 7

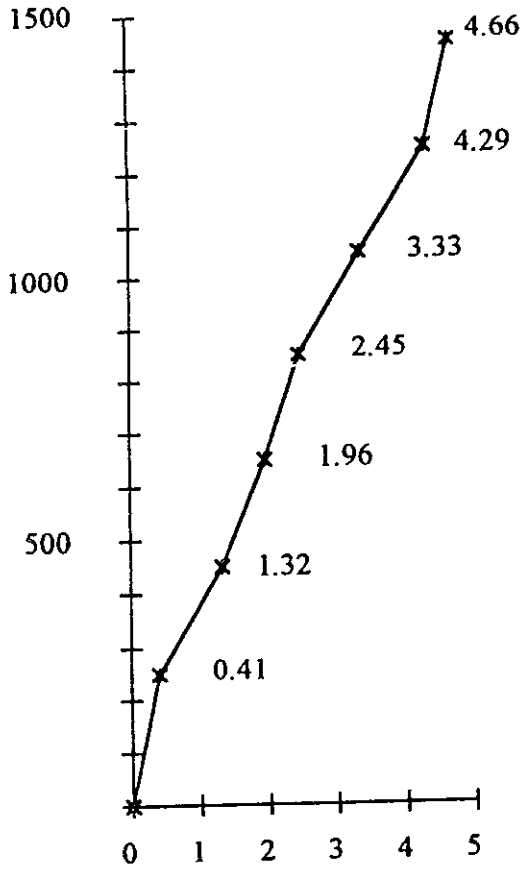

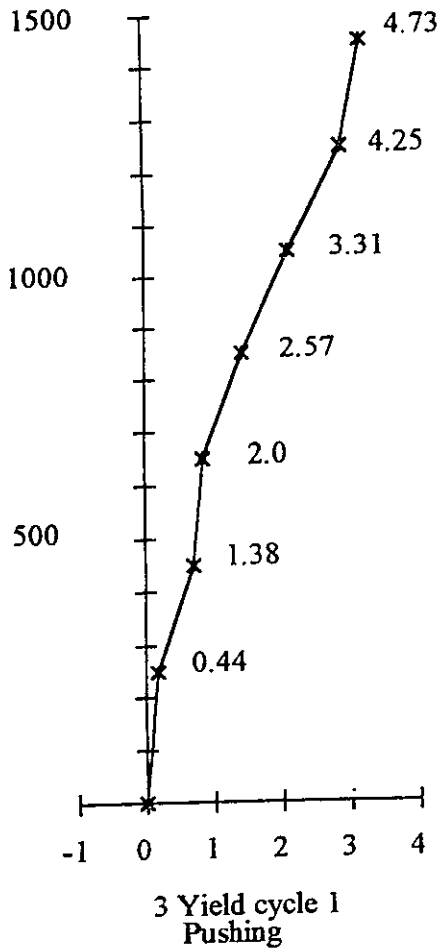

Figure 3.40c Shear Deformation Profile for Wall 7

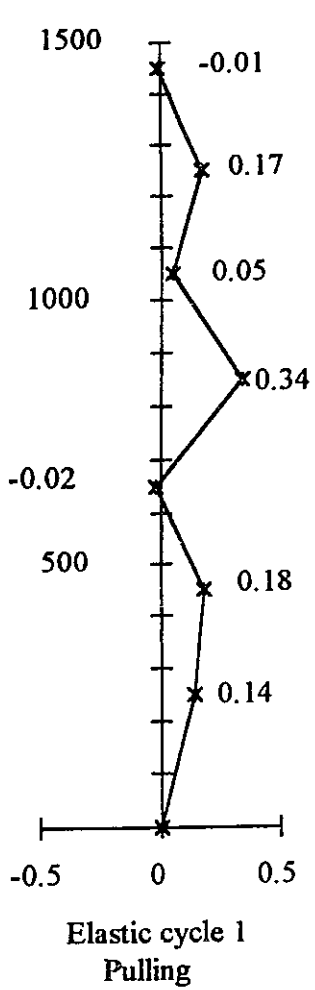

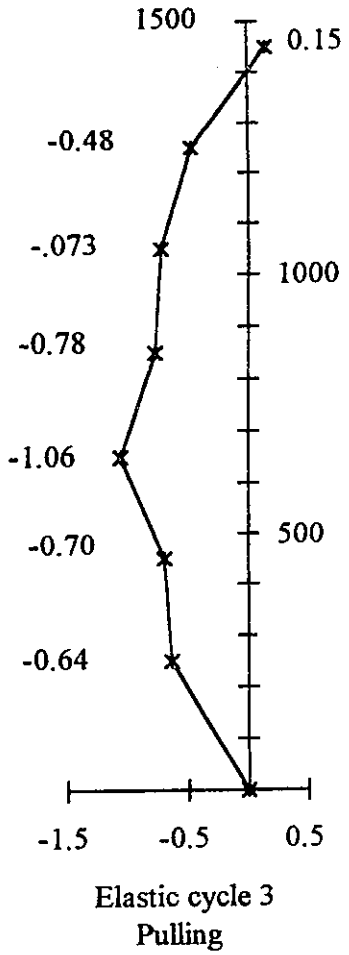

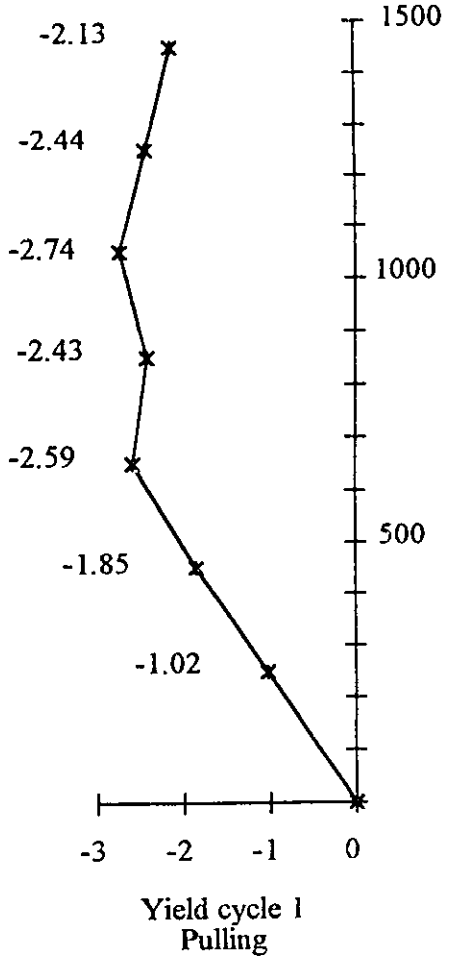

Figure 3.40d Shear Deformation Profile for Wall 7

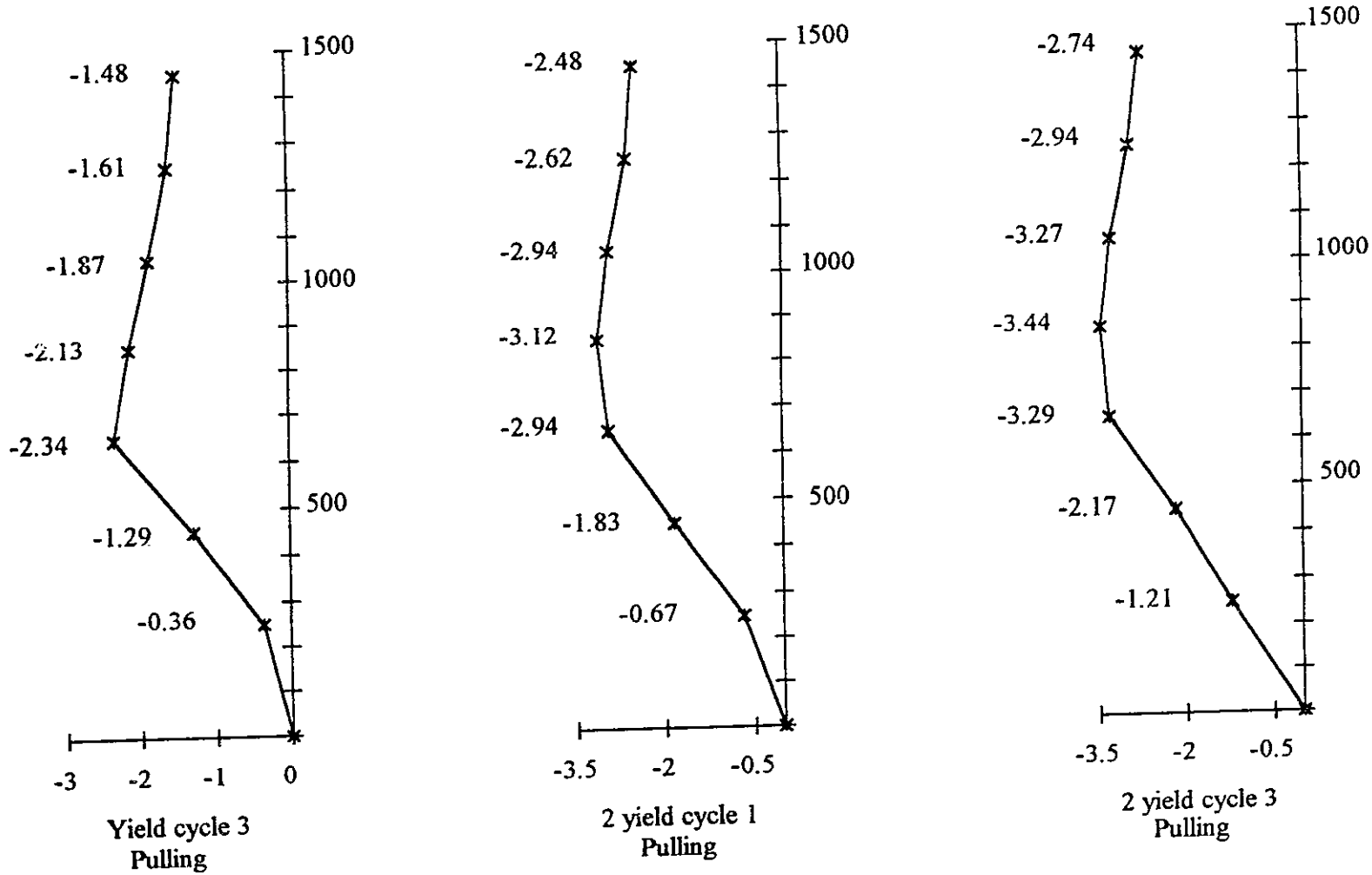

Figure 3.40e Shear Deformation Profile for Wall 7

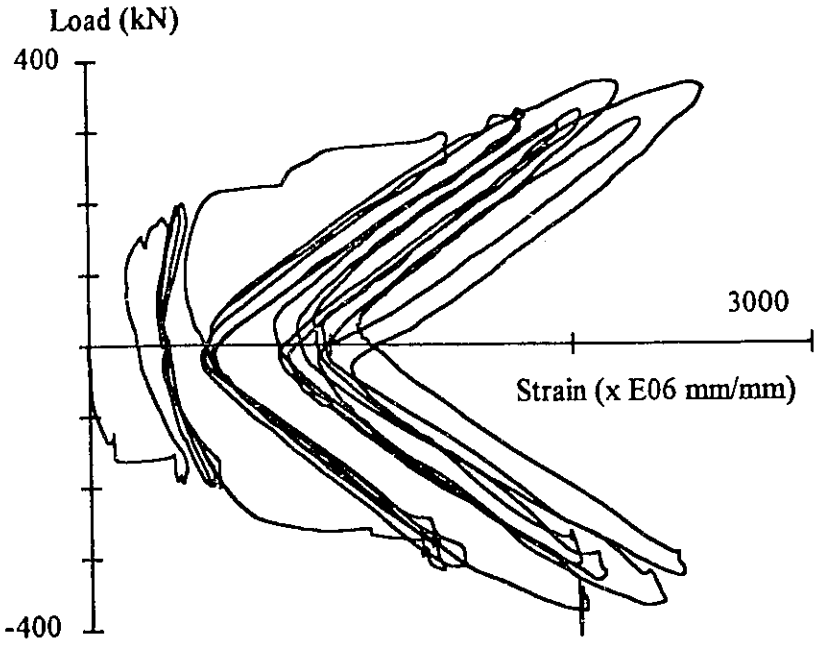

Figure 3.41 Load-Strain Relationship for Vertical Bar,V743, Wall7

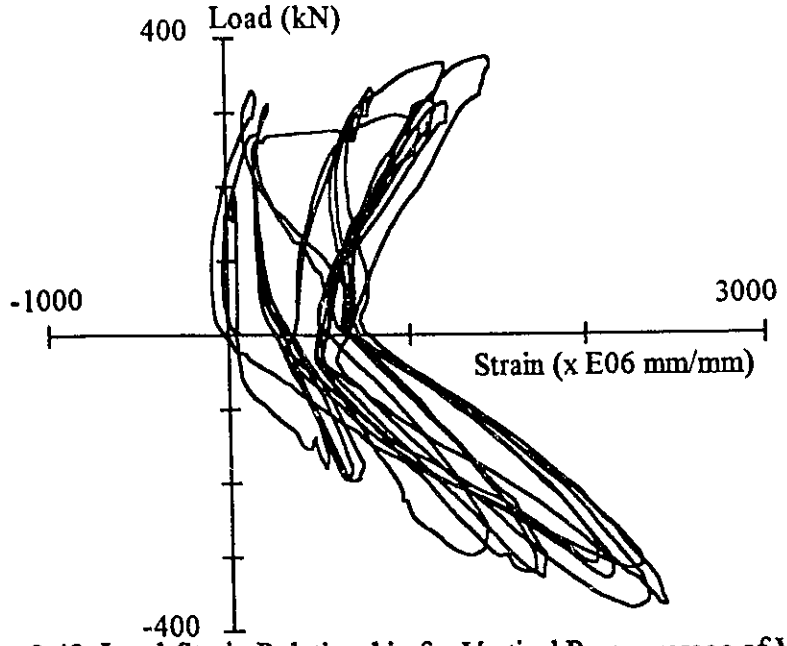

Figure 3.42 Load-Strain Relationship for Vertical Bars, average of V762 and V763, Wall 7

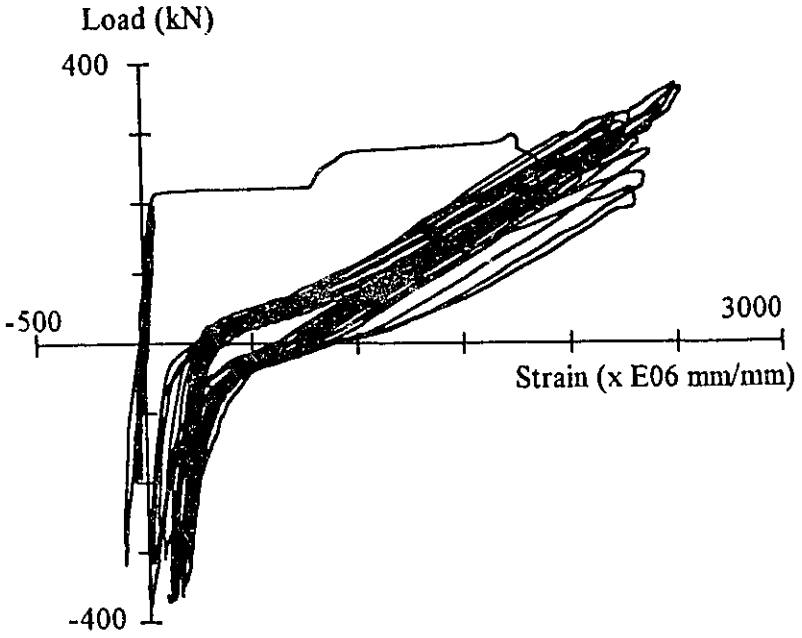

Figure 3.43 Load-Strain Relationship for Vertical bars, average of V764 and V765 Wall 7

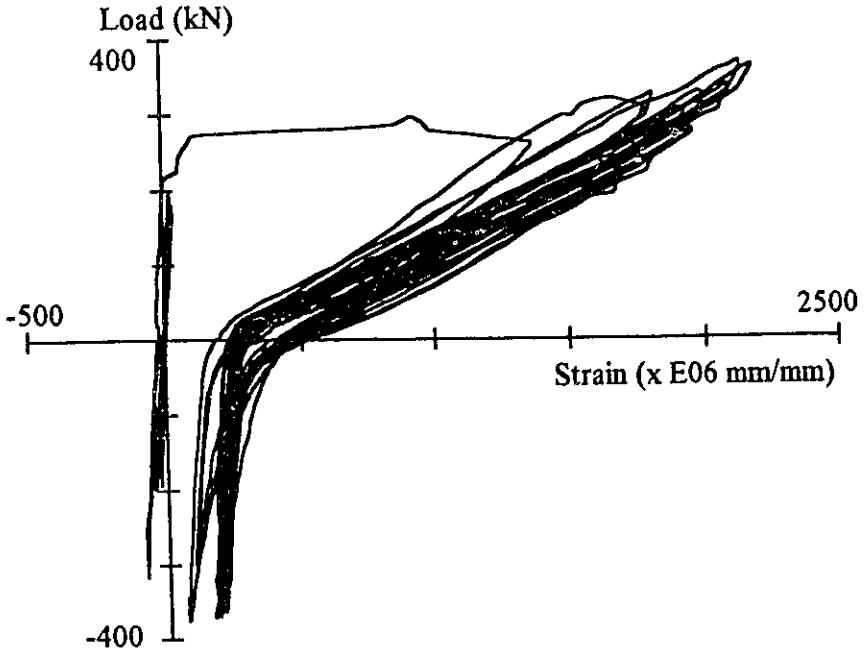

Figure 3.44 Load-Strain Relationship for Vertical bars, average of V772 and V773 Wall 7

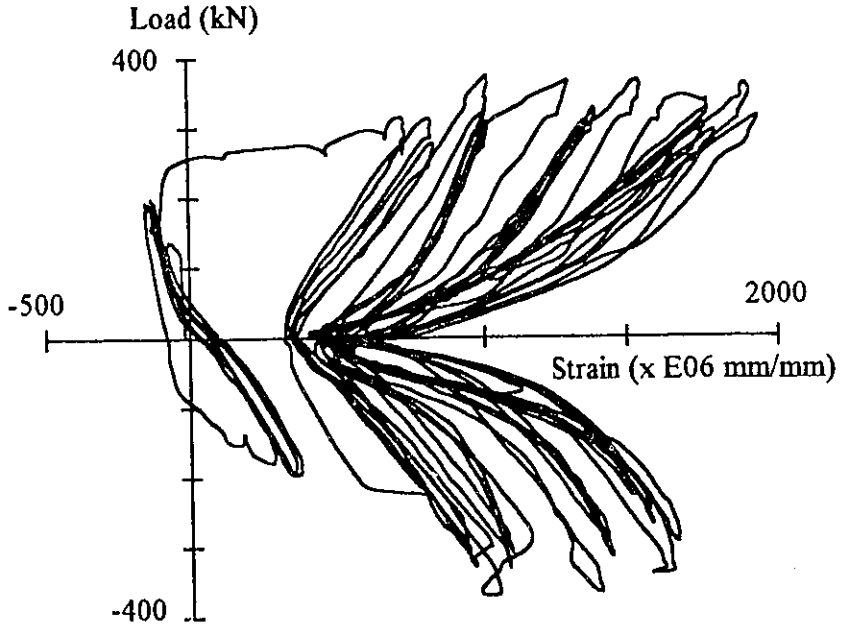

Figure 3.45 Load-Strain Relationship for Horizontal bars, average of H721 and H722, Wall 7

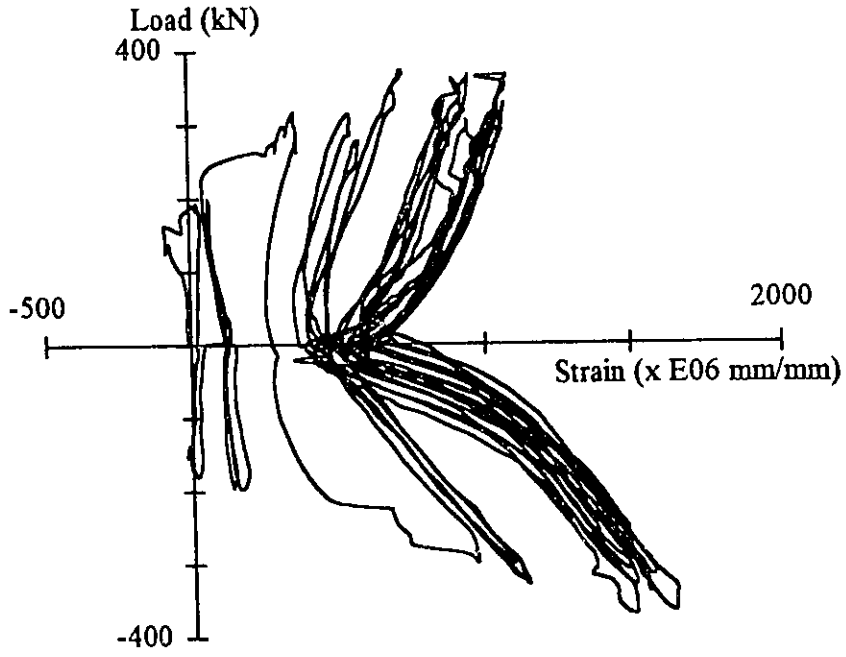

Figure 3.46 Load-Strain Relationship for Horizontal bar, H724, Wall 7

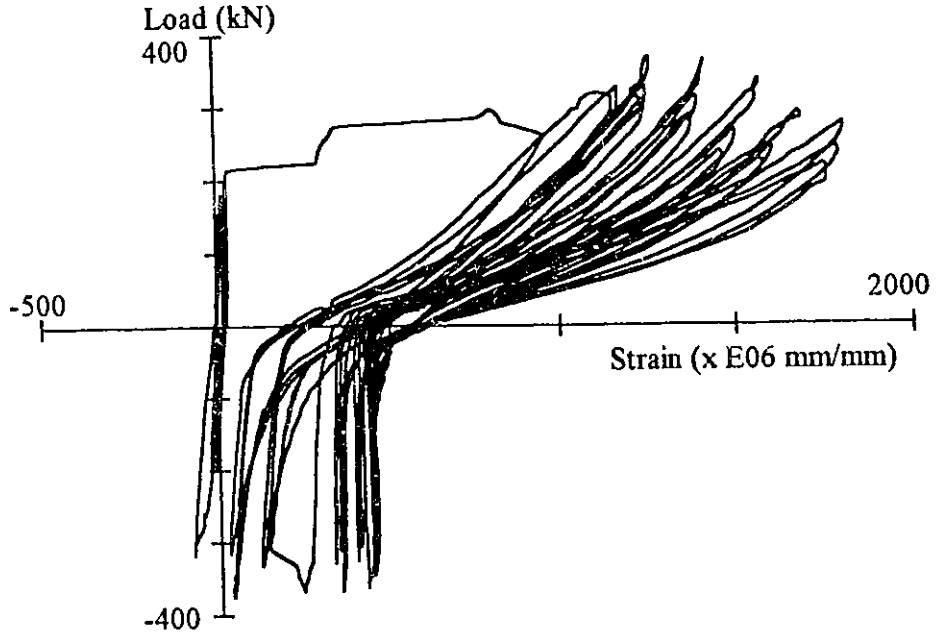

Figure 3.47 Load-Strain Relationship for Horizontal Bars, average of H741 and H742 Wall 7

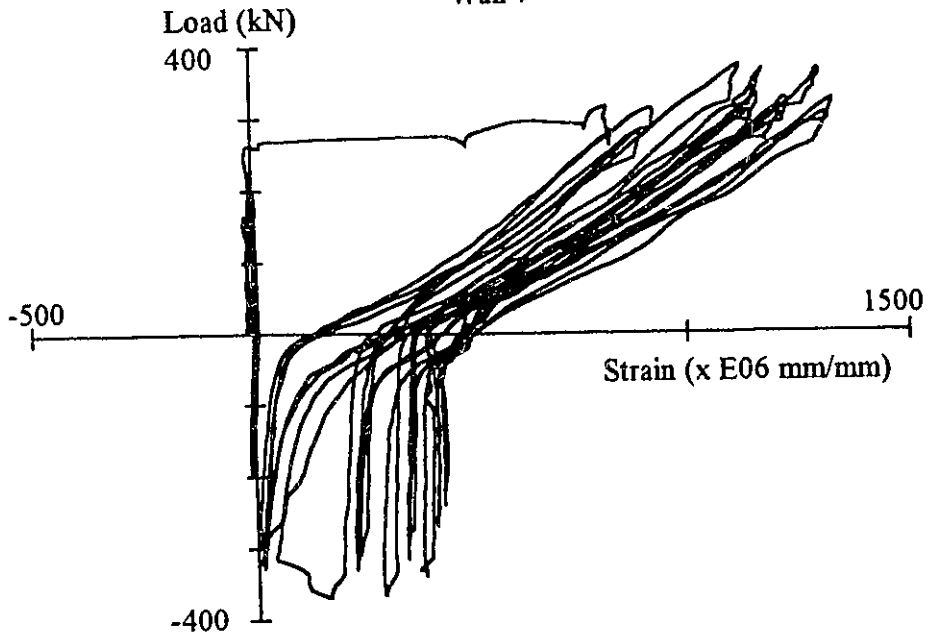

Figure 3.48 Load-Strain Relationship for Horizontal bars, average of H743 and H744 Wall 7

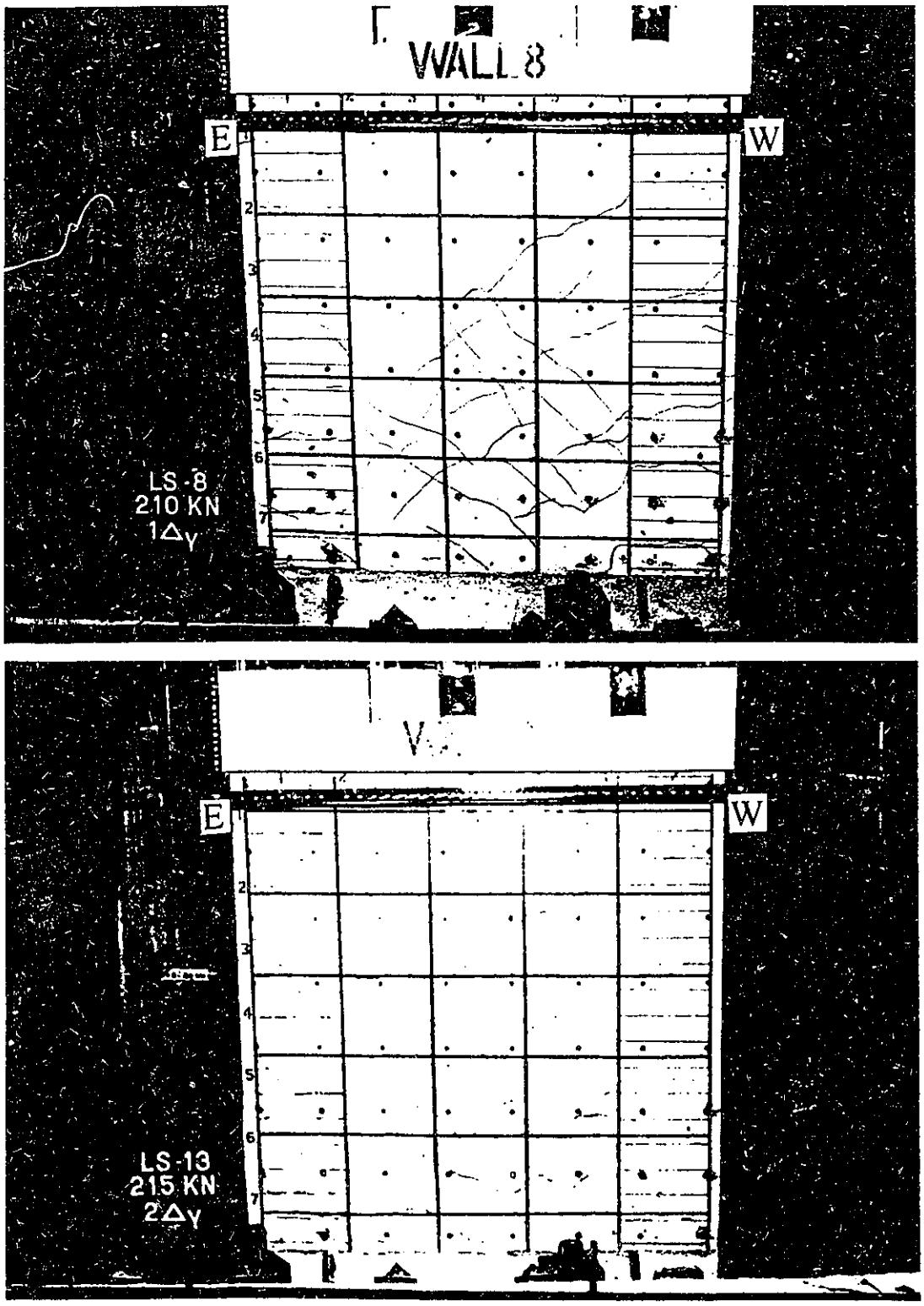

Figure 3.49 Wall 8 Crack Pattern, Cycle 1 (pulling) at $1\Delta_y$ (above) and Cycle 1 (pushing) at $2\Delta_y$ (below)

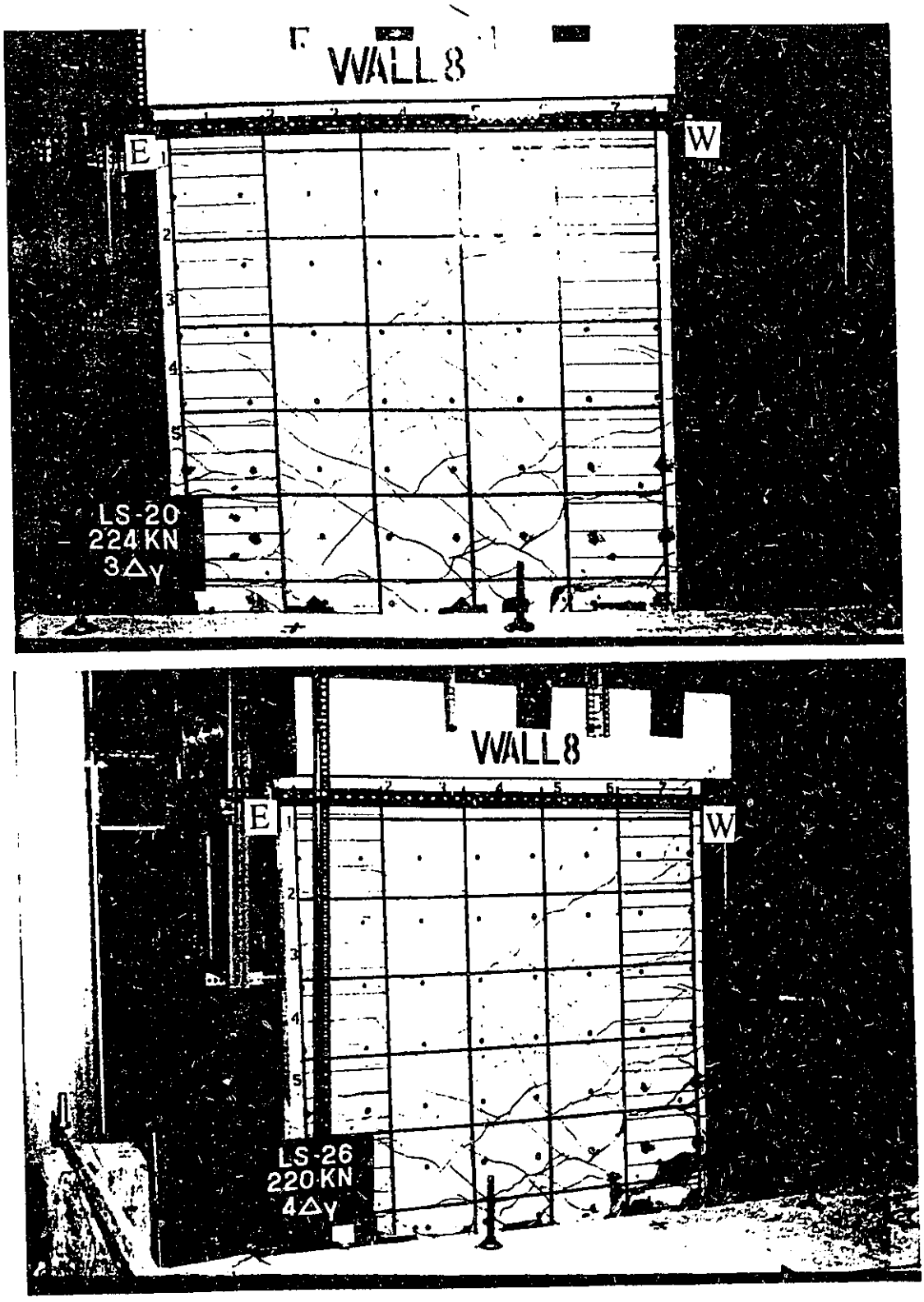

Figure 3.50 Wall 8 Crack Pattern, Cycle 1 (pulling) at $3\Delta_y$ (above) and Cycle 1 (pulling) at $4\Delta_y$ (below)

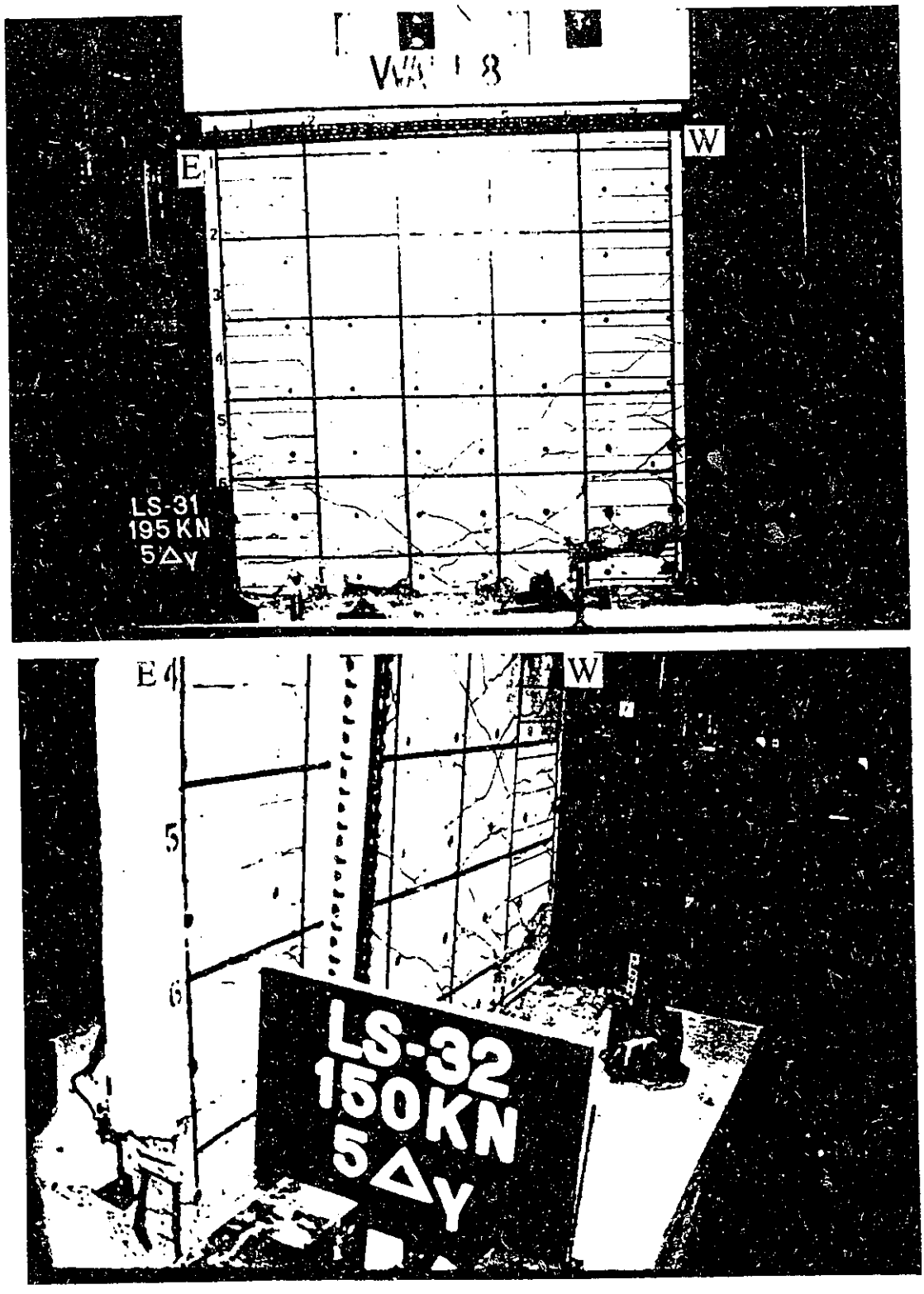

Figure 3.51 Wall 8 Crack Pattern, Cycle 1 (pushing) at $5\Delta_y$ (above) and Cycle 1 (pulling) at $5\Delta_y$ (below)

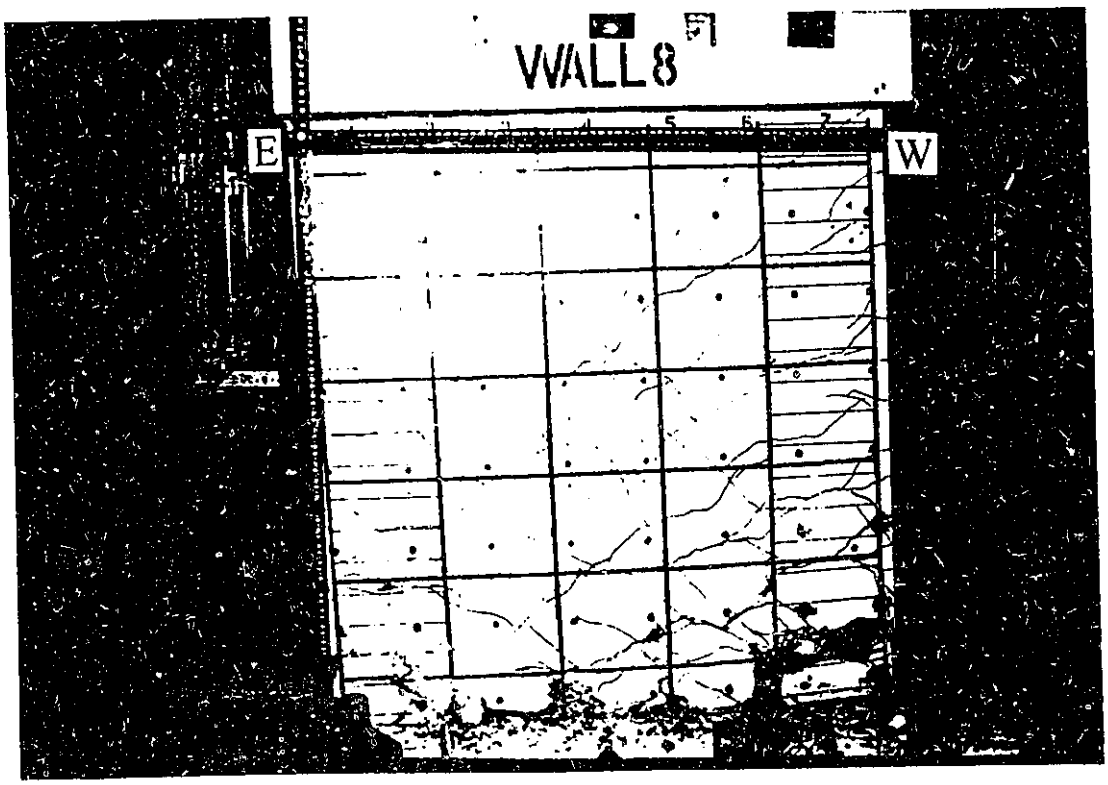

Figure 3.52 Wall 8 Crack Pattern at the End of Test

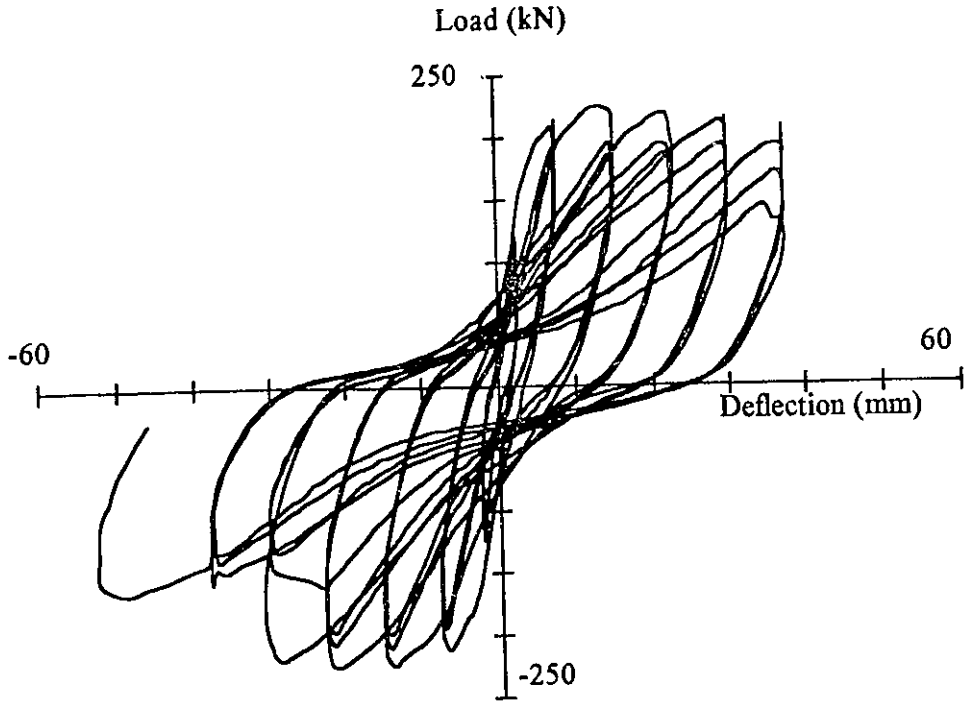

Figure 3.53 Load-East Top Horizontal Deflection for Wall 8
at the Level of Potentiometer

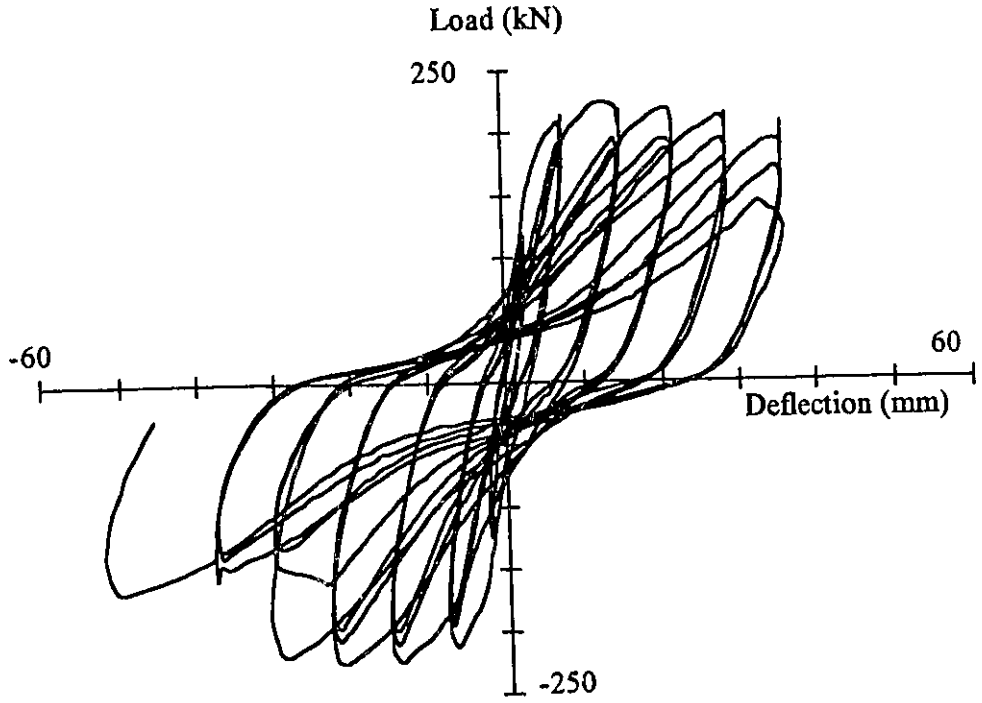

Figure 3.54 Load-West Top Horizontal Deflection for Wall 8
at the Level of Potentiometer

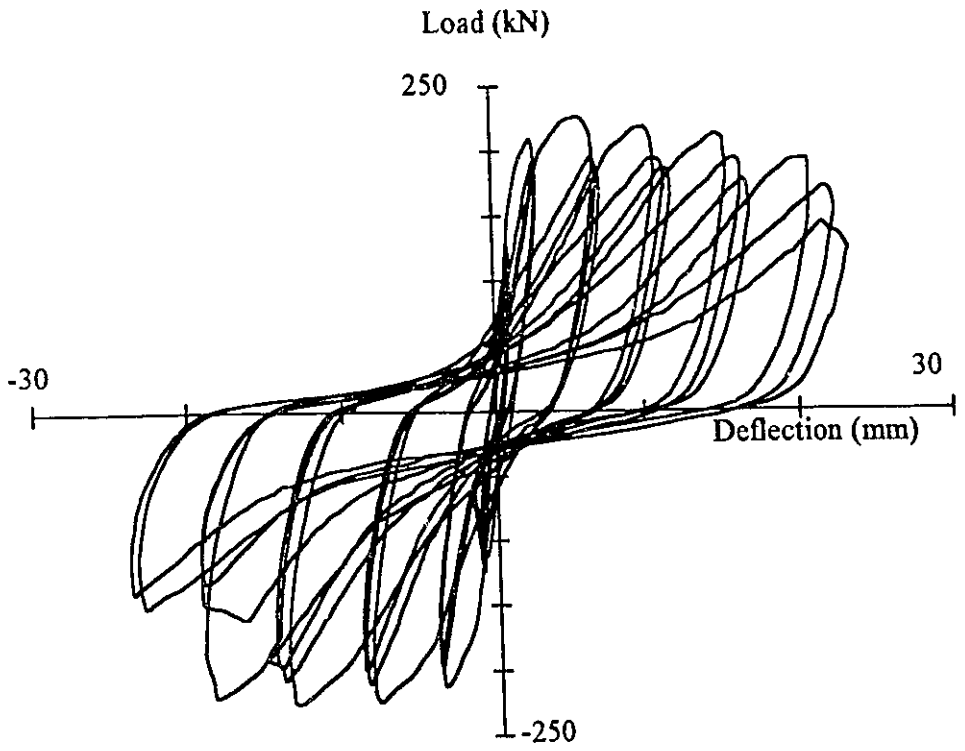

Figure 3.55 Load Mid-Height Horizontal Deflection for Wall 8

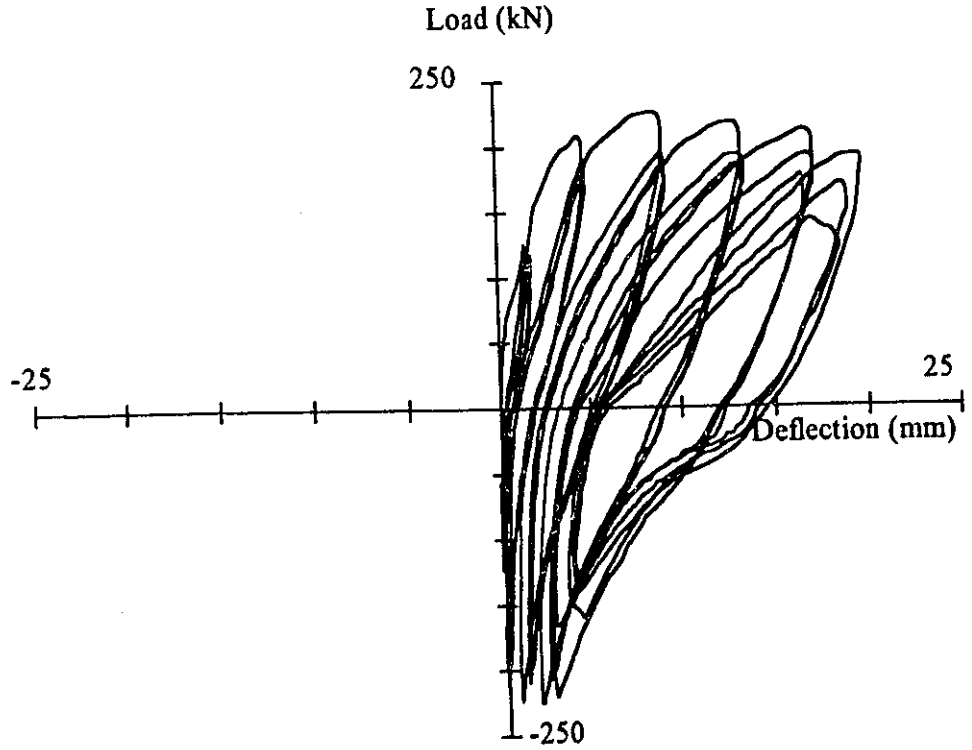

Figure 3.56 Load-East Top Vertical Deflection for Wall 8

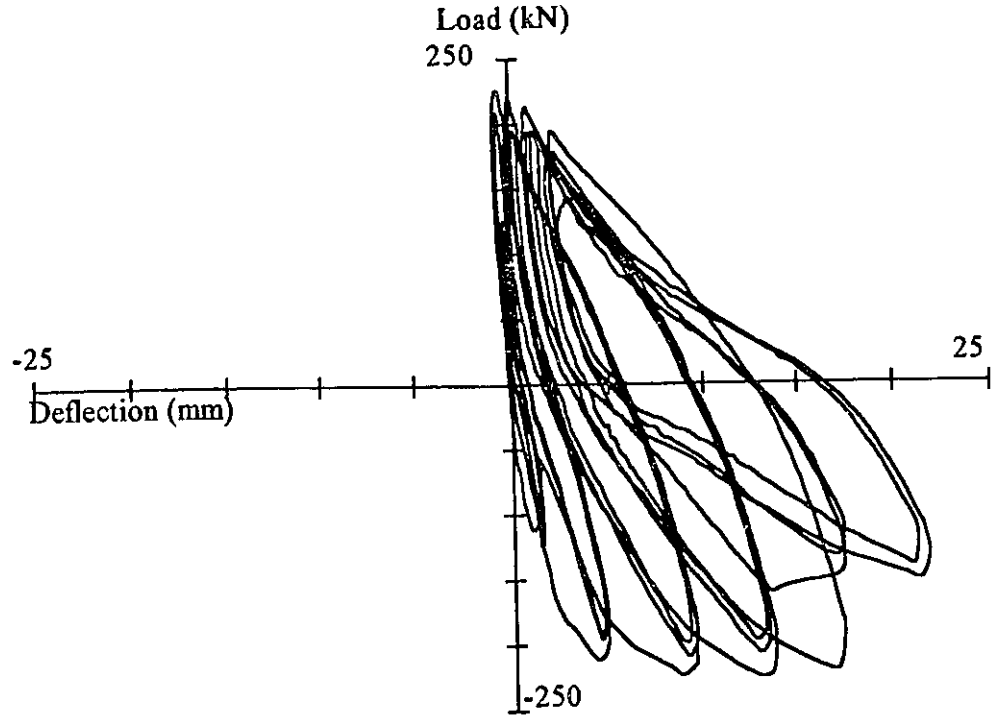

Figure 3.57 Load-West Top Vertical Deflection for Wall 8

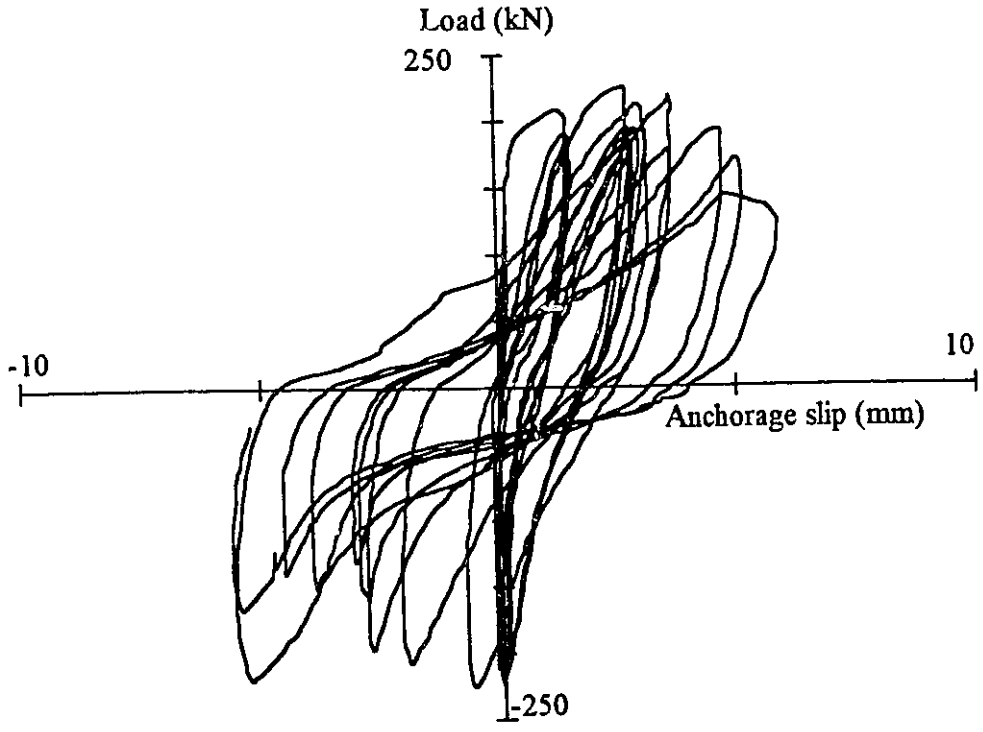

Figure 3.58 Load-East Anchorage Slip for Wall 8

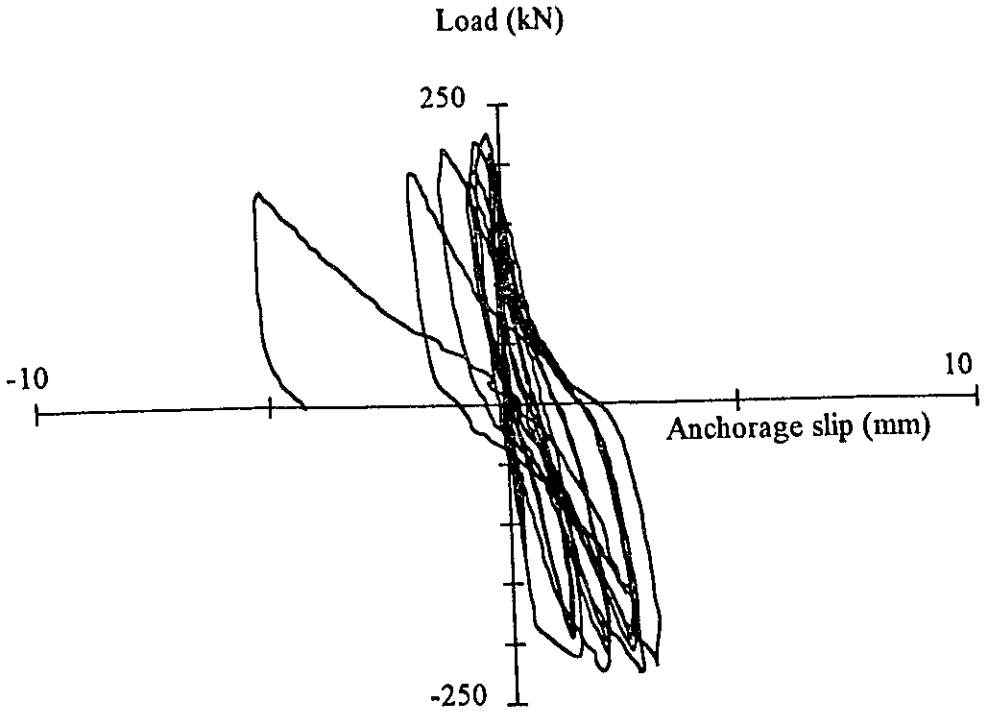

Figure 3.59 Load-West Anchorage Slip for Wall 8

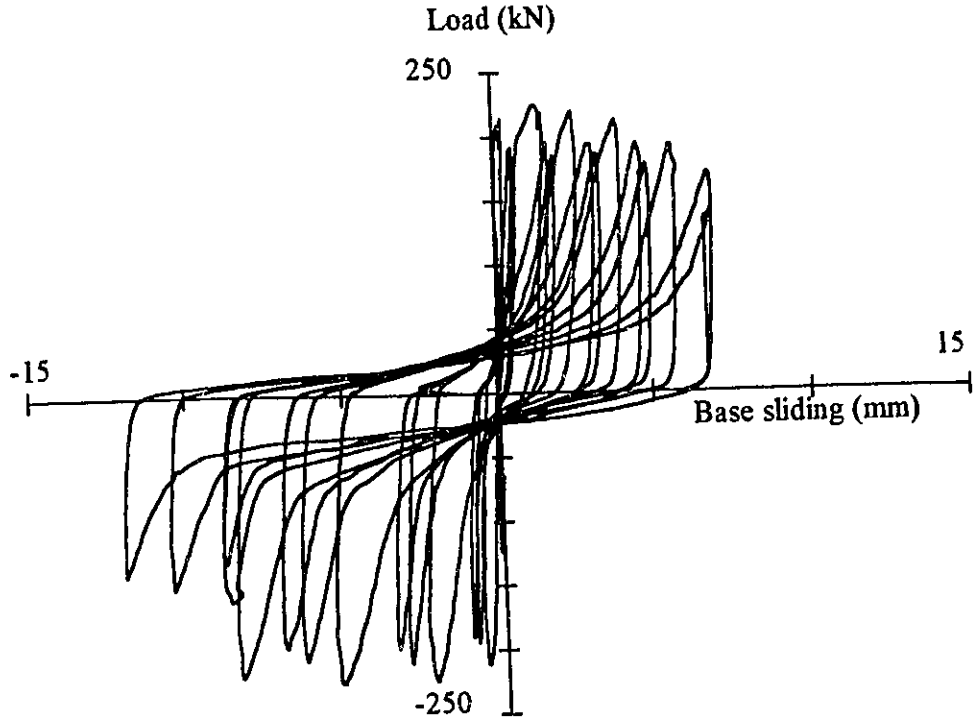

Figure 3.60 Load-East Base Sliding for Wall 8

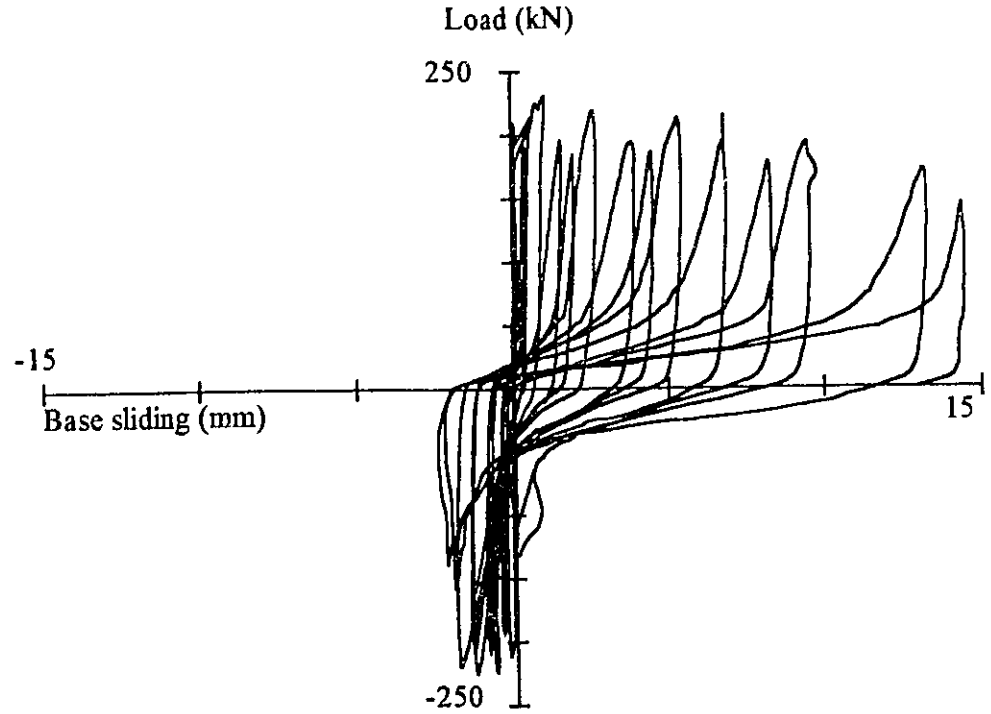

Figure 3.61 Load-West Base Sliding for Wall 8

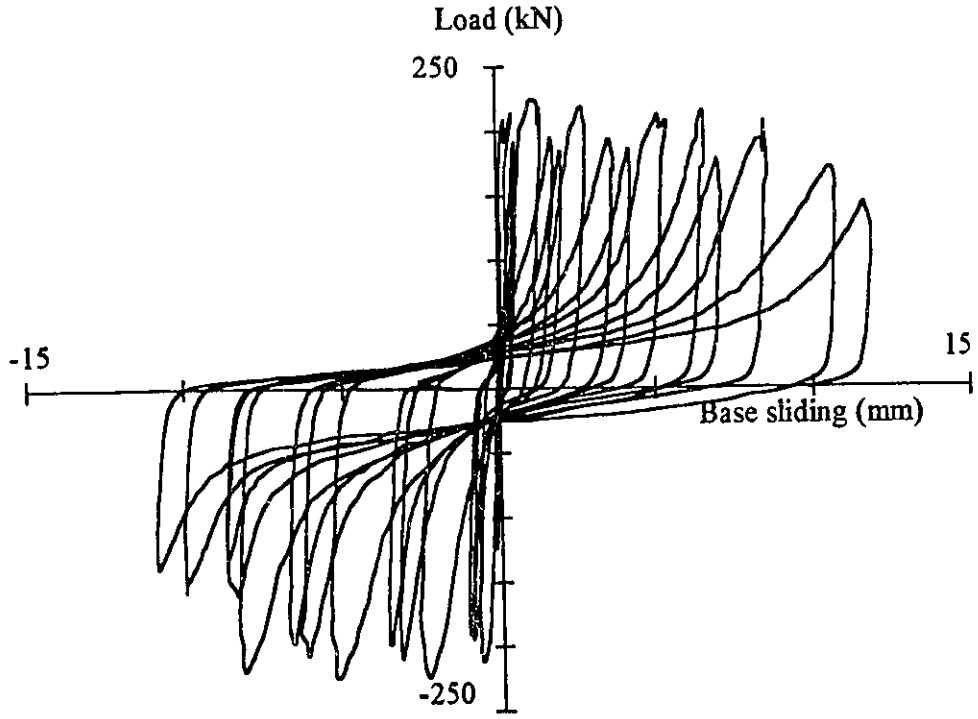

Figure 3.62 Load-Center Base Sliding for Wall 8

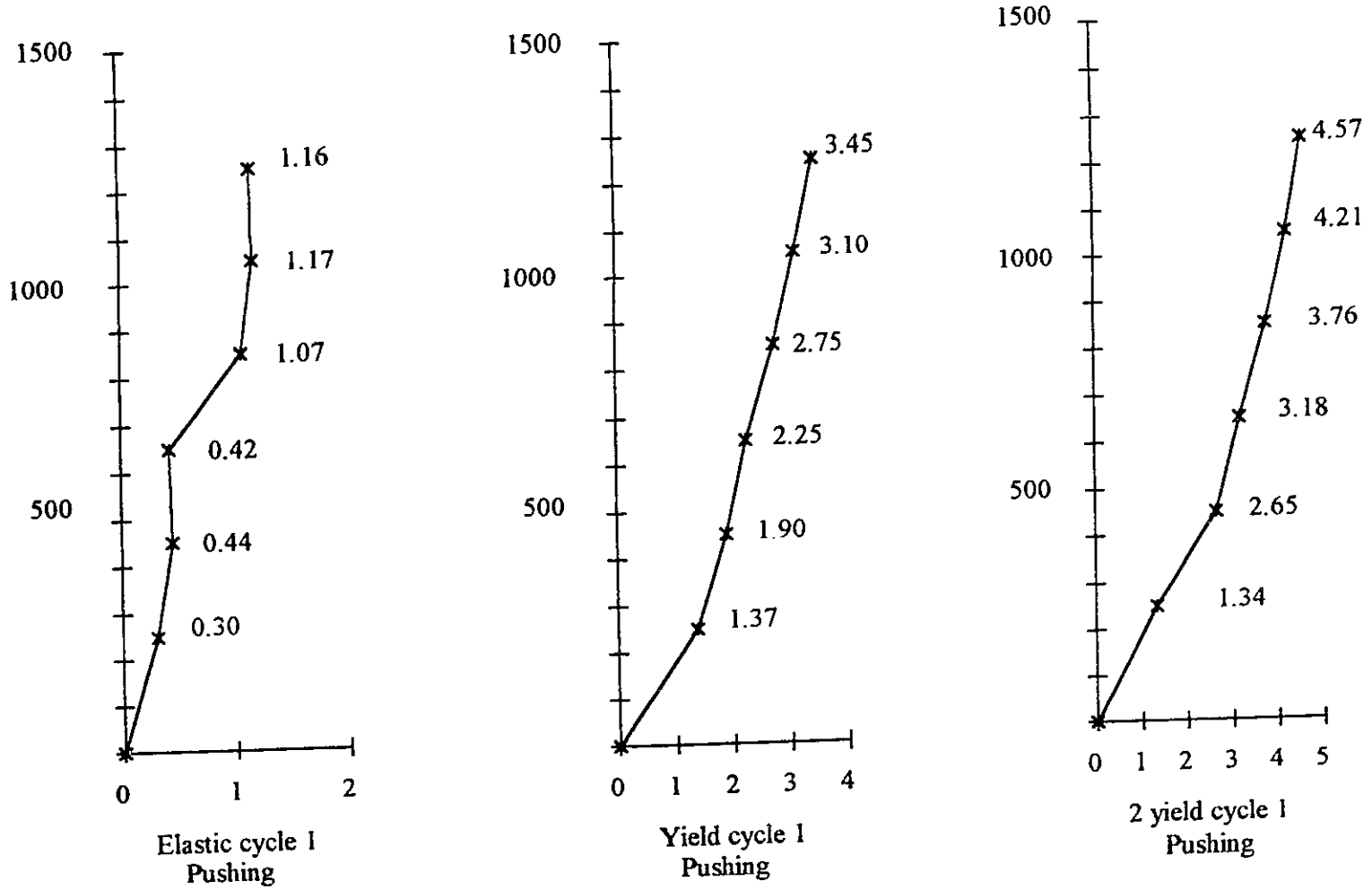

Figure 3.63a Shear Deformation Profile for Wall 8

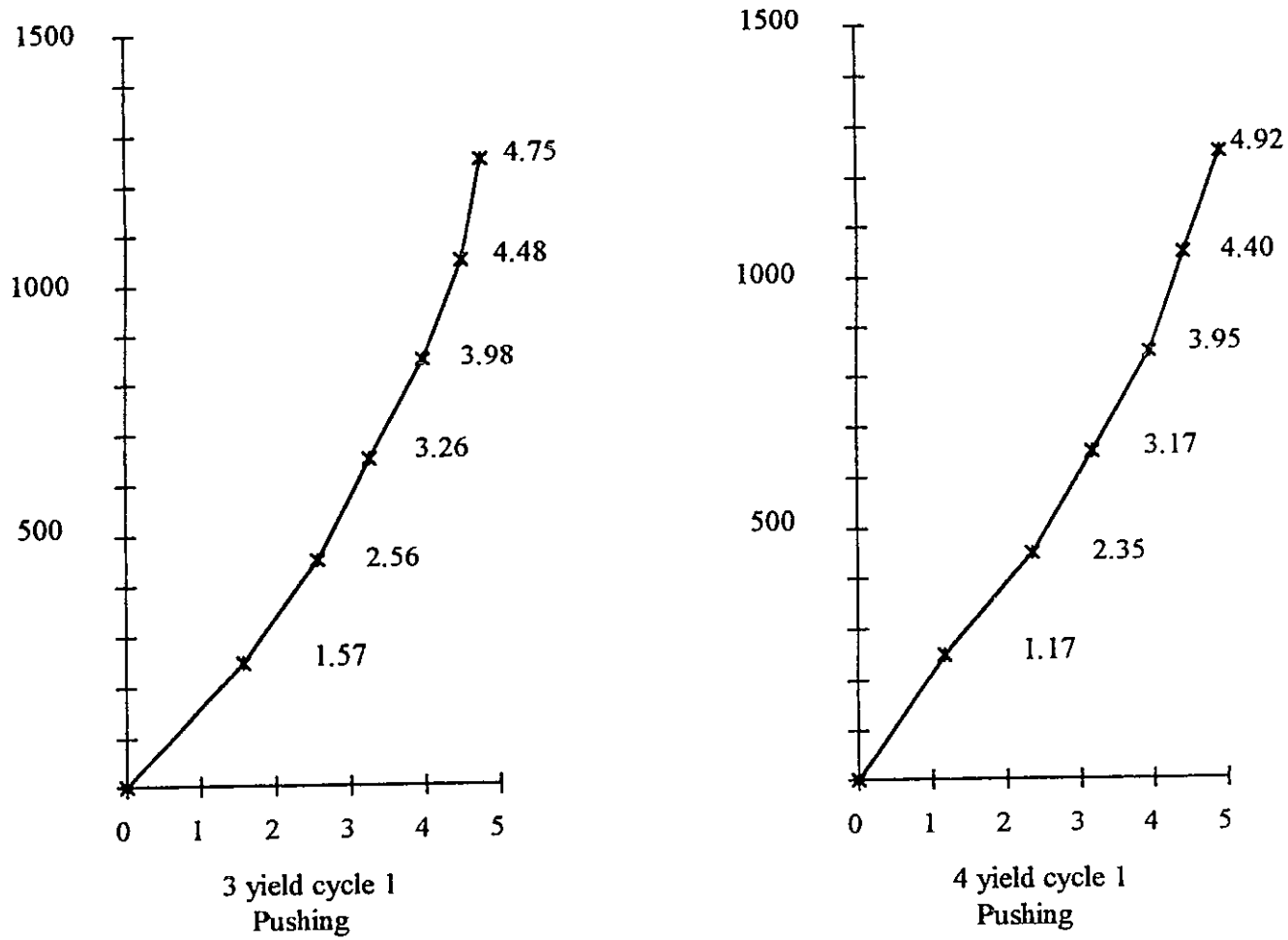

Figure 3.63b Shear Deformation Profile for Wall 8

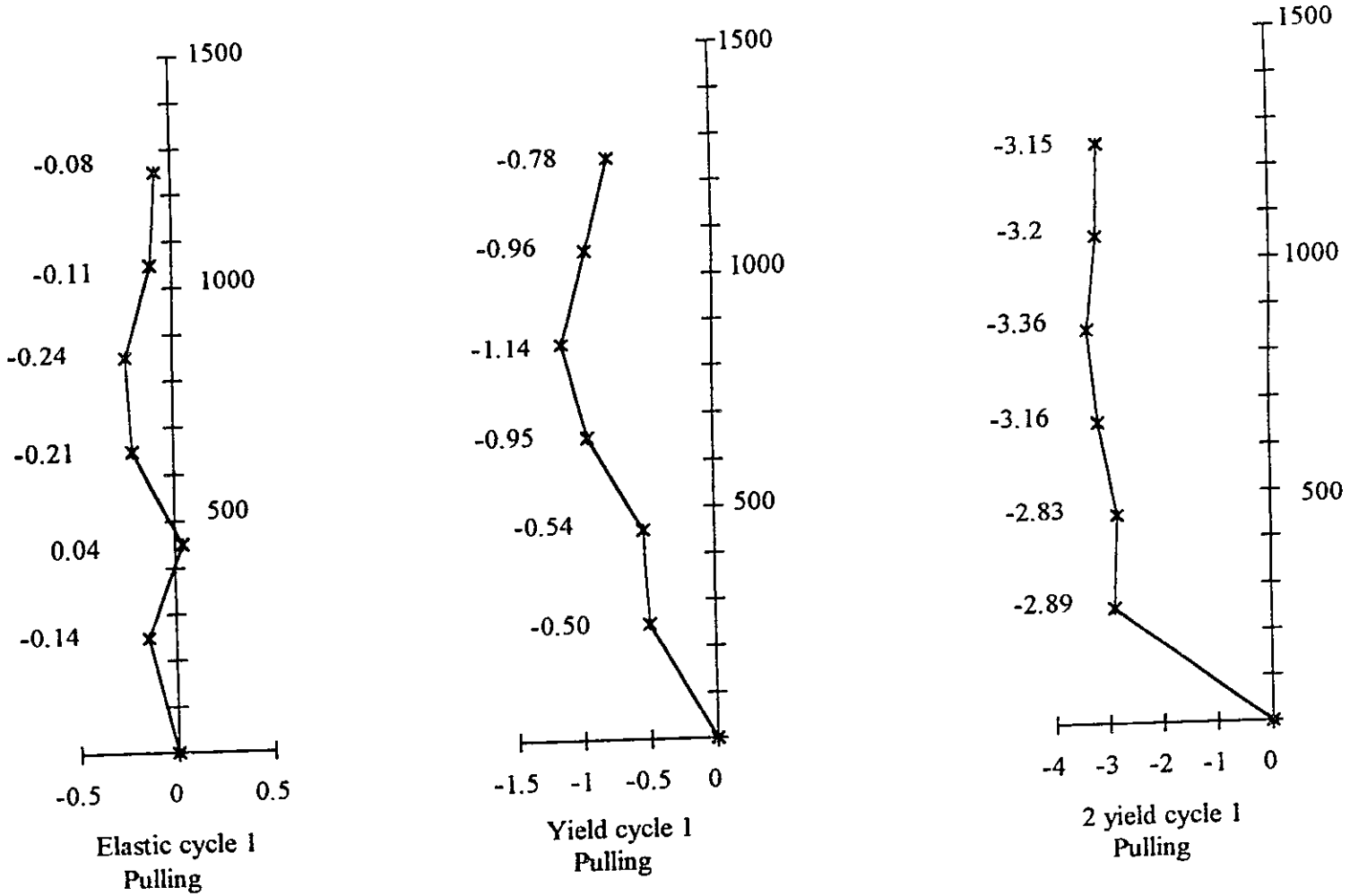

Figure 3.63c Shear Deformation Profile for Wall 8

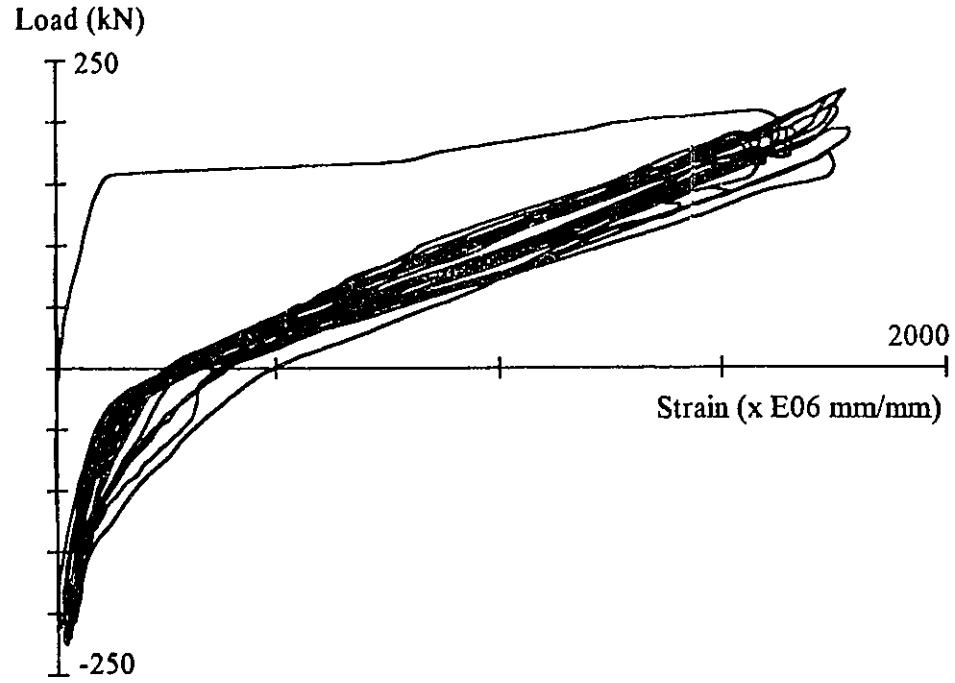

Figure 3.64 Load-Strain Relationship for Vertical bars, average of V814 and V815 Wall 8

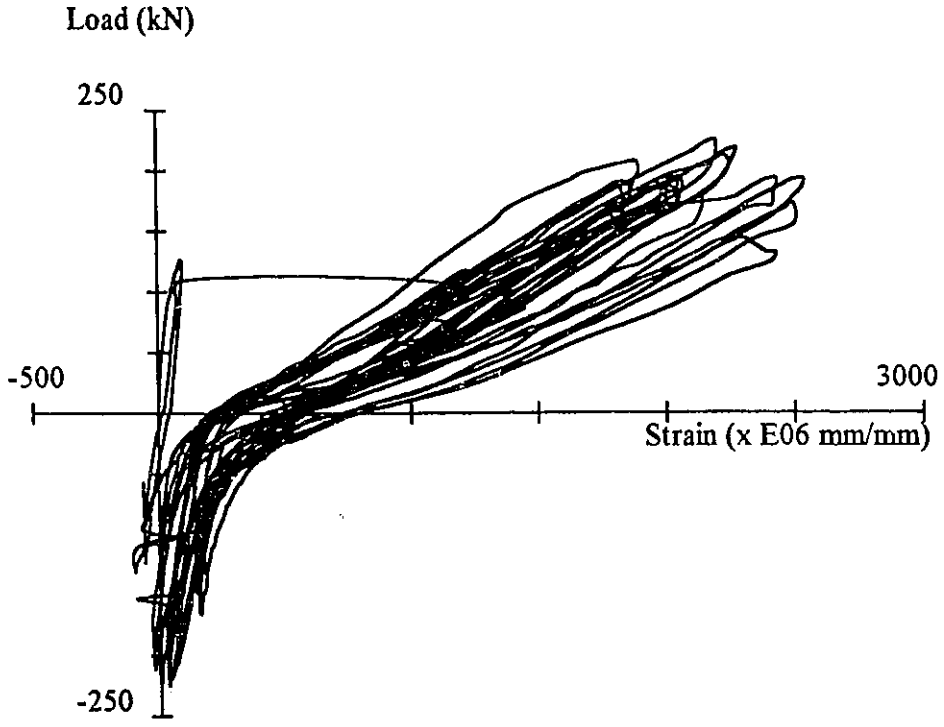

Figure 3.65 Load-Strain Relationship for Vertical bar, V824, Wall 8

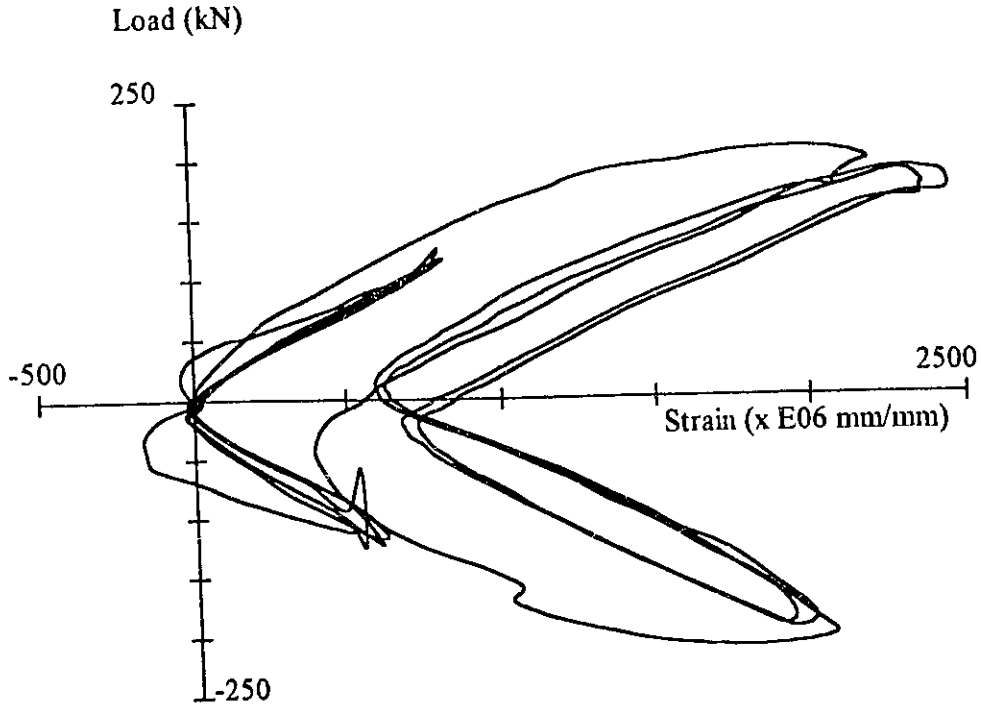

Figure 3.66 Load-Strain Relationship for Vertical Bar, V831, Wall8

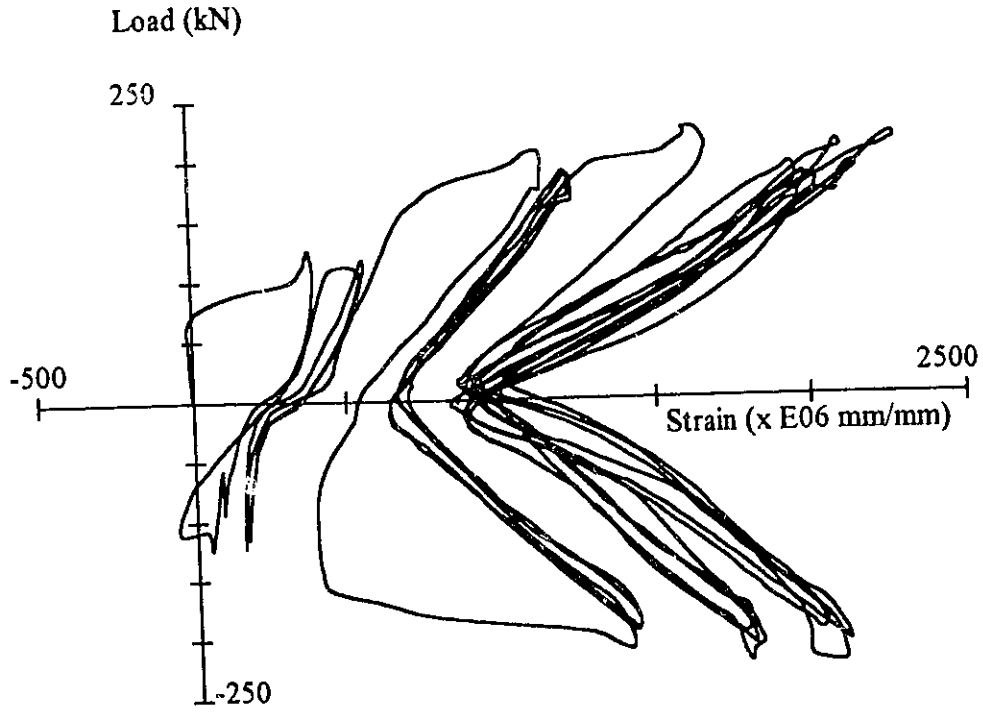

Figure 3.67 Load-Strain Relationship for Horizontal Bar, H823, Wall8

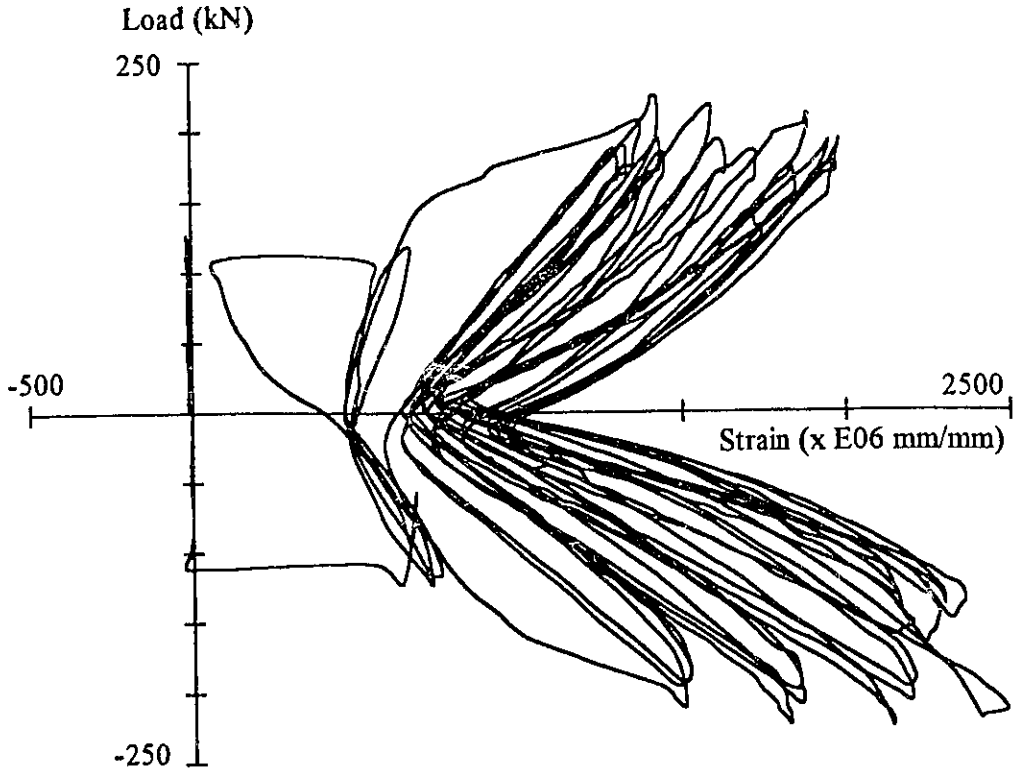

Figure 3.68 Load-Strain Relationship for Horizontal Bar, H832, Wall 8

Chapter 4

Discussion of Test Results

4.1 General

Behaviour of Wall 7 and Wall 8 are discussed in this chapter based on their force-deformation characteristics. Experimentally recorded force-horizontal displacement relationships consist of deflection components due to flexure, shear, anchorage slip, and shear sliding. These displacement components can be either directly obtained or computed from measured data reported in Chapter 3. The magnitude and hysteretic relationship of each displacement component provide insight into the mode of behaviour of walls and importance of each deformation component.

When a crack is formed at the base of the wall, the reinforcing steel crossing the crack is stressed within the foundation. Yielding of the reinforcement at the critical section penetrates into the foundation causing extension of reinforcement within the foundation. This leads to widening of the crack at the wall-footing interface, producing rigid body rotations of the wall. This is referred to as anchorage slip. Horizontal wall deflection due to anchorage slip is a result of the rigid body rotation of the wall with respect to its base. Wall rotation due to anchorage slip is determined from vertical displacement readings recorded at the base. The difference between east and west readings of vertical displacements, shown in Figures 3.35, 3.36, 3.58, and 3.59, measured by potentiometers 1 and 5 (Figures 3.23a and 3.23b) divided by the distance between these potentiometers gives wall rotation due to anchorage slip. The horizontal deflection component due to anchorage slip is then determined from this rotation if multiplied by the wall height. However, the targets for potentiometers 1 and 5 were located slightly above (45 mm) the

wall base. Therefore, these readings contain flexural rotation of the wall within the bottom 45 mm strip. The flexural rotation in this region is computed from recorded data as explained in Appendix A, and subtracted from the readings for anchorage slip, leaving only the deformations due to anchorage slip.

Total wall rotation is determined from vertical displacement readings of the top beam shown in Figures 3.33, 3.34, 3.56, and 3.57 recorded by potentiometers 7 and 9 (Figures 3.23a and 3.23b). The difference in east and west readings divided by the horizontal distance between the potentiometers gives total wall rotation due to flexure and anchorage slip. Flexural rotation is determined from the total by subtracting the rotation due to anchorage slip.

Base sliding is another component of total horizontal deflection. This component was measured using LVDT's installed at west end, center, and east end of the wall (LVDT's 2, 3 and 4 in Figures 3.23a and 3.23b). Due to the formation of wide cracks at later stages of loading near LVDT's 2 and 4 (readings of which are shown in Figures 3.37, 3.38, 3.60, and 3.61) values measured by LVDT No.3 located at the center of the wall base (Figures 3.39 and 3.62) were used as a measure of base slip for both walls.

Shear deformation was determined from concrete strains recorded by a Demec gauge. The strain measurements were taken on all four sides and two diagonals of square grids formed by Demec targets. The wall was divided into horizontal strips along each row of grids, and the grid on the assumed inclined failure plane was used for shear deformation of each strip. It was assumed that the calculated shear deformation for each grid represented the average shear deformation of the corresponding strip. The average value of strains measured along top and bottom horizontal sides of each grid was used as horizontal strain, "ε_x". Similarly the average value of measured strains along the vertical sides of each grid was used as vertical strain "ε_y". Using these two strains and the strain along one of the two diagonals "ε_{l1}", or "ε_{l2}", enabled calculation of shear deformations as shown below;

$$\gamma_{xy} = \varepsilon_x + \varepsilon_y - 2\varepsilon_{l1} \tag{4.1}$$

or

$$\gamma_{xy} = 2\varepsilon_{l2} - (\varepsilon_x + \varepsilon_y) \tag{4.2}$$

$$\Delta_{sh} = \gamma_{xy} h_s \tag{4.3}$$

where "h_s" is the height of each grid. The total shear deformation of the wall was then calculated as the summation of shear deformations for each horizontal strip. The equations used above are approximate in the sense that the angle of principal strains is assumed to be 45 degrees.

The components of horizontal deflections are discussed in the following sections and the summation of all four components is compared with experimentally calculated top horizontal deflection at the center of the top beam.

4.2 Behaviour of Wall 7

4.2.1 Hysteretic Behaviour of Top Horizontal Deflection

Hysteretic force-top horizontal deflection relationship for Wall 7 is shown in Figure 4.1. Displacements shown in this figure represent those of the centerline of the top loading beam and are obtained from linear interpolation between the displacements recorded by potentiometer 10 located at 185 mm above the beam and LVDT 6 located near mid-height, 890 mm above the base. The wall capacity attained in the positive (pushing) and negative (pulling) directions were 380 kN and 370 kN respectively. The hysteresis loops show significant pinching due to shear distortions and shear sliding. The wall strength is maintained until the first cycle at $5\Delta_y$ (1.6 % drift) in the positive direction and the first cycle at $3\Delta_y$ (0.92 % drift) in the negative direction. Significant stiffness degradation is

observed between the consecutive deformation cycles at each level. Although the sustained deformation level may be considered to be adequate in terms of expected drift levels, the energy absorption capacity, as depicted by the area under hysteresis loops, may be considered to be poor due to pinching of the loops.

4.2.2 Horizontal Component of Deflection due to Anchorage Slip Rotation

Experimental moment rotation relationship due to anchorage slip for Wall 7 is shown in Figure 4.2. Envelope curve of load deflection relationship due to anchorage slip is shown in Figure 4.3. The values plotted in the figure includes the correction due to flexural rotation of the wall within the gauge length, as discussed earlier and as explained in Appendix A. The results indicate a steady increase in horizontal deflection due to anchorage slip. Although this component is zero during elastic loading, it's contribution to total deflection becomes 17.0 % at $1\Delta_y$, 18.4 % at $2\Delta_y$, and 12.5 % at $3\Delta_y$. Horizontal displacement due to anchorage slip is in general larger than shear sliding, but smaller than shear and flexural displacements.

4.2.3 Horizontal Component of Deflection due to Flexure

Hysteretic moment-total rotation relationship for Wall 7 is illustrated in Figure 4.4. This relationship was measured at the top of the top loading beam and hence represents total rotations, including those due to flexure and anchorage slip. The loops are more rounded as compared to those observed in Figure 4.1 for horizontal displacements. This is to be expected since both flexural and anchorage slip loops typically exhibit higher energy dissipation characteristics and little pinching. Figure 4.5 depicts moment-rotation relationship for flexure alone, obtained by subtracting that caused by anchorage slip.

Flexural behaviour of Wall 7 was also computed analytically. Plane section analysis was conducted for this purpose for different load stages. Analytically determined curvature diagrams along the wall height are shown in Figure 4.6. Curvature diagrams computed from experimental data are shown in Figure 4.7. These experimental quantities were

computed from moment-flexural rotation relationship by assuming bi-linear variation of curvatures and adopting a procedure similar to that explained in Appendix A. Comparisons of envelope curves for experimental and analytical moment-curvature, moment-rotation and force-flexural displacement relationships are shown in Figures 4.8, 4.9, and 4.10 respectively. The results generally indicate good correlation between the experimental and analytical values. The results further indicate that horizontal displacement due to flexure accounts for approximately 40 % of total wall displacement.

4.2.4 Horizontal Component of Deflection due to Shear Sliding

Hysteretic shear force-shear sliding relationship, measured by LVDT No. 3 located at the center of the wall base is reproduced in Figure 4.11. The relationship indicates symmetrical deformations up to $2\Delta_y$ for both positive and negative loading. Larger values of shear sliding was recorded for negative loading when the wall was pulled beyond $2\Delta_y$. The envelope curve is shown in Figure 4.12. The results indicate that horizontal displacement due to shear sliding along the construction joint is limited to 10 % of total horizontal displacement.

4.2.5 Horizontal Component of Deflection due to Shear Deformations

Shear deformations were measured by Demec gauges at peak displacements of each deformation level. These readings were taken during the first and third cycles of each deformation level for Wall 7. The readings were terminated after the first cycle of $3\Delta_y$ for positive loading and the third cycle of $2\Delta_y$ for negative loading. The limit of the Demec gauge was exceeded beyond these deflection levels. Shear deformations calculated from measured data for Wall 7 are plotted in Figure 4.13, as shear force-shear deformation relationship. The plots indicate some degradation of shear stiffness between the first and third cycle readings. In general shear displacements account for 35 % to 40 % of total horizontal displacement.

4.2.6 Discussion of Deformation Components

The make up of total horizontal displacement for Wall 7 is shown in Figure 4.14 as a function of displacement ductility ratio. Percentage of each deformation component, either directly measured or computed from measured data, is shown in the figure. The results indicate that shear and flexure played equally important roles on response of Wall 7, and each contributed approximately 40 % to the overall displacement. Pinching of force-displacement relationship of total horizontal displacement during the earlier part of testing indicates that shear was a major contributor to overall wall response. Significant increase in pinching of hysteresis loops beyond the 0.92 % drift level suggests that shear sliding was another contributor to the reduction in the energy dissipation mechanism of the wall.

The remaining displacement components made up 20 % of total displacement. Anchorage slip initially accounted for a larger portion of the remaining displacement. Beyond the displacement ductility ratio of 2, however, anchorage slip and shear sliding contributed approximately 10 % each, with a growing influence of shear sliding with increasing inelasticity and number of cycles. The anchorage slip was essentially due to the extension of vertical reinforcement in the foundation, rather than slippage of the same reinforcement. Hence the hysteresis loops were similar to those for flexure, showing capacity for energy dissipation. Shear sliding did not appear to be very significant for Wall 7, and became the governing mode of behaviour after approximately 0.92 % lateral drift. There was, a significant increase in shear sliding going from the first to third cycles within the same total displacement level. This suggests that as the number of inelastic cycles increased, the influence of shear sliding became more dominant. Shear sliding increased up to 40 % of total displacement at about 1.6 % lateral drift, beyond which compression crushing of concrete led to a significant strength decay.

The deformation components recorded, and observation made on overall wall response lead to the conclusion that the wall developed its full flexural capacity associated with flexural yielding. Analytical calculations based on plain section assumption produced

reasonably good agreement with flexural response. The wall also developed significant diagonal tension cracking, and failed due to the crushing of concrete in the highly compressed toe region of the wall. Diagonal compression crushing was observed at the onset of strength decay. While shear sliding along the construction joint was not significant within 0.92 % lateral drift, it became very significant thereafter.

The deformation components presented above were determined separately and individually. The summation of these components are compared with total recorded horizontal displacement in Figure 4.15. The comparison shows a good agreement, indicating that the error involved in some of the assumptions made to compute displacements from measured data is small.

4.3 Behaviour of Wall 8

4.3.1 Hysteretic Behaviour of Top Horizontal Deflection

Hysteretic force-top horizontal deflection relationship for Wall 8 is shown in Figure 4.16. Displacements shown in this figure represent those of the centerline of the top loading beam and are obtained from linear interpolation between the displacements recorded by potentiometer 10 located at 185 mm above the beam and LVDT 6 located near mid-height, 890 mm above the base. The wall capacity attained in the positive (pushing) and negative (pulling) directions were 225 kN and 224 kN respectively. The hysteresis loops show pinching due to shear distortions and shear sliding at later stages of loading, particularly beyond $3\Delta_y$ deformation level. The wall strength is maintained until the first cycle at $4\Delta_y$ (1.83 % drift) in both positive and negative directions. Significant stiffness degradation is observed between the consecutive deformation cycles at each level. The sustained deformation level may be considered to be adequate in terms of expected drift levels. Beyond the drift level of 1.83 % the energy absorption capacity, as depicted by the area under hysteresis loops, may be considered to be poor due to pinching of the loops.

4.3.2 Horizontal Component of Deflection due to Anchorage Slip Rotation

Experimental moment rotation relationship due to anchorage slip for Wall 8 is shown in Figure 4.17. Envelope curve of load deflection relationship due to anchorage slip is shown in Figure 4.18. The values plotted in the figure includes the correction due to flexural rotation of the wall within the gauge length, as discussed earlier and as explained in Appendix A. The results indicate a steady increase in horizontal deflection due to anchorage slip. Although this component is zero during elastic loading, it's contribution to total deflection becomes 16.3 % at $1\Delta_y$, 19.2 % at $2\Delta_y$, and 18.1 % at $3\Delta_y$. Horizontal displacement due to anchorage slip is in general larger than shear sliding, but smaller than shear and flexural displacements.

4.3.3 Horizontal Component of Deflection due to Flexure

Hysteretic moment-total rotation relationship for Wall 8 is illustrated in Figure 4.19. This relationship was measured at the top of the top loading beam and hence represents total rotations, including those due to flexure and anchorage slip. The loops are more rounded as compared to those observed in Figure 4.16 for horizontal displacements. This is to be expected since both flexural and anchorage slip loops typically exhibit higher energy dissipation characteristics and little pinching. Figure 4.20 depicts moment-rotation relationship for flexure alone, obtained by subtracting that caused by anchorage slip.

Flexural behaviour of Wall 8 was also computed analytically. Plane section analysis was conducted for this purpose for different load stages. Analytically determined curvature diagrams along the wall height are shown in Figure 4.21. Curvature diagrams computed from experimental data are shown in Figure 4.22. These experimental quantities were computed from moment-flexural rotation relationship by assuming bi-linear variation of curvatures and adopting a procedure similar to that explained in Appendix A. Comparisons of envelope curves for experimental and analytical moment-curvature, moment-rotation and force-flexural displacement relationships are shown in Figures 4.23, 4.24, and 4.25 respectively. The results generally indicate a very good correlation between

the experimental and analytical values. The results further indicate that horizontal displacement due to flexure accounts for approximately 40 % to 45 % of total wall displacement.

4.3.4 Horizontal Component of Deflection due to Shear Sliding

Hysteretic shear force-shear sliding relationship, measured by LVDT No. 3 located at the center of the wall base is reproduced in Figure 4.26. The relationship indicates near symmetrical deformations for both positive and negative loading. The envelope curve is shown in Figure 4.27. The results indicate that horizontal displacement due to shear sliding along the construction joint is limited to 8 % of total horizontal displacement.

4.3.5 Horizontal Component of Deflection due to Shear Deformations

Shear deformations were measured by Demec gauges at peak displacements of each deformation level. These readings were taken during the first cycle of each deformation level for Wall 8. The readings were terminated after the first cycle of $4\Delta_y$ for positive loading and the first cycle of $2\Delta_y$ for negative loading. The limit of the Demec gauge was exceeded beyond these deflection levels. Shear deformations calculated from measured data for Wall 8 are plotted in Figure 4.28, as shear force-shear deformation relationship. In general shear displacement accounts for 25 % to 35 % of total horizontal displacement.

4.3.6 Discussion of Deformation Components

The make up of total horizontal displacement for Wall 8 is shown in Figure 4.29 as a function of displacement ductility ratio. Percentage of each deformation component, either directly measured or computed from measured data, is shown in the figure. The results indicate that flexure and shear played important roles on response of Wall 8, and contributed approximately 45 % and 35 % to the overall displacement respectively. Limited pinching observed in the force-displacement relationship of total horizontal displacement during the earlier part of testing indicates that shear was a contributor to overall wall response although its contribution was not as high as that for Wall 7. This

may be explained by the higher aspect ratio of Wall 8. Significant increase in pinching of hysteresis loops beyond the 1.83 % drift level suggests that shear sliding was another contributor to the reduction in the energy dissipation mechanism of the wall at later stages of loading.

The remaining displacement components made up 20 % of total displacement. Anchorage slip accounted for a larger portion of the remaining displacement. The anchorage slip was essentially due to the extension of vertical reinforcement in the foundation, rather than slippage of the same reinforcement. Hence the hysteresis loops were similar to those for flexure, showing capacity for energy dissipation. Shear sliding appear to increase at a constant rate with displacement ductility for Wall 8, and became significant after approximately 1.83 % lateral drift. There was a significant increase in shear sliding going from the first to third cycles within the same total displacement level. This suggests that as the number of inelastic cycles increased, the influence of shear sliding became more dominant. Shear sliding increased up to 35 % of total displacement at about 1.83 % lateral drift, beyond which compression crushing of concrete led to a significant strength decay. However, within the expected level of drift, the contribution of shear sliding was negligibly small.

The deformation components recorded and observation made on overall wall response lead to the conclusion that the wall developed its full flexural capacity associated with flexural yielding. Analytical calculations based on plain section assumption produced reasonably good agreement with flexural response. The contribution of flexure to overall wall response increased with increasing inelasticity. The wall also developed significant diagonal tension cracking, and failed due to the crushing of concrete in the highly compressed toe region of the wall. Diagonal compression crushing was observed at the onset of strength decay. The contribution of shear to overall wall response decreased with increasing level of deformations and reduced to 25 % at approximately $3\Delta_y$ (1.4 % drift).

While shear sliding along the construction joint was not significant within 1.4 % lateral drift, it increased gradually thereafter.

The deformation components presented above were determined separately and individually. The summation of these components are compared with total recorded horizontal displacement in Figure 4.30. The comparison shows a good agreement, indicating that the error involved in some of the assumptions made to compute displacements from measured data is small.

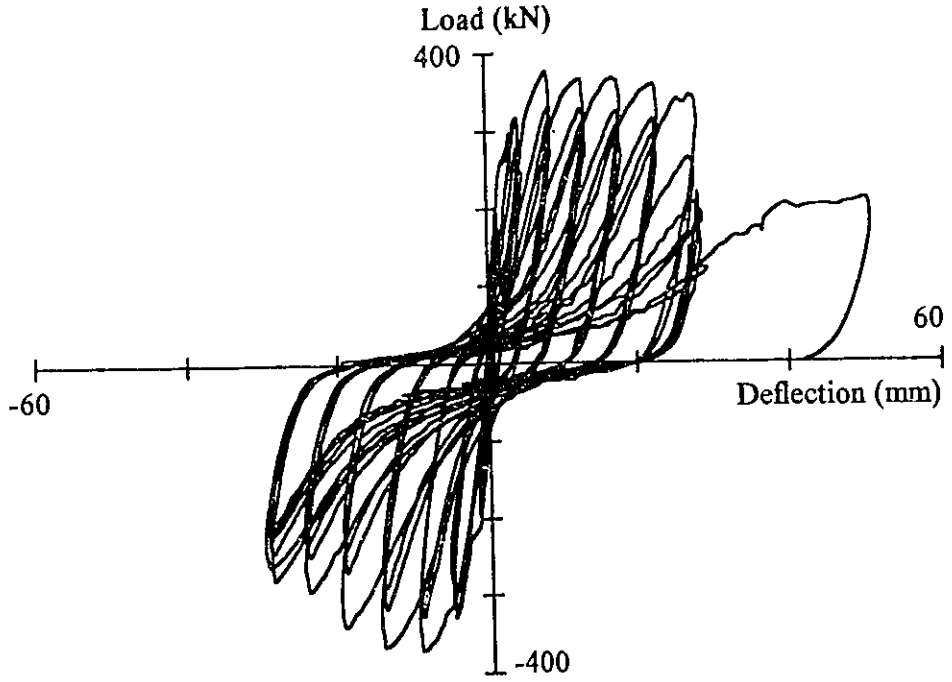

Figure 4.1 Hysteretic Load-Top Horizontal Deflection for Wall 7
at the Center of the Top Beam

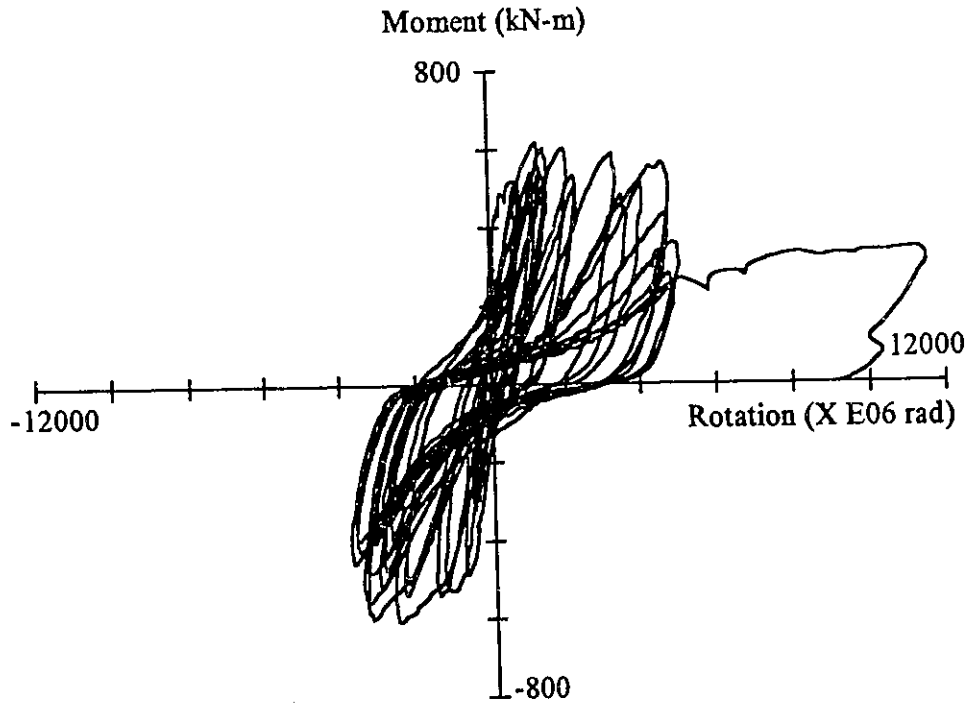

Figure 4.2 Hysteretic Moment Anchorage Slip Rotation for Wall 7

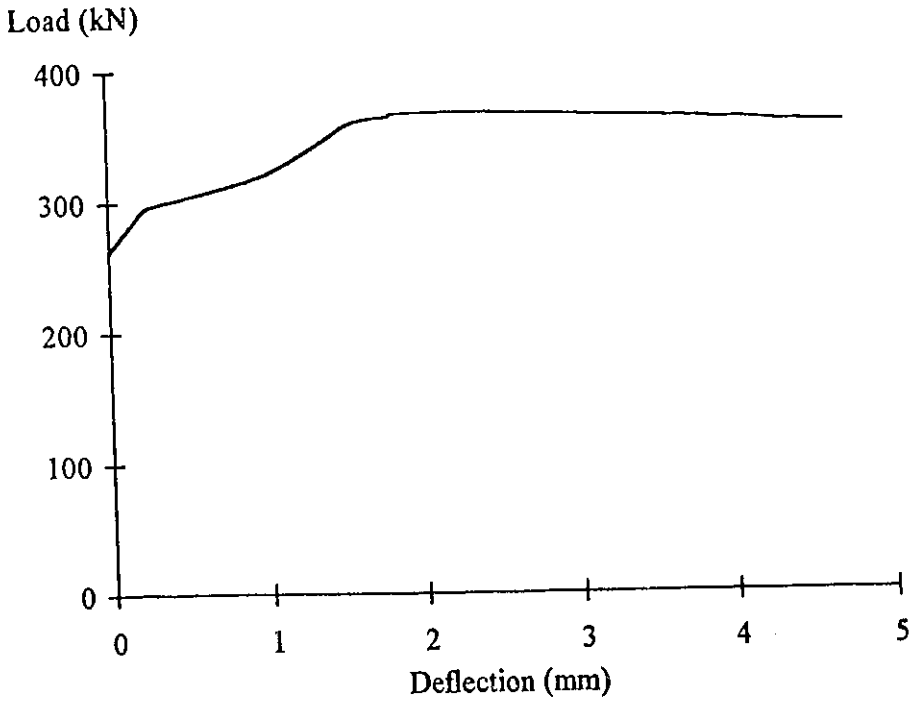

Figure 4.3 Horizontal Deflection due to Anchorage Slip for Wall 7

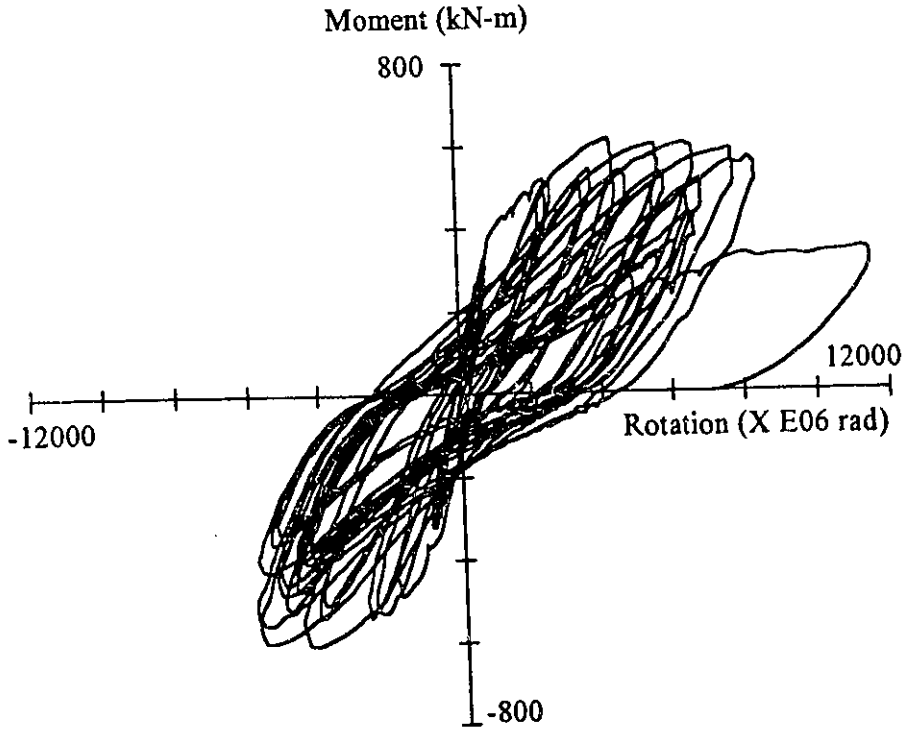

Figure 4.4 Hysteretic Moment Total Rotation for Wall 7

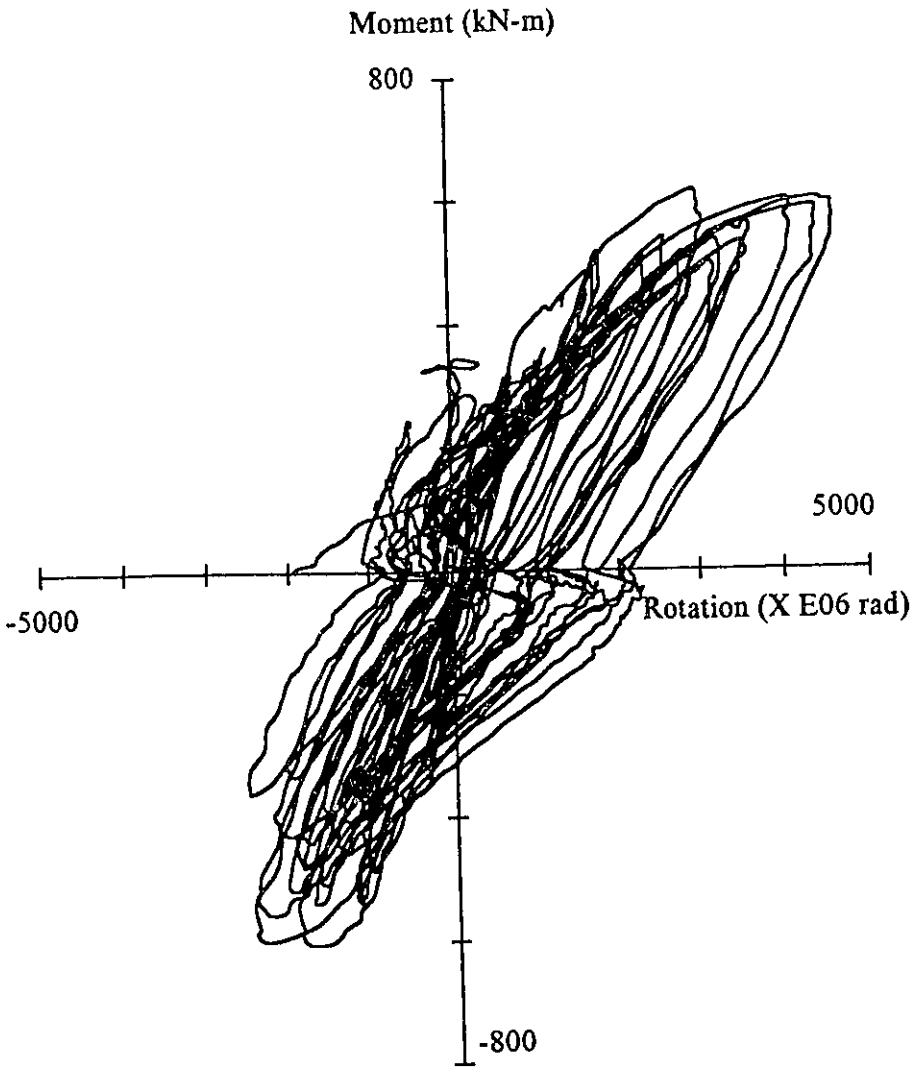

Figure 4.5 Hysteretic Moment Flexural Rotation for Wall 7

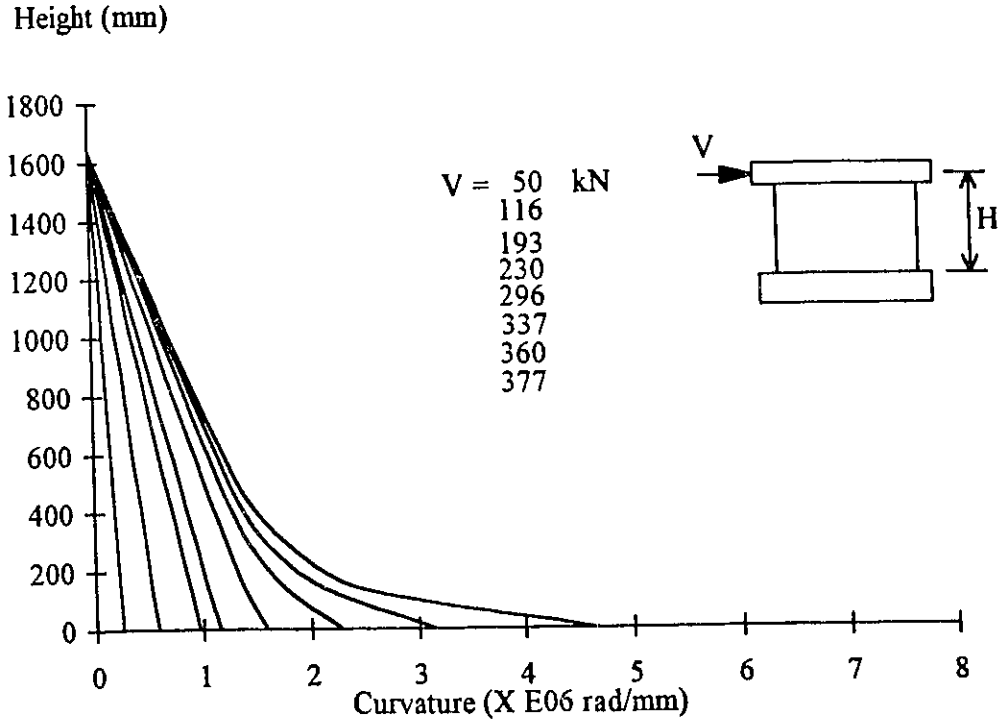

Figure 4.6 Analytical Curvature Distribution along the Height of Wall 7

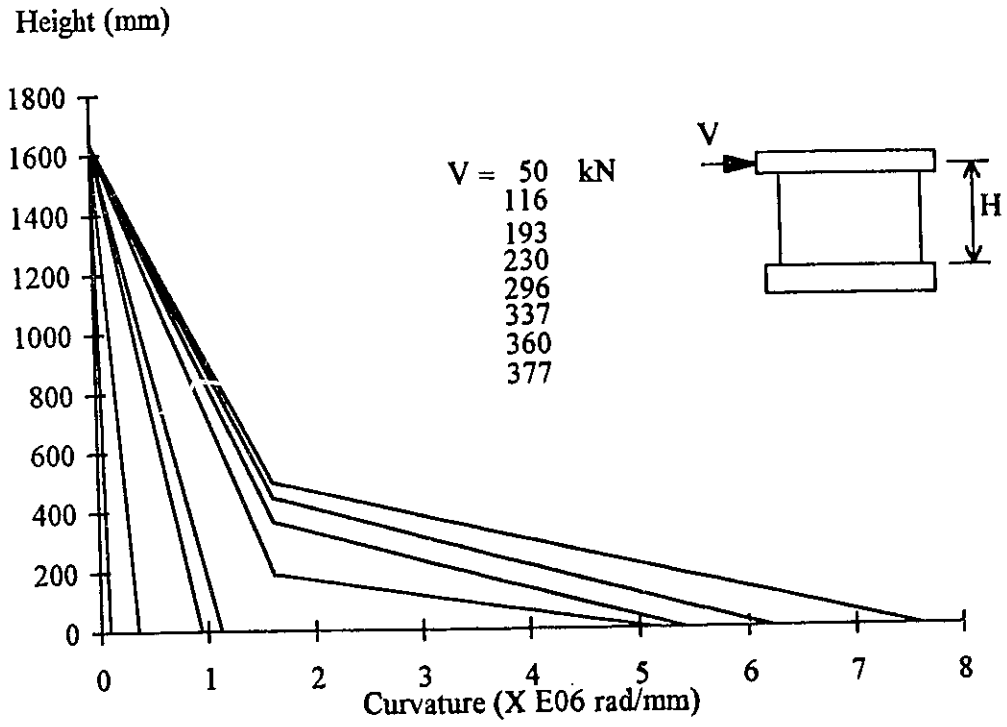

Figure 4.7 Experimental Curvature Distribution along the Height of Wall 7

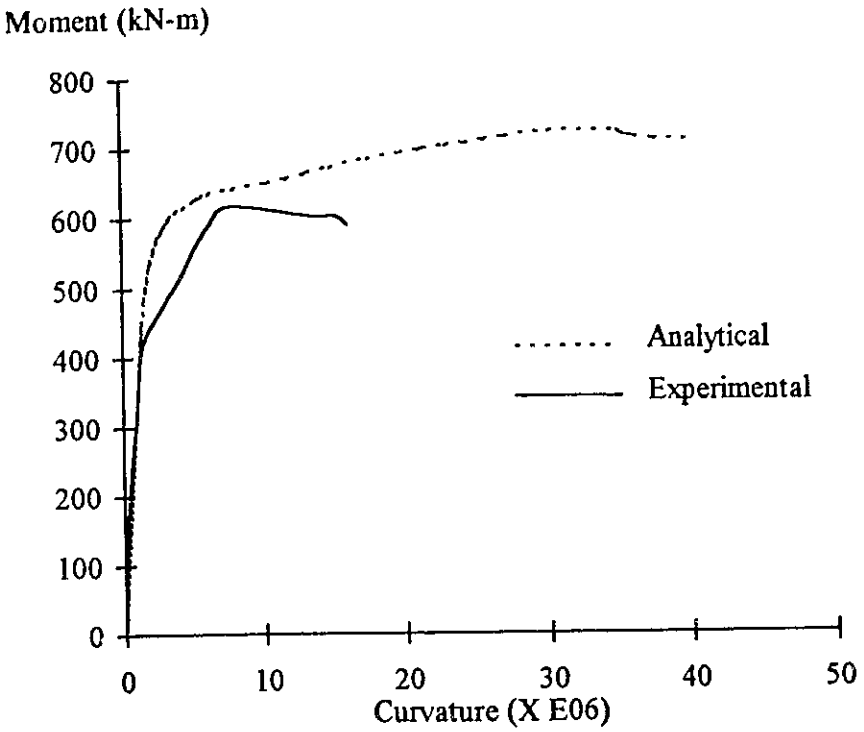

Figure 4.8 Moment Curvature Diagram for Wall 7

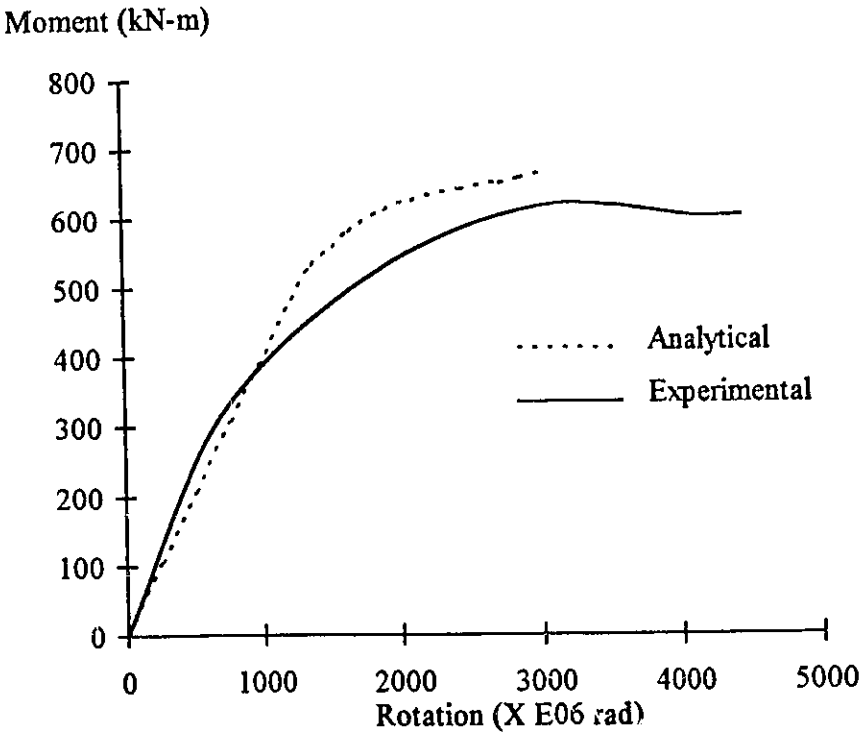

Figure 4.9 Moment Flexural Rotation Diagram for Wall 7

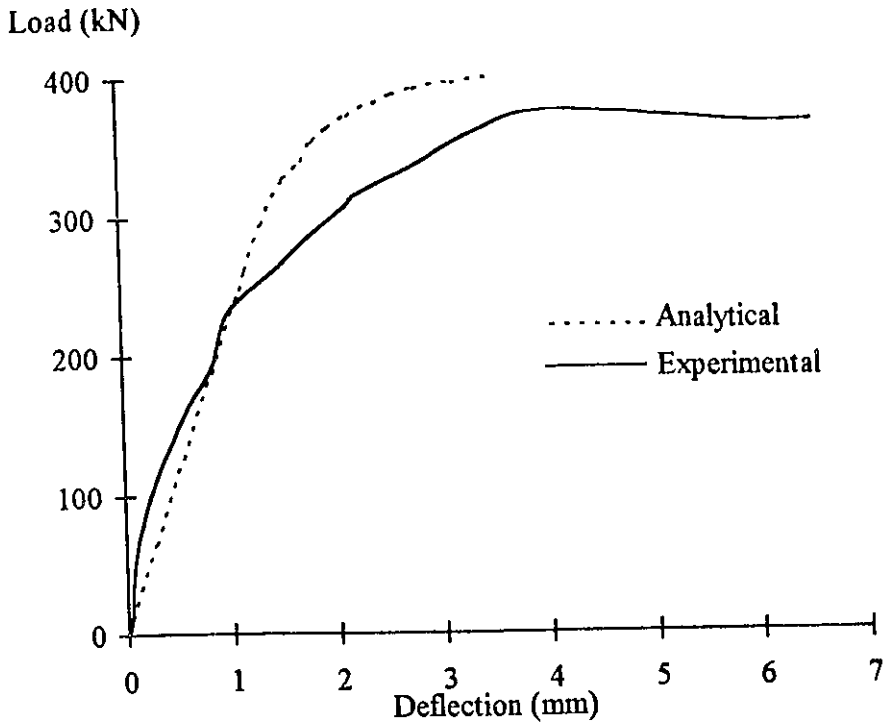

Figure 4.10 Force-Flexural Deflection Diagram for Wall 7

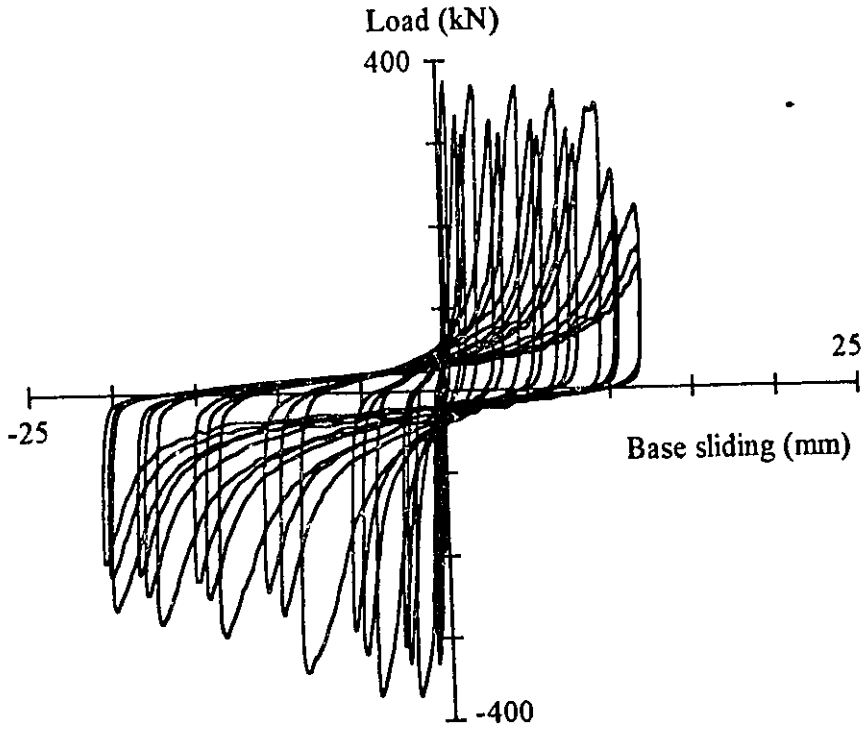

Figure 4.11 Load Center Base Sliding for Wall 7

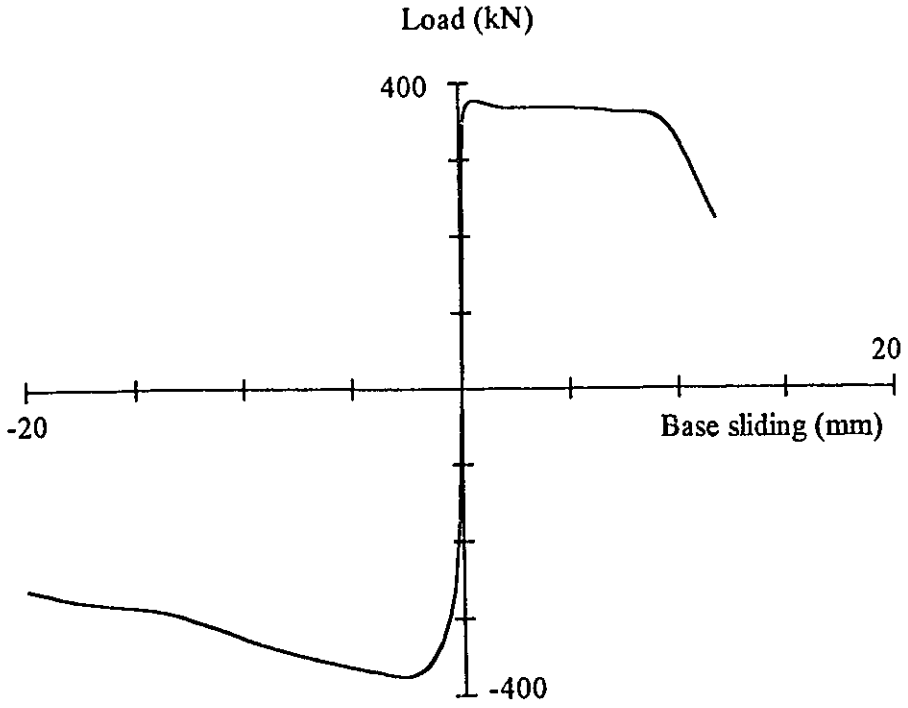

Figure 4.12 Experimental Load Base Sliding Diagram for Wall 7

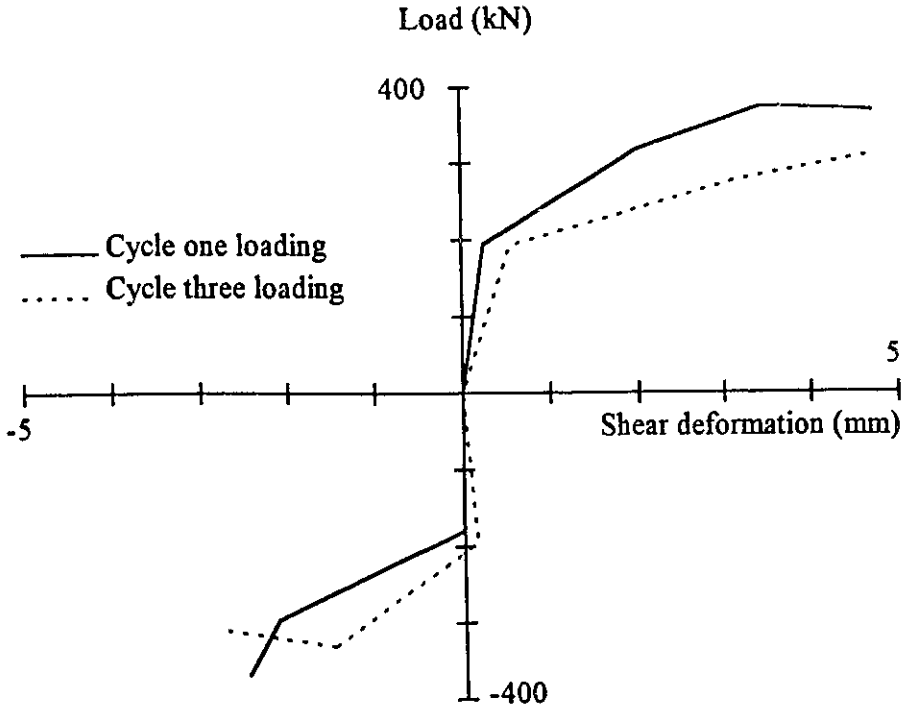

Figure 4.13 Experimental Load Shear Deformation Diagram for Wall 7

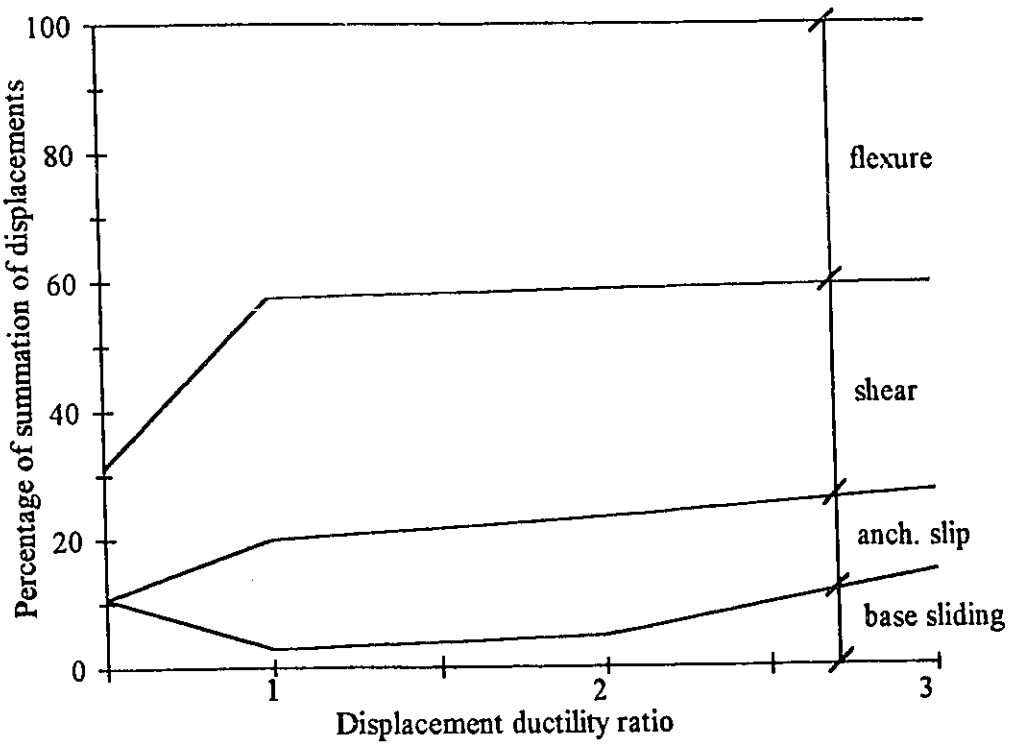

Figure 4.14a Horizontal Displacement Components for Wall 7 , Cycle 1

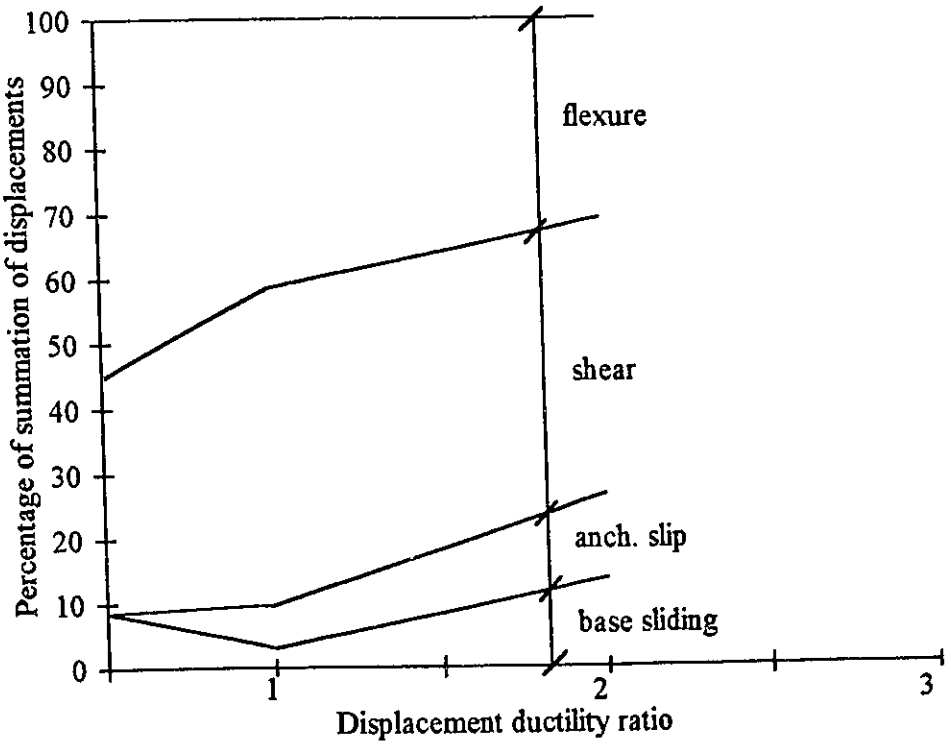

Figure 4.14b Horizontal Displacement Components for Wall 7 , Cycle 3

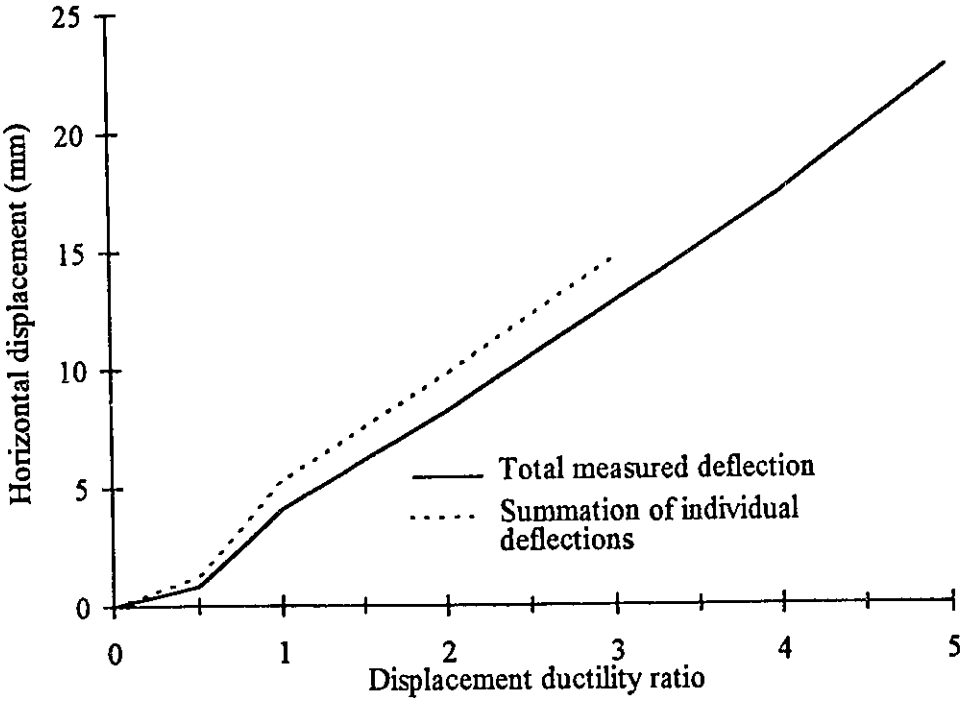

Figure 4.15a Experimental Horizontal Displacements for Wall 7, Cycle 1

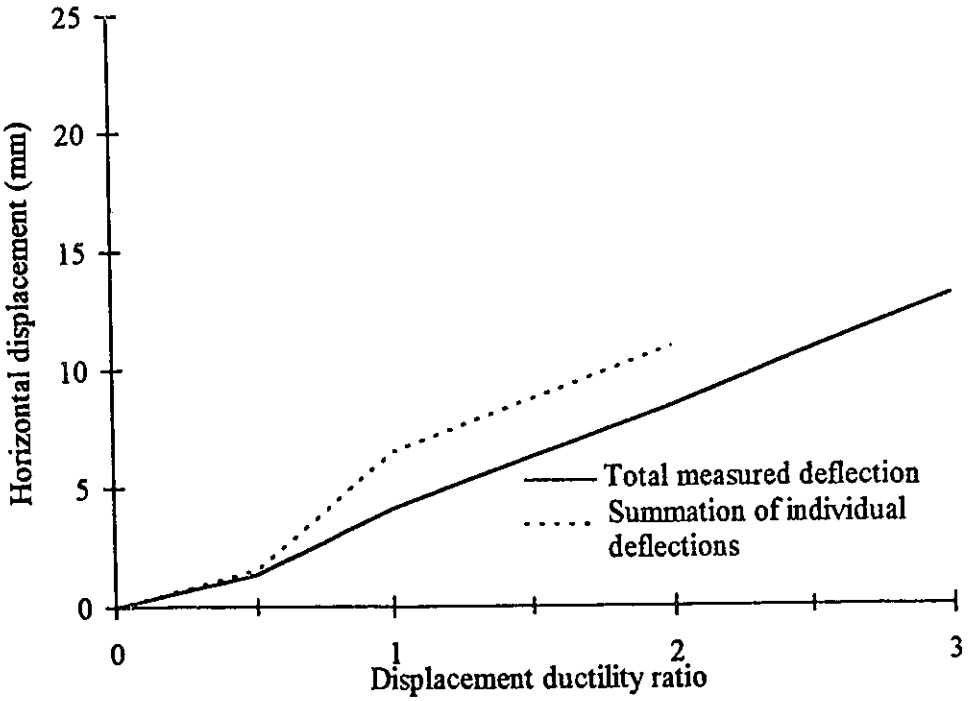

Figure 4.15b Experimental Horizontal Displacements for Wall 7, Cycle 3

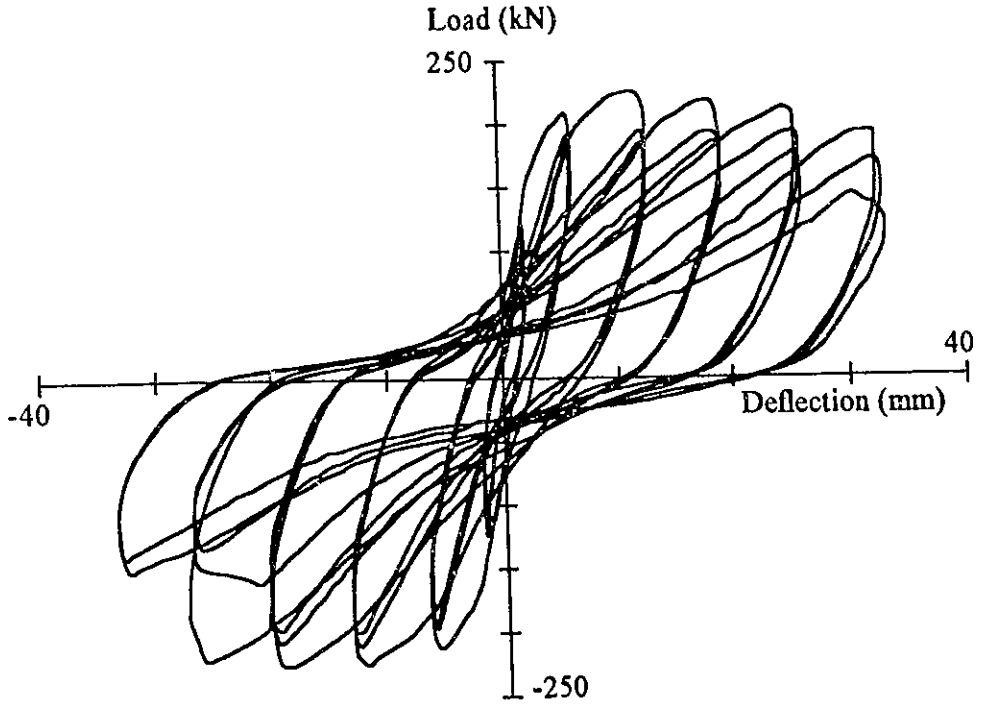

Figure 4.16 Hysteretic Load Top Horizontal Deflection for Wall 8 at the Center of the Top Beam

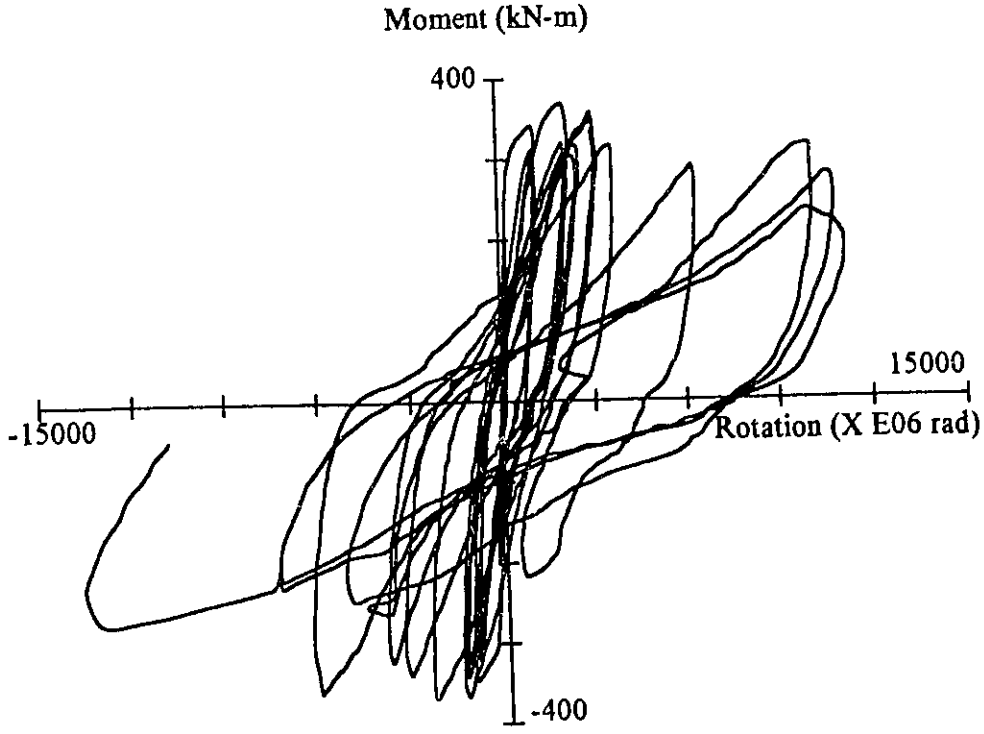

Figure 4.17 Hysteretic Moment Anchorage Slip Rotation for Wall 8

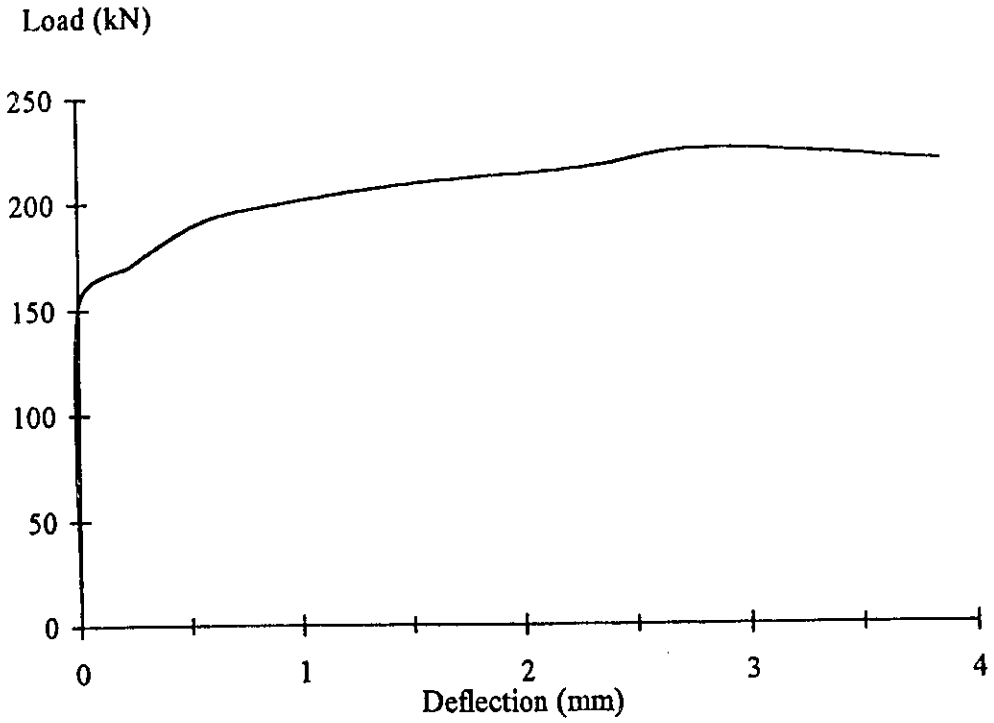

Figure 4.18 Horizontal Deflection due to Anchorage Slip for Wall 8

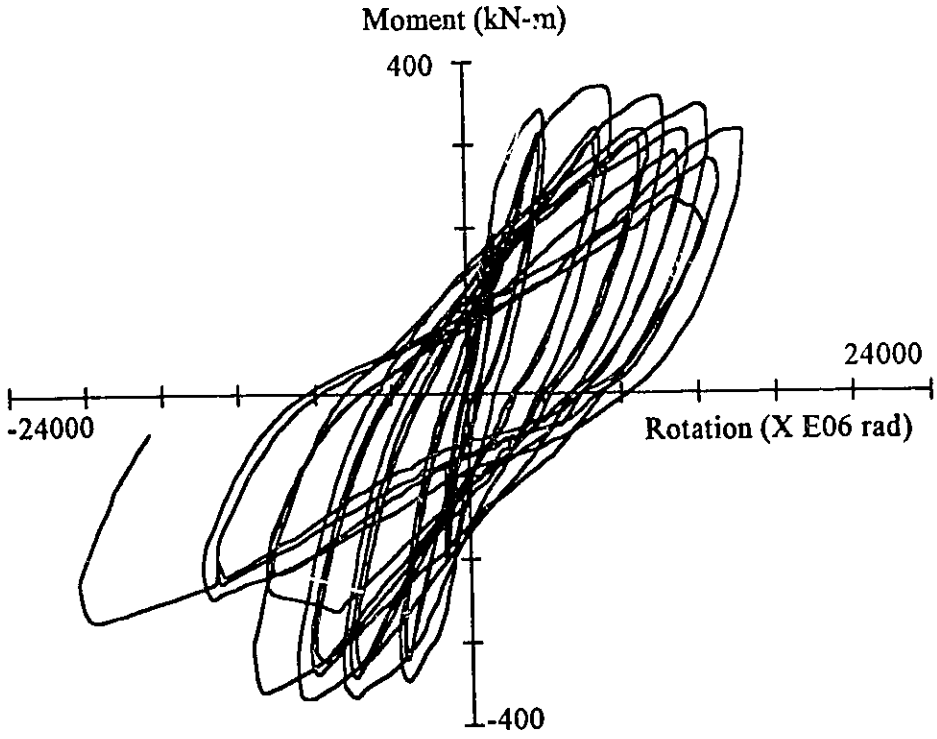

Figure 4.19 Hysteretic Moment Total Rotation for Wall 8

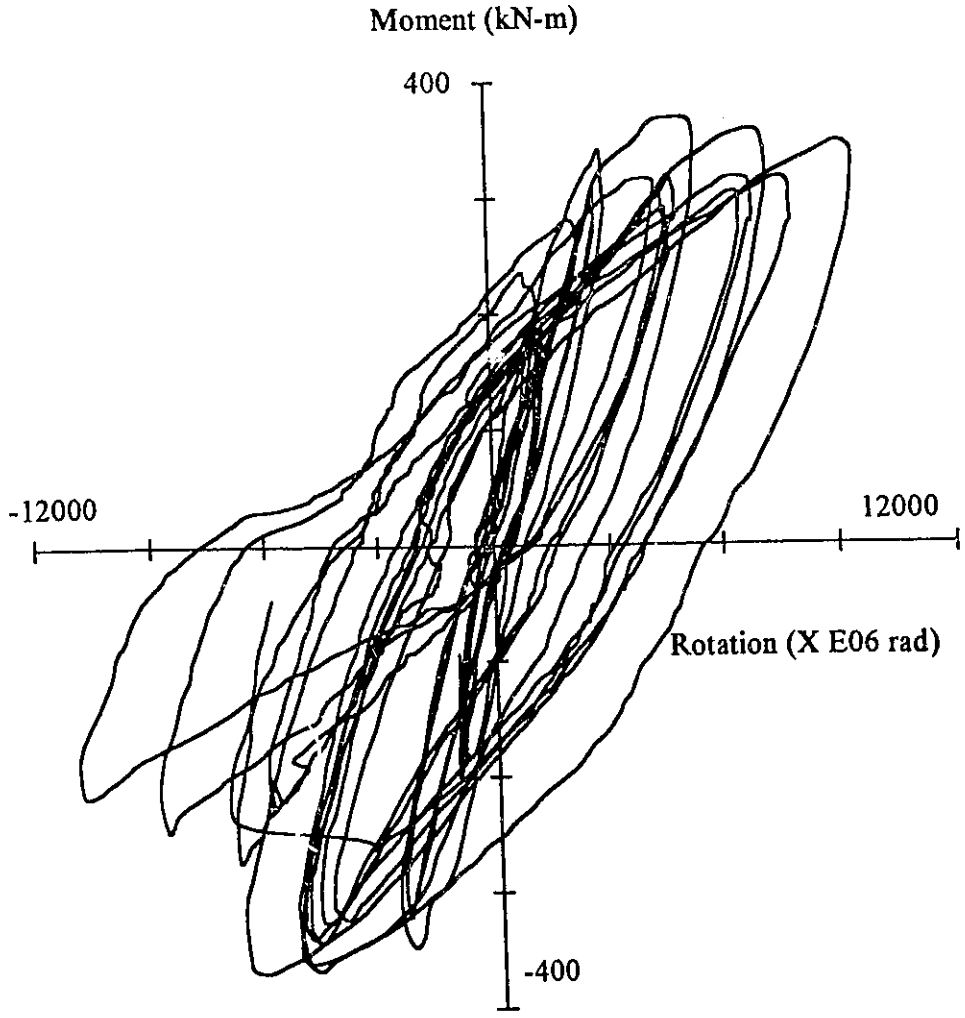

Figure 4.20 Hysteretic Moment Flexural Rotation for Wall 8

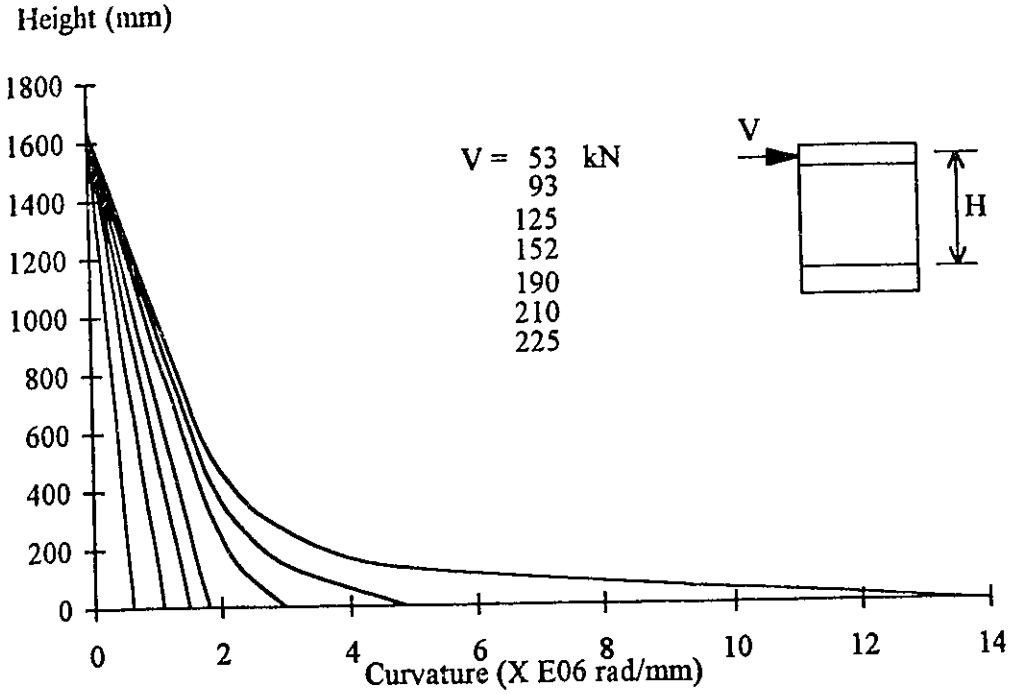

Figure 4.21 Analytical Curvature Distribution along the Height of Wall 8

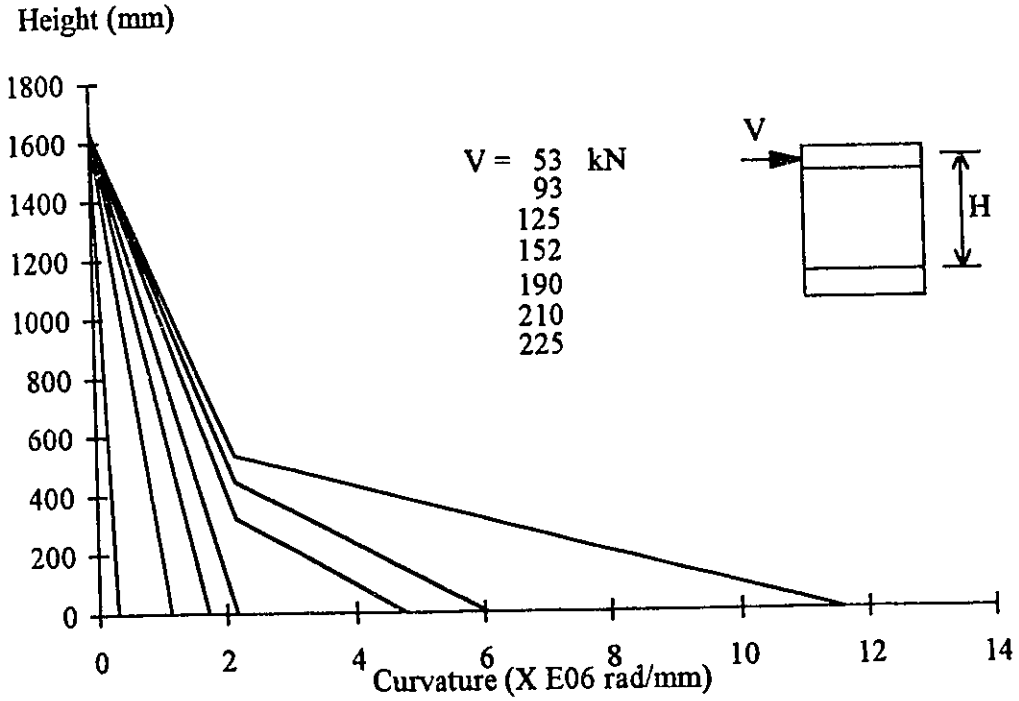

Figure 4.22 Experimental Curvature Distribution along the Height of Wall 8

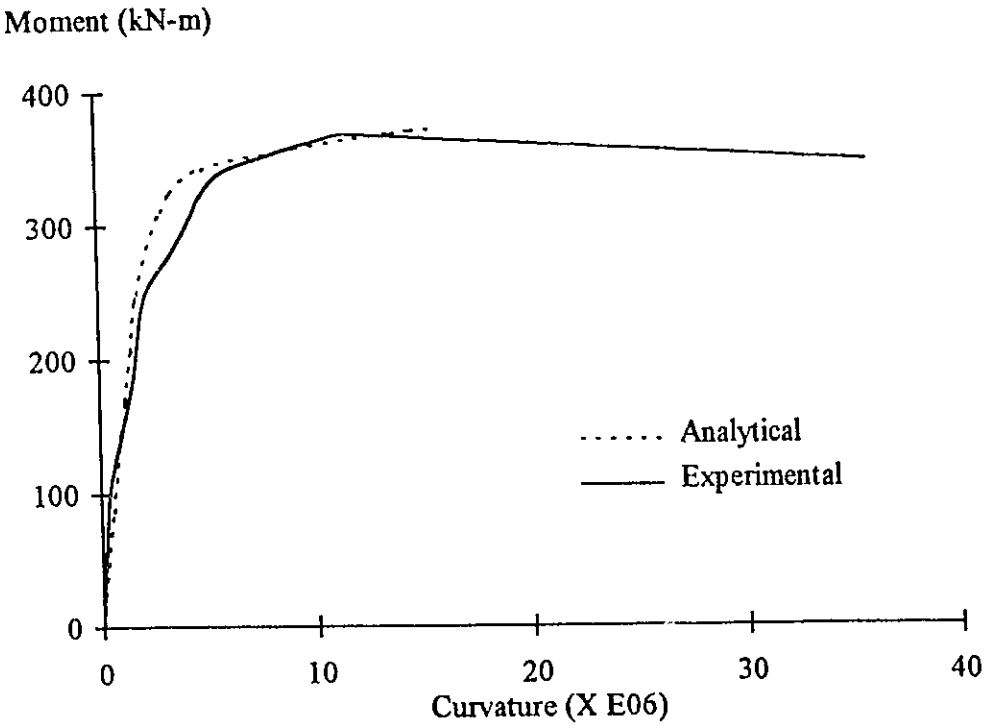

Figure 4.23 Moment Curvature Diagram for Wall 8

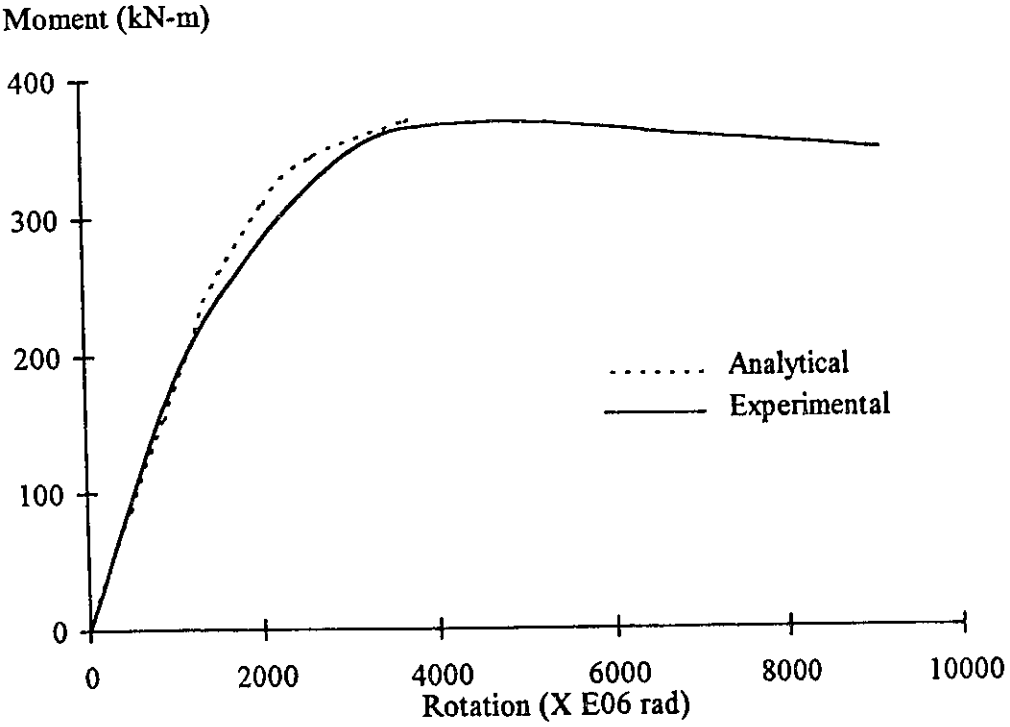

Figure 4.24 Moment Flexural Rotation Diagram for Wall 8

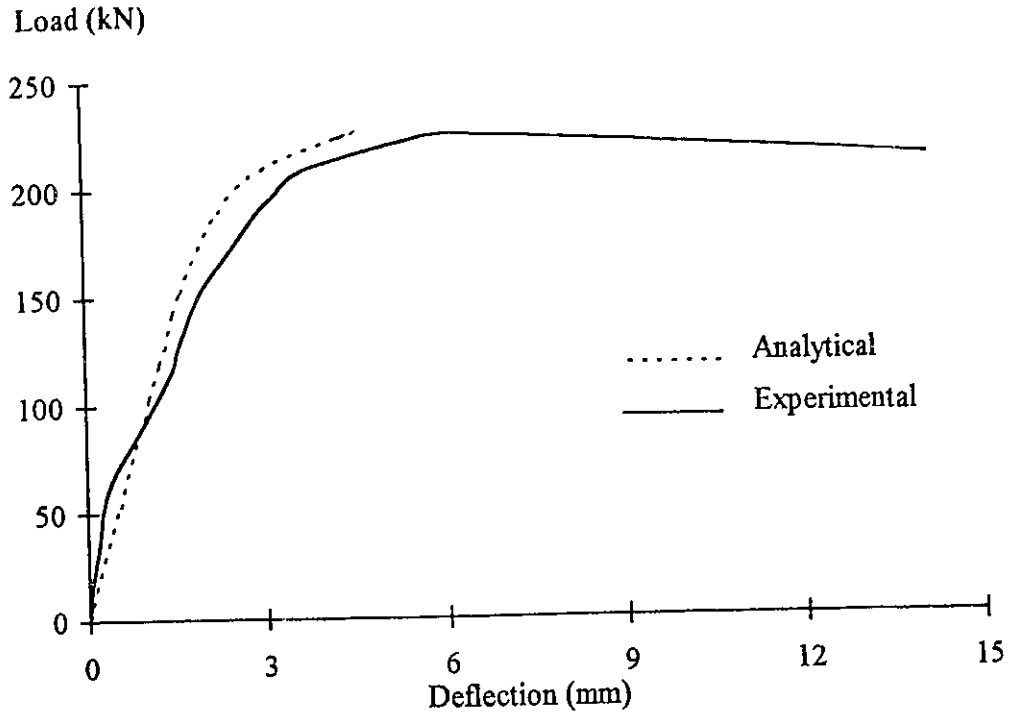

Figure 4.25 Load Flexural Deflection Diagram for Wall 8

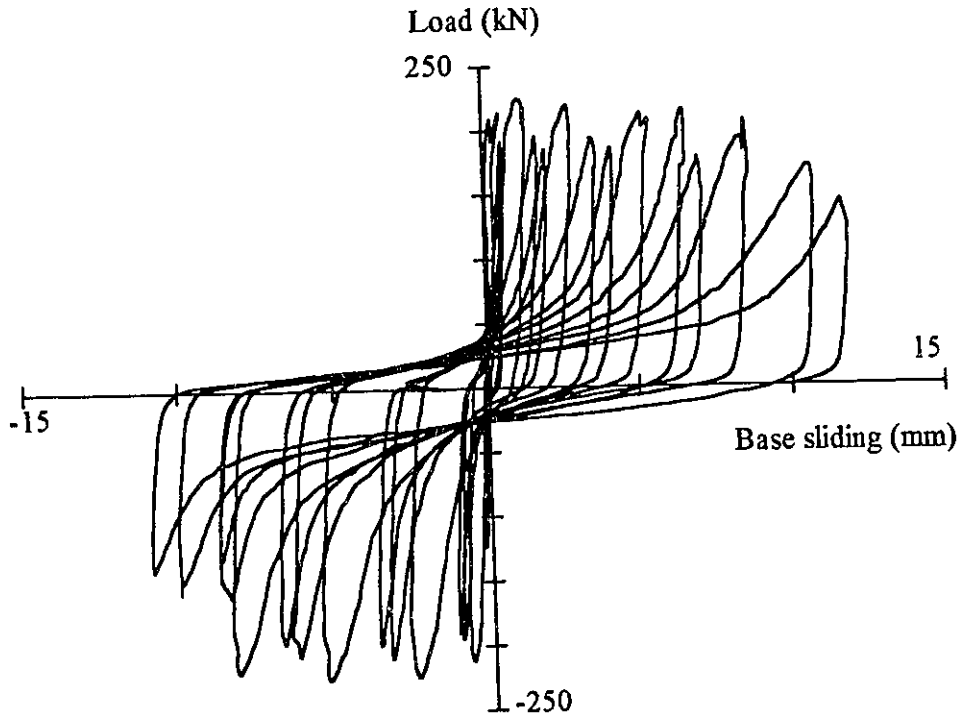

Figure 4.26 Load Center Base Sliding for Wall 8

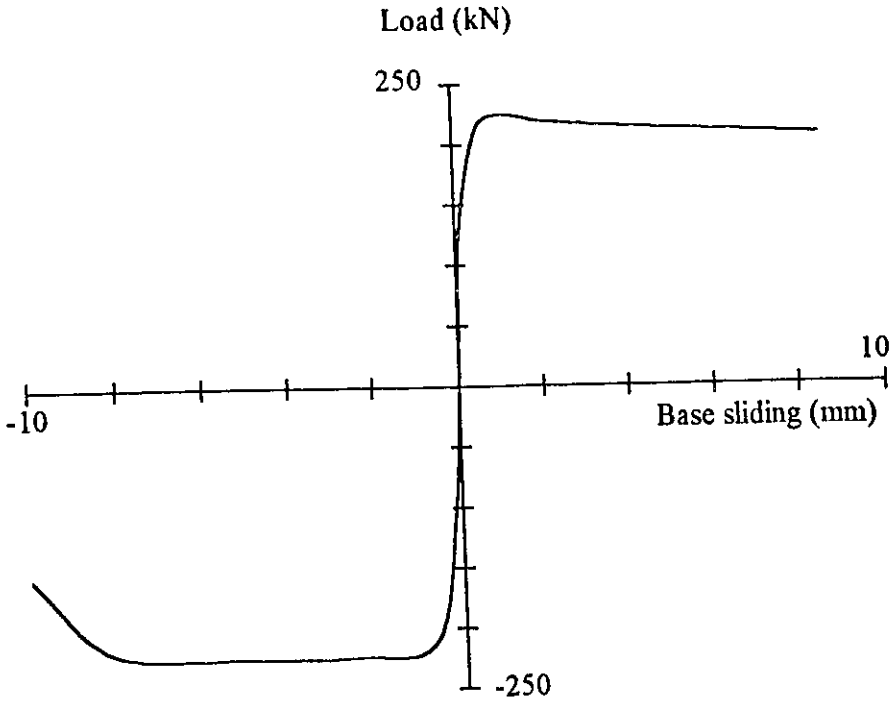

Figure 4.27 Experimental Load Base Sliding Diagram for Wall 8

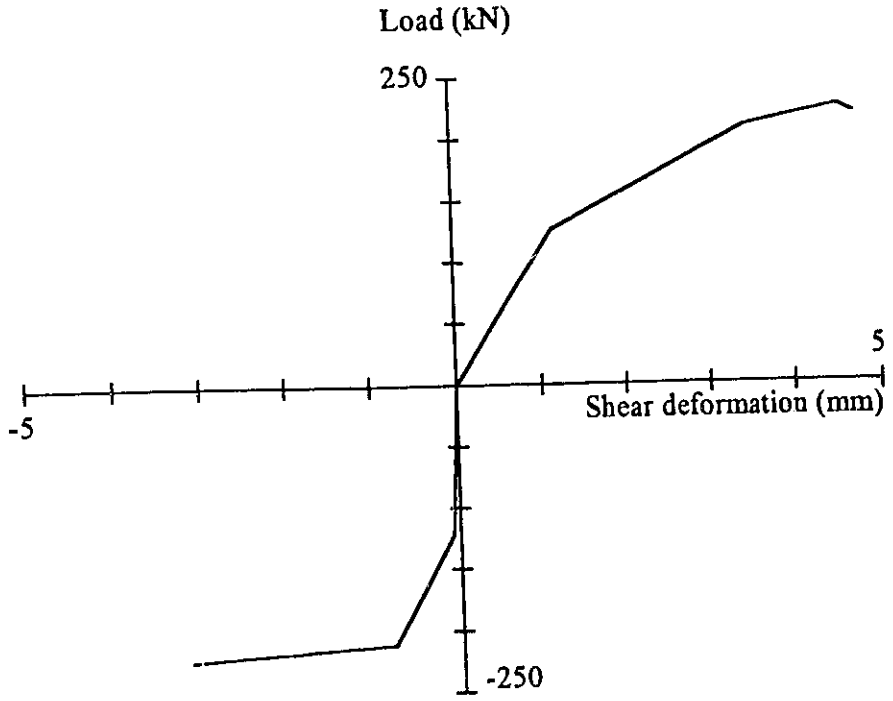

Figure 4.28 Experimental Load Shear Deformation Diagram for Wall 8

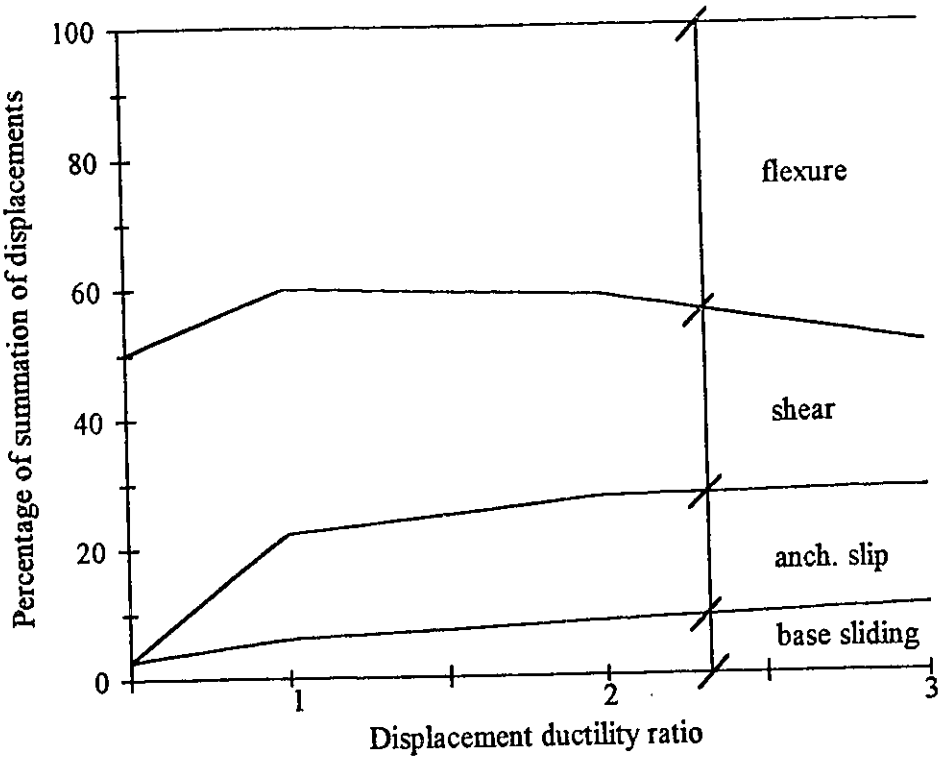

Figure 4.29 Horizontal Displacement Components for Wall 8

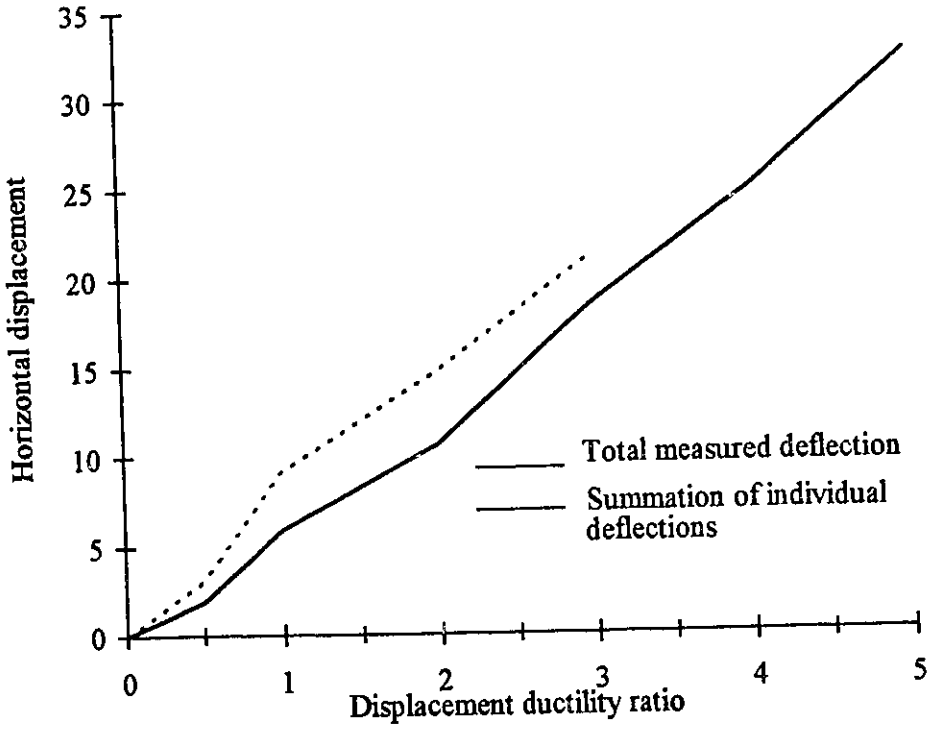

Figure 4.30 Experimental Horizontal Displacements for Wall 8

Chapter 5

Development of Analysis Procedure for Low-Rise Shear Walls

5.1 General

Behaviour of low-rise shear walls is generally determined by approximate empirical expressions. Recently, significant advances have been made in more accurate and elaborate non-linear finite element analyses of concrete shear walls. While the former has obvious limitations and lack of accuracy, the latter requires significant computational effort and analytical expertise for reliable results which hinders its applicability as a design tool in practice. Therefore, there is need for a reasonably simple and yet rational analytical procedure that combines the effects of shear, flexure and axial load on low-rise shear walls. Such a procedure may be used for design. It may also be used for establishing force-deformation relationships of shear dominant low-rise walls within the inelastic range.

A new procedure has been developed for analysis of low-rise shear walls under combined shear, flexure and axial load, based on equilibrium, compatibility, and material models. The procedure has been verified against available test data. This chapter contains a discussion and presentation of the analytical procedure, as well as the verification of the procedure against experimental data.

5.2 Proposed Analytical Procedure

The mechanisms of load resistance and governing failure modes in low-rise shear walls are discussed in Chapter 3. It is clear that the mechanisms of load resistance, and the behaviour of

low-rise shear walls are different than those for flexure dominant beams and tall structural walls, as well as shear dominant deep beams. Therefore, conventional methods used for analysis of beams and tall walls are not applicable to low-rise walls.

The first step of the proposed approach involves determination of potential failure planes. In low-rise shear walls the potential failure planes typically include the horizontal plane at the base, and an inclined plane with an inclination of 45 degrees or smaller, between the corner of the wall at the loading end and the beginning of the compression zone at the base. Figure 5.1 illustrates the potential failure planes. The horizontal plane at the base is critical against flexure and sliding shear, whereas the inclined plane is critical against diagonal tension caused by shear and flexure. Compression crushing of concrete may occur either at the toe near the base, or along the compression strut parallel to the inclined failure plane. Figure 5.2 illustrates the critical concrete struts in walls with different aspect ratios. It is assumed that premature failures of walls due to sliding along the base, lift-up and tilting due to poor foundation design, failure of the improperly detailed boundary elements due to the buckling of longitudinal reinforcement, and out of plane instability are prevented. This implies that the failure occurs within the wall panel either due to flexure at the horizontal section near the base, or due to diagonal tension and/or diagonal compression, along the inclined failure plane. Therefore, the analysis procedure includes plane section analysis of the horizontal wall section at the base, inclined section analysis of the potential failure plane, and checking for compression crushing of concrete within the concrete strut. The strains obtained from the inclined section analysis lead to the computation of shear distortions and shear displacements of the wall.

Plane Section Analysis

Under seismic induced inertia loads, walls with uniform vertical reinforcement throughout the height of the wall panel, have their critical sections for flexure at the base where bending stresses are highest. Analysis of this section under pure bending, using the conventional plane section analysis produce good correlations with test data (Park and Paulay, 1975, Paulay, 1981, Paulay et. al, 1982). Furthermore, although the assumption of plane sections before

bending remaining plane after bending has been verified extensively for beams and columns, or members with high aspect ratios in general, it has also been shown by Paulay et. al, (1982), Pilette (1988), and Wasiewicz (1988) that the same assumption holds true for walls with low aspect ratios. Figure 5.3 shows experimentally recorded strain profiles at different stages of loading for Wall 4 tested by Pilette (Pilette, 1988). Figure 5.4 shows strain profiles in flexural reinforcement and moment curvature relationship for Wall 6 (Wasiewicz, 1988). A comparison of experimental and analytical moment rotation diagrams for Wall 1 tested by Wiradinata (Wiradinata, 1985) is shown in Figure 5.5. These figures indicate that the flexural capacity of low-rise walls can be established by the conventional flexural analysis of the horizontal plane at the base, and that plane sections do remain approximately plane after bending at the wall base section.

Flexural analysis of the critical section provides strain and stress distributions along the section near the base, as well as bending moment resistances at each stage of loading. The bending resistance is related to the applied shear force through equilibrium, and hence the magnitude of applied shear force associated with bending resistance can be established for each stage of loading. The flexural analysis also defines the width of the compression zone near the base for each stage of loading. This information sets the stage for inclined section analysis under diagonal tension and compression, which leads to the computation of wall capacity under combined shear, flexure, and axial load, as well as inelastic deformations due to shear.

Inclined Section Analysis

The wall section considered in "inclined section analysis" includes the inclined potential failure plane and the compression zone of the horizontal section near the base. Figure 5.6 shows the free-body diagram of the portion of a wall element cut by the inclined plane. Internal forces along the plane are also indicated, and can be computed using strain compatibility, material stress-strain relationships and equilibrium of forces. This can be done if the strain profile along the inclined section is known.

Analysis of experimental data obtained from tests of large scale shear walls indicate that the initial inclination of diagonal tension cracks is approximately 45 degrees, and that these cracks are captured by top and bottom beams which do not permit further straining near the beams. This results in an increase of horizontal strains in the middle portions of walls. Experimentally measured strains on horizontal reinforcement confirm that the walls are in fact strained high in the middle relative to top and bottom regions (Synge, 1980). This is also illustrated by Figures 5.7 and 5.8 which show experimentally measured horizontal strains along the inclined failure plane of Wall 7 and Wall 8 recorded by Demec gauges during testing, as part of this research program. Although the strains are relatively small near the beams, they are not zero.

A strain profile perpendicular to the inclined section is assumed based on the experimental observations. The strain profile has non-zero strains at the ends and maximum strain at mid-height, and the variation between these strains is assumed to be linear for simplicity. Figure 5.9 illustrates the assumed distribution of strains perpendicular to the inclined section. The end strains are computed from boundary conditions. The mid-height strain is determined through iterations such that equilibrium is satisfied. Hence the procedure is analogous to the familiar sectional analysis for flexure.

The strain at one end of the inclined section, coinciding with neutral axis for the horizontal section is labelled as ε_{1b}, and is computed such that the strain compatibility in the vertical direction is maintained, i.e. strain is zero in the vertical direction ($\varepsilon_v = 0.0$). Mohr's circle of strains, shown in Figure 5.10 can be used to compute ε_{1b} using the boundary condition of ε_v being equal to zero. The other strain needed for this computation is the strain parallel to the inclined section ε_{2b}. This strain is determined from the stress-strain relationship of concrete in the strut and the stress f_{c2} computed in the previous stage of loading as explained later under "Check for Concrete Crushing in Compression Strut". For the first load stage under a small load increment, both ε_{2b} and ε_{1b} can be taken to be zero.

$$\varepsilon_v = \varepsilon_{1b} \cos^2 \theta + \varepsilon_{2b} \sin^2 \theta = 0 \qquad (5.1)$$

$$\varepsilon_{1b} = -\varepsilon_{2b} \tan^2 \theta \tag{5.2}$$

The strain at the top of the inclined section (ε_{1t}) can be established using the Mohr's circle of strains as shown below:

$$\varepsilon_{1t} = \frac{\varepsilon_{1tv} - \varepsilon_{2t} \sin^2 \theta}{\cos^2 \theta} \tag{5.3}$$

The vertical component of strain at this point, ε_{1tv}, is determined approximately by superimposing the effects of flexure and shear, computed separately and independently.

$$\varepsilon_{1tv} = (\varepsilon_{1tv})_{flexure} + (\varepsilon_{1tv})_{shear} \tag{5.4}$$

The flexural component of vertical strain, $(\varepsilon_{1tv})_{flexure}$, is computed from a plane section analysis. The shear component, $(\varepsilon_{1tv})_{shear}$, is determined by considering diagonal compression and axial tension effects of shear force as illustrated in Figure 5.11. The contribution of tension concrete is neglected, and it is assumed that the resistance to axial tension is provided uniformly by the longitudinal reinforcement.

The component of strain parallel to the inclined section, ε_{2t}, is computed from the concrete stress in the strut at this location (f_{2t}), computed in the previous load stage and the stress-strain relationship of concrete as explained later. For the first load stage under a small increment of load both ε_{2t} and f_{2t} can be assume to be zero.

Once the end strains are established, an iterative process can be employed to determine the mid-height strain perpendicular to the inclined section (ε_{1c}) such that equilibrium of forces is satisfied. For an assumed value of ε_{1c}, the strain profile along the inclined section is completely defined. Axial strains in vertical and horizontal reinforcement are then computed from Mohr's circle of strains as ε_{vi} and ε_{hi} respectively for the i^{th} vertical and i^{th} horizontal reinforcement.

Assuming that the shear stress resisted by reinforcement is negligible, the Mohr's circle expressions become;

$$\varepsilon_{vi} = \varepsilon_{1vi} \cos^2 \theta + \varepsilon_{2vi} \sin^2 \theta \tag{5.5}$$

$$\varepsilon_{hi} = \varepsilon_{1hi} \sin^2 \theta + \varepsilon_{2hi} \cos^2 \theta \tag{5.6}$$

Stress and force in each reinforcing steel are computed using the stress-strain relationship for steel and the area of each reinforcing bar.

$$f_{svi} = \varepsilon_{vi} E_{svi} \leq f_{yvi} \tag{5.7}$$

$$f_{shi} = \varepsilon_{hi} E_{shi} \leq f_{yhi} \tag{5.8}$$

$$F_{svi} = f_{svi} A_{svi} \tag{5.9}$$

$$F_{shi} = f_{shi} A_{shi} \tag{5.10}$$

The vertical compressive force in compression concrete, C_c, is established by integrating the area under the parabolic stress-strain relationship for concrete up to the extreme compression fibre strain of ε_{cc}. With the forces in steel and concrete computed as explained above, the only other unknown forces left on the free-body diagram shown in Figure 5.6 are the shear forces along the inclined section (V_d) and the concrete compression zone (V_f). Taking moments about point B eliminates these unknown forces and the moment equilibrium is checked. If it is not satisfied, another value of ε_{1c} is assumed and the previous calculations are repeated until the equilibrium is satisfied. When equilibrium is satisfied, the assumed ε_{1c} is correct, and the analysis is extended into computing the unknown shear forces V_d and V_f from force equilibrium.

$$\sum F_v = 0 \tag{5.11}$$

$$\sum F_h = 0 \tag{5.12}$$

The inclined section analysis is continued until the steel ruptures in tension or concrete crushes in the compression strut.

Check for Concrete Crushing in Compression Strut

The inclined section analysis can be continued until the crushing of concrete in the compression strut. Therefore, the compressive stress in the strut should be checked at the end of each load stage. This is done by computing both the applied compressive stress and the capacity in the strut in a direction parallel to the inclined section. The stress condition in the compression strut is shown in Figure 5.12. Concrete in the strut is subjected to shearing stresses in combination with longitudinal stresses caused by flexure in the vertical direction. The compressive stress in concrete (f_{c2}) parallel to the inclined section can be computed if the shearing stress (τ) and stress perpendicular to the inclined section (f_{c1}) are known.

Shear stress in the strut is computed from equilibrium of forces acting on the free body diagram shown in Figure 5.6. The contribution of horizontal forces in horizontal reinforcement and the horizontal force component of inclined shear force along the inclined section can be accounted for to establish the variation of shear along the height of the wall. This is done by dividing the free body diagram into horizontal strips, and assuming constant shear within each strip.

$$v_{av} = \frac{V_{strip}}{0.8wt} \tag{5.13}$$

where, "w" is the web width of the strip (see Figure 5.6) and "t" is the web thickness of the wall.

The concrete stress perpendicular to the inclined section can be attained from the strain value in the same direction, readily available from the inclined section analysis. The stress

so calculated is limited to the cracking strength of concrete, since a new crack is expected to form when the cracking stress is exceeded.

$$f_{c1} = \varepsilon_1 E_c \leq f_{cr} \tag{5.14}$$

$$f_{cr} = 0.315\sqrt{f_c'} \quad \text{(MPa)} \tag{5.15}$$

Compressive stresses along the length of the strut are then computed from Mohr's circle of stress for concrete.

$$f_{c2} = 2v_{av} \tan\theta - f_{c1} \tan^2\theta \tag{5.16}$$

The applied stress, computed above, is checked against the compressive capacity of concrete in the strut. Concrete strength in a compressive strut may not be equal to the cylinder strength of concrete. It was shown by Vecchio (Vecchio and Collins, 1986) that, concrete in a strut between two cracks has a reduced strength due to transverse tensile strains. Hence, the following expression was suggested by Vecchio for strength of concrete in a compression strut.

$$f_{c2m} = \frac{f_c'}{0.8 - 0.34\dfrac{\varepsilon_1}{\varepsilon_0}} \leq f_c' \tag{5.17}$$

Eq. (5.17) provides concrete compressive strength in the strut at each horizontal strip, having a specific value of ε_1. These strength values are compared with compressive stresses generated under applied loading and computed by Eq. (5.16). The following inequality signifies concrete crushing in the inclined strut.

$$f_{c2} \geq f_{c2m} \tag{5.18}$$

Strain in concrete struts can also be established from the stress-strain relationship of concrete suggested by Vecchio (Vecchio and Collins, 1986). These strains at the top and

the bottom of the strut, ε_{2t}, and, ε_{2b}, respectively are used in establishing the end strain conditions for the strain diagram along the inclined section. The concrete strain, ε_{2i}, at each level is calculated from Eq. (5.19) and is assumed to be uniform within each strip.

$$\varepsilon_{2i} = \varepsilon_0(1-\sqrt{1-\frac{f_{c2}}{f_{c2m}}}) \tag{5.19}$$

Computation of Shear Deformations

Shear deformations are computed from strains computed in the inclined section analysis. It is assumed that shear distortions are concentrated along the inclined failure plane. Therefore, shear distortion for each horizontal strip is computed at the intersection of the strip with the inclined failure plane, and is assumed to be the representative of distortion of the whole strip. Shear distortion for each strip, γ_{strip}, can be computed from Mohr's circle for strains as shown below:

$$\gamma_{strip} = 2(\varepsilon_1 - \varepsilon_h)\tan\theta = (\varepsilon_1 - \varepsilon_2)\sin 2\theta \tag{5.20}$$

where, ε_h is the horizontal strain of the strip at the inclined crack, and ε_1 and ε_2 are the strains at the same location perpendicular and parallel to the inclined plane, respectively, and are available from the inclined section analysis.

Horizontal shear displacement of each strip is computed by multiplying the above computed shear distortion by the strip height. Total horizontal shear displacement is then computed by summing displacement of each strip along the height of the wall.

$$\Delta_{shear} = \sum \gamma_{strip} h_{strip} \tag{5.21}$$

The complete shear force-shear displacement response is obtained by repeating the above procedure for each stage of loading, with new set of strain values computed from inclined section analysis.

The above procedure was verified against available test data. The results produced good correlations with recorded data, as explained in the next section. However, additional improvement in displacement computations can be made if additional inclined sections are considered below the assumed inclined failure plane with inclinations gradually decreasing to 0, at which case the crack coincides with the horizontal crack along the construction joint. Prelimenary analyses conducted for some walls indicated that the improvements could not be justified in view of the excessive computaional effort involved in such refinement, and relatively small values of shear displacement obtained in this region.

5.3 Step-by-Step Solution Technique for Proposed Analysis Procedure

Complete response of low-rise shear walls can be determined using the following step-by-step solution technique:

Step 1

Assume the following strains are zero:

1. Compressive strain in inclined concrete strut, ε_2.
2. Strain perpendicular to inclined failure plane at the base (point 'B' in Figure 5.9) ε_{1b}.

Step 2

Assume a linear strain distribution for vertical strains along the horizontal critical section at the wall base for conventional plane section analysis. Assume a value for extreme compressive strain in concrete, ε_{cc}, and determine the following:

1. The neutral axis depth, and strains and stresses in vertical bars crossing horizontal critical section along the construction joint.
2. Moment, M, at the base of the wall and the value of applied shear load V associated with M.

Step 3

Select an inclined section between the top wall corner on the loading side and the neutral axis at the wall base (Figure 5.9). Assume a trapezoidal strain distribution

along the inclined failure plane for strains perpendicular to this plane, ε_1. Compute top and bottom strains, ε_{1t} and ε_{1b}, respectively from the following expressions:

$$\varepsilon_{1t} = \frac{\varepsilon_{1tv} - \varepsilon_{2t} \sin^2 \theta}{\cos^2 \theta} \tag{5.3}$$

$$\varepsilon_{1b} = -\varepsilon_0 (1 - \sqrt{1 - \frac{f_{c2}}{f_{c2m}}}) \tan^2 \theta \tag{5.22}$$

Having established the end strains of the trapezoidal strain distribution, assume a value for the mid-depth strain ε_{1c}. This defines the trapezoidal strain distribution completely.

Step 4

Calculate ε_{vi} and ε_{hi} axial strains in vertical and horizontal reinforcing bars cut by the inclined plane. These are determined from assumed strain distribution along the inclined plane and strain transformation using Mohr's circle of strains.

$$\varepsilon_{vi} = \varepsilon_{1vi} \cos^2 \theta + \varepsilon_{2vi} \sin^2 \theta \tag{5.5}$$

$$\varepsilon_{hi} = \varepsilon_{1hi} \sin^2 \theta + \varepsilon_{2hi} \cos^2 \theta \tag{5.6}$$

If ε_{vi} or ε_{hi} exceeds tensile rupturing strain of steel replace these values with zero.

Step 5

Determine axial stresses and forces in vertical and horizontal reinforcing bars cut by the inclined plane using calculated strains in step 4 and reinforcing bar properties.

Step 6

Verify the validity of the assumed strain ε_{1c} through moment equilibrium about point 'B' (Figure 5.6). If the moment equilibrium is not satisfied change the assumed value of strain ε_{1c}, and go to step 4, and repeat the procedure until moment equilibrium is satisfied.

Step 7

Compute the remaining internal forces, i.e., shear forces along the inclined plane, V_d, and concrete compression zone at the base, V_f, from equilibrium of vertical and horizontal forces.

Step 8

Compute concrete compressive strain along the length of the inclined strut. Divide the wall into a number of horizontal strips for this purpose.

Step 9

Calculate concrete tensile stress perpendicular to the inclined strut using a trapezoidal strain distribution for ε_1. Assuming concrete tensile stress remains uniform within each strip, compute the tensile stress f_{c1i} for each strip.

$$f_{c1i} = \varepsilon_{1i} E_c \leq f_{cr} \tag{5.23}$$

$$f_{cr} = 0.315\sqrt{f_c'} \qquad \text{(MPa)} \tag{5.15}$$

Step 10

Assuming uniform distribution of shear along the inclined section and accounting for the effect of horizontal reinforcement, compute horizontal shear at the level of each strip. Using the horizontal shear for each strip calculate the average horizontal shear stress in concrete at the middle of each strip.

$$v_{av} = \frac{V_{strip}}{0.8wt} \tag{5.13}$$

where V_{strip} is the horizontal shear load at the middle of each strip, w is the wall width on one side of the inclined plane and t is the wall thickness.

Step 11

Determine compressive stress in concrete in the inclined compressive strut at the middle of each strip.

$$f_{c2} = 2v_{av} \tan\theta - f_{c1} \tan^2 \theta \tag{5.16}$$

Step 12

Compute maximum diagonal compressive strength of concrete in the inclined strut.

$$f_{c2m} = \frac{f_c'}{0.8 - 0.34\frac{\varepsilon_1}{\varepsilon_0}} \leq f_c' \tag{5.17}$$

where, ε_0 is concrete strain at maximum stress, determined from stress-strain diagram.

Step 13

Compare the applied compressive stress f_{c2} with the capacity of concrete, f_{c2m}. If $f_{c2} \geq f_{c2m}$, compression failure occurs in the strut. This makes the end of the analysis. If $f_{c2} < f_{c2m}$ go to the next step.

Step 14

Calculate compressive strain in the inclined strut for each strip.

$$\varepsilon_{2i} = \varepsilon_0\left(1 - \sqrt{1 - \frac{f_{c2}}{f_{c2m}}}\right) \tag{5.19}$$

Step 15

Calculate, γ_{xyi}, shearing strain in each strip from one of the following equations:

$$\gamma_{xyi} = 2(\varepsilon_{1i} - \varepsilon_{hi})\tan\theta \tag{5.24a}$$

$$\gamma_{xyi} = (\varepsilon_{1i} - \varepsilon_{2i})\sin 2\theta \tag{5.24b}$$

Step 16

Calculate horizontal shear displacement at each strip

$$\Delta_{shi} = \gamma_{xyi} h_i \tag{5.25}$$

where h_i is the depth of the i^{th} strip.

Step 17

Calculate total shear displacement by summing shear displacement of each strip along the wall height. Go to step 2 for the next load stage and associated ε_{cc} value.

A computer program 'Walls' for evaluating the reponse of low-rise shear walls using the proposed analytical procedure is described in Appendix C.

5.4 Verification of the Proposed Analysis Procedure

The analytical approach developed in this thesis has been verified extensively against available test data. A total of 110 low-rise shear walls were analyzed for this purpose. The walls considered had aspect ratios of 1.0 or less, with rectangular, barbell, and flanged sections. A large volume of test data were obtained from a paper in which the available experimental data had been compiled (Wood, 1990). Additional test data were obtained from other published papers and reports (Barda et. al, 1977, Benjamin and Williams, 1985, Synge, 1980, Wiradinata, 1985, and Lefas et. al, 1990). The experimental data compiled was believed to be near complete at the time the verification were done.

The verification of analytical procedure was done in two stages. The first stage involved comparisons of strength values. All the experimental data reported contained this information. The second stage involved comparisons of shear force-shear displacement relationships. Few researchers in the past measured and reported shear displacement as a separate displacement component. Hence these comparisons were made using limited test data. A total of 14 walls were analyzed for this purpose.

Verification of Strength Values

A total of 76 barbell, 14 flanged, and 20 rectangular walls were analyzed to determine wall strength. Thirty eight walls had aspect ratios of 0.5 and less, where the aspect ratio is defined as wall height-to-length ratio. The wall height used in this definition is not the same as the height measured to the centroid of the applied load, which yield slightly higher aspect ratios. The vertical web reinforcement ratio varied between 0.35 % and 2.89 %, and the horizontal reinforcement ratio varied between 0.25 % and 1.89 %. Most walls contained boundary elements with 0.71 % to 8.88 % reinforcement ratio. The loading was monotonic for 76 walls, and cyclic or reversed cyclic for the remainder. Details of wall properties are included in Appendix B. Barbell, flanged, and rectangular walls were starting with letters "B", "F", and "R" respectively. Wall labels, researchers, reinforcement ratios, material properties, loading type, and the wall geometry are included in Appendix B, in Tables B.1 through B.3. All walls were reported to had failed in shear.

Wall capacities based on the shear strength provisions of ACI 318-89 Building Code were also computed for each wall. These quantities (V_{ACI}), as well as the capacities computed based on the proposed procedure (V_{prop}), are listed in Table 5.1. Also included are the experimentally recorded shear capacities (V_{exp}). The concrete compressive strain at the extreme fiber of the horizontal wall section along the construction joint are included in the table as ε_{cc}. These strain values, obtained from plane section analyses, reflect the strain condition under flexure when the failure takes place due to shear compression.

The comparisons of experimentally recorded and analytically computed strength values are given in Figures 5.13 through 5.15 in three different scales of plots. The figures also include comparisons of wall strengths based on ACI 318 with recorded experimentally. The results indicate that good correlations were obtained with the proposed analytical procedure. The computed strengths for barbell and rectangular walls were especially in good agreement with experimental strengths. In general, analytically computed strengths showed better correlations with experimental quantities than those based on the ACI provisions.

Verification of Shear Deformations

Verification of shear deformation computaions were done in the form of reproducing shear force-shear displacement relationships of walls using the proposed analytical procedure. The resulting analytical relationships were for monotonically increasing loading. Experimental force-deformation relationships were available in the form of hysteretic relationships under cyclic loading. Therefore, the comparisons were made with the envelopes of these hysteresis loops, assumed to be equivalent to the monotonic curve.

As was mentioned earlier, experimentally recorded shear force-shear displacement relationships for low-rise walls are scarce in the literature. The two walls (Wall 7 and Wall 8) tested as part of this investigation were instrumented for shear deformation measurements. Four other walls, tested in the previous phase of the same overall investigation, were also instrumented for shear displacement measurements. These 6 walls were selected for analysis. Material and geometric properties of Walls 3 through 8 are included in Appendix B.

In order to extend the verifications to walls tested in other research programs, an additional 8 shear walls, tested at the Portland Cement Association (PCA) with aspect ratios of 2.4 (Osterle et. al, 1976), were considered. These walls were instrumented to measure shear displacements at the lower portions of wall, within a height (6 ft)

approcximately equal to the wall width (6 ft 3 in). Therefore, these wall segments had low aspect ratios, and hence were included in the verification.

Two of these walls had rectangular cross-sections, one had a flange section, and the remaining 5 had barbell sections. The horizontal reinforcement ratio varied between 0.31% and 0.71 %, and the vertical web reinforcement ratio varied between 0.25 % and 0.30 %. The walls had boundary elements with reinforcement ratios ranging from 1.0 % to 4.0%. Four walls contained confined boundary elements. The proposed procedure was modified for these walls to account for concrete confinement based on the analytical model proposed by Saaticioglu and Razvi (Saatcioglu and Razvi, 1992). The applied loading was cyclic for all but B4, which was tested under monotonically increasing lateral loading. With these walls, total number of walls used in verification of inelastic shear deformation became 14.

The comparisons between analytical and experimental force-displacement relationships are shown in Figures 5.16 to 5.29. Walls 3 through 6 had an I-shaped concrete foundation, secured to the laboratory strong floor at the flanges. The researchers who tested these walls reported some flexibility of the base, which may have resulted in a more flexible behaviour of the walls. The comparisons for Wall 7 and Wall 8 show good predictions. Among the PCA walls, R1,R2 , B1, and B3 developed premature failure due to inelastic bar buckling or instability of compression zone. For flanged walls, in general, the prediction of the wall response using the proposed analytical procedure leads to somewhat poorer correlation with experimental results. The experimental results for the remaining walls show good agreement with those obtained from the proposed analytical procedure. The above comparisons indicate that the strength and inelastic deformation computations, based on the analytical procedure developed in this thesis, lead to reasonably accurate results.

5.5 Observations on Wall Behaviour Based on Analysis Results

Some observations were made on wall behaviour and the effects of design parameters, while analyzing 110 low-rise walls. The results indicate that the increase in vertical web reinforcement increases not only the flexural capacity but also the shear capacity. This is to be expected since the vertical reinforcement does contribute to controlling tension crack. In fact, for walls with aspect ratios less than 1.0, the contribution of vertical reinforcement is more than that of horizontal web reinforcement due to the inclination of corner-to-corner crack. The results of recent wall tests also support the role of vertical web reinforcement on ultimate capacity (Barda et. al, 1977, Cardenas et. al, 1990). As for the horizontal web reinforcement, it is concluded that they are effective in producing more uniform crack pattern, and may enhance the diagonal tension capacity. However, usually because of the low aspect ratio of these walls, the vertical reinforcement ratio associated with flexural yielding appears to be sufficient to prevent diagonal tension failure that may occur along a corner-to-corner failure plane, and increasing horizontal reinforcement ratio, as stipulated in ACI 318-89 does not improve the shear capacity. In all the walls analyzed, failure was associated with compression crushing of inclined concrete struts, even for walls with very low percentage of horizontal reinforcement. The analysis results clearly indicate that the wall aspect ratio is the single most important parameter that changes the failure mode from diagonal compression to flexure. Because sliding shear failure was not considered in the analytical procedure developed, the above observations apply to those cases where shear sliding does not result in premature failure.

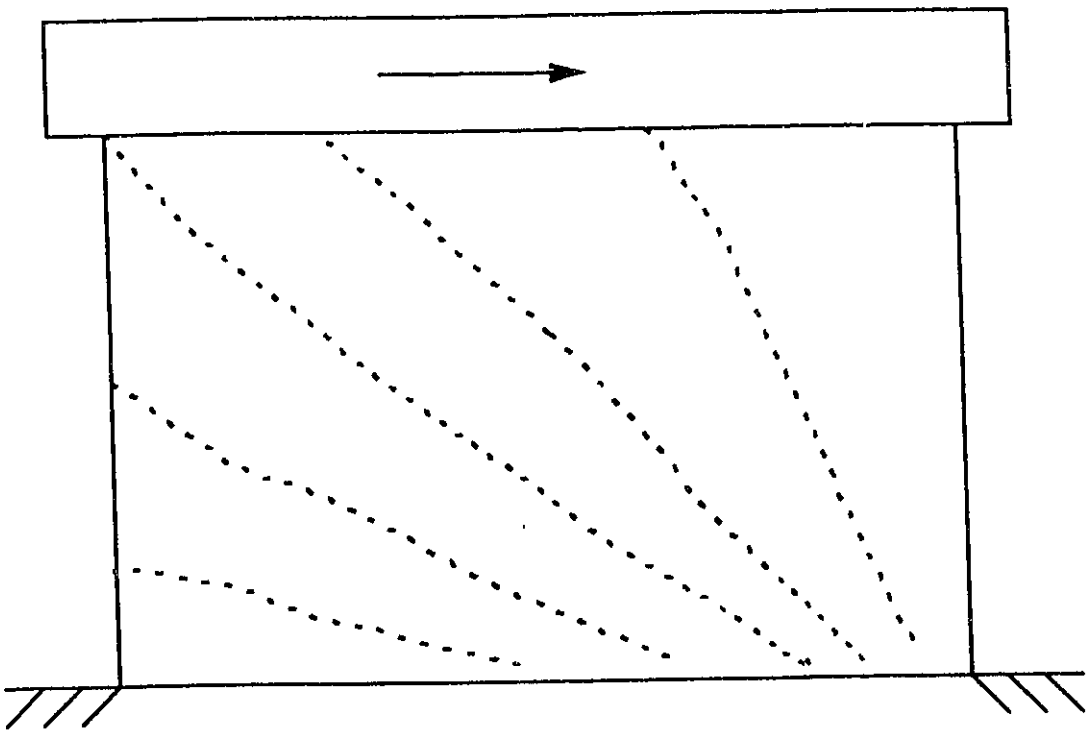

Figure 5.1a Crack Pattern in Low-Rise Shear Walls

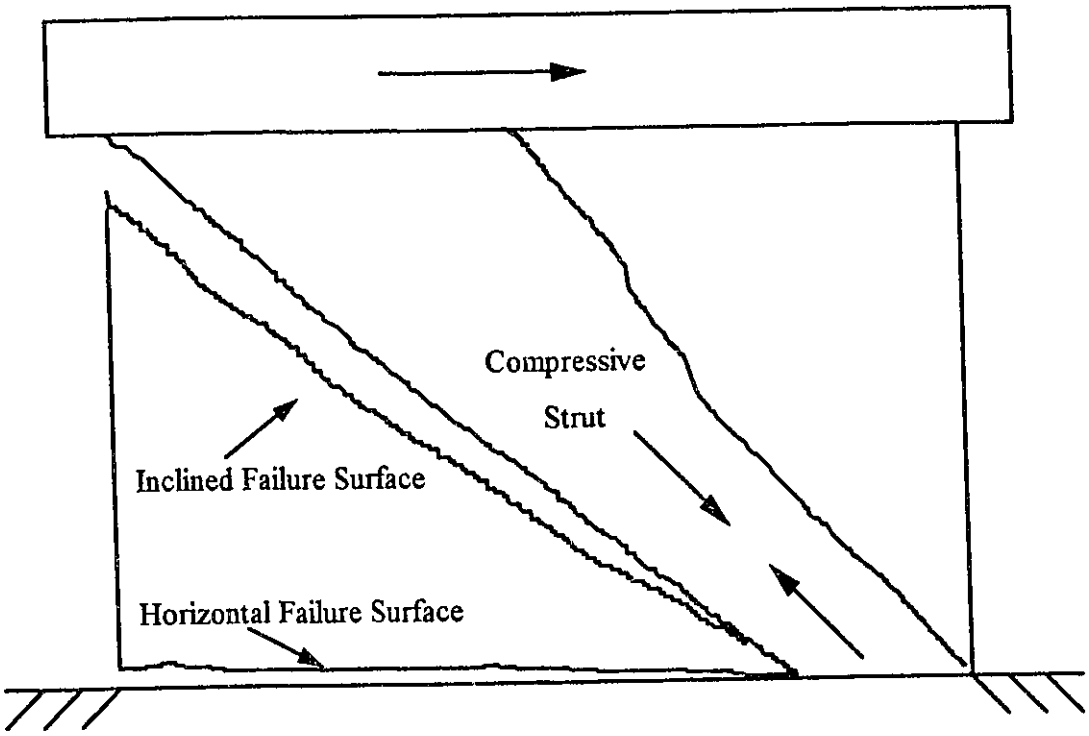

Figure 5.1b Potential Failure Planes for Low-Rise Shear Walls

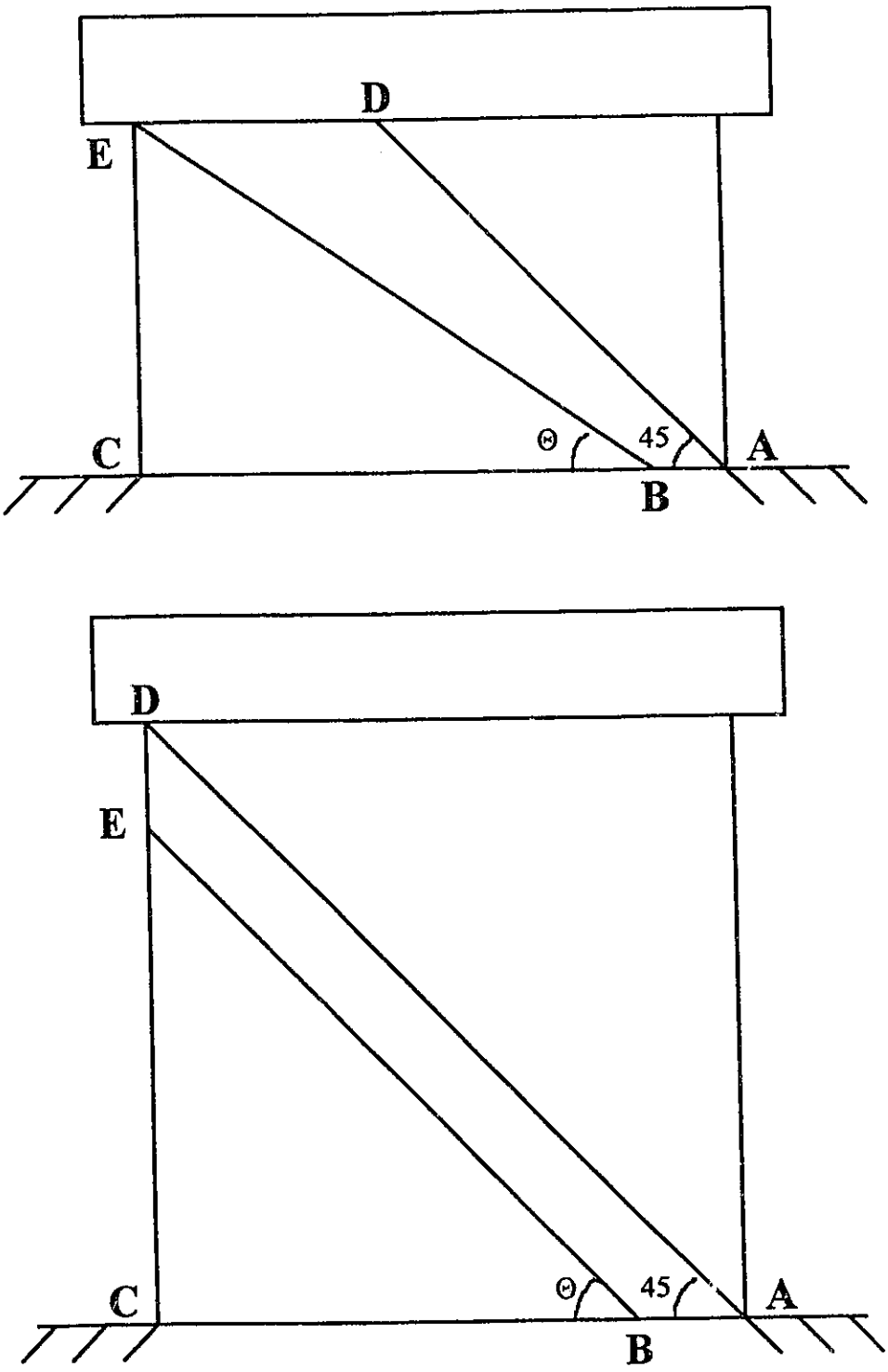

Figure 5.2 Critical Concrete Struts in Walls with Different Aspect Ratios

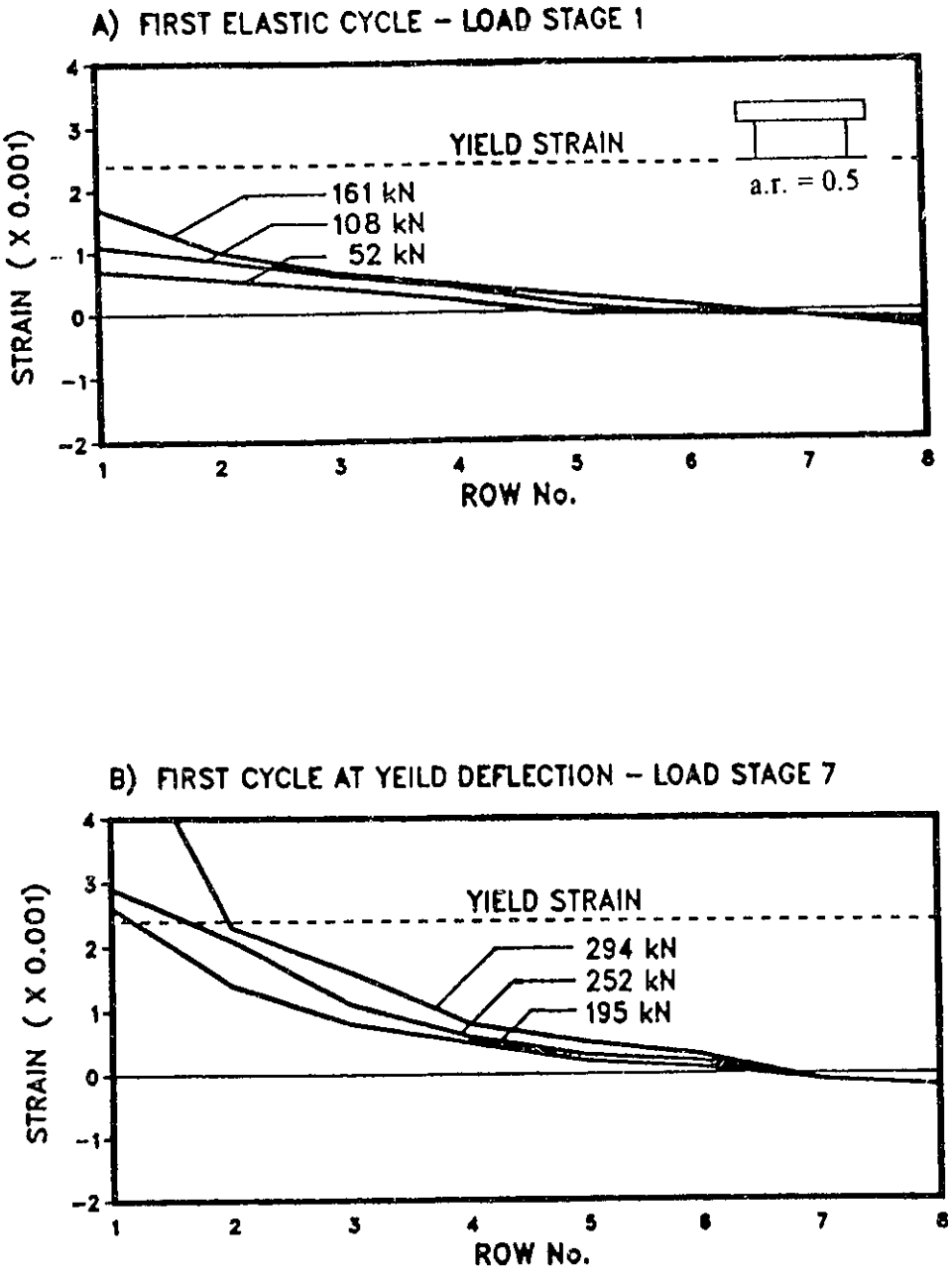

Figure 5.3 Strain Distributions in Flexural Reinforcement for Wall 4
(adopted from Pilette, 1988)

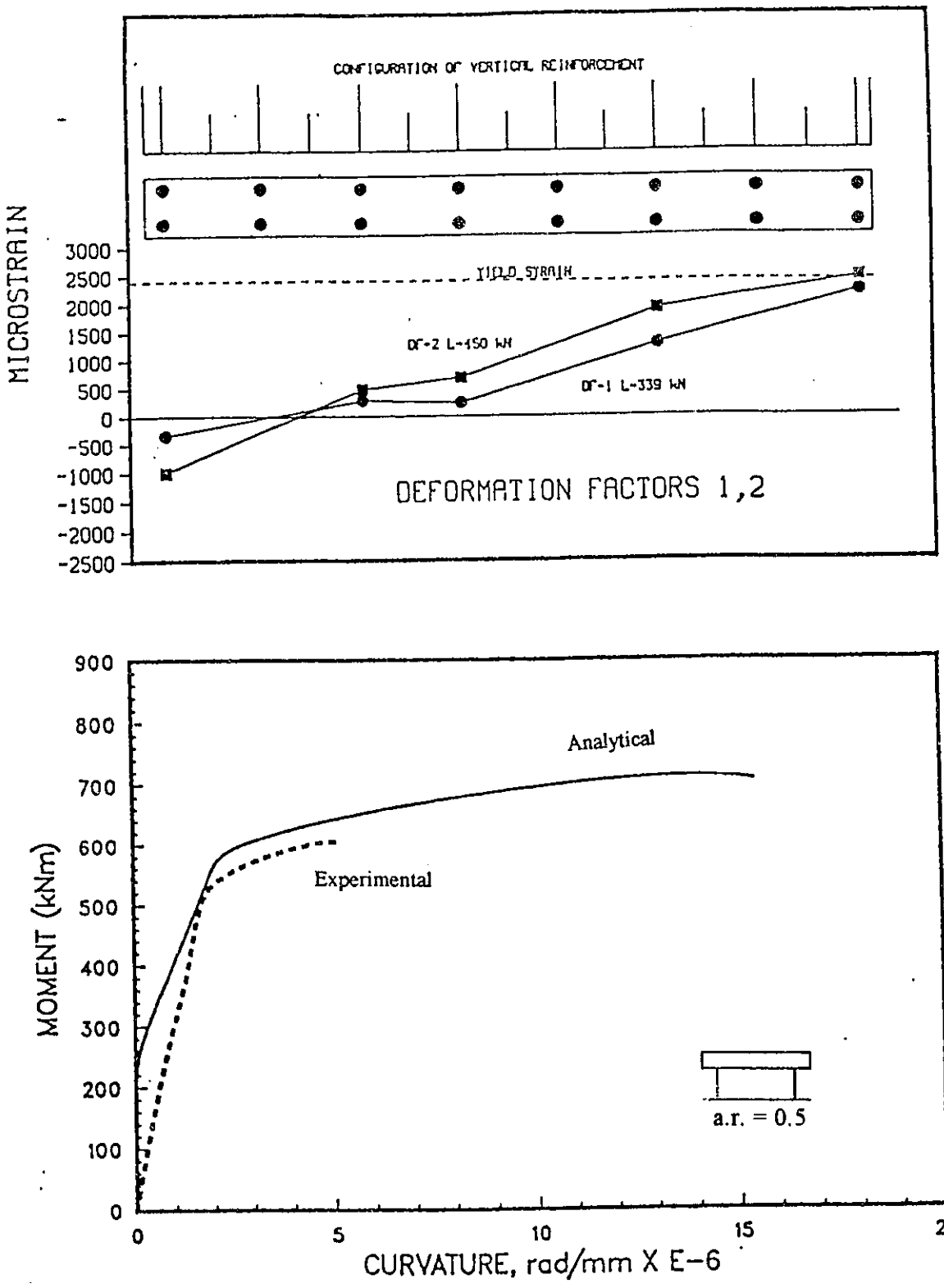

Figure 5.4 Strain Profiles in Flexural Reinforcement (above) and Moment Curvature Relationship for Wall 6 (adopted from Wasiewicz, 1988)

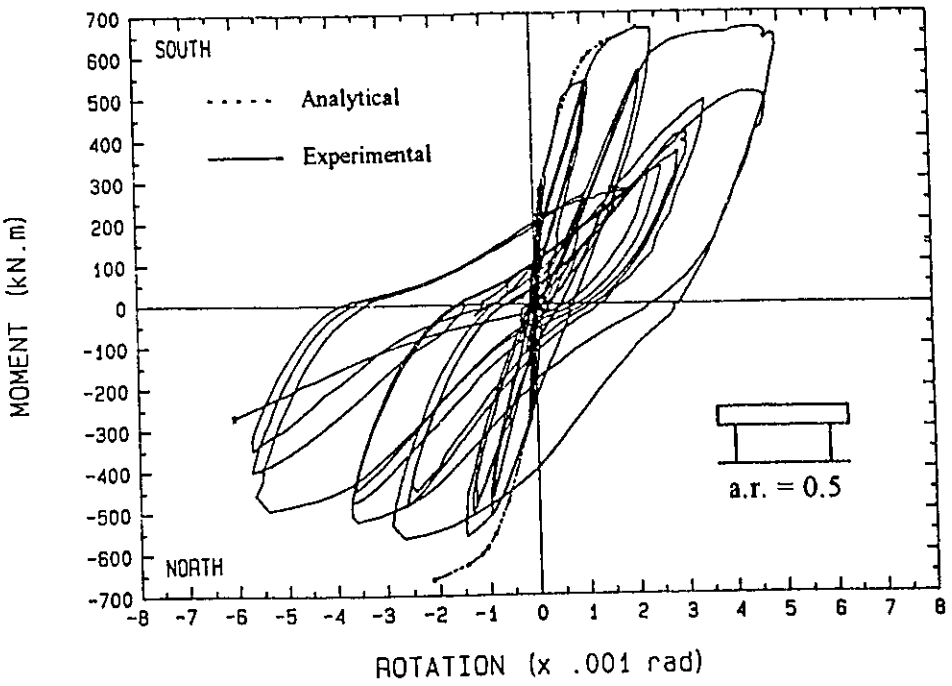

Figure 5.5 Moment Rotation Diagram for Wall 1
(adopted from Wiradinata, 1985)

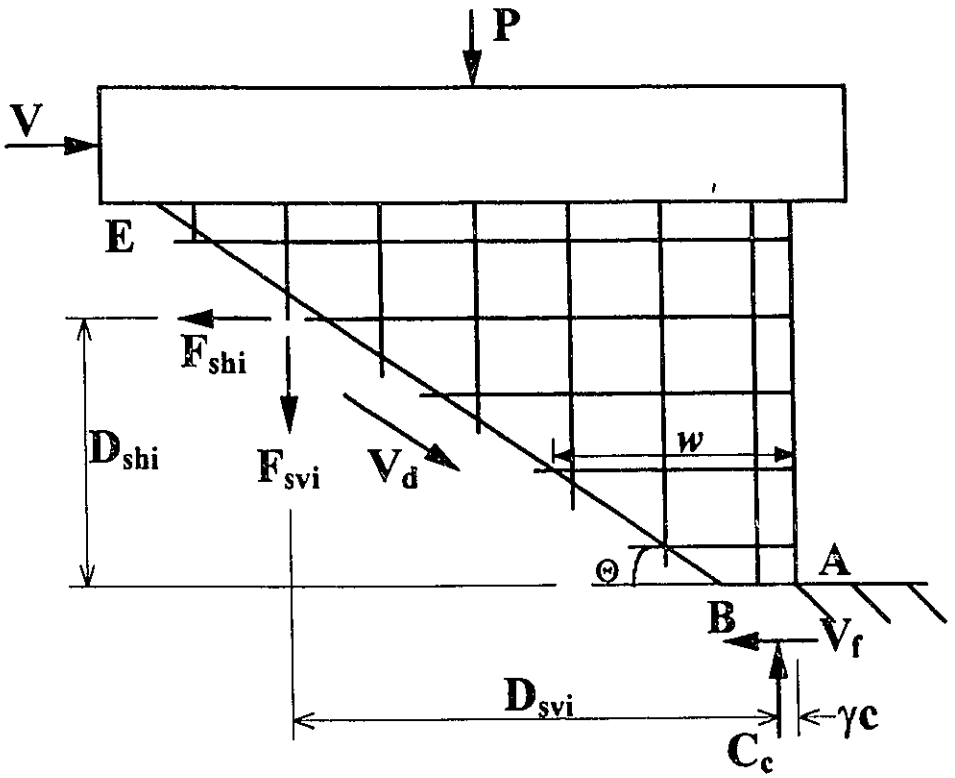

Figure 5.6 Free Body Diagram to One Side of the Potential Failure Plane

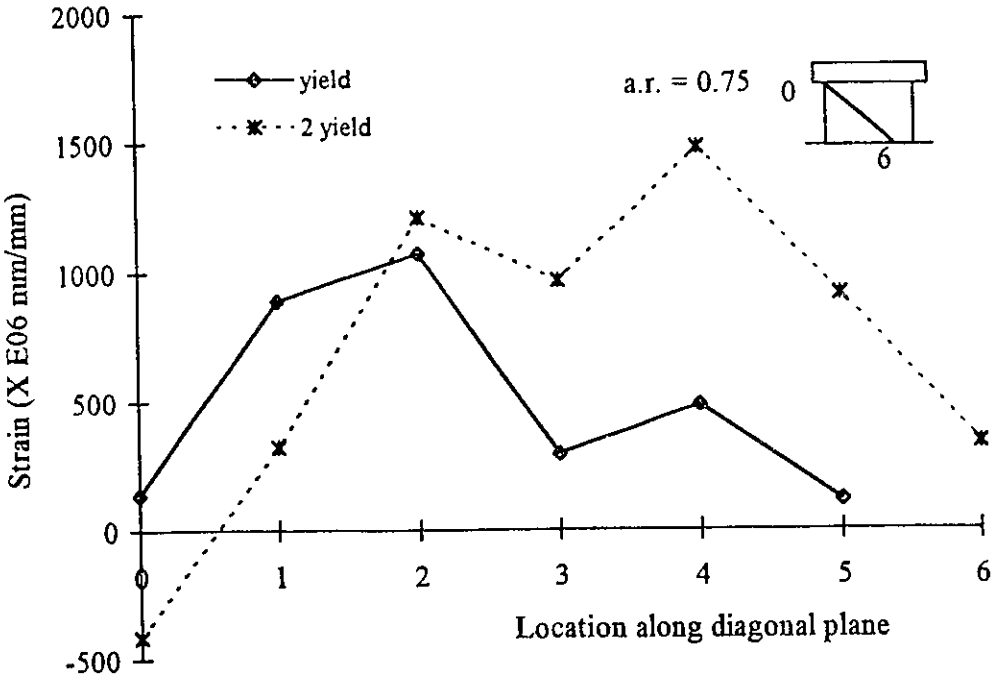

Figure 5.7 Variation of Horizontal Strains along Diagonal Failure Plane Recorded by Demec Gauge for Wall 7

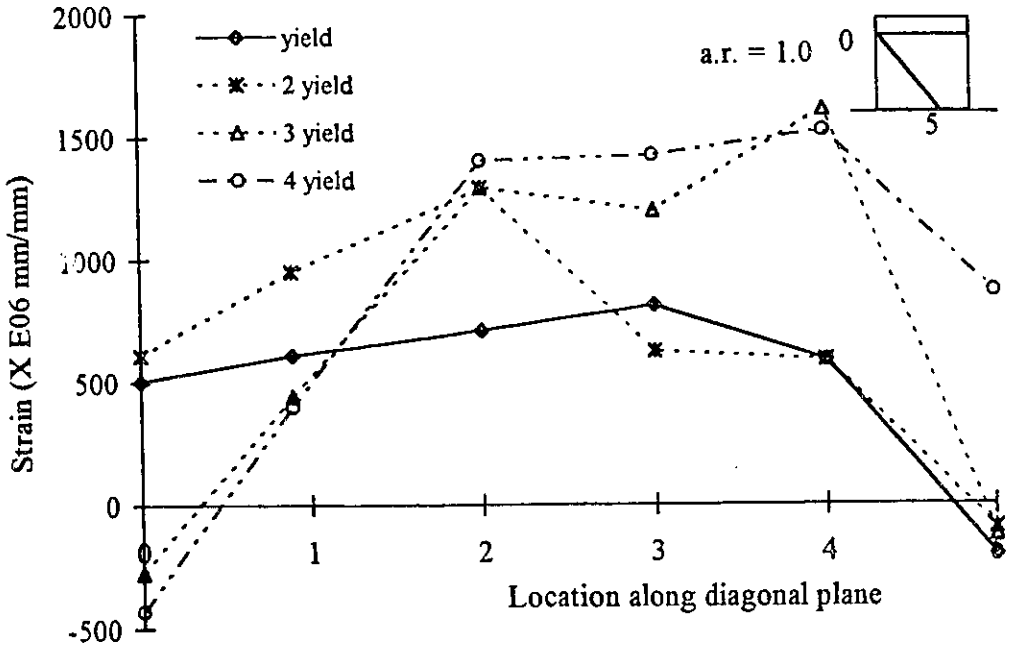

Figure 5.8 Variation of Horizontal Strains along Diagonal Failure Plane Recorded by Demec Gauge for Wall 8

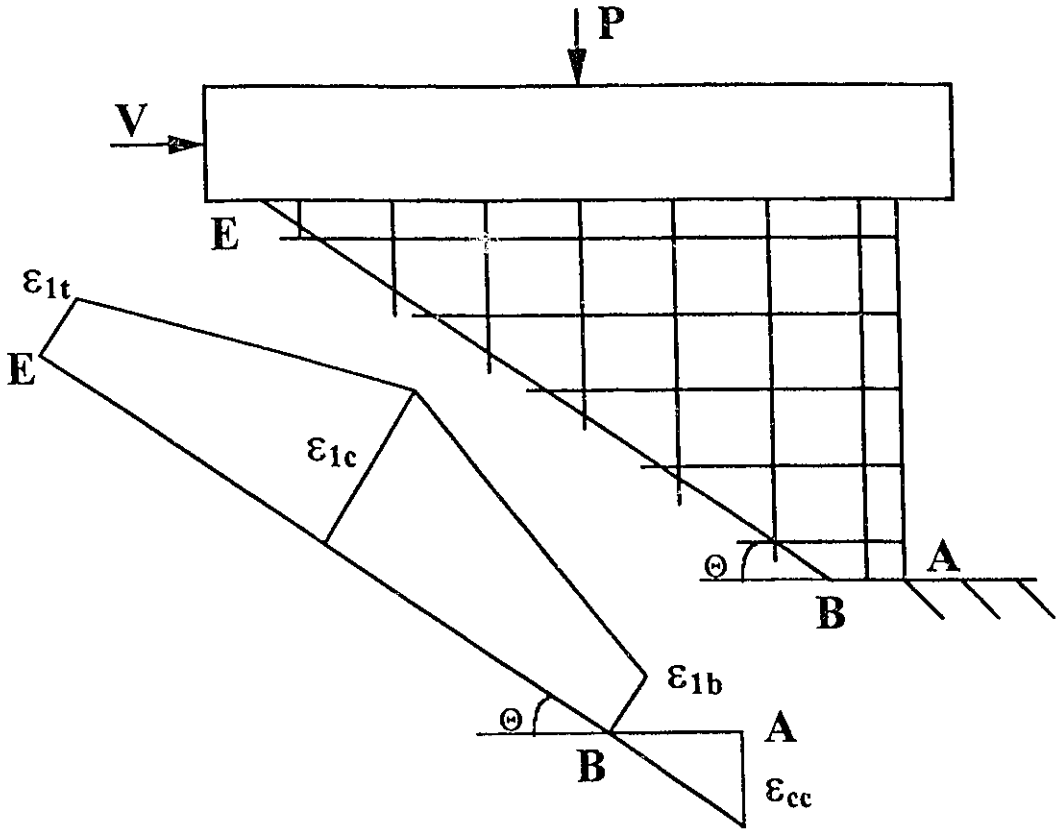

Figure 5.9 Assumed Strain Distribution Perpendicular to the Inclined Section

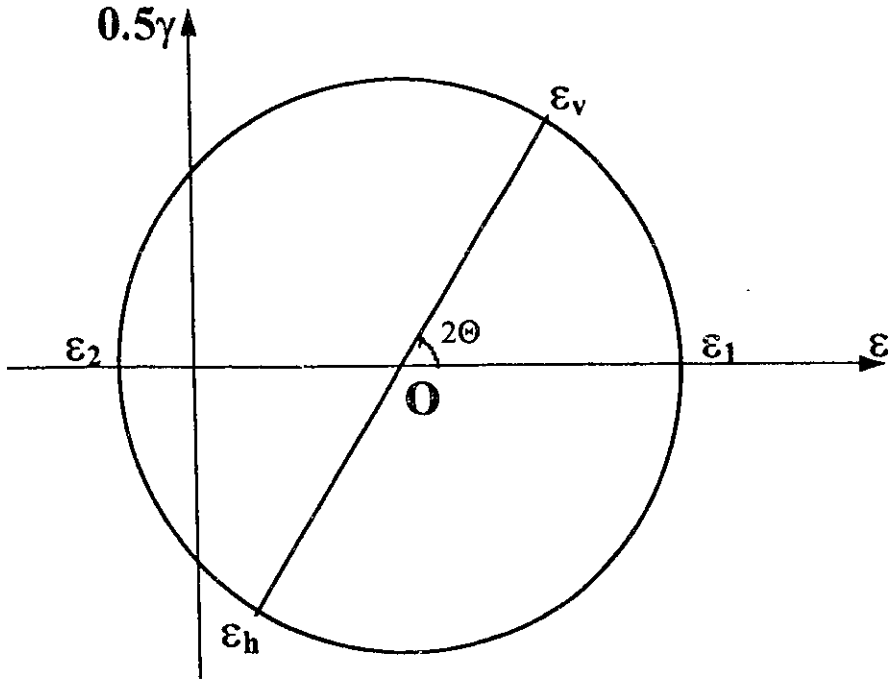

Figure 5.10 Mohr's Circle of Strains

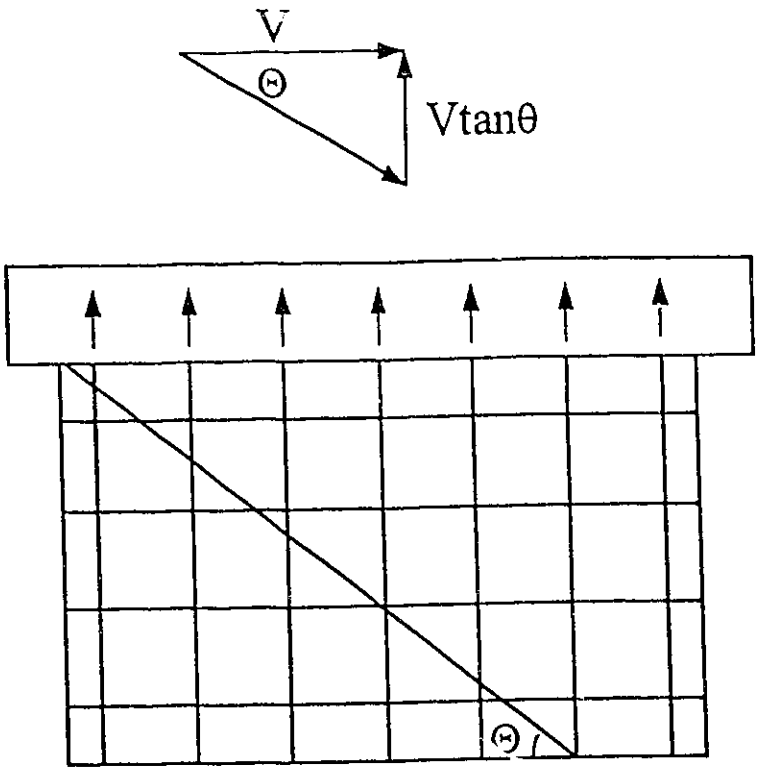

Figure 5.11 Vertical Component of Shear Load in Reinforcement

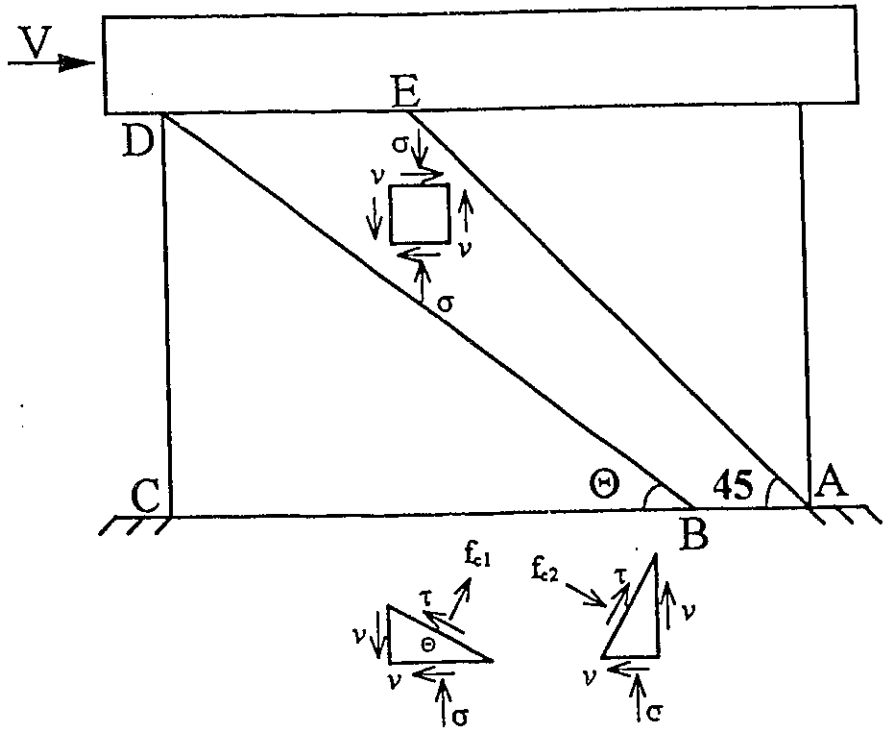

Figure 5.12 Stress Conditions Within the Wall

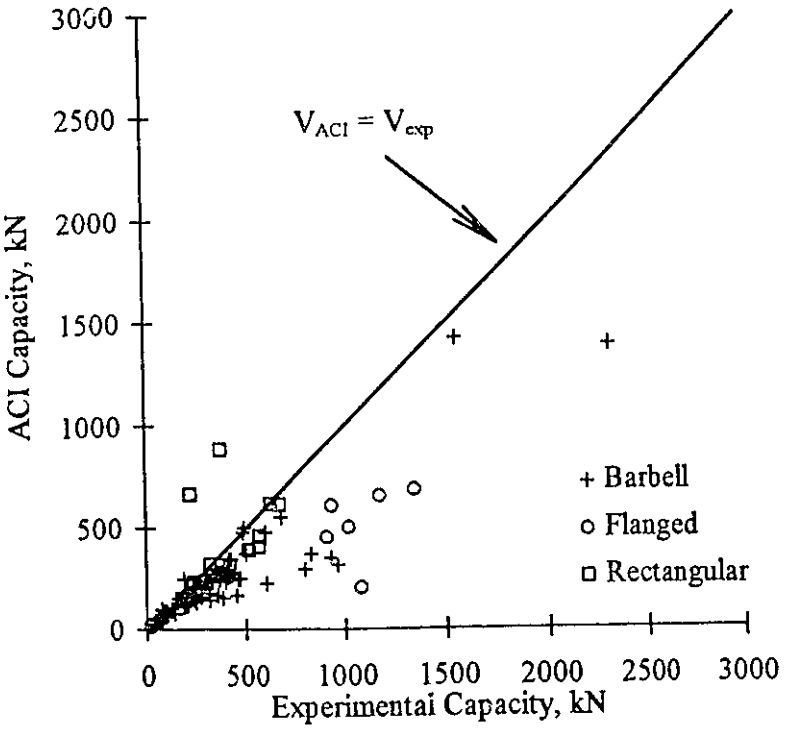

Figure 5.13a ACI Versus Experimental Capacity

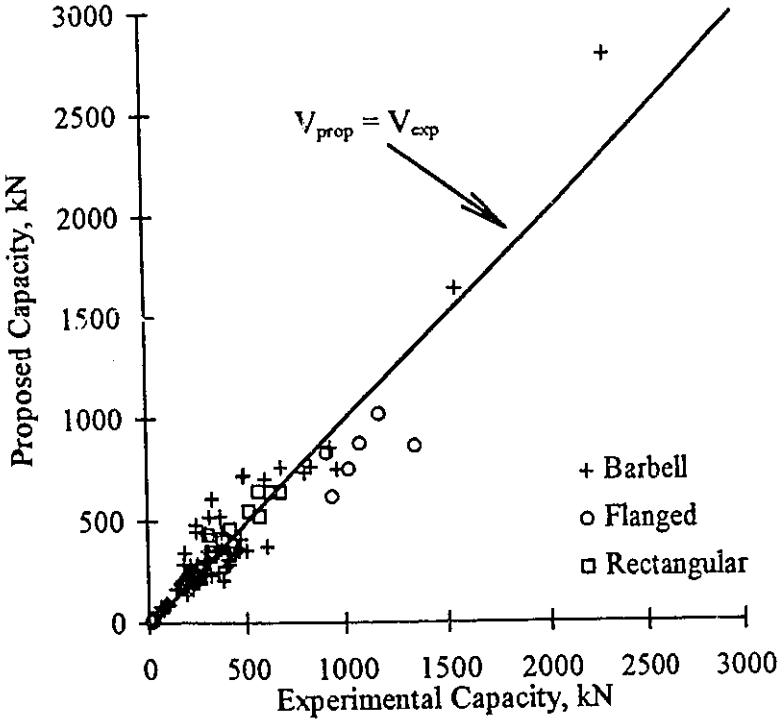

Figure 5.13b Proposed Versus Experimental Capacity

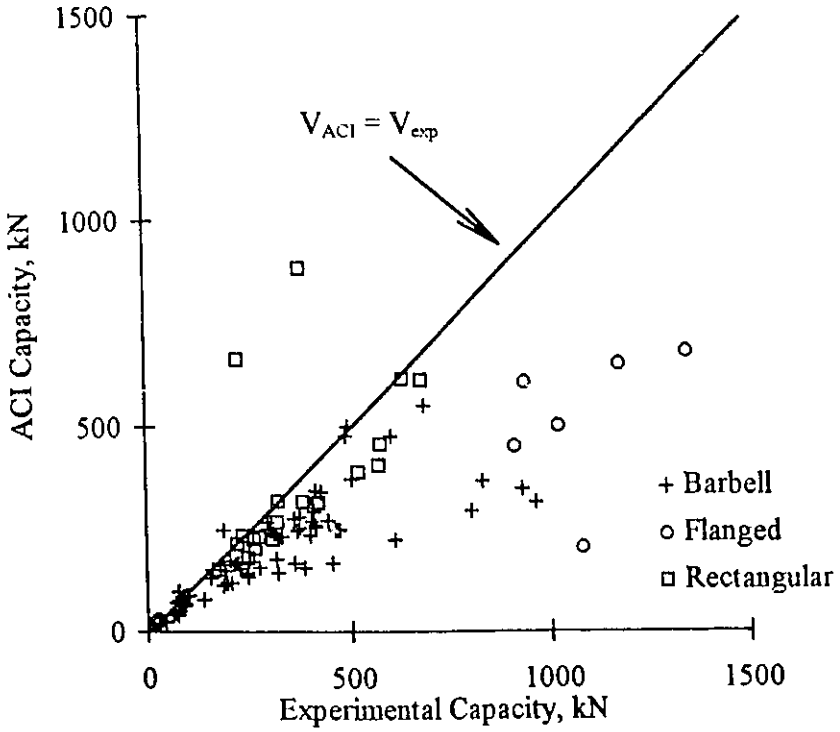

Figure 5.14a ACI Versus Experimental Capacity (new scale)

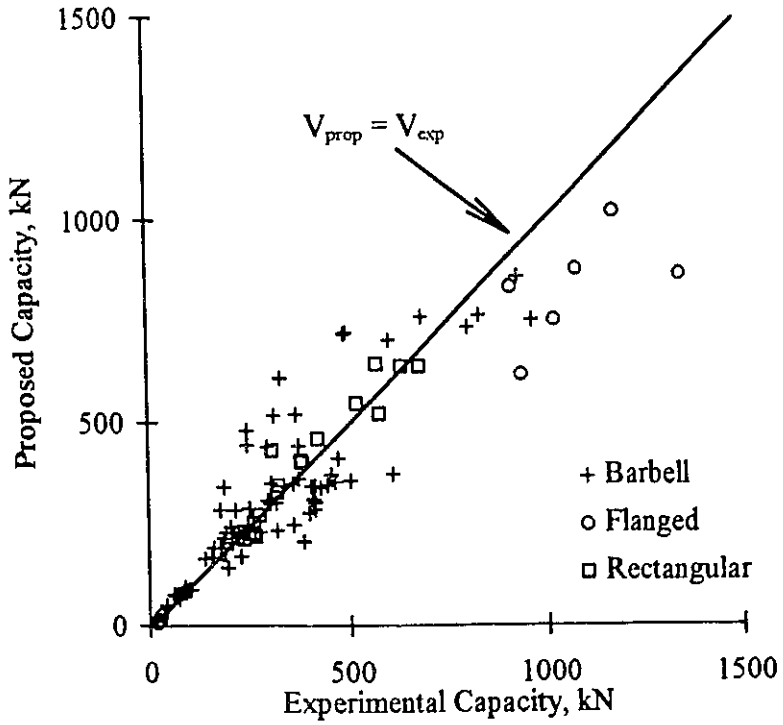

Figure 5.14b Proposed Versus Experimental Capacity (new scale)

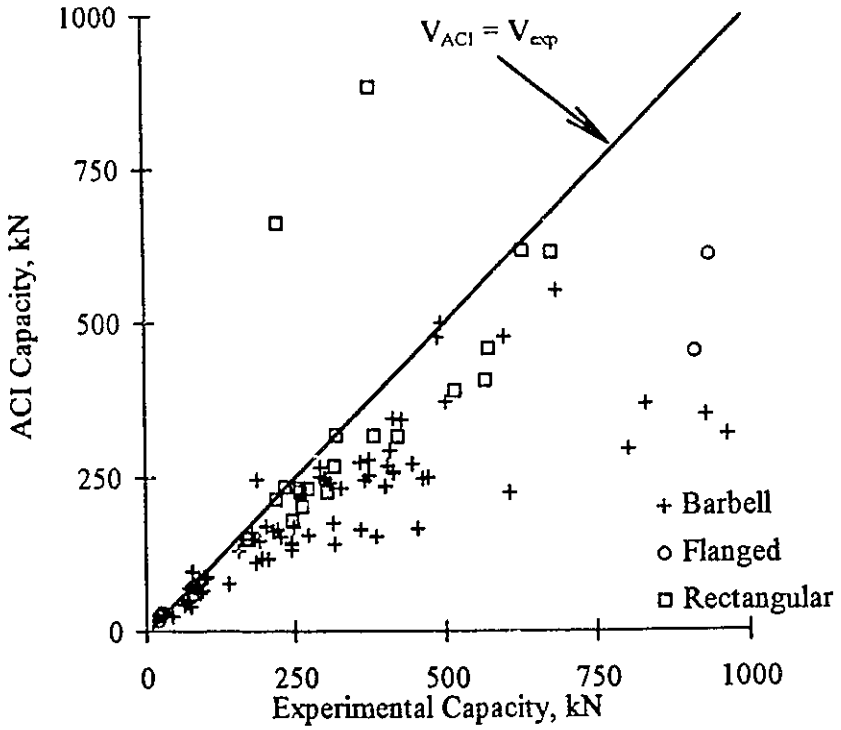

Figure 5.15a ACI Versus Experimental Capacity (new scale)

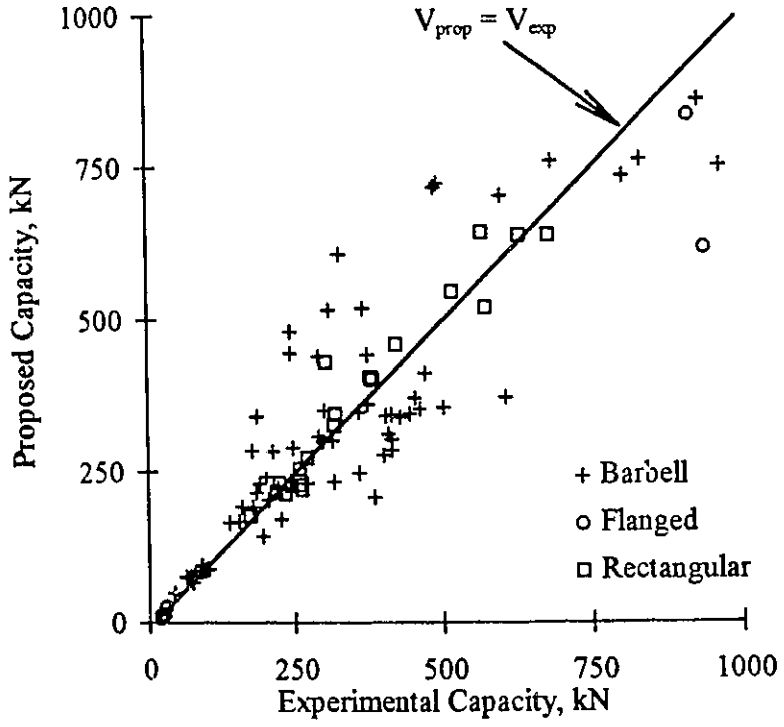

Figure 5.15b Proposed Versus Experimental Capacity (new scale)

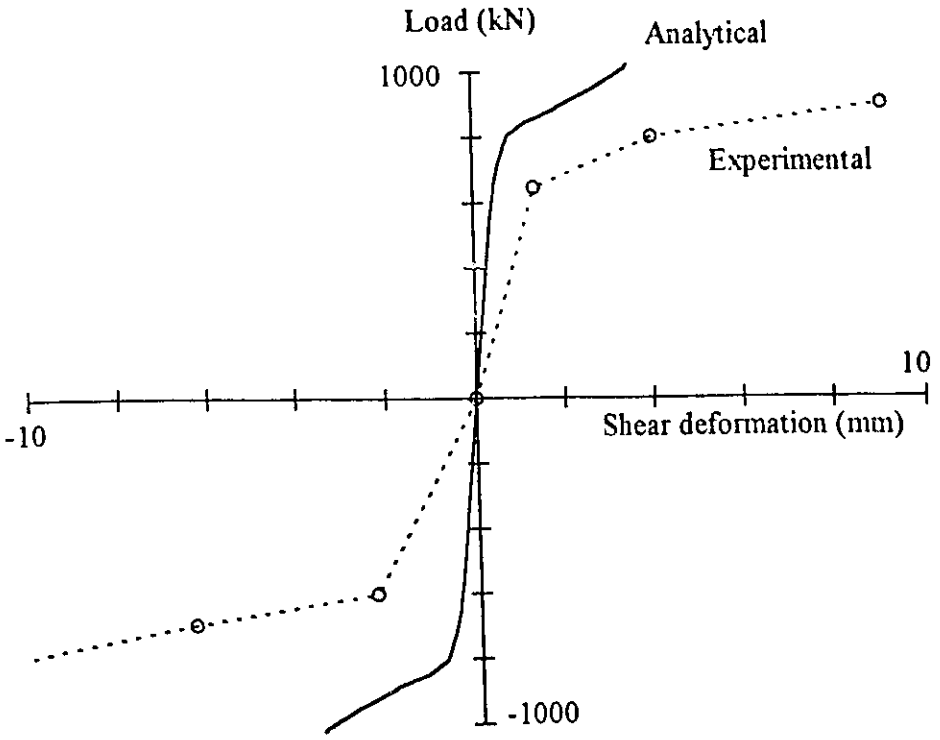

Figure 5.16 Shear Load-Shear Deformation Diagram for Wall 3

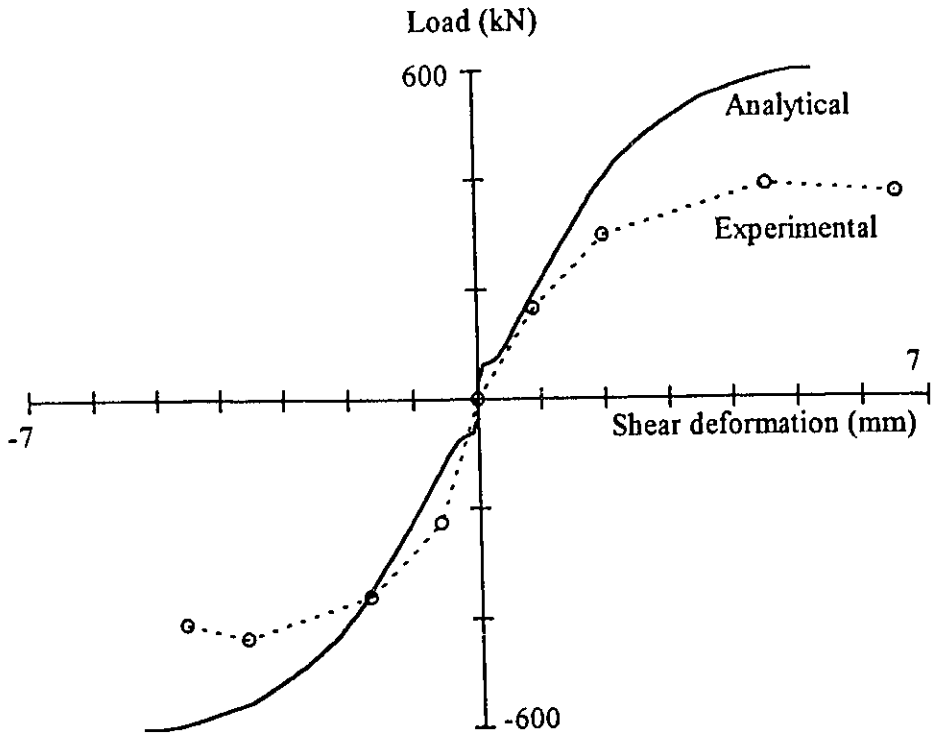

Figure 5.17 Shear Load-Shear Deformation Diagram for Wall 4

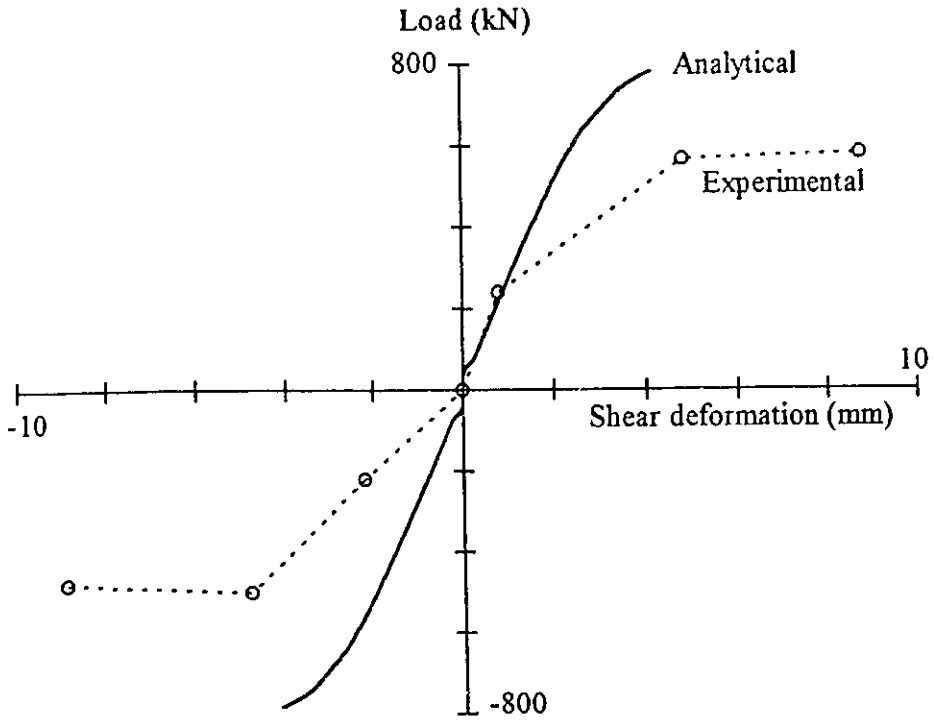

Figure 5.18 Shear Load-Shear Deformation Diagram for Wall 5

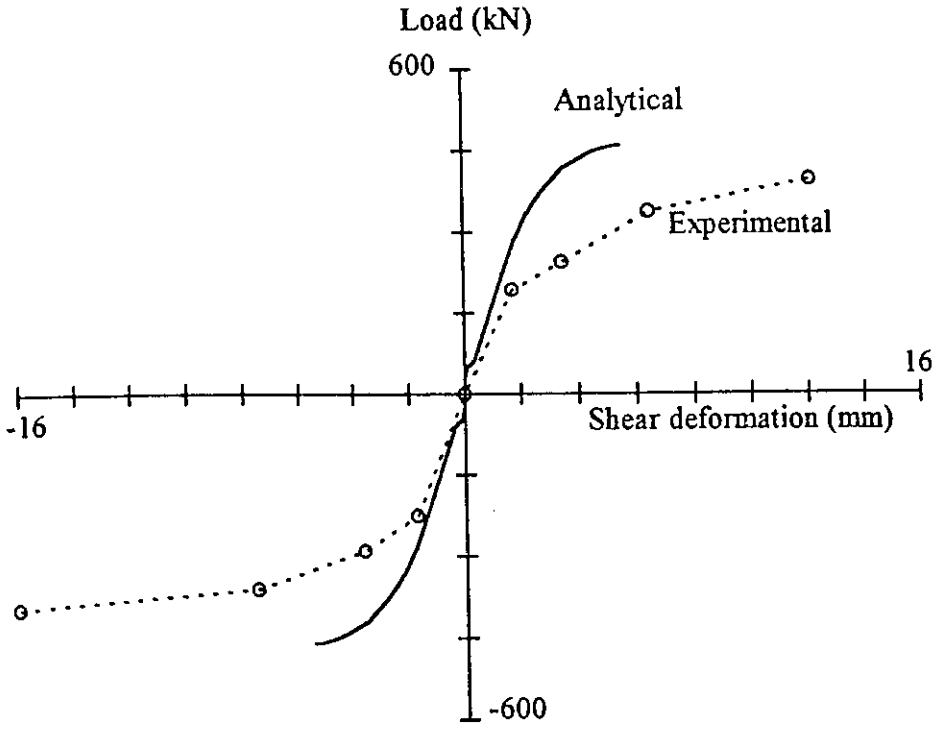

Figure 5.19 Shear Load-Shear Deformation Diagram for Wall 6

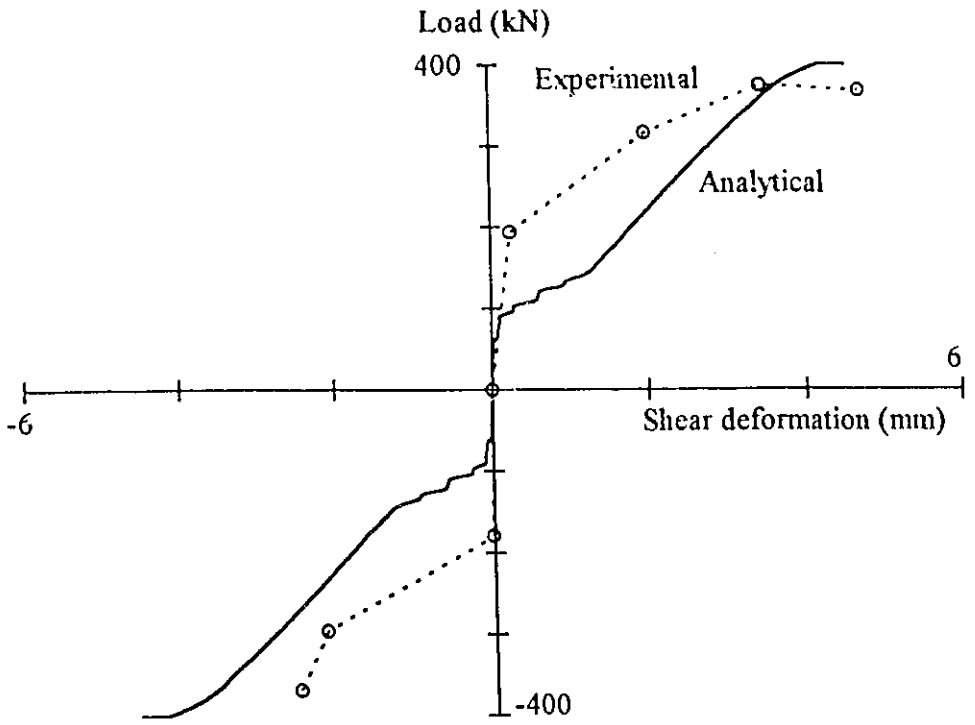

Figure 5.20 Shear Load-Shear Deformation Diagram for Wall 7

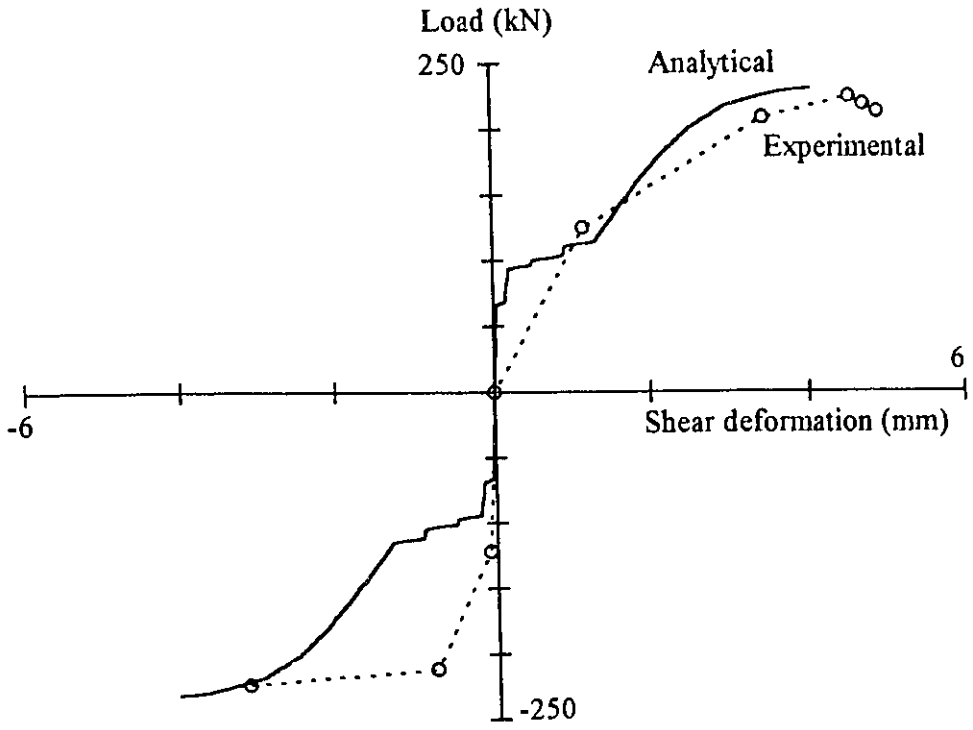

Figure 5.21 Shear Load-Shear Deformation Diagram for Wall 8

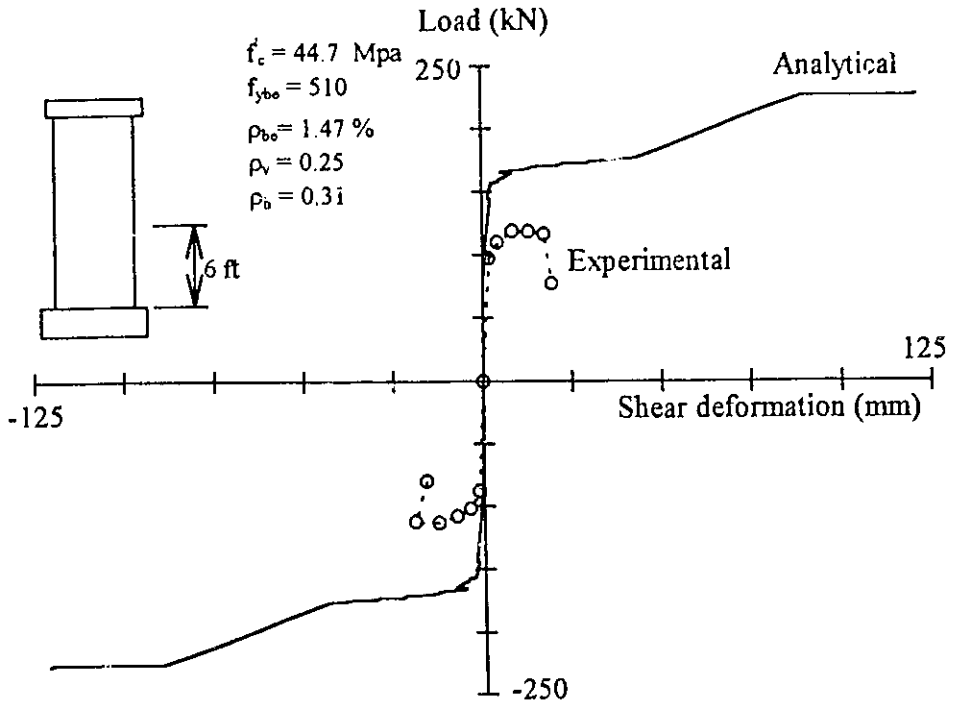

Figure 5.22 Shear Load-Shear Deformation Diagram for PCA Wall R1

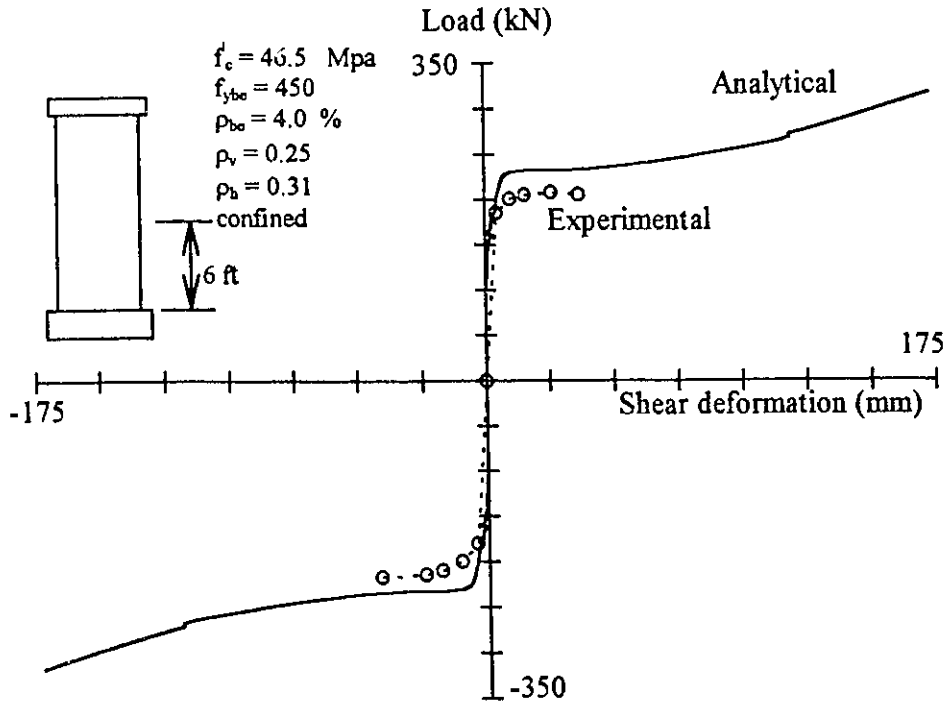

Figure 5.23 Shear Load-Shear Deformation Diagram for PCA Wall R2

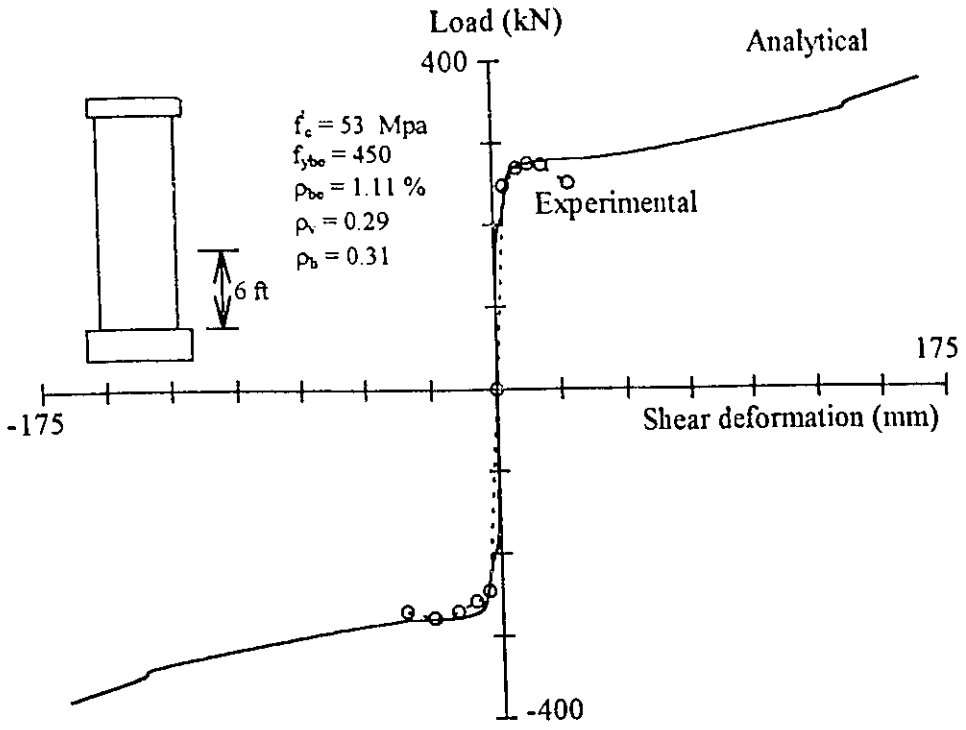

Figure 5.24 Shear Load-Shear Deformation Diagram of PCA Wall B1

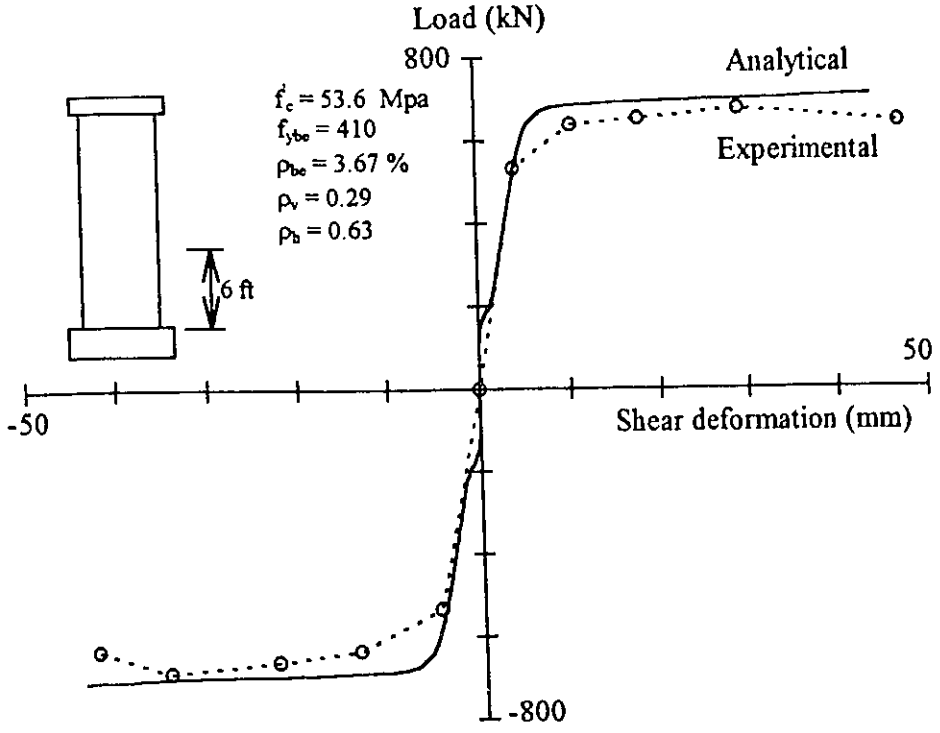

Figure 5.25 Shear Load-Shear Deformation Diagram of PCA Wall B2

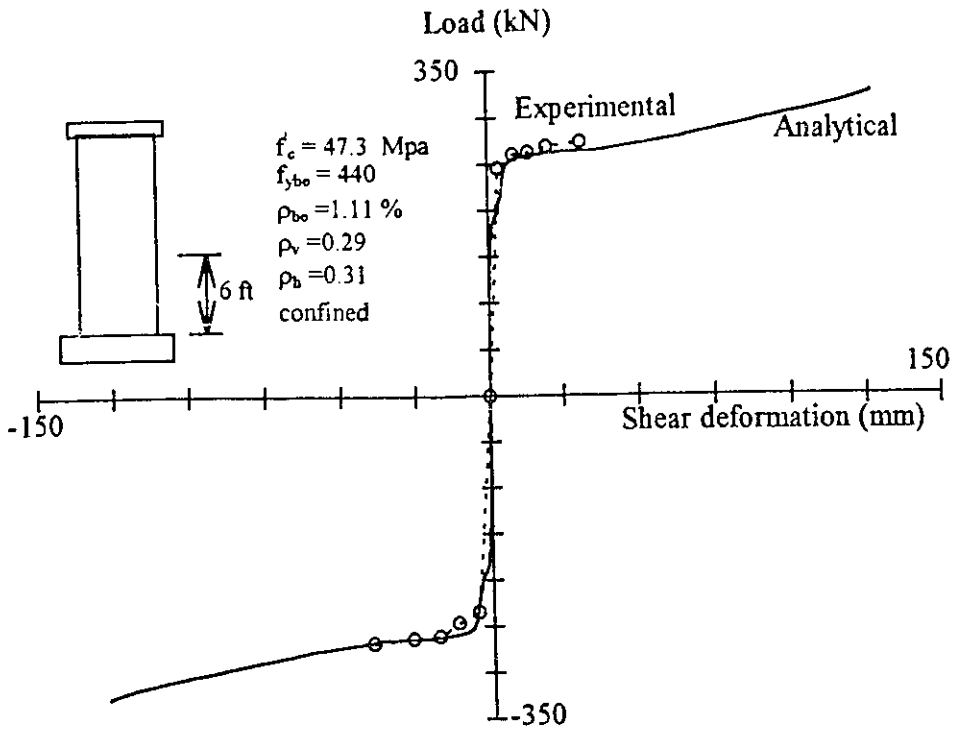

Figure 5.26 Shear Load-Shear Deformation Diagram for PCA Wall B3

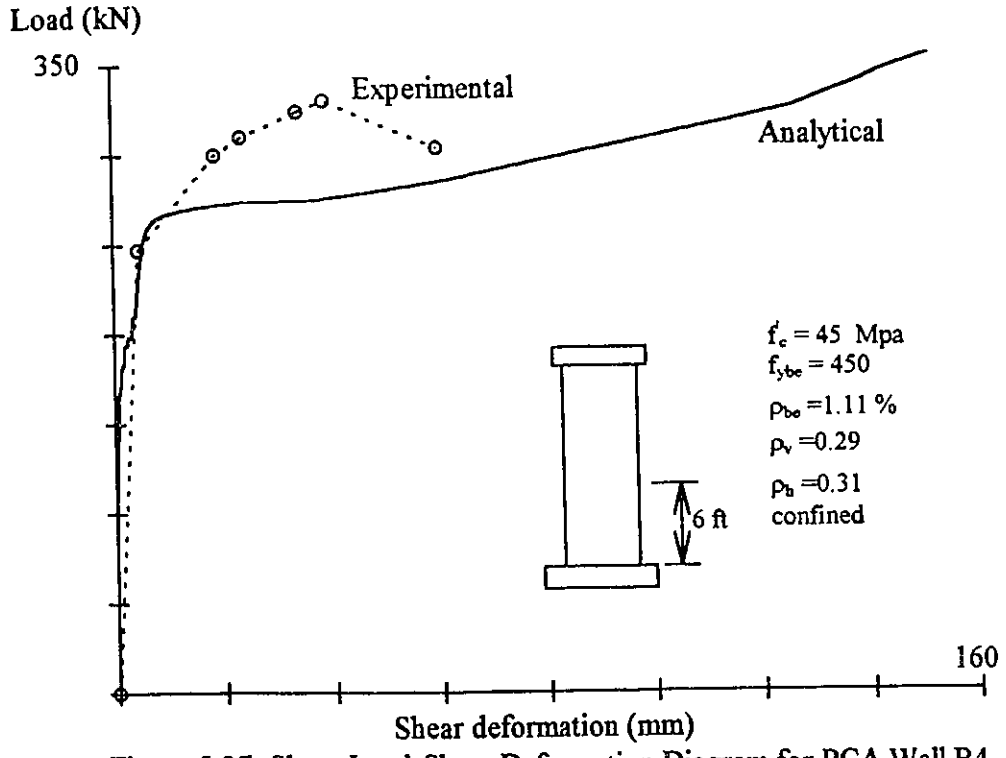

Figure 5.27 Shear Load-Shear Deformation Diagram for PCA Wall B4

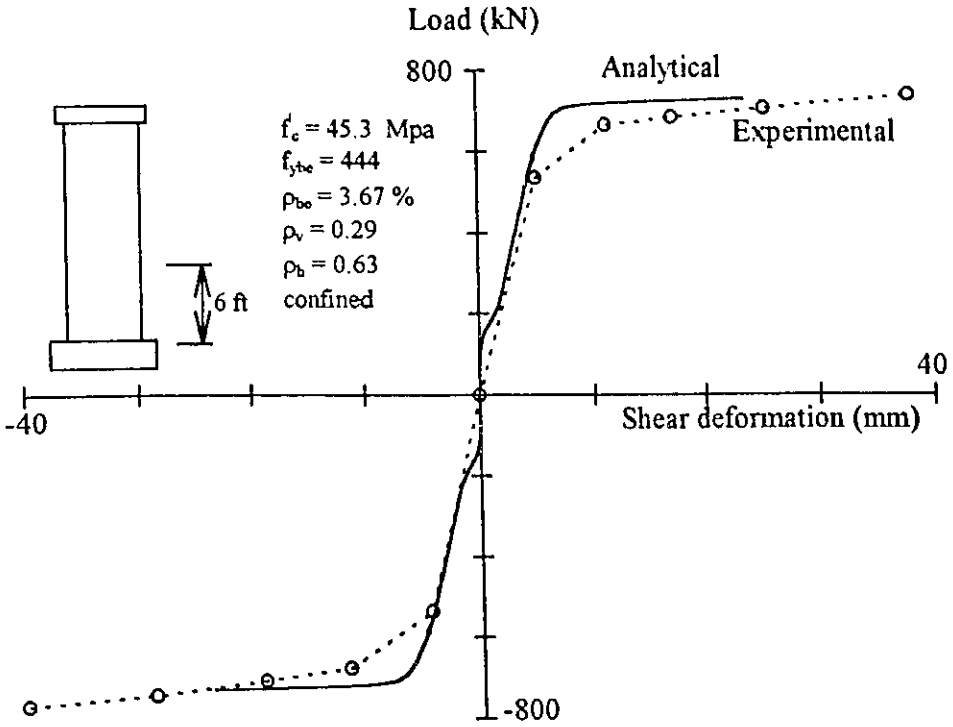

Figure 5.28 Shear Load-Shear Deformation Diagram for PCA Wall B5

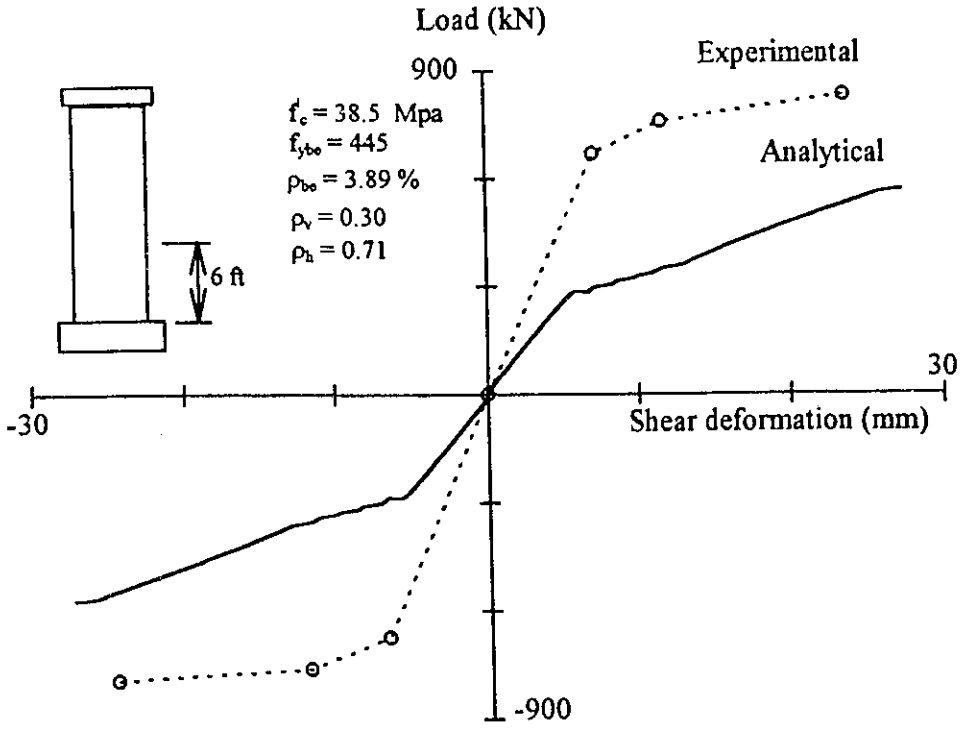

Figure 5.29 Shear Load-Shear Deformation Diagram for PCA Wall F1

Table 5.1 Ultimate Shear Capacity of Barbel Walls

Wall Code	ε_{cc}	V_{prop} kN	V_{sl} kN	V_{ACI} kN	V_{exp} kN	$\frac{V_{prop}}{V_{exp}}$	$\frac{V_{ACI}}{V_{exp}}$	θ Deg
B1	-.00040	248	218	166	360	0.69	0.46	37
B2	-.00041	371	345	167	454	0.82	0.37	39
B3	-.00067	304	255	257	414	0.73	0.62	36
B4	-.00126	311	320	293	409	0.76	0.72	32
B5	-.00066	345	298	272	445	0.78	0.61	35
B6	-.00065	342	292	269	405	0.84	0.66	35
B7	-.00067	349	303	275	360	0.97	0.76	34
B8	-.00046	412	356	250	472	0.87	0.53	40
B9	-.00071	286	257	259	414	0.69	0.63	34
B10	-.00060	277	235	236	400	0.69	0.59	37
B11	-.00078	345	290	345	414	0.83	0.83	36
B12	-.00079	356	297	372	503	0.71	0.74	36
B13	-.00077	340	277	343	428	0.79	0.80	37
B14	-.00051	725	575	500	494	1.47	1.01	21
B15	-.00052	718	575	477	489	1.47	0.98	22
B16	-.00053	705	562	477	601	1.17	0.79	22
B17	-.00067	94	82	85	89	1.06	0.96	45
B18	-.00070	168	152	131	155	1.08	0.84	34
B19	-.00066	241	208	171	202	1.19	0.85	27
B20	-.00063	439	385	267	294	1.49	0.91	18

Table 5.1 Ultimate Shear Capacity of Barbel Walls

Wall Code	ε_{cc}	V_{prop} kN	V_{sl} kN	V_{ACI} kN	V_{exp} kN	$\frac{V_{prop}}{V_{exp}}$	$\frac{V_{ACI}}{V_{exp}}$	θ Deg
B21	-.00066	340	288	247	187	1.82	1.32	32
B22	-.00042	289	253	170	249	1.16	0.68	32
B23	-.00055	353	296	248	463	0.76	0.54	31
B24	-.00055	360	304	253	374	0.96	0.68	30
B25	-.00114	308	295	251	294	1.05	0.85	27
B26	-.00054	204	184	117	205	1.0	0.57	36
B27	-.00050	166	158	77	138	1.20	0.56	37
B28	-.00054	86	78	62	90	0.96	0.69	31
B29	-.00055	762	627	552	685	1.11	0.81	31
B30	-.00088	300	280	249	301	1.0	0.83	25
B31	-.00056	224	182	166	222	1.01	0.75	45
B32	-.00062	443	363	279	374	1.18	0.75	18
B33	-.00055	351	293	247	303	1.16	0.81	31
B34	-.00043	301	259	176	316	0.95	0.56	32
B35	-.00075	516	420	240	[illegible]	1.66	0.77	20
B36	-.00074	520	423	246	367	1.42	0.67	19
B37	-.00084	608	483	232	329	1.85	0.71	21
B38	-.00043	283	250	163	214	1.32	0.76	35
B39	-.00044	284	252	161	178	1.60	0.91	35
B40	-.00047	480	440	144	245	1.96	0.59	19
B41	-.00052	445	413	133	245	1.82	0.54	19

Table 5.1 Ultimate Shear Capacity of Barbel Walls

Wall Code	ε_{cc}	V_{prop} kN	V_{sl} kN	V_{ACI} kN	V_{exp} kN	$\frac{V_{prop}}{V_{exp}}$	$\frac{V_{ACI}}{V_{exp}}$	θ Deg
B42	-.00070	192	170	151	178	1.08	0.85	31
B43	-.00070	192	170	151	178	1.08	0.85	31
B44	-.00070	192	170	151	160	1.20	0.94	31
B45	-.00066	231	200	157	274	0.84	0.57	40
B46	-.00067	233	184	142	318	0.73	0.45	43
B47	-.00081	171	152	154	227	0.75	0.68	38
B48	-.00088	208	180	154	385	0.54	0.40	39
B49	-.00060	230	196	147	191	1.20	0.77	42
B50	-.00063	234	186	141	245	0.96	0.58	43
B51	-.00049	754	700	317	966	0.78	0.33	36
B52	-.00045	861	800	394	932	0.92	0.37	35
B53	-.00051	373	307	225	608	0.61	0.37	45
B54	-.00049	764	693	369	834	0.92	0.44	36
B55	-.00045	737	700	295	804	0.92	0.37	35
B56	-.00070	76	60	42	63	1.21	0.67	44
B57	-.00065	66	54	40	75	0.88	0.53	44
B58	-.00070	77	61	43	63	1.21	0.68	44
B59	-.00086	86	71	66	94	0.91	0.70	41

Table 5.1 Ultimate Shear Capacity of Barbel Walls

Wall Code	ε_{cc}	V_{prop} kN	V_{sl} kN	V_{ACI} kN	V_{exp} kN	$\frac{V_{prop}}{V_{exp}}$	$\frac{V_{ACI}}{V_{exp}}$	θ Deg
B60	-.00084	85	70	65	90	0.94	0.72	42
B61	-.00084	85	70	64	86	0.98	0.75	42
B62	-.00096	87	74	85	98	0.89	0.87	41
B63	-.00098	88	75	88	97	0.91	0.91	40
B64	-.00098	88	75	89	102	0.87	0.87	40
B65	-.00133	50	53	24	43	1.16	0.56	37
B66	-.00111	49	52	24	44	1.12	0.54	37
B67	-.00076	75	66	47	69	1.08	0.69	40
B68	-.00080	77	68	51	71	1.08	0.71	39
B69	-.00089	76	68	70	71	1.08	0.98	39
B70	-.00091	78	72	75	77	1.01	0.97	39
B71	-.00103	79	74	98	78	1.01	1.25	38
B72	-.00101	78	73	97	77	1.02	1.25	39
B73	-.00097	143	121	118	195	0.73	0.61	45
B74	-.00080	216	147	112	185	1.17	0.60	45
B75	-.00155	1642	1338	1426	1555	1.06	0.92	27
B76	-.00054	2793	2450	1392	2310	1.21	0.60	34

Table 5.1 Ultimate Shear Capacity of Flanged Walls

Wall Code	ε_{cc}	V_{prop} kN	V_{sl} kN	V_{ACI} kN	V_{exp} kN	$\frac{V_{prop}}{V_{exp}}$	$\frac{V_{ACI}}{V_{exp}}$	θ Deg
F1	-.00056	845	628	683	1348	0.64	0.51	31
F2	-.00038	754	655	503	1023	0.74	0.49	36
F3	-.00050	1022	827	654	1176	0.87	0.56	33
F4	-.00052	878	718	206	1080	0.81	0.19	34
F5	-.00047	835	706	453	915	0.91	0.50	34
F6	-.00064	620	375	609	940	0.66	0.65	45
F7	-.00041	26	37	29	29	0.89	1.0	29
F8	-.00039	25	36	29	28	0.88	1.05	29
F9	-.00027	13	19	28	25	0.50	1.13	45
F10	-.00026	11	18	24	24	0.44	0.99	45
F11	-.00028	11	19	24	20	0.56	1.19	45
F12	-.00025	7	13	17	20	0.36	0.84	45
F13	-.00032	14	21	26	25	0.56	1.05	45
F14	-.00029	12	20	25	26	0.47	0.97	45

Table 5.1 Ultimate Shear Capacity of Rectangular Walls

Wall Code	ε_{cc}	V_{prop} kN	V_{sl} kN	V_{ACI} kN	V_{exp} kN	$\frac{V_{prop}}{V_{exp}}$	$\frac{V_{ACI}}{V_{exp}}$	θ Deg
R1	-.00102	547	406	390	519	1.05	0.75	45
R2	-.00220	645	552	406	570	1.13	0.71	45
R3	-.00206	640	562	615	679	0.94	0.90	45
R4	-.00083	430	431	226	306	1.41	0.74	45
R5	-.00206	640	562	617	632	1.01	0.98	45
R6	-.00126	177	118	150	174	1.02	0.86	45
R7	-.00108	213	174	234	235	0.91	0.99	40
R8	-.00088	217	180	214	220	0.98	0.97	40
R9	-.00091	253	200	233	260	0.97	0.89	41
R10	-.00091	272	210	232	274	0.99	0.85	42
R11	-.00119	344	306	318	322	1.07	0.99	32
R12	-.00093	326	285	267	319	1.02	0.84	31
R13	-.00101	402	342	317	383	1.05	0.83	33
R14	-.00100	460	376	316	422	1.09	0.75	34
R15	-.00210	228	203	226	260	0.88	0.87	45
R16	-.00215	220	180	203	265	0.83	0.77	45
R17	-.00219	227	193	180	247	0.92	0.73	45
R18	-.00151	521	452	458	575	0.91	0.80	31
R19	-.00163	404	427	884	380	1.06	2.33	40
R20	-.00170	230	248	663	225	1.02	2.95	45

Chapter 6

Design Recommendation

6.1 Introduction

A design procedure is presented in this chapter for earthquake resistant low-rise concrete shear walls. The procedure is based on experimental observations and the analytical procedure developed in this thesis. The analysis procedure was simplified and used for computation of ultimate wall capacity. The details of the design procedure are presented in the following sections.

6.1 A Simplified Approach for Wall Capacity

The analysis procedure described in Chapter 5 has been simplified for use in design. The simplified approach is limited to the calculation of wall strength in diagonal compression. It is assumed that the shear force applied at the floor level is transferred to the storey below (or the foundation) through a single diagonal strut. This strut is assumed to form between a 45-degree inclined crack, propagating from the compression corner at the toe of the wall, and the corner-to-corner crack extending to the neutral axis of the horizontal wall section at the base. Figure 6.1 illustrates the assumed diagonal compression strut. The strut width at the base of the wall is equal to the distance perpendicular to the diagonal strut, drawn from the neutral axis. The location of the neutral axis is obtained from plane section analysis of the horizontal wall section along the construction joint. Therefore, plane section analysis of the wall section at the base is needed to establish the strut width at each load stage. The width of the strut varies along its length, and becomes minimum

near the base, producing highest compressive stress within the strut. The shear force associated with each level of bending moment and corresponding neutral axis location is computed from equilibrium. The diagonal force, in the direction of the center-line of the strut, is calculated from applied shear force. The compressive stress in the strut is computed by dividing the diagonal force by the area of the strut perpendicular to the diagonal force at the base.

$$V_{strut} = \frac{V}{\cos\beta} \tag{6.1}$$

$$\beta = 0.5(\theta + 45) \tag{6.2}$$

$$f_{c2} = \frac{V_{strut}}{A} \tag{6.3}$$

The applied compressive stress in the strut concrete, f_{c2}, is compared with concrete compressive strength determined by a standard cylinder test. The concrete strength in this region is assumed to be equal to the cylinder strength since the transverse tensile strain in the strut, in this region is small. The reduction in concrete strength in the strut due to transverse tensile strain was considered in the analysis procedure discussed in Chapter 5. However, compressive force assumed constant within the strut leads to the maximum stress near the base where the strut width is minimum. It was found earlier in the detailed analysis procedure discussed in Chapter 5 that the rate of decrease in applied shear compression in the strut going from the base to the mid-height of the wall is faster than the rate at which concrete strength decreased due to the transverse tensile strain. This implies that the critical region for concrete crushing is near the base, rather than the mid-height region. Therefore, checking for concrete crushing at the base of the compression strut, against concrete cylinder strength, can be justified.

The aforementioned approach is based on the premise that shear capacity of low-rise walls with aspect ratios of less than or equal to 1.0 is governed by diagonal crushing of concrete. Both experimental observations and analyses of walls based on the procedure discussed in Chapter 5 confirm that walls with low aspect ratios do fail in diagonal compression, even if some yielding of web reinforcement takes place. In fact all the walls analyzed in this thesis also indicate that for walls with low aspect ratios, diagonal compression crushing precedes flexural failure even if flexural yielding may develop at the horizontal critical section. Hence, the diagonal compression capacity computed by the simplified approach provides ultimate load capacity for the wall.

The simplified approach was verified against 110 low-rise walls with aspect ratios of 1.0 or smaller. Geometric and material characteristics of the walls are tabulated in Appendix B, Tables B.1 to B.3. Wall capacities were also determined using the ACI 318-89 Building Code provisions. The analytically determined capacities are compared against those obtained by test in Table 6.1 and Figures 6.2 to 6.4. The comparisons indicate that the simplified approach provides sufficiently accurate estimates of experimentally obtained wall capacities. They further indicate that the analytical capacities based on the simplified approach show much better correlation with experimental data than those computed on the bases of ACI 318-89. Therefore, the above approach is recommended for computing the lateral load capacity of an earthquake resistant low-rise wall for design purposes.

6.3 Reinforcement Requirements

Low-rise walls usually have sufficiently high internal lever arm for required capacity in flexure. Therefore, minimum vertical reinforcement ratio of 0.25 % provides sufficiently high bending moment capacity for most applications. When higher bending moment capacity is required for high seismic loads the percentage of vertical web reinforcement may be increased. This may result in improvement in diagonal compression capacity

because of the increased compression area of the strut, associated with the position of the neutral axis. Concentration of vertical reinforcement at the boundary elements in rectangular, flanged and barbell sections provides more efficient means of improving flexural capacity.

Horizontal reinforcement in low-rise walls with aspect ratios of 1.0 and smaller is not effective in increasing shear capacity. This point was proven by both experimental and analytical investigations. However, minimum horizontal web reinforcement ratio of 0.25 % provides better distribution of cracks and hence is recommended in low-rise shear walls.

6.4 Design Against Shear Sliding

Sliding shear is one of the failure modes for low-rise shear walls that may lead to premature failure prior to the development of capacities in flexure and diagonal compression. Furthermore, shear sliding results in excessive pinching of hysteresis loops, producing significant reduction in energy dissipation capacity of walls. One of the major objectives of the experimental part of the current investigation was the assessment of the importance of shear sliding in low-rise walls with different aspect ratios. In the earlier phases of the same investigation it was shown that walls with aspect ratios of 0.5 and 0.25 were susceptible of premature failure due to shear sliding along the construction joint. The lateral load capacity of these walls were limited to 70 % to 81 % of their diagonal compression capacities, based on the procedure outlined in Chapter 5, and 65 % to 70 % of their flexural capacities, based on plane section analysis of critical wall section. Walls tested in the current investigation, with 0.75 and 1.0 aspect ratios, showed improved performance in terms of shear sliding. The walls with aspect ratios of 0.75 and 1.0 were able to sustain 95 % and 97 % of their diagonal compression capacities, respectively, and 86 % of their flexural capacities. While the capacity was improved in walls with relatively high aspect ratios, sliding shear deformation formed an appreciable portion of total

displacements in Wall 7 and Wall 8, reaching up to 35 % to 40 % of total lateral displacement at approximately 1.6 % and 1.83 % lateral drift, respectively. Sliding shear reinforcement was developed in the previous phase of this investigation (Wasiewicz, 1988), consisting of short vertical bars, placed perpendicular to the construction joint, between the vertical web bars. These bars were placed in two wall specimens with aspect ratios of 0.25 and 0.5 and were shown to be effective eliminating shear sliding. Therefore, sliding shear reinforcement, developed in the earlier phase of this investigation for walls with aspect ratios of 0.25 and 0.5, is recommended to be used for all walls with aspect ratios of 1.0 and smaller. The sliding shear reinforcement should consist of uniformly distributed vertical reinforcement, placed between the vertical web reinforcement, extending at least by development length into the foundation or storey below and extending into the web by the larger of 15 times the bar diameter or the wall thickness. Figure 6.5 illustrates the details of the sliding shear reinforcement.

6.5 Design Against Bar Buckling

Although low-rise walls generally have the required internal lever arm and hence the flexural capacity with uniformly distributed web reinforcement, buckling of exterior longitudinal bars under compression can be prevented if at least four end bars are concentrated to form a boundary element, and laterally supported by close hoops. One of the walls, without such detailing was tested earlier by Wasiewicz (Wasiewicz,1988) and was shown to develop bar buckling at about 2 % drift under reversed cyclic loading. Hence, the recommendation made by the same researcher against bar buckling is adopted here. Accordingly, the two end bars in the compression region will be supported laterally by closed hoops, with a maximum spacing of 16 hoop bar diameter or the wall thickness. This requirement is also illustrated in Figure 6.5.

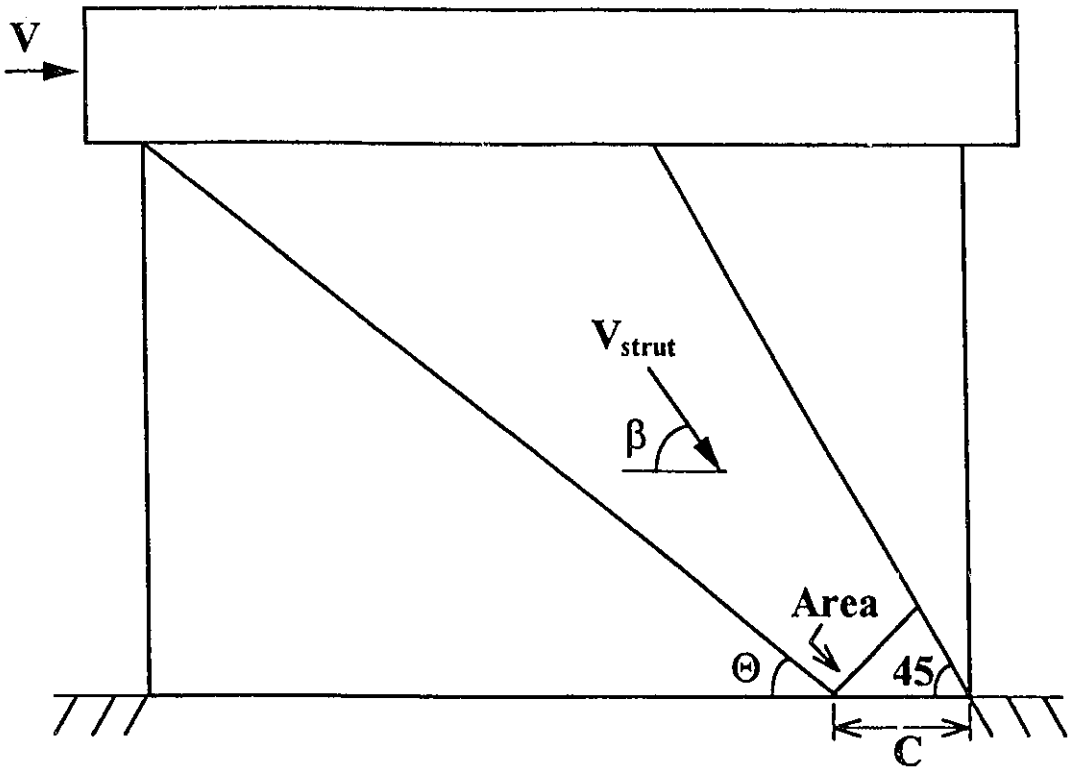

Figure 6.1 Assumed Diagonal Compression Strut

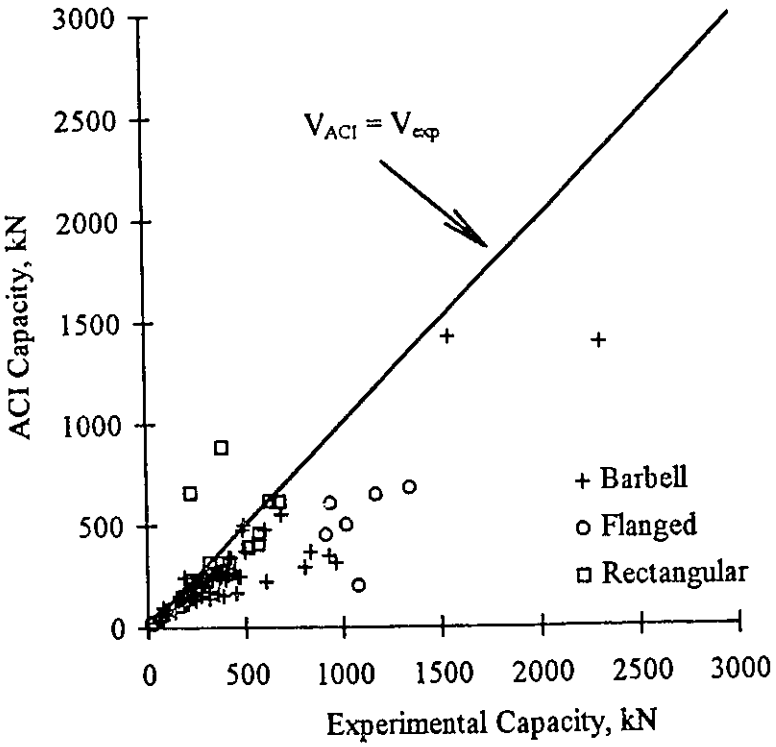

Figure 6.2a ACI Versus Experimental Capacity

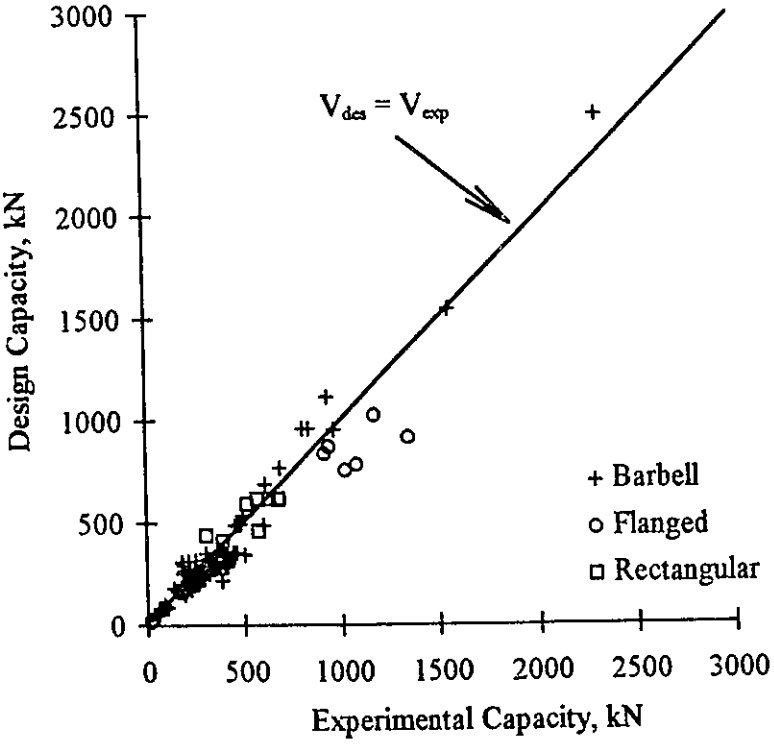

Figure 6.2b Design Versus Experimental Capacity

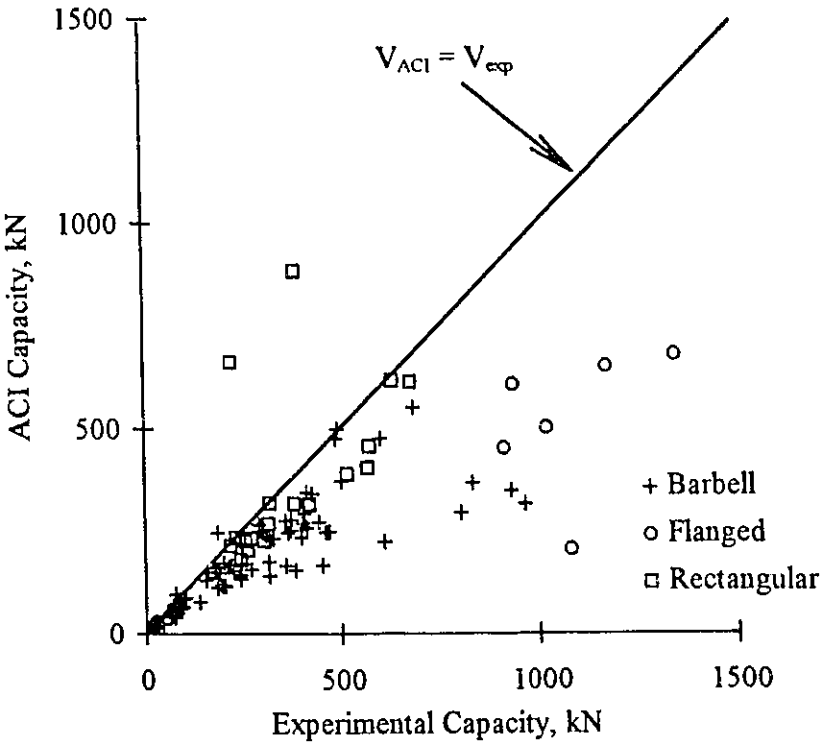

Figure 6.3a ACI Versus Experimental Capacity (new scale)

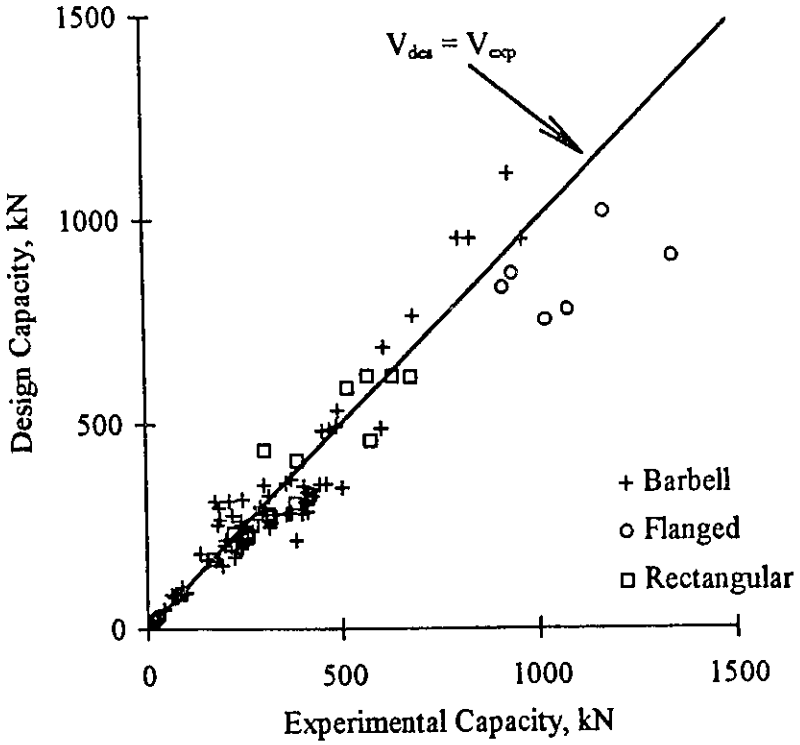

Figure 6.3b Design Versus Experimental Capacity (new scale)

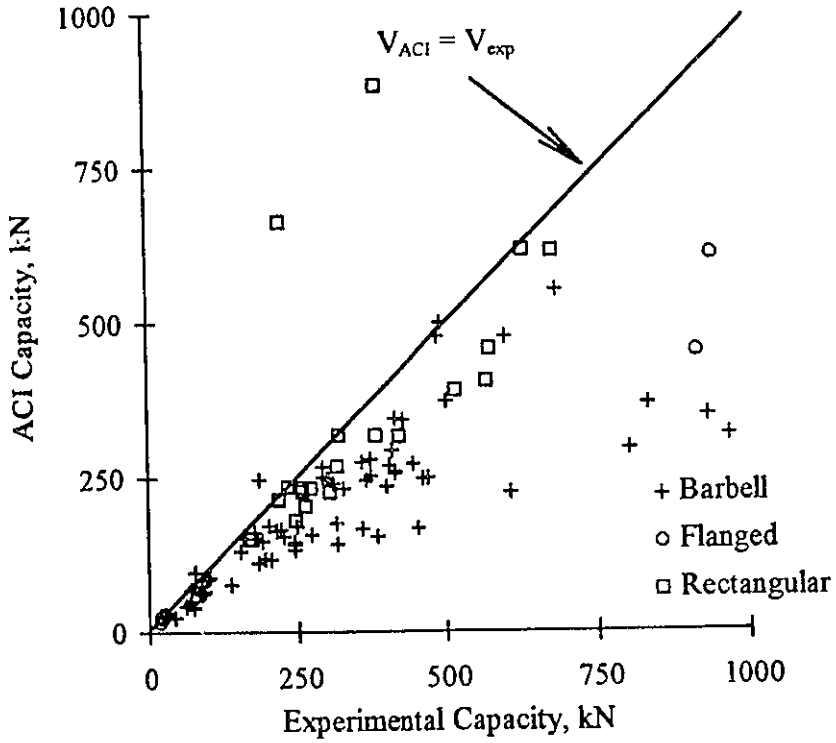

Figure 6.4a ACI Versus Experimental Capacity (new scale)

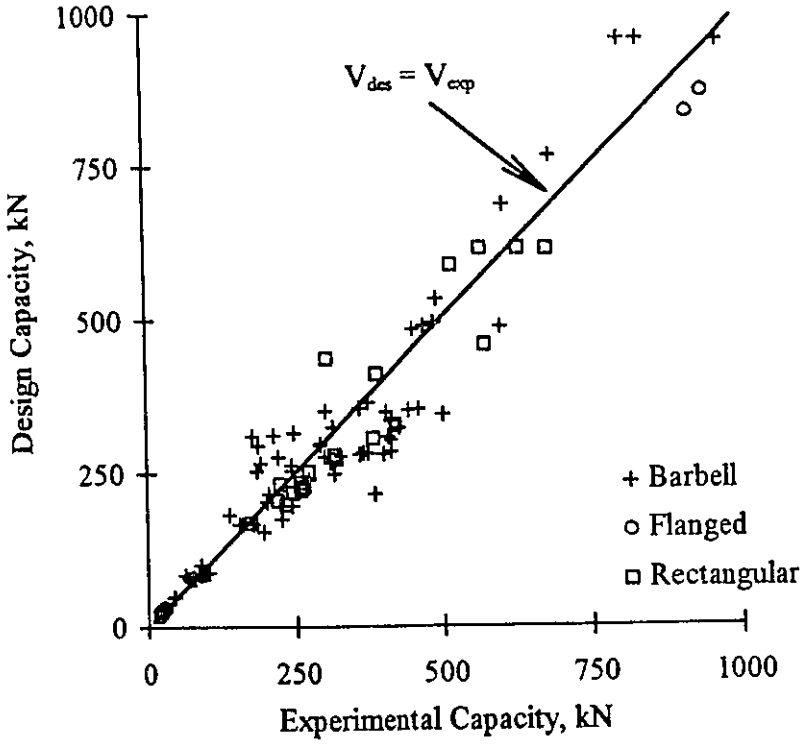

Figure 6.4b Design Versus Experimental Capacity (new scale)

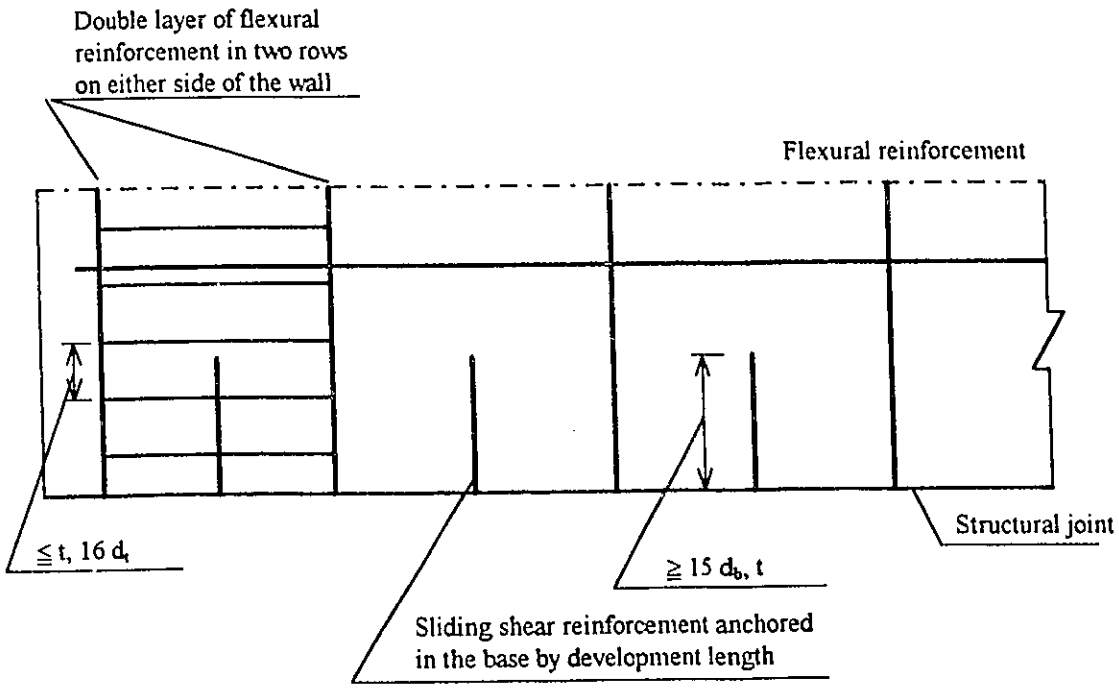

Figure 6.5 Details of the Sliding Shear Reinforcement (adopted from Wasiewicz, 1988)

Table 6.1 Design Shear Capacity of Barbell Walls

Wall Code	ε_{cc}	V_{des} kN	V_{ACI} kN	V_{exp} kN	$\frac{V_{des}}{V_{exp}}$	$\frac{V_{ACI}}{V_{exp}}$	β Deg
B1	-.00066	280	166	360	0.78	0.46	39
B2	-.00054	483	167	454	1.06	0.37	42
B3	-.00067	304	257	414	0.73	0.62	41
B4	-.00091	309	293	409	0.75	0.72	39
B5	-.00075	352	272	445	0.79	0.61	39
B6	-.00073	349	269	405	0.86	0.66	40
B7	-.00077	355	275	360	0.99	0.76	39
B8	-.00055	489	250	472	1.04	0.53	42
B9	-.00069	285	259	414	0.69	0.63	40
B10	-.00063	281	236	400	0.70	0.59	41
B11	-.00069	335	345	414	0.81	0.83	41
B12	-.00070	345	372	503	0.69	0.74	41
B13	-.00067	324	343	428	0.76	0.80	42
B14	-.00033	534	500	494	1.08	1.01	33
B15	-.00033	494	477	489	1.01	0.98	34
B17	-.00033	489	477	601	0.81	0.79	34
B17	-.00120	101	85	89	1.14	0.96	44
B18	-.00067	166	131	155	1.07	0.84	39
B19	-.00046	203	171	202	1.0	0.85	37
B20	-.00031	298	267	294	1.01	0.91	32

Table 6.1 Design Shear Capacity of Barbell Walls

Wall Code	ε_{cc}	V_{des} kN	V_{ACI} kN	V_{exp} kN	$\frac{V_{des}}{V_{exp}}$	$\frac{V_{ACI}}{V_{exp}}$	β Deg
B21	-.00051	295	247	187	1.58	1.32	39
B22	-.00052	315	170	249	1.26	0.68	38
B23	-.00055	354	248	463	0.76	0.54	38
B24	-.00057	365	253	374	0.97	0.68	38
B25	-.00068	295	251	294	1.0	0.85	37
B26	-.00060	215	117	205	1.05	0.57	40
B27	-.00055	182	77	138	1.32	0.56	41
B28	-.00053	86	62	90	0.95	0.69	38
B29	-.00056	767	552	685	1.12	0.81	38
B30	-.00055	277	249	301	0.92	0.83	36
B31	-.00082	276	166	222	1.24	0.75	45
B32	-.00031	282	279	374	0.75	0.75	32
B33	-.00055	351	247	303	1.16	0.81	38
B34	-.00052	325	176	316	1.03	0.56	38
B35	-.00031	268	240	311	0.86	0.77	33
B36	-.00032	283	246	367	0.77	0.67	33
B37	-.00032	278	232	329	0.85	0.71	33
B38	-.00056	311	163	214	1.46	0.76	39
B39	-.00056	310	161	178	1.74	0.91	39
B40	-.00024	254	144	245	1.03	0.59	32
B41	-.00022	196	133	245	0.80	0.54	32

Table 6.1 Design Shear Capacity of Barbell Walls

Wall Code	ε_{cc}	V_{des} kN	V_{ACI} kN	V_{exp} kN	$\frac{V_{des}}{V_{exp}}$	$\frac{V_{ACI}}{V_{exp}}$	β Deg
B42	-.00051	167	151	178	0.94	0.85	39
B43	-.00051	167	151	178	0.94	0.85	39
B44	-.00051	167	151	160	1.04	0.94	39
B45	-.00075	239	157	274	0.87	0.57	42
B46	-.00075	249	142	318	0.78	0.45	44
B47	-.00095	174	154	227	0.77	0.68	41
B48	-.00101	215	154	385	0.56	0.40	42
B49	-.0007	266	147	191	1.39	0.77	44
B50	-.00071	262	141	245	1.07	0.58	44
B51	-.00063	954	317	966	0.99	0.33	40
B52	-.00067	1116	394	932	1.20	0.37	39
B53	-.00104	688	225	608	1.13	0.37	45
B54	-.00063	957	369	834	1.15	0.44	40
B55	-.00063	957	295	804	1.19	0.37	40
B56	-.00090	84	42	63	1.34	0.67	43
B57	-.00086	81	40	75	1.09	0.53	44
B58	-.00090	85	43	63	1.34	0.68	43
B59	-.00095	87	66	94	0.93	0.70	43

Table 6.1 Design Shear Capacity of Barbell Walls

Wall Code	ε_{cc}	V_{des} kN	V_{ACI} kN	V_{exp} kN	$\frac{V_{des}}{V_{exp}}$	$\frac{V_{ACI}}{V_{exp}}$	β Deg
B60	-.00094	87	65	90	0.96	0.72	43
B61	-.00093	86	64	86	1.01	0.75	43
B62	-.00095	87	85	98	0.89	0.87	43
B63	-.00097	88	88	97	0.91	0.91	43
B64	-.00097	88	89	102	0.87	0.87	43
B65	-.00105	49	24	43	1.13	0.56	41
B66	-.00104	48	24	44	1.10	0.54	41
B67	-.00112	79	47	69	1.14	0.69	42
B68	-.00116	79	51	71	1.12	0.71	41
B69	-.00111	78	70	71	1.10	0.98	42
B70	-.00115	79	75	77	1.03	0.97	41
B71	-.00114	79	98	78	1.02	1.25	41
B72	-.00113	79	97	77	1.03	1.25	42
B73	-.00150	154	118	195	0.79	0.61	45
B74	-.00097	252	112	185	1.36	0.60	45
B75	-.00071	1544	1426	1555	0.99	0.92	37
B76	-.00048	2498	1392	2310	1.08	0.60	39

Table 6.1 Design Shear Capacity of Flanged Walls

Wall Code	ε_{cc}	V_{des} kN	V_{ACI} kN	V_{exp} kN	$\frac{V_{des}}{V_{exp}}$	$\frac{V_{ACI}}{V_{exp}}$	β Deg
F1	-.00060	914	683	1348	0.68	0.51	38
F2	-.00038	755	503	1023	0.74	0.49	41
F3	-.00050	1023	654	1176	0.87	0.56	39
F4	-.00046	782	206	1080	0.72	0.19	40
F5	-.00047	837	453	915	0.91	0.50	39
F6	-.00102	871	609	940	0.93	0.65	45
F7	-.00066	31	29	29	1.08	1.0	36
F8	-.00066	32	29	28	1.13	1.05	36
F9	-.00089	29	28	25	1.17	1.13	44
F10	-.00087	26	24	24	1.06	0.99	44
F11	-.00098	25	24	20	1.24	1.19	43
F12	-.00089	19	17	20	0.94	0.84	44
F13	-.00105	28	26	25	1.11	1.05	43
F14	-.00103	27	25	26	1.06	0.97	44

Table 6.1 Design Shear Capacity of Rectangular Walls

Wall Code	ε_{cc}	V_{des} kN	V_{ACI} kN	V_{exp} kN	$\frac{V_{des}}{V_{exp}}$	$\frac{V_{ACI}}{V_{exp}}$	β Deg
R1	-.00146	589	390	519	1.13	0.75	45
R2	-.00177	617	406	570	1.08	0.71	45
R3	-.00173	615	615	679	0.91	0.90	45
R4	-.00107	436	226	306	1.42	0.74	45
R5	-.00173	616	617	632	0.98	0.98	45
R6	-.00111	169	150	174	0.97	0.86	45
R7	-.00088	199	234	235	0.85	0.99	43
R8	-.00074	205	214	220	0.93	0.97	43
R9	-.00076	234	233	260	0.90	0.89	44
R10	-.00078	252	232	274	0.92	0.85	44
R11	-.00067	272	318	322	0.85	0.99	39
R12	-.00056	279	267	319	0.87	0.84	39
R13	-.00059	306	317	383	0.80	0.83	39
R14	-.00060	327	316	422	0.78	0.75	40
R15	-.00176	221	226	260	0.85	0.87	45
R16	-.00276	227	203	265	0.86	0.77	45
R17	-.00178	217	180	247	0.88	0.73	45
R18	-.00089	458	458	575	0.80	0.80	38
R19	-.00192	410	884	380	1.08	2.33	42
R20	-.00174	231	663	225	1.03	2.95	45

Chapter 7

Summary and Conclusions

7.1 Summary

A combined experimental and analytical research was conducted on behaviour, analysis and design of low-rise concrete shear walls. The objective for the experimental part was to investigate strength and deformation characteristics of low-rise walls under inelastic reversed cyclic loading, simulating seismic effects. One of the main test parameters was the wall aspect ratio, as it affected failure modes, particularly shear sliding. The test program included two large scale reinforced concrete shear walls, with aspect ratios of 0.75 and 1.0. The walls were 1500 mm high and 100 mm thick. One of the walls was 2000 mm wide, producing an aspect ratio of 0.75, and the other was 1500 mm wide, producing an aspect ratio of 1.0. Uniformly placed horizontal and vertical web reinforcement was placed in two rows to reflect the actual construction practice. Strong and stiff loading beams were cast with the walls for application of uniform shear at the top. The walls were built in two stages. First a stiff foundation was cast to secure the walls to the laboratory strong floor for full fixity. A construction joint was prepared between the footing and the wall before casting the wall at a later date.

The walls were well instrumented for load and deformation measurements. An important aspect of instrumentation was the measurement of deformation components separately. Aside form horizontal displacements, flexural rotations, shear distortions and anchorage slip were measured. Hysteretic behaviour of these deformation components were examined to assess the significance of each deformation component on wall behaviour. This information provided

insight into the governing mode of behaviour, as well as data for development and verification of the analytical procedure developed.

The analytical part included development of a rational analysis procedure for strength and inelastic deformation computations for low-rise shear walls. An effort was made to develop the procedure such that it would be reasonably straight forward for use in practice. An inclined section analysis was developed and recommended, analogous to plane section analysis under bending. Equilibrium and strain compatibility were used as the basis for the procedure. Simplifying assumptions were made based on experimental observations in establishing the strain distribution along the inclined plane. Strain transformation was used, based on Mohr's circle of strains to compute internal forces in horizontal and vertical reinforcement. Mohr's circle of stresses was used to compute diagonal compressive stress in concrete struts. The strain condition in the web provided information on shear deformations.

An extensive verification of the analysis procedure was conducted against 110 low-rise walls. Additional verification was done against available test data on inelastic shear force-shear deformation relationships. The comparisons indicate reasonably good correlations between the results based on the analysis procedure and data recorded during large scale tests of shear walls.

A simplified method was developed for design purposes to estimate wall capacity. A design procedure was outlined, using the simplified procedure, for earthquake resistant design of shear walls with aspect ratios of 1.0 and smaller.

7.2 Conclusions

The following conclusions were drawn from the combined experimental and analytical investigation reported in this thesis:

- Low-rise shear walls with aspect ratios between 0.75 and 1.0, reinforced with 0.8% horizontal and vertical reinforcement ratio develop lateral load capacities near their flexural strengths. These walls failed in diagonal crushing shortly before developing their flexural strengths under reversed cyclic loading. The walls tested in this investigation indicated that Wall 7, with an aspect ratio of 0.75, and Wall 8 with an aspect ratio of 1.0, developed 86 % of their flexural capacities. These walls, however, possess deformabilities of 0.92 % and 1.83 % lateral drift, when they have aspect ratios of 0.75 and 1.0, respectively. This may be viewed as sufficient ductility for low-rise concrete walls with aspect ratios of 0.75 to 1.0.

- Investigation of hysteretic relationships of deformation components indicates that shear and flexure play equally significant roles on walls with aspect ratios of 0.75 and 1.0. Flexural and shear deformations formed approximately 40% each, of total lateral displacement in Wall 7 with an aspect ratio of 0.75. This breakdown was approximately 45% flexure and 35% shear in Wall 8 with an aspect ratio of 1.0, with increasing contribution of flexure at later stages of loading.

- Walls with aspect ratios of 0.75 and 1.0 developed limited shear sliding along the construction joint prior to the onset of strength degradation. Horizontal shear sliding formed 8 % to 10 % of total lateral displacement in the walls tested in this investigation, within the range mentioned. However, shear sliding increased significantly thereafter, forming 35% and 40% of total lateral displacement at 1.6 % and 1.83 % lateral drift for Wall 7 and Wall 8, respectively.

- Although deformabilities of walls with aspect ratios of 0.75 to 1.0 appear to be satisfactory in terms of expected drift levels, energy absorption capacities as indicated by hysteretic force-deformation relationships are less than those expected in flexure dominant members. Significant pinching of hysteresis loops and stiffness degradation between the consecutive load cycles at the same deformation level were observed in the experimental data recorded. A marked increase in pinching of force-displacement hysteretic relationship is attributed to the increase in shear sliding at later stages of loading, a phenomenon that may be minimized through the use of sliding shear reinforcement.

- Plane section analysis of low-rise walls produces reasonably good estimates of sectional flexural response. Analytical calculations of flexural rotations for walls tested in this investigation agree fairly well with those recorded experimentally.

- The analysis procedure developed in this investigation, for walls with aspect ratios of 1.0 or smaller, produces good correlations with experimentally recorded wall capacities. The same procedure also produces reasonably good agreement with experimentally recorded inelastic shear force-shear deformation relationships.

- Wall aspect ratio is clearly the most important parameter for low-rise concrete shear walls that dictates the failure mode. The analyses of a large number of walls with different aspect ratios indicated that, irrespective of the reinforcement ratio used, walls with aspect ratios of less than 1.0 develop diagonal compression failure when sliding shear failure is prevented. Walls with aspect ratios of 0.5 and smaller may fail in sliding shear if shear sliding is not prevented by special reinforcement provided perpendicular to the construction joint.

- In walls with aspect ratios less than 1.0, vertical wall reinforcement plays a substantially more important role than horizontal web reinforcement. Vertical reinforcement improves both flexural and diagonal compression capacities of walls. While horizontal reinforcement improves crack distribution within the web, it does not add to the strength of low-rise walls with aspect ratios less than 1.0. Hence, the ACI318-89 requirement for low-rise walls are not applicable to walls with aspect ratios of less than 1.0.

7.3 Recommendations for Further Research

The following recommendations are made for future research:

1. More experimental data are needed to establish mechanism of shear resistance in low-rise walls with aspect ratios in the range of 1.0 to 2.0. Therefore, more tests of shear walls are recommended in the aspect ratio range mentioned.

2. The analysis procedure developed in this investigation can be used to conduct a comprehensive parametric investigation to establish the influence of geometric and material parameters on wall behaviour.

3. The analysis procedure developed in this investigation is limited to walls with aspect ratios of 1.0 or less. The procedure can easily be extended to other ranges of wall aspect ratios.

4. Shear sliding is not included as a failure criterion in the proposed analysis procedure. A study of shear sliding, with underlining conditions is recommended.

5. The analysis procedure can be refined in the area of concrete strength in diagonal strut. Biaxial stress condition, and strength of concrete under cyclic loading form two important areas of recommended research.

6. The simplified approach described in Chapter 6 and associated design procedure can be put into a form suitable for recommendation to building code committees. Further development of the design procedure is recommended.

Bibliography

American Concrete Institute, "Building Code Requirements for Reinforced Concrete," ACI 318-9, Detroit, 1989, 346 pp.

Barda, F., Hanson, J. M., and Corley, W. G., "Shear Strength of Low-Rise Walls with Boundary Elements," Reinforced Concrete Structures in Seismic Zones, ACI Special Publication SP-53, American Concrete Institute, Detroit, 1977, pp. 149-202.

Benjamin, J. R., and Williams, H., "The Behavior of One-Story Reinforced Concrete Shear Walls," Proceedings of the American Society of Civil Engineers; Journal of the Structural Division, ASCE, Vol. 83, 1957, pp. 1-49.

Birkeland, P. W., and Birkeland, H. W., "Connections in Precast Concrete Construction," Proceedings of the American Concrete Institute, Journal ACI, Vol. 63, 1966, pp. 345-368.

Canadian Standard Association, "Design of Concrete Structures for Buildings," CAN3-A23.3-M84, Canadian Portland Cement Association, Ottawa, Canada 1985.

Cheng, F. Y., Mertz, G. E., Sheu, M. S., and Ger, J. F., "Computed Versus Observed Inelastic Seismic Low-Rise RC Shear Walls," Journal of Structural Engineering, Vol. 119, No. 11, November 1993, pp. 3255-3275.

Collins, M. P., "Towards a Rational Theory for RC Members in Shear," ASCE Proceedings, Journal of the Structural Division, ST. 104, 1978, pp. 649-666.

Collins, M. P., and Mitchell, D., "Prestressed Concrete Structures," Prentice Hall, Englewood Cliffs, New Jersey, 1991, 766 pp.

Farrar, C. R., Baker, W. E., and Dove, R.C., "Static and Simulated Seismic Testing of the TRG-7 through -16 Shear Wall Structures," Los Alamos National Laboratory Report No. NUREG/CR-5660, LA-11992-MS, RD, September 1991.

Hsu, T. T. C., "Unified Theory of Reinforced Concrete," CRC Press, Inc. Florida, 1993, 313 pp.

Hsu, T. T. C., and Mo, Y. L., "Softening of Concrete in Low-Rise Shear Walls," Journal ACI, Proceedings, Vol. 82, No. 6, November-December 1985, pp. 883-889.

Lefas, L. D., Kotsovos, M. D., and Ambraseys, N. N., "Behavior of Reinforced Concrete Structural Walls: Strength, Deformation Characteristics, and Failure Mechanism," ACI Structural Journal, Vol. 7, No. 1, January-February 1990, pp. 23-31.

Lefas, L. D., and Kotsovos,M. D., "Strength and Deformation Characteristics of Reinforced Concrete Walls under Load Reversals," ACI Structural Journal, Vol. 87, No. 6, November-December 1990, pp. 716-726.

Mac Gregor, J. G., "Reinforced Concrete, Mechanics and Design," 2 nd Edition, Prentice Hall Inc, Englewood Cliffs, New Jersey, 1992, 848 pp.

Marti, P., "Basic Tools of Reinforced Concrete Beam Design," Journal ACI, Proceedings, Vol. 82, No. 1, January-February 1985, pp. 46-56.

Marti, P., "Truss Model in Detailing," Concrete International, Design and Construction, Journal ACI, Proceedings, Vol. 7, No. 12, December 1985, pp. 66-73.

Mast, R. F., "Auxiliary Reinforcement in Concrete Connections," Journal of the Structural Division, ASCE, Vol. 94, June 1968, pp. 1485-1504.

Mattock, A. H., and Hawkins, N. M., "Shear Transfer in Reinforced Concrete; Recent Research," PCI Journal, March-April 1972, pp. 55-75.

Mau, S. T., and Hsu, T. T. C., "Shear Design and Analysis of Low-Rise Structural Walls," Journal ACI, Proceedings, Vol. 83, No. 2, March-April 1986, pp. 306-315.

Oesterle, R. G., "Inelastic Analysis for In-Plane Strength of Reinforced Concrete Shear Walls," Ph.D. Thesis, Northwestern University, Evanston, Illinois, June 1986, 332 pp.

Oesterle, R. G., Fiorato A. E., Johal, L. S., Carpenter, J. E., Russel, H. G., and Corley, W. G., "Earthquake Resistant Structural Walls; Tests of Isolated Walls," Report to National Science Foundation; PCA, Skokie, Illinois, November 1976, 44 pp.

Oesterle, R. G., Aristizabal-Ochoa, J. D., Fiorato, A. E., Russel, H. G., and Corley, W. G, "Earthquake Resistant Structural Walls; Tests of Isolated Walls-Phase II," Report to National Science Foundation; PCA, Skokie, Illinois, October 1979, 84 pp.

Ogata, K., and Kabeyasawa, T., "Experimental Study on the Hysteretic Behavior of Reinforced Concrete Shear Walls under the Loading of Different Moment-to-Shear Ratios," Transaction of the Japan Concrete Institute, Tokyo, Vol. 6, 1984, pp. 717-724.

Onozato, N., and Mochizuki, M., "Analysis of Skeleton Curve of Multistory Framed Shear Walls using Macro Models," Transactions of the Japan Concrete Institute, Vol. 13, 1991, pp. 303-310.

Park, R., and Paulay, T., "Reinforced Concrete Structures," John Wiley and Sons Inc. New York, 1975, 769 pp.

Paulay, T., "Ductility of Reinforced Concrete Shear Walls for Seismic Areas," Reinforced Concrete Structures in Seismic Zones, ACI Special Publication SP-53, American Concrete Institute, Detroit, 1977, pp. 127-147.

Paulay, T., "The Design of Reinforced Concrete Ductile Shear Walls for Earthquake Resistance," Research Report No. 81-1; Department of Civil Engineering, University of Canterbury, Christchurch New Zealand, February 1981, 125pp.

Paulay, T., Priestley, M. J. N., and Synge, A. J., "Ductility in Earthquake Resisting Squat Shear Walls," Journal ACI, No. 79-26, July-August 1982, pp. 257-269.

Pilette, C. F., "Behavior of Earthquake Resistant Squat Shear Walls," M. A. Sc. Thesis, University of Ottawa, Canada, 1987, 143 pp.

Saatcioglu, M., "Hysteretic Shear Response of Low-Rise Walls," Preliminary Proceedings Volume of International Workshop on Concrete Shear in Earthquake, University of Houston, Texas, U. S. A., January 13-16, 1991, pp. I12-1-I12-10.

Saatcioglu, M., and Razvi, S. R., "Strength and Ductility of Confined Concrete," Journal of Structural Engineering, Vol. 118, No. 6, June 1992, pp. 1590-1607.

Shaikh, A. F., "Proposed Revision to Shear-Friction Provisions," PCI Journal, Prestressed Concrete Institute, Vol. 23, No.2, March-April 1978, pp. 12-21.

Siao, W. B., "Shear Strength of Short Reinforced Concrete Walls, Corbels, and Deep Beams," ACI Structural Journal, Vol. 91, No. 2, March-April 1994, pp. 123-132.

Synge, A. J., "Ductility of Squat Shear Walls," Research Report 80-8, Department of Civil Engineering, University of Canterbury, Christchurch New Zealand, February 1980, 141 pp.

Vecchio, F., and Collins, M. P., "The Modified Compression-Field Theory for Reinforced Concrete Elements Subjected to Shear," Journal ACI, Proceedings, Vol. 83, No. 2, March-April 1986, pp. 219-231.

Wasiewicz, Z. F., "Sliding Shear in Low-Rise Shear Walls under Lateral Load Reversals," M. A. Sc. Thesis, University of Ottawa, Canada, 1988, 127 pp.

Wiradinata, S., "Behavior of Squat Shear Walls Subjected to Load Reversals," M. A. Sc. Thesis, University of Toronto, Canada, 1985, 171 pp.

Wiradinata, S., and Saatcioglu, M., "Tests of Squat Shear Wall Under Lateral Load Reversals," Third U. S. National Conference on Earthquake Engineering, Charleston, South Carolina, V.2, 1986, pp. 1395-1406.

Wood, S. L., "Shear Strength of Low-Rise Reinforced Concrete Walls," ACI Structural Journal, Vol. 87, No. 1, January-February 1990, pp. 99-107.

APPENDIX A

Horizontal Component for Deflection due to Flexure and Adjustments for the Component of Deflection due to Anchorage Slip

The experimental data for flexural response consist of total rotation of the top beam and the rotation due to anchorage slip, which also includes a portion of flexural rotation within the LVDT gauge length. Because it was nearly impossible to attach the LVDT's without a gauge length, what was meant to record anchorage slip rotation also included flexural rotation within the bottom 45 mm portion of the wall. This information was used in computing lateral deflection due to flexure, and also in computing actual rotations due to anchorage slip.

The flexural displacement was computed from curvature diagram along the wall height. The curvature diagram was established such that the variation along the wall height would be bilinear, and the area under the diagram (integration of curvatures) would be equal to the experimentally measured rotation. The experimentally measured flexural rotation, obtained by subtracting the anchorage slip reading from that for total rotation, gives the flexural rotation between the point of application of the load at the top and the section 45 mm above the base. The area under the curvature diagram between these two stations should be equal to the experimental values obtained. Using this condition, and establishing the yield point at moment corresponding to analytically computed yield curvature, the curvature diagram was constructed, as illustrated in Figure A.1. Extending the curvature diagram to the base of the wall, completely defined the curvature diagram. This curvature diagram was used in computing horizontal displacement due to flexure (as moment of the area), and in adjusting anchorage slip rotations to exclude that portion of rotations associated with flexural rotation of the bottom 45 mm region (shaded area in Figure A.1).

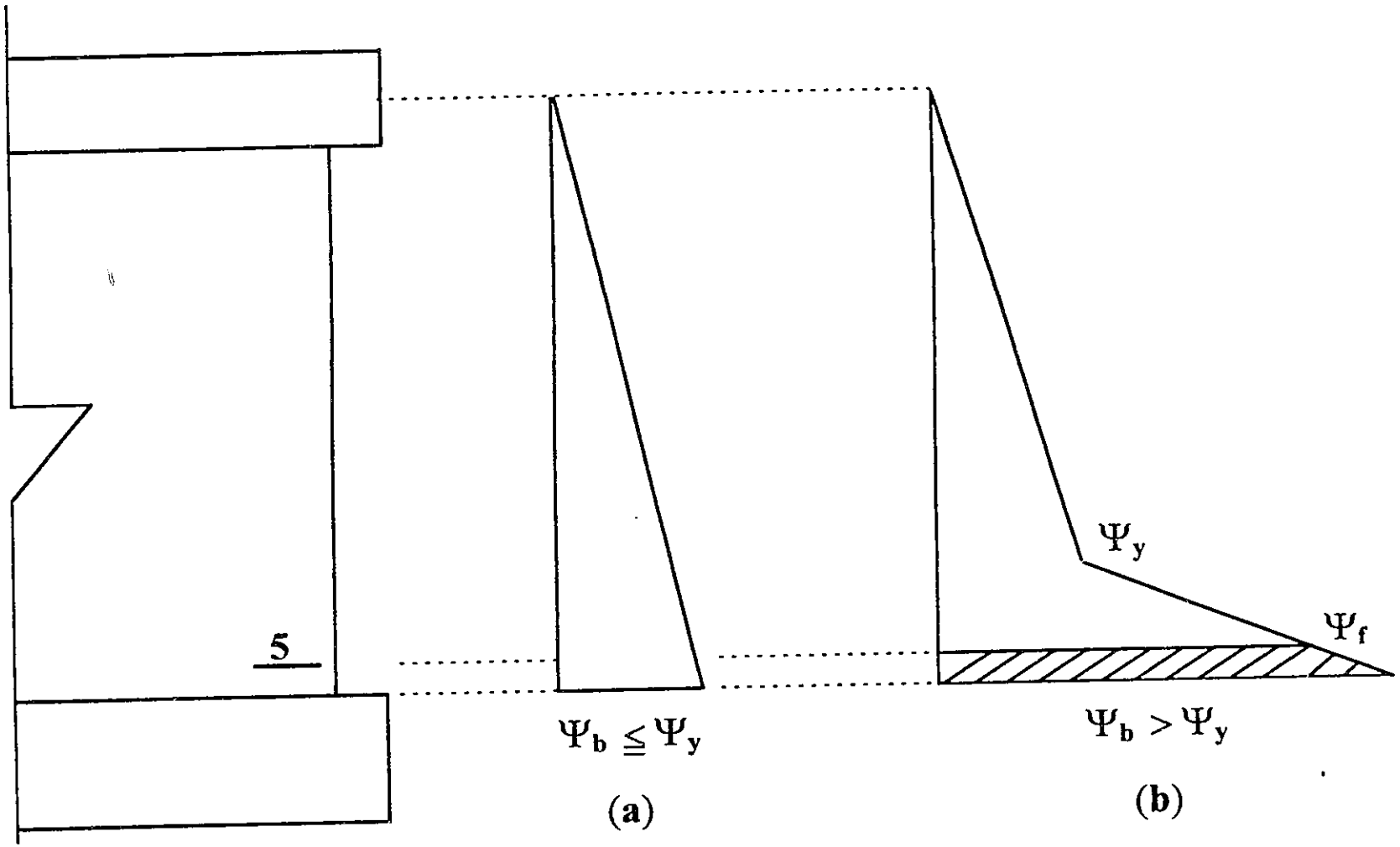

Figure A.1 Assumed Curvature Diagram for Base Curvature Less than or Equal to Yield Curvature (a) and Larger than Yield Curvature (b)

APPENDIX B

Identification, Dimensions and Properties of Low-Rise Walls

Table B.1 Identification of Barbell Walls

Wall Code	Wall ID	Researcher	Reference
B1	6	Antebi	Cited in Wood, 1990
B2	10	=	=
B3	13	=	=
B4	25	=	=
B5	32	=	=
B6	35	=	=
B7	37	=	=
B8	41	=	=
B9	45	=	=
B10	49	=	=
B11	50	=	=
B12	51	=	=
B13	54	=	=
B14	55	=	=
B15	58	=	=
B16	60	=	=
B17	4BII-1	Benjamin and williams	Benjamin and Willimas, 1957
B18	4BII-2	=	Cited in Wood, 1990
B19	4BII-3	=	=
B20	4BII-4	=	=

Table B.1 Identification of Barbell Walls

Wall Code	Wall iD	Researcher	Reference
B21	3BI-1	Benjamin and williams	Benjamin and Willimas, 1957
B22	1BII-1	=	==
B23	1BII-2a	=	==
B24	1BII-2b	=	==
B25	3BI-3	=	==
B26	3AII-1	=	Cited in Wood, 1990
B27	3AII-2	=	==
B28	1BII-1a	=	==
B29	1BII-3	=	Benjamin and Willimas, 1957
B30	NV-1	=	Cited in Wood, 1990
B31	NV-11	=	==
B32	NV-18	=	==
B33	VR-3	=	Benjamin and Willimas, 1957
B34	R-1	=	==
B35	A1-A	=	==
B36	A1-B	=	==
B37	A2-B	=	==
B38	M-1	=	==
B39	M-4	=	==
B40	MR-2	=	Cited in Wood, 1990
B41	MR-4	=	==

Table B. 1 Identification of Barbell Walls

Wall Code	Wall ID	Researcher	Reference
B42	SD-1A	Benjamin and williams	Cited in Wood, 1990
B43	SD-1B	=	=
B44	SD-1C	=	=
B45	A-8	Galletly	=
B46	A-4	=	=
B47	B-8	=	=
B48	B-4	=	=
B49	C-8	=	=
B50	C-4	=	=
B51	29	Ryo	=
B52	30	=	=
B53	31	=	=
B54	70	Sugano	=
B55	71	=	=
B56	101	Tanabe	=
B57	102	=	=
B58	103	=	=
B59	104	=	=

Table B.1 Identification of Barbell Walls

Wall Code	Wall ID	Researcher	Reference
B60	105	Tanabe	Cited in Wood, 1990
B61	106	=	==
B62	107	=	==
B63	108	=	==
B64	109	=	==
B65	110	=	==
B66	111	=	==
B67	112	=	==
B68	113	=	==
B69	114		==
B70	115	=	==
B71	116	=	==
B72	117	=	==
B73	134	Tsuboi	==
B74	135	=	==
B75	150	Aoyagi	==
B76	152	=	==

Table B.1 Identification of Flanged Walls

Wall Code	Wall ID	Researcher	Reference
F1	B1-1	Barda	Barda et. al, 1973
F2	B2-1	=	=
F3	B3-2	=	=
F4	B4-3	=	=
F5	B6-4	=	=
F6	B8-5	=	=
F7	46	Kokusho	Cited in Wood, 1990
F8	47	=	=
F9	50	=	=
F10	51	=	=
F11	52	=	=
F12	53	=	=
F13	54	=	=
F14	55	=	=

Table B.1 Identification of Rectangular Walls

Wall Code	Wall ID	Researcher	Reference
R1	SW-7	Cardenas	Cardenas et, al. 1973
R2	SW-8	=	==
R3	SW-9	=	==
R4	SW-10	=	==
R5	SW-13	=	==
R6	169	Yoshizaki	Cited in Wood, 1990
R7	171	=	==
R8	172	=	==
R9	173	=	==
R10	174	=	==
R11	176	=	==
R12	177	=	==
R13	178	=	==
R14	179	=	==
R15	SW11	Lefas	Lefas et. al, 1990a
R16	SW14	=	==
R17	SW17	=	==
R18	W1	Saatcioglu and Wiradinata	Wiradinata, 1985
R19	W7	Saatcioglu and Mohammadi	Mohammadi, 1994
R20	W8	=	==

Table B.2 Reinforcement Ratios and Material Properties of Barbell Walls

Wall Code	f_c' Psi	ρ_{be} %	ρ_v %	ρ_h %	f_{ybe} Ksi	f_{yv} Ksi	f_{yh} Ksi
B1	3160	2.09	0.25	0.25	47.0	39.3	39.3
B2	3360	4.72	0.25	0.25	44.3	39.3	39.3
B3	2670	2.09	0.50	0.50	43.0	57.0	57.0
B4	5970	2.09	0.50	0.50	40.0	48.0	48.0
B5	3880	2.09	0.50	0.50	50.0	50.0	50.0
B6	3700	2.09	0.50	0.50	50.0	50.0	50.0
B7	4100	2.09	0.50	0.50	50.0	50.0	50.0
B8	3310	4.72	0.50	0.50	49.0	46.9	46.9
B9	2950	2.09	0.25	0.25	42.9	45.4	45.4
B10	2030	2.09	0.25	0.25	45.5	46.3	46.3
B11	2380	2.09	0.50	0.50	46.3	44.4	44.4
B12	2470	2.09	0.50	0.50	46.2	49.8	49.8
B13	2090	2.09	0.50	0.50	45.3	50.2	50.2
B14	3310	2.09	0.50	0.50	46.5	52.3	52.3
B15	2900	2.09	0.50	0.50	48.7	50.5	50.5
B16	2840	2.09	0.50	0.50	46.2	50.8	50.8
B17	2900	2.21	0.50	0.50	45.3	49.5	49.5
B18	3100	2.21	0.50	0.50	45.3	49.5	49.5
B19	2800	2.21	0.50	0.50	45.3	49.5	49.5
B20	3830	2.21	0.50	0.50	45.3	49.5	49.5

Table B.2 Reinforcement Ratios and Material Properties of Barbell Walls

Wall Code	f_c' Psi	ρ_{be} %	ρ_v %	ρ_h %	f_{ybe} Ksi	f_{yv} Ksi	f_{yh} Ksi
B21	3100	4.19	0.50	0.50	45.3	49.5	49.5
B22	2900	2.09	0.25	0.25	45.3	49.5	49.5
B23	3200	2.09	0.50	0.50	45.3	49.5	49.5
B24	3500	2.09	0.50	0.50	45.3	49.5	49.5
B25	3300	1.31	0.50	0.50	45.3	49.5	49.5
B26	3600	3.31	0.50	0.50	45.3	49.5	49.5
B27	2800	3.31	0.25	0.25	45.3	49.5	49.5
B28	3100	2.01	0.50	0.50	45.3	49.5	49.5
B29	3000	2.0	0.50	0.50	45.3	49.5	49.5
B30	3900	1.76	0.50	0.50	45.3	49.5	49.5
B31	3600	4.96	0.50	0.50	45.3	49.5	49.5
B32	3000	1.76	0.50	0.50	45.3	49.5	49.5
B33	3100	2.09	0.50	0.50	45.3	49.5	49.5
B34	3000	2.09	0.25	0.25	47.0	52.0	52.0
B35	3140	2.21	1.0	1.0	43.0	49.5	49.5
B36	3280	2.21	1.0	1.0	43.0	49.5	49.5
B37	2960	2.21	1.50	1.50	43.0	49.5	49.5
B38	3200	2.25	0.25	0.25	47.0	52.0	52.0
B39	3100	2.25	0.25	0.25	47.0	52.0	52.0
B40	2890	3.20	0.25	0.25	47.0	52.0	52.0
B41	2090	3.20	0.25	0.25	47.0	52.0	52.0

Table B.2 Reinforcement Ratios and Material Properties of Barbell Walls

Wall Code	f_c' Psi	ρ_{be} %	ρ_v %	ρ_h %	f_{ybe} Ksi	f_{yv} Ksi	f_{yh} Ksi
B42	2340	2.75	0.50	0.50	42.5	42.5	42.5
B43	2340	2.75	0.50	0.50	42.5	42.5	42.5
B44	2340	2.75	0.50	0.50	42.5	42.5	42.5
B45	5200	4.91	0.79	0.79	46.0	50.0	50.0
B46	4300	4.91	1.57	1.57	45.3	50.0	50.0
B47	4900	2.76	0.79	0.79	49.7	50.0	50.0
B48	5000	2.76	1.57	1.57	49.7	50.0	50.0
B49	4600	5.51	0.79	0.79	53.5	50.0	50.0
B50	4300	5.51	1.57	1.57	53.2	50.0	50.0
B51	3370	2.55	0.18	0.18	67.8	48.6	48.6
B52	4780	2.55	0.19	0.19	67.8	48.6	48.6
B53	2520	2.55	0.17	0.18	67.8	70.4	70.4
B54	3500	2.54	0.18	0.18	60.7	79.6	79.6
B55	3660	2.54	0.07	0.07	60.7	66.8	66.8
B56	4980	4.70	1.83	1.83	53.3	41.2	41.2
B57	4370	4.70	1.83	1.83	53.3	41.2	41.2
B58	5060	4.70	1.83	1.83	53.3	41.2	41.2
B59	5160	4.70	1.22	1.22	53.3	41.2	41.2

Table B.2 Reinforcement Ratios and Material Properties of Barbell Walls

Wall Code	f_c' Psi	ρ_{be} %	ρ_v %	ρ_h %	f_{ybe} Ksi	f_{yv} Ksi	f_{yh} Ksi
B60	4980	4.70	1.22	1.22	53.3	41.2	41.2
B61	4910	4.70	1.22	1.22	53.3	41.2	41.2
B62	4770	4.70	0.92	0.92	53.3	41.2	41.2
B63	5120	4.70	0.92	0.92	53.3	41.2	41.2
B64	5190	4.70	0.92	0.92	53.3	41.2	41.2
B65	6640	4.70	1.83	1.83	42.5	42.7	42.7
B66	6300	4.70	1.83	1.83	42.5	42.7	42.7
B67	6230	4.70	1.83	1.83	42.5	42.7	42.7
B68	7070	4.70	1.83	1.83	42.5	42.7	42.7
B69	5800	4.70	1.22	1.22	42.5	42.7	42.7
B70	6690	4.70	1.22	1.22	42.5	42.7	42.7
B71	6570	4.70	0.92	0.92	42.5	42.7	42.7
B72	6170	4.70	0.92	0.92	42.5	42.7	42.7
B73	4310	3.96	1.97	1.89	37.8	43.0	43.0
B74	4150	8.26	1.97	1.89	43.8	43.0	43.0
B75	4270	1.74	0.58	0.62	52.6	49.2	49.2
B76	4240	6.48	0.58	0.62	39.5	49.2	49.2

Table B.2 Reinforcement Ratios and Material Properties of Flanged Walls

Wall Code	f_c' Psi	ρ_{be} %	ρ_v %	ρ_h %	f_{ybe} Ksi	f_{yv} Ksi	f_{yh} Ksi
F1	4200	1.83	0.50	0.50	76.2	78.8	71.9
F2	2370	6.46	0.50	0.50	70.6	80.0	72.4
F3	3920	4.17	0.50	0.50	60.0	79.0	74.4
F4	2760	4.17	0.50	0.0	76.5	77.6	
F5	3080	4.17	0.25	0.50	76.7	72.0	72.0
F6	3400	4.17	0.50	0.50	70.9	77.0	72.7
F7	2890	0.71	0.70	0.73	58.3	46.9	46.9
F8	2700	0.71	0.67	0.70	58.3	46.9	46.9
F9	2060	1.52	0.40	0.38	59.1	58.3	58.3
F10	2060	1.52	0.45	0.43	59.1	46.9	46.9
F11	2350	1.52	0.50	0.48	59.1	46.9	46.9
F12	2000	1.52	0.69	0.66	59.1	46.9	46.9
F13	2600	1.52	0.73	0.72	59.1	46.9	46.9
F14	2430	1.52	0.73	0.72	59.1	46.9	46.9

Table B.2 Reinforcement Ratios and Material Properties of Rectangular Walls

Wall Code	f_c' Psi	ρ_{be} %	ρ_v %	ρ_h %	f_{ybe} Ksi	f_{yv} Ksi	f_{yh} Ksi
R1	6240	8.27	0.86	0.27	65.0	65.0	60.0
R2	6160	0.0	2.89	0.27		65.0	67.5
R3	6240	0.0	2.89	1.0		65.0	60.0
R4	5850	0.0	1.63	0.0		65.0	
R5	6300	0.0	2.89	1.0		65.0	66.0
R6	3410	8.88	1.17	1.17	50.1	62.9	62.9
R7	3560	3.92	0.78	0.82	49.7	62.9	62.9
R8	3560	5.53	0.44	0.41	49.7	62.9	62.9
R9	3560	5.92	0.78	0.82	50.1	62.9	62.9
R10	3560	5.92	1.17	1.17	50.1	62.9	62.9
R11	3700	2.94	0.80	0.82	49.7	62.9	62.9
R12	3700	4.44	0.36	0.41	50.1	62.9	62.9
R13	3700	4.44	0.80	0.82	50.1	62.9	62.9
R14	3700	4.73	1.17	1.17	50.9	62.9	62.9
R15	6450	3.10	2.40	1.10	68.2	68.2	75.4
R16	5190	3.10	2.40	1.10	68.2	68.2	75.4
R17	5950	3.10	2.40	0.37	68.2	68.2	75.4
R18	3600	0.0	0.80	0.25		63.0	61.6
R19	6525	0.0	0.80	0.80		65.25	65.25
R20	6525	0.0	0.80	0.80		65.25	65.25

Table B.3 Loading and Dimensions of Barbell Walls

Wall Code	* Load	b_f in	h_f in	t_w in	l_w in	h_w in	Aspect ratio
B1	M	7.5	5.0	2.0	71.0	40.0	0.63
B2	M	7.5	5.0	2.0	71.0	40.0	0.63
B3	M	7.5	5.0	2.0	71.0	40.0	0.63
B4	M	7.5	5.0	2.0	71.0	40.0	0.63
B5	M	7.5	5.0	2.0	71.0	40.0	0.63
B6	M	7.5	5.0	2.0	71.0	40.0	0.63
B7	M	7.5	5.0	2.0	71.0	40.0	0.63
B8	M	7.5	5.0	2.0	71.0	40.0	0.63
B9	M	7.5	5.0	3.0	71.0	40.0	0.63
B10	M	7.5	5.0	3.0	71.0	40.0	0.63
B11	M	7.5	5.0	3.0	71.0	40.0	0.63
B12	M	7.5	5.0	3.0	71.0	40.0	0.63
B13	M	7.5	5.0	3.0	71.0	40.0	0.63
B14	M	7.5	5.0	2.0	131.0	40.0	0.34
B15	M	7.5	5.0	2.0	131.0	40.0	0.34
B16	M	7.5	5.0	2.0	131.0	40.0	0.34
B17	M	5.0	4.0	2.0	24.0	20.0	0.92
B18	M	5.0	4.0	2.0	36.0	20.0	0.61
B19	M	5.0	4.0	2.0	48.0	20.0	0.46
B20	M	5.0	4.0	2.0	70.0	20.0	0.31

* M- Montonic Loading

Table B.3 Loading and Dimensions of Barbell Walls

Wall Code	* Load	b_f in	h_f in	t_w in	l_w in	h_w in	Aspect ratio
B21	M	3.75	5.0	2.0	68.0	33.5	0.53
B22	M	7.5	5.0	2.0	68.0	33.3	0.53
B23	M	7.5	5.0	2.0	68.0	33.5	0.53
B24	M	7.5	5.0	2.0	68.0	33.5	0.53
B25	M	12.0	5.0	2.0	68.0	33.5	0.53
B26	M	5.0	4.0	1.75	36.0	20.0	0.61
B27	M	5.0	4.0	1.75	36.0	20.0	0.61
B28	M	3.75	2.5	1.0	34.0	16.75	0.53
B29	M	11.25	7.5	3.0	102.0	50.25	0.53
B30	M	5.0	5.0	2.0	65.0	27.5	0.46
B31	M	5.0	5.0	2.0	45.0	37.5	0.89
B32	M	5.0	5.0	2.0	77.0	21.25	0.31
B33	M	7.5	5.0	2.0	68.0	33.5	0.53
B34	M	7.5	5.0	2.0	68.0	33.5	0.53
B35	M	5.0	4.0	1.75	70.0	19.75	0.31
B36	M	5.0	4.0	1.75	70.0	19.75	0.31
B37	M	5.0	4.0	1.75	70.0	19.75	0.31
B38	M	7.5	4.75	2.0	62.0	34.0	0.56
B39	M	7.5	4.75	2.0	62.0	34.0	0.56
B40	M	5.0	5.0	1.75	64.75	16.5	0.29
B41	M	5.0	5.0	1.75	64.75	16.5	0.29

* M- Monotonic Loading

Table B.3 Loading and Dimensions of Barbell Walls

Wall Code	* Load	b_f in	h_f in	t_w in	l_w in	h_w in	Aspect ratio
B42	M	4.0	4.0	2.0	48.0	23.0	0.52
B43	M	4.0	4.0	2.0	48.0	23.0	0.52
B44	M	4.0	4.0	2.0	48.0	23.0	0.52
B45	M	4.0	4.0	1.75	36.0	20.0	0.72
B46	M	4.0	4.0	1.75	36.0	20.0	0.72
B47	M	4.0	4.0	1.75	36.0	20.0	0.72
B48	M	4.0	4.0	1.75	36.0	20.0	0.72
B49	M	4.0	4.0	1.75	36.0	20.0	0.72
B50	M	4.0	4.0	1.75	36.0	20.0	0.72
		mm	**mm**	**mm**	**mm**	**mm**	
B51	C	250	250	78	2300	1200	0.63
B52	RC	250	250	75	2300	1200	0.63
B53	RC	250	250	80	1550	110	0.94
B54	RC	250	250	74	2300	1200	0.63
B55	RC	250	250	83	2300	1200	0.63
B56	M	60	60	20	570	400	0.84
B57	M	60	60	20	570	400	0.84
B58	M	60	60	20	570	400	0.84
B59	M	60	60	20	570	400	0.84

* M- Montonic Loading C- Cyclic Loading RC- Reversed Cyclic Loading

Table B.3 Loading and Dimensions of Barbell Walls

Wall Code	* Load	b_f mm	h_f mm	t_w mm	l_w mm	h_w mm	Aspect ratio
B60	M	60	60	30	570	400	0.84
B61	M	60	60	30	570	400	0.84
B62	M	60	60	40	570	400	0.84
B63	M	60	60	40	570	400	0.84
B64	M	60	60	40	570	400	0.84
B65	M	60	60	10	570	400	0.84
B66	M	60	60	10	570	400	0.84
B67	M	60	60	20	570	400	0.84
B68	M	60	60	20	570	400	0.84
B69	M	60	60	30	570	400	0.84
B70	M	60	60	30	570	400	0.84
B71	M	60	60	40	570	400	0.84
B72	M	60	60	40	570	400	0.84
B73	C	107	120	67	507	300	0.99
B74	C	107	120	67	507	300	0.99
B75	RC	320	320	160	2720	1200	0.55
B76	RC	320	320	160	2720	1200	0.55

* M- Montonic Loading C- Cyclic Loading RC- Reversed Cyclic Loading

Table B.3 Loading and Dimensions of Flanged Walls

Wall Code	* Load	b_f in	h_f in	t_w in	l_w in	h_w in	Aspect ratio
F1	M	24.0	4.0	4.0	75.0	37.5	0.54
F2	M	24.0	4.0	4.0	75.0	37.5	0.54
F3	RC	24.0	4.0	4.0	75.0	37.5	0.54
F4	RC	24.0	4.0	4.0	75.0	37.5	0.54
F5	RC	24.0	4.0	4.0	75.0	37.5	0.54
F6	RC	24.0	4.0	4.0	75.0	75.0	1.04
		mm	mm	mm	mm	mm	
F7	RC	145	30	23	430	200	0.50
F8	RC	145	30	24	430	200	0.50
F9	RC	145	30	27	430	340	0.85
F10	RC	145	30	24	430	340	0.85
F11	RC	145	30	22	430	340	0.85
F12	RC	145	30	16	430	340	0.85
F13	RC	145	30	22	430	340	0.85
F14	RC	145	30	22	430	340	0.85

* M- Montonic Loading RC- Reversed Cyclic Loading

Table B.3 Loading and Dimensions of Rectangular Walls

Wall Code	* Load	t_w in	l_w in	h_w in	Aspect ratio
R1	M	3.0	75.0	75.0	1.08
R2	M	3.0	75.0	75.0	1.08
R3	M	3.0	75.0	75.0	1.08
R4	M	3.0	75.0	75.0	1.08
R5	RC	3.0	75.0	75.0	1.08
		mm	**mm**	**mm**	
R6	RC	60	800	800	1.07
R7	RC	60	1200	800	0.72
R8	RC	60	1200	800	0.72
R9	RC	60	1200	800	0.72
R10	RC	60	1200	800	0.72
R11	RC	60	1600	800	0.54
R12	RC	60	1600	800	0.54
R13	RC	60	1600	800	0.54
R14	RC	60	1600	800	0.54
R15	M	70	750	750	1.1
R16	M	70	750	750	1.1
R17	M	70	750	750	1.1
R18	RC	100	2000	1000	0.57
R19	RC	100	2000	1500	0.82
R20	RC	100	1500	1500	1.09

* M- Montonic Loading RC- Reversed Cyclic Loading

Table B.4a Identification of Rectangular Walls W3, W4, W5 and W6

Wall Code	Wall ID	Researcher	Reference
R21	W3	Saatcioglu and Wasiewicz	Wasiewicz, 1988
R22	W6	=	==
R23	W4	Saatcioglu and Pilette	Pilette, 1988
R24	W5	=	==

Table B.4b Reinforcement Ratics and Material Properties of Rectangular Walls W3, W4, W5 and W6

Wall Code	f_c' Psi	ρ_{be} %	ρ_v %	ρ_h %	f_{ybe} Ksi	f_{yv} Ksi	f_{yh} Ksi
R21	5075	0.0	0.80	0.39		69.6	36.0
R22	5075	0.0	0.80	0.80		69.6	69.6
R23	4785	0.0	0.80	0.80		69.6	69.6
R24	3915	0.0	1.20	1.20		69.6	69.6

Table B.4c Loading and Dimensions of Rectangular Walls W3, W4, W5 and W6

Wall Code	* Load	t_w mm	l_w mm	h_w mm	Aspect ratio
R21	RC	100	2000	500	0.33
R22	RC	100	2000	1000	0.58
R23	RC	100	2000	1000	0.58
R24	RC	100	2000	1000	0.58

* M- Montonic loading RC- Reversed Cyclic loading

APPENDIX C

Walls Fortran Program and Data File

Walls Fortran Program

Walls Fortran program is used to determine the complete response of low-rise shear walls based on the proposed analytical procedure. The program is listed in this section.

Walls Data File

The input data for Walls Fortran program is compiled in Walls Data file in free format form. The input data consists of the following series of data:

Line 1. Flange width, flange height, wall height, wall thickness, wall length, thickness of the top beam, and the distance from top horizontal reinforcement to the bottom of the top beam.

Line 2. Concrete cylinder strength (negative quantity), yield strength of horizontal reinforcement, modulus of elasticity of vertical reinforcement, modulus of elasticity of horizontal reinforcement, ultimate strength of horizontal reinforcement, strain at the beginning of strain hardening of horizontal reinforcement, and ultimate strain of horizontal reinforcement.

Line 3. Number of vertical reinforcement bars.

Line 4. Dimensions and properties of i^{th} vertical reinforcement, including: distance from the face of the wall, cross-sectional area, yield strength, strain at the beginning of strain hardening, ultimate strain, ultimate strength, and modulus of elasticity.

Line 5. Number of horizontal reinforcement bars.

Line 6. Distance of horizontal reinforcement from construction joint at base of the wall and cross-sectional area of horizontal reinforcement.

Line 7. Applied axial load and experimentally obtained shear capacity of the wall.

FILE: WALLS FORTRAN *

```
C     WALLS FORTRAN PROGRAM IS USED TO DETERMINE THE COMPLETE SHEAR LOAD
C     SHEAR DEFORMATION RESPONSE OF LOW-RISE SHEAR WALLS BASED ON THE
C     PROPOSED ANALYTICAL PROCEDURE. THE INPUT IS COMPILED IN WALLS DATA
C     FILE IN FREE FORMAT FORM.
      DIMENSION D(900),E1V(900),EV(900),FV(900),FSV(900)
      DIMENSION ESHV(900),EUV(900),FUV(900),VFH(900),YQQ(900)
      DIMENSION D1(900),E1H(900),FH(900),EH(900),FSH(900),ESS(900)
      DIMENSION FYV(900),EYV(900),FV3(900),EV3(900),FSV3(900)
      DIMENSION DH(900),AV(900),AH(900),FT1(900),YFC2M(900),YFCA(900)
      DIMENSION SH(900),X(900),Y(900),AMC(900),AMT(900),DDX(900)
      DIMENSION E2V(900),E2H(900),VFXX(900),HDX(900),GXY(900),DEL(900)
      DIMENSION AMH(900),AMV(900),RMH(900),RMV(900),RM(900),FSV1(900)
      DIMENSION TITLE(20),VY(900),ETT(900),BX(900),BY(900),BE1(900)
      DIMENSION BE2(900),BG(900),BH(900),BDL(900),AEE(900),AED(900)
      DIMENSION EP(200),PP(200),APM(200),AMP(200)
      DIMENSION EECC(9000),EBM(9000),EVT(9000),EEV(9000)
      READ(5,180)(TITLE (I),I=1,20)
      WRITE(6,180)(TITLE (I),I=1,20)
  180 FORMAT(20A4)
C     INPUT LINE ONE
      READ(5,*)BF,HF,H,T,AL,HT,HCOV
C     INPUT LINE TWO
      READ(5,*)FCP,FYH,ES,ES1,FUH,ESHH,EUH
C     INPUT LINE THREE
      READ(5,*)N
      DO 10 I=1,N
C     INPUT LINE FOUR
   10 READ(5,*)D(I),AV(I),FYV(I),ESHV(I),EUV(I),FUV(I),ESS(I)
C     TO BE USED WHEN PARAMETERS ARE IN U.S CUSTOMARY UNITS.
C     READ(5,*)D(I),AV(I),FYV(I),ESHV(I),EUV(I),FUV(I),ESS(I)
C     D(I)=D(I)*25.4
C     AV(I)=AV(I)*(25.4**2)
C     FYV(I)=FYV(I)*6.895
C     FUV(I)=FUV(I)*6.895
C     ESS(I)=ESS(I)*6.895
C  10 CONTINUE
C     INPUT LINE FIVE
      READ(5,*)M
      JJ=M+1
C     INPUT LINE SIX
      DO 11 J=1,M
   11 READ(5,*)SH(J),AH(J)
C     READ(5,*)SH(J),AH(J)
C     SH(J)=SH(J)*25.4
C     AH(J)=AH(J)*(25.4**2)
C  11 CONTINUE
C     INPUT LINE SEVEN
      READ(5,*)AX,VSUS
      ERR=1.0
      E2=0.0
      E0=-.002
      AVS=0.0
C     PARAMETERS FOR CONCRETE CONFINEMENT
      E085=-.0038
C     RHO= ?
```

```
FILE: WALLS    FORTRAN  *

      RHO=0.0
C     FK= ?
      FK=0.0
C     FPC= ?
      FPC=FCP
      E01=E0*(1.+5.*FK)
      E85=260.*E01*RHO+E085
      E20=(0.8*E85-0.65*E01)/0.15
      POW=1./(1.+2.*FK)
      KJ=0
      ID=0
C     THE FOLLOWING IS THE COEFFICIENT OF FRICTION ALONG A CRACK PLANE.
      CF=1.0
C     THE FOLLOWING COEFFICIENT IS USED TO ACCOUNT FOR THE EFFECT OF
C     CYCLIC LOADING ON 'FCP'. COE2 = 1.0 IF NOT APPLICABLE.
      COE2=1.0
C     AX=AX*4.448
C     FCP=FCP*.006895
C     FYH=FYH*6.895
C     FUH=FUH*6.895
C     ES=ES*6.895
C     ES1=ES1*6.895
C     BF=BF*25.4
C     HF=HF*25.4
C     H=H*25.4
C     T=T*25.4
C     AL=AL*25.4
C     HT=HT*25.4
C     HCOV=HCOV*25.4
      KB=0
      FCPX=FCP*COE2
      FCPX1=-FCPX
      FCP1=-FCP
      ASPC=(H+.5*HT)/AL
      ARH=0.0
      DO 8012 J=1,M
      ARH=ARH+AH(J)
 8012 CONTINUE
      DO 889 I=1,N
  889 AVS=AVS+AV(I)
      DO 51 I=1,N
   51 E2V(I)=0.0
      DO 52 J=1,M
   52 E2H(J)=0.0
      E1B=0.0
      RHOH=100.*ARH/(H*T)
      EC=4730.*SQRT(FCPX1)
      EYH=FYH/ES1
      WRITE(6,12)BF,HF,H,T,AL
   12 FORMAT(/5X,'BF =',F6.0,2X,'HF =',F6.0,2X,'H =',F6.0,2X,'T =',F6.0,
     12X,'L =',F6.0/4X,'_____
     1_____'//)
      WRITE(6,2222)
C2222 FORMAT(7X,'ECC',8X,'V',8X,'DEF'/6X,'--------------------------')
 2222 FORMAT(7X,'DEF',8X,'V'/6X,'-----------------------')
```

FILE: WALLS FORTRAN *

```
      ECC=-.000001
      C=0.0
      IZ=0
      DO 1614 IM=1,3000
      IZ=IZ+1
      IF(ABS(ECC)-0.010)1060,1060,1614
 1060 IF(ABS(ECC)-ABS(E0))1017,1017,1018
 1017 ALF=ECC*(1.-ECC/(3.*E0))/E0
      GAM=1.-(2./3.-ECC/(4.*E0))/(1.-ECC/(3.*E0))
      GOTO 1019
 1018 IF(ABS(ECC)-.0073)1020,1020,1021
 1020 ALF=(1.3*ECC+75.*(ECC**2)-.633*E0-75.*(E0**2))/ECC
      DS=.65*(ECC**2)+50.*(ECC**3)-.233*(E0**2)-50.*(E0**3)
      DS1=ECC*(1.3*ECC+75.*(ECC**2)-.633*E0-75.*(E0**2))
      GAM=1.-DS/DS1
      GOTO 1019
 1021 ALF=(-.00403-.633*E0-75.*(E0**2)+.2*ECC)/ECC
      DDS=.000009857-.233*(E0**2)+50.*(E0**3)+.1*(ECC**2)
      DDS1=ALF*(ECC**2)
      GAM=1.-DDS/DDS1
 1019 C=C-100.0
      IF(C)1022,1022,1023
 1022 C=0.005
 1023 IF(C-AL/2.)1024,1024,1025
 1024 AP=0.0
      AP1=0.0
      BM=0.0
      VB=0.0
      BMC=0.0
      BMT=0.0
      VB1=0.0
      IF(C-HF)1026,1026,1027
 1026 CC=ALF*FCP*BF*C
      GOTO 1028
 1027 CC=ALF*FCP*(BF*HF+T*(C-HF))
 1028 DO 1029 I=1,N
      EYV(I)=FYV(I)/ESS(I)
      EV(I)=ECC*(C-D(I))/C
      IF(ABS(EV(I))-EYV(I))1030,1031,1031
 1030 FV(I)=EV(I)*ESS(I)
      GOTO 1032
 1031 IF(ABS(EV(I))-ESHV(I))1033,1034,1034
 1033 FV(I)=FYV(I)*(ABS(EV(I)))/EV(I)
      GOTO 1032
 1034 FV(I)=(FUV(I)-FYV(I))*(ABS(EV(I))-ESHV(I))/(EUV(I)-ESHV(I))
      FV(I)=FV(I)+FYV(I)
      FV(I)=FV(I)*(ABS(EV(I)))/EV(I)
 1032 FSV(I)=FV(I)*AV(I)
      IF(FSV(I))1035,1035,1036
 1035 AP=AP+FSV(I)
      AMC(I)=FSV(I)*(D(I)-C)
      BMC=BMC+AMC(I)
      GOTO 1029
 1036 AP1=AP1+FSV(I)
      AMT(I)=FSV(I)*(D(I)-C)
```

```
FILE: WALLS     FORTRAN  *

      BMT=BMT+AMT(I)
 1029 CONTINUE
      AP=AP/1000.
      AP1=AP1/1000.
      CC=CC/1000.
      VB=AP+AP1+CC
      IF(ABS(VB)-ERR)1038,1038,1039
 1039 C=C+0.05
      GOTO 1023
 1025 WRITE(6,1040)C
 1040 FORMAT(3X,'C =',F7.2,2X,'NO ANSWER FOR THIS CASE.'/2X,'INCREASE
     1THE SPECIFIED ERROR AND RERUN THE PROGRAM')
      GOTO 41
 1038 PMC=CC*(GAM*C-C)*1000.
      BM=(BMT+BMC+PMC)/1000000.
      VT=BM*1000./(HT/2.+H)
      EECC(IM)=ECC
      EVT(IM)=VT
      EBM(IM)=BM
      EEV(IM)=EV(N)
      ECC=ECC-.000001
 1614 CONTINUE
C     BEGINING OF PLANE SECTION ANALYSIS
      ECC=-.00001
      EHA=0.0
      VMAX=0.0
      EMAX=0.0
      C=0.0
      JA=0
      JB=0
      JC=0
      JD=0
      JE=0
      KX=0
      KY=0
   14 IF(ABS(ECC)-0.010)22,22,1646
   22 C=0.005
   23 IF(C-AL)24,24,25
   24 AP=0.0
      AP1=0.0
      BM=0.0
      VB=0.0
      BMC=0.0
      BMT=0.0
      VB1=0.0
      IF(C-10.)5000,5000,5001
 5000 BN=2.0
      GOTO 5002
 5001 IF(C-100.)5003,5003,5004
 5003 BN=5.0
      GOTO 5002
 5004 IF(C-1000.)5006,5006,5007
 5006 BN=50.0
      GOTO 5002
 5007 BN=100.
```

FILE: WALLS FORTRAN *

```
 5002 DT=C/BN
      NB=BN
      DD=0.0
      APS=0.0
      AMPS=0.0
      DO 5008 IP=1,NB
      DD=DD+DT
      EP(I)=DD*ECC/C
      IF(ABS(EP(I))-ABS(E01))8001,8001,8002
 8001 PP(I)=-FPC*(2.*EP(I)/E01-(EP(I)/E01)**2)**POW
      GOTO 8007
 8002 IF(ABS(EP(I))-ABS(E20))8003,8003,8004
 8003 PP(I)=-FPC*(1.+.15*(EP(I)-E01)/(E01-E85))
      GOTO 8007
 8004 PP(I)=-.20*FPC
 8007 CL=C-HF
      IF(IP-NB)6000,6001,6001
 6000 IF(DD-CL)7000,7000,7001
 7000 DD2=DD+0.5*DT
      IF(DD2-CL)7002,7002,7003
 7002 APM(I)=PP(I)*DT*T/1000.
      AMP(I)=APM(I)*DD/1000.
      GOTO 7004
 7003 DD3=DD2-CL
      DD4=DT-DD3
      APM(I)=PP(I)*(DD3*BF+DD4*T)/1000.
      AMP(I)=PP(I)*DD3*BF*(CL+0.5*DD3)+PP(I)*DD4*T*(CL-0.5*DD4)
      AMP(I)=AMP(I)/1000000.
      GOTO 7004
 7001 DD1=DD-CL
      IF(DD1-0.5*DT)7005,7005,7006
 7005 APM(I)=(PP(I)*0.5*DT*BF+PP(I)*BF*DD1+PP(I)*(0.5*DT-DD1)*T)
      APM(I)=APM(I)/1000.
      AMP(I)=PP(I)*.5*DT*BF*(DD+.25*DT)+PP(I)*BF*DD1*(DD-.5*DD1)
      AMP(I)=AMP(I)+PP(I)*(.5*DT-DD1)*T*(CL-.5*(.5*DT-DD1))
      AMP(I)=AMP(I)/1000000.
      GOTO 7004
 7006 APM(I)=PP(I)*DT*BF/1000.
      AMP(I)=APM(I)*DD/1000.
 7004 APS=APS+APM(I)
      AMPS=AMPS+AMP(I)
      GOTO 5008
 6001 APM(I)=.5*PP(I)*DT*BF/1000.
      APS=APS+APM(I)
      AMP(I)=APM(I)*(DD-.25*DT)/1000.
      AMPS=AMPS+AMP(I)
 5008 CONTINUE
      DO 29 I=1,N
      EYV(I)=FYV(I)/ESS(I)
      EV(I)=ECC*(C-D(I))/C
      RM(I)=ABS(EV(I))/EYV(I)
      IF(ABS(EV(I))-EYV(I))30,31,31
   30 FV(I)=EV(I)*ESS(I)
      GOTO 32
   31 IF(ABS(EV(I))-ESHV(I))33,34,34
```

FILE: WALLS FORTRAN *

```
   33 FV(I)=FYV(I)*(ABS(EV(I)))/EV(I)
      GOTO 32
   34 FV(I)=(FUV(I)-FYV(I))*(ABS(EV(I))-ESHV(I))/(EUV(I)-ESHV(I))
      FV(I)=FV(I)+FYV(I)
      FV(I)=FV(I)*(ABS(EV(I)))/EV(I)
   32 FSV(I)=FV(I)*AV(I)
      IF(FSV(I))35,35,36
   35 AP=AP+FSV(I)
      AMC(I)=FSV(I)*(D(I)-C)
      BMC=BMC+AMC(I)
      GOTO 29
   36 AP1=AP1+FSV(I)
      AMT(I)=FSV(I)*(D(I)-C)
      BMT=BMT+AMT(I)
   29 CONTINUE
      AP=AP/1000.
      AP1=AP1/1000.
      CC=-APS
      VB=AP+AP1+CC+AX
C     CHECK FOR EQUILIBRIUM OF FORCES FOR A GIVEN VALUE OF 'ECC'
      IF(ABS(VB)-ERR)38,38,39
   39 C=C+0.05
      GOTO 23
   25 WRITE(6,40)C
   40 FORMAT(3X,'C =',F7.2,2X,'NO ANSWER FOR THIS CASE.'/2X,'INCREASE
     1THE SPECIFIED ERROR AND RERUN THE PROGRAM')
      GOTO 167
   38 PMC=AMPS*1000000.
      GAM=1.-1000.*AMPS/(APS*C)
      BM=(BMT+BMC+PMC)/1000000.+AX*(.5*AL-C)/1000.
      UET=ECC*(C-AL)/C
C     SHEAR FORCE CALCULATED FOR A GIVEN VALUE OF 'ECC'
      VT=BM*1000./(.5*HT+H)
      BMX=VT*(H+.5*HT-HX)/1000.
C     BEGINING OF INCLINED SECTION ANALYSIS
      IF(C-HF)6500,6500,6501
 6500 ARS=BF*C
      GOTO 6502
 6501 ARS=BF*HF+T*(C-HF)
 6502 IF(VMAX-VT)432,433,433
  432 VMAX=VT
      EMAX=ECC
      RVM=VMAX/VSUS
  433 ALX=AL-C
      WE=T+2.*HF
      IF(WE-BF)600,600,601
  601 WE=BF
  600 IF(C-HF)602,602,603
  603 AF=.5*(WE+T)*HF+(C-HF)*T
      GOTO 604
  602 WE1=T+2.*(HF-C)
      IF(WE1-BF)605,605,606
  606 WE1=BF
  605 AF1=.5*(WE1+WE)*C
  604 AA=H/ALX
```

FILE: WALLS FORTRAN *

```
      ZX=0.5
      IF(AA-1.0)300,301,301
  301 AA=1.0
  300 RAD=ATAN(AA)
      TE=57.29577951*RAD
      S5=TAN(RAD)
      S1=SIN(RAD)
      S2=COS(RAD)
      S4=1./S5
      HX=ALX*S5
      ALR=ALX/S2
      ALRZ=ZX*ALR
      HEF=H-2.*HCOV
      ALLA=AL-HF
      DO 1615 K=1,IZ
      J=K-1
      IF(BMX-EBM(K))1617,1616,1615
 1616 EVZ1=EEV(K)
      GOTO 1619
 1617 EVZ1=EEV(J)
      GOTO 1619
 1615 CONTINUE
      WRITE(6,1620)
 1620 FORMAT('PROGRAM DID NOT FIND EQUAL MOMENT')
      GOTO 41
 1619 EVZ=1000.*VT*S5/(AVS*ES)+EVZ1
      E1Z=(EVZ-EHA*(S1**2))/(S2**2)
      OM=M
      PHI=-1000000.*ECC/C
      E1T=0.0
C     TRIAL VALUE FOR CENTER STRAIN PERPENDICULAR TO INCLINED SECTION
   43 E1T=E1T+0.00001
      IF(E1T-1.5)44,44,45
   44 K=0
      DO 46 J=1,M
      K=M-J+1
      DH(K)=HX-SH(J)
   46 CONTINUE
      XB=0.0
      BMH=0.0
      DO 49 K=1,M
      IF(DH(K))302,303,303
  302 FSH(K)=0.0
      FH(K)=0.0
      EH(K)=0.0
      RMH(K)=0.0
      XB=XB+FSH(K)
      GOTO 49
  303 D1(K)=DH(K)/S1
      IF(D1(K)-ALRZ)700,700,701
  700 E1H(K)=D1(K)*(E1T-E1Z)/ALRZ+E1Z
      GOTO 702
  701 E1H(K)=(E1T-E1B)*(ALR-D1(K))/(ALR-ALRZ)+E1B
  702 EH(K)=E1H(K)*(S1**2)+E2H(K)*(S2**2)
      IF(EH(K)-EYH)58,59,59
```

FILE: WALLS FORTRAN *

```
   58 FH(K)=EH(K)*ES1
      GOTO 60
   59 IF(EH(K)-ESHH)61,62,62
   61 FH(K)=FYH
      GOTO 60
   62 FH(K)=FYH+(FUH-FYH)*(EH(K)-ESHH)/(EUH-ESHH)
   60 FSH(K)=FH(K)*AH(K)/1000.
      RMH(K)=ABS(EH(K))/EYH
      XB=XB+FSH(K)
      AMH(K)=FSH(K)*(HX-DH(K))/1000.
      BMH=BMH+AMH(K)
   49 CONTINUE
      YB=0.0
      FVV=0.0
      BMY=0.0
      DO 63 I=1,N
      X(I)=D(I)-C
      IF(X(I))263,263,64
  263 EV3(I)=EV(I)
      FV3(I)=FV(I)
      RMV(I)=ABS(EV3(I))/EYV(I)
      FSV3(I)=FSV(I)/1000.
      E1V(I)=0.0
      E2V(I)=0.0
      GOTO 63
   64 Y(I)=X(I)/S2
      ALRU=ALR-ALRZ
      IF(Y(I)-ALRU)703,703,704
  703 E1V(I)=Y(I)*(E1T-E1B)/ALRU+E1B
      GOTO 705
  704 E1V(I)=(E1T-E1Z)*(ALR-Y(I))/ALRZ+E1Z
  705 EV3(I)=E1V(I)*(S2**2)+E2V(I)*(S1**2)
      IF(EV3(I)-EYV(I))65,65,66
   65 FV3(I)=EV3(I)*ESS(I)
      GOTO 67
   66 IF(EV3(I)-ESHV(I))68,69,69
   68 FV3(I)=FYV(I)
      GOTO 67
   69 FV3(I)=(FUV(I)-FYV(I))*(EV3(I)-ESHV(I))/(EUV(I)-ESHV(I))
      FV3(I)=FV3(I)+FYV(I)
   67 FSV3(I)=FV3(I)*AV(I)/1000.
      YB=YB+FSV3(I)
      AMV(I)=FSV3(I)*X(I)/1000.
      BMY=BMY+AMV(I)
      RMV(I)=ABS(EV3(I))/EYV(I)
   63 CONTINUE
      IF(VT-500.)830,830,831
   30 ERR1=3.
      GOTO 832
  831 IF(VT-1000.)833,833,834
  833 ERR1=4.
      GOTO 832
  834 ERR1=5.
  832 DIF=BMT/1000000.-(BMH+BMY)
C     CHECK FOR MOMENT EQUILIBRIUM AT NEUTRAL AXIS FOR INCLINED SECTION
```

```
FILE: WALLS    FORTRAN  *

C      ANALYSIS
       IF(ABS(DIF)-ERR1)47,47,43
   47  VF=(AP1-YB)/S1
       VSL=VT-XB+VF*S2
       AREA=(ALLA-HF)*T+(WE+T)*HF
       CC1=-(CC+AP)
       ZET=22.5+.5*TE
       ZET1=ZET*.017453292
       DIA=VSL*COS(ZET1)+CC1*SIN(ZET1)
       ARS2=ARS*SIN(ZET1)
       FDIA3=DIA*1000./ARS2
       FDIA4=-FDIA3
       RV=VT/VSUS
       BSST=VT*1250./AREA
       IF(C-HF)800,800,801
  800  AREA1=AF1
       GOTO 802
  801  AREA1=AF
  802  BSS=VSL*1250./AREA1
       VFX=1000.*VF/(T*ALR)
       YH=HEF/(OM-1.)
       PFA=0.0
       PFC=0.0
       KA=0
       XB1=0.0
       WB=0.0
       WF=0.0
       W1=(0.5*YH+HCOV)/S1
       VVH=0.0
       QQX=0.0
       QQ4=0.0
       KP=0
       DSHX=0.0
       GA=0.0
       AA1=H/ALX
       IF(AA1-1.0)306,306,307
   306 JM=0
       DO 308 K=1,M
       IF(K-1)309,309,310
   309 WB=0.0
       WF=W1
       DDX(K)=AL-0.5*HCOV/S5
       HDX1=.5*HCOV
       IF(DDX(K)-ALLA)803,803,804
   803 AREA2=(DDX(K)-HF)*T+.5*(WE+T)*HF
       GOTO 805
   804 X3=DDX(K)-ALLA
       WE2=T+2.*X3
       IF(WE2-BF)607,607,608
   608 WE2=BF
   607 AREA2=(AL-2.*HF)*T+.5*(WE+T)*HF+.5*(WE2+T)*X3
   805 ETT(K)=(E1T-E1Z)*(.5*HCOV/(S1*ALRZ))+E1Z
       IF(ETT(K)-.0000666)311,312,312
   312 FT1(K)=0.315*SQRT(FCPX1)
       GOTO 313
```

FILE: WALLS FORTRAN *

```
  311 FT1(K)=ETT(K)*EC
  313 QM=FT1(K)*(S5**2)
      YFC2M(K)=FCPX/(0.8-0.34*ETT(K)/E0)
      VFXX(K)=VFX*.5*HCOV*T*S2/(S1*1000.)
      VY(K)=VT+VFXX(K)-XB1
      XB1=XB1+FSH(K)
      YFCA(K)=-(2500.*VY(K)*S5/(AREA2)-QM)
      IF(YFCA(K))190,190,3080
 3080 DEL1=0.0
      DSHX=DSHX+DEL1
      GOTO 308
  190 IF(ABS(YFC2M(K))-ABS(FCPX))314,314,315
  315 YFC2M(K)=FCPX
  314 YQQ(K)=YFCA(K)/YFC2M(K)
      IF(YQQ(K)-1.)102,102,41
C     CALCULATION OF SHEAR DISTORTIONS AND DISPLACEMENTS AT EACH STRIP
  102 EHA=E0*(1.-SQRT(1.-YQQ(K)))
      AEX=ETT(K)*(S1**2)+EHA*(S2**2)
      AEV=ETT(K)*(S2**2)+EHA*(S1**2)
      GXY1=2.*S1*S2*(ETT(K)-EHA)
      DEL1=GXY1*HDX1
      DSHX=DSHX+DEL1
      GA=GA+GXY1
      DO 520 I=1,N
      IF(D(I)-DDX(K))520,521,521
  521 E2V(I)=E0*(1.-SQRT(1.-YQQ(K)))
  520 CONTINUE
      IF(QQX-YQQ(K))316,316,308
  316 QQX=YQQ(K)
      KA=K
      PFA=YFCA(K)
      PFC=YFC2M(K)
      GOTO 308
  310 IF(K-M)317,317,308
  317 WB=WF
      WF=WB+YH/S1
      KP=K-1
      DDX(K)=AL-WB*S2
      ALZ=AL-ALRZ*S2
      IF(DDX(K)-ALLA)806,806,807
  806 AREA2=(DDX(K)-HF)*T+.5*(WE+T)*HF
      GOTO 808
  807 X3=DDX(K)-ALLA
      WE2=T+2.*X3
      IF(WE2-BF)609,609,610
  610 WE2=BF
  609 AREA2=(AL-2.*HF)*T+.5*(WE+T)*HF+.5*(WE2+T)*X3
  808 IF(DDX(K)-ALZ)709,709,710
  710 ETT(K)=WB*(E1T-E1Z)/ALRZ+E1Z
      GOTO 711
  709 ETT(K)=(E1T-E1B)*(ALR-WB)/ALRU+E1B
  711 VFXX(K)=VFX*WB*T*S2/1000.
      VY(K)=VT+VFXX(K)-XB1
      IF(ETT(K)-.0000666)318,319,319
  319 FT1(K)=0.315*SQRT(FCPX1)
```

FILE: WALLS FORTRAN *

```
      GOTO 320
  318 FT1(K)=ETT(K)*EC
  320 QM=FT1(K)*(S5**2)
      XB1=XB1+FSH(K)
      YFCA(K)=-(2500.*VY(K)*S5/(AREA2)-QM)
      IF(YFCA(K))191,191,3080
  191 YFC2M(K)=FCPX/(0.8-0.34*ETT(K)/E0)
      IF(ABS(YFC2M(K))-ABS(FCPX))321,321,322
  322 YFC2M(K)=FCPX
  321 YQQ(K)=YFCA(K)/YFC2M(K)
      IF(YQQ(K)-1.)103,103,41
  103 IF(K-2)522,522,523
  522 E2H(KP)=E0*(1.-SQRT(1.-YQQ(K)))
      HDX(KP)=.5*(YH+HCOV)
      GXY(KP)=2.*S1*S2*(ETT(K)-E2H(KP))
      DEL(KP)=GXY(KP)*HDX(KP)
      DSHX=DSHX+DEL(KP)
      GA=GA+GXY(KP)
      AEE(KP)=ETT(K)*(S1**2)+E2H(KP)*(S2**2)
      AED(KP)=ETT(K)*(S2**2)+E2H(KP)*(S1**2)
      DO 524 I=1,N
      IF(D(I)-DDX(K))524,525,525
  525 IF(D(I)-DDX(KP))526,524,524
  526 E2V(I)=E0*(1.-SQRT(1.-YQQ(K)))
  524 CONTINUE
      GOTO 527
  523 E2H(KP)=E0*(1.-SQRT(1.-YQQ(K)))
      HDX(KP)=YH
      GXY(KP)=2.*S1*S2*(ETT(K)-E2H(KP))
      DEL(KP)=GXY(KP)*HDX(KP)
      DSHX=DSHX+DEL(KP)
      GA=GA+GXY(KP)
      AEE(KP)=ETT(K)*(S1**2)+E2H(KP)*(S2**2)
      AED(KP)=ETT(K)*(S2**2)+E2H(KP)*(S1**2)
      DO 528 I=1,N
      IF(D(I)-DDX(K))528,529,529
  529 IF(D(I)-DDX(KP))530,528,528
  530 E2V(I)=E0*(1.-SQRT(1.-YQQ(K)))
  528 CONTINUE
  527 IF(QQX-YQQ(K))323,323,308
  323 QQX=YQQ(K)
      KA=K
      PFA=YFCA(K)
      PFC=YFC2M(K)
  308 CONTINUE
      ETTX=E1B
      IF(ETTX-.0000666)277,278,278
  278 FT1X=.315*SQRT(FCPX1)
      GOTO 279
  277 FT1X=ETTX*EC
  279 QM=FT1X*(S5**2)
      IF(C-HF)809,809,810
  809 AREA4=AF1
      GOTO 811
  810 AREA4=AF
```

FILE: WALLS FORTRAN *

```
  811 FCAB=-2500.*VSL*S5/AREA4+QM
      IF(FCAB)192,192,1670
 1670 DEL2=0.0
      DSHX=DSHX+DEL2
      GOTO 9971
  192 FC2MB=FPC/(.8-.34*E1B/E01)
      IF(ABS(FC2MB)-ABS(FPC))280,280,281
  281 FC2MB=FPC
  280 QQB=FCAB/FC2MB
      IF(QQB-1.)104,104,41
  104 RFC2=FDIA4/FCPX
      JM=K-1
      E2H(JM)=E0*(1.-SQRT(1.-QQB))
      HDX2=.5*YH+HCOV
      GXY2=2.*S1*S2*(E1B-E2H(JM))
      DEL2=GXY2*HDX2
      DSHX=DSHX+DEL2
      GA=GA+GXY2
      AEX1=E1B*(S1**2)+E2H(JM)*(S2**2)
      AEV1=E1B*(S2**2)+E2H(JM)*(S1**2)
      E1B=-E0*(1.-SQRT(1.-QQB))*(S5**2)
      DO 531 I=1,N
      IF(D(I)-C)531,532,532
  532 IF(D(I)-DDX(JM))533,531,531
  533 E2V(I)=E0*(1.-SQRT(1.-QQB))
  531 CONTINUE
      IF(QQX-QQB)91,91,92
   91 QQX=QQB
      PFA=FCAB
      PFC=FC2MB
      IF(QQX-1.)9971,41,41
   92 IF(QQX-1.)9971,41,41
  307 LA=0
      DO 73 K=1,M
      IF(DH(K))74,74,73
   74 LA=LA+1
   73 CONTINUE
      LB=M-LA
      BL=LB
      ZY=(BL-1.0)*YH+HCOV
      ZZ=HX-ZY
      WA1=(0.5*YH+ZZ)/S1
      DO 75 LC=1,LB
      K=LC+LA
      IF(LC-1)76,76,77
   76 WB=0.0
      WF=WA1
      VY(K)=VT
      DDX(K)=AL
      AREA1=(ALLA-HF)*T+(WE+T)*HF
      ETT(K)=E1Z
      IF(ETT(K)-.0000666)78,79,79
   79 FT1(K)=0.315*SQRT(FCPX1)
      GOTO 80
   78 FT1(K)=ETT(K)*EC
```

FILE: WALLS FORTRAN *

```
   80 QM=FT1(K)*(S5**2)
      XB1=XB1+FSH(K)
      YFC2M(K)=FCPX/(0.8-0.34*ETT(K)/E0)
      YFCA(K)=-(2500.*VY(K)*S5/(AREA1)-QM)
      IF(YFCA(K))193,193,7500
 7500 DEL1=0.0
      DSHX=DSHX+DEL1
      GOTO 75
  193 IF(ABS(YFC2M(K))-ABS(FCPX))81,81,82
   82 YFC2M(K)=FCPX
   81 YQQ(K)=YFCA(K)/YFC2M(K)
      IF(YQQ(K)-1.)105,105,41
C 105 HDX1=H-HX
  105 HDX1=0.0
      EHA=E0*(1.-SQRT(1.-YQQ(K)))
      GXY1=2.*S1*S2*(ETT(K)-EHA)
      DEL1=GXY1*HDX1
      DSHX=DSHX+DEL1
      GA=GA+GXY1
      AEX=ETT(K)*(S1**2)+EHA*(S2**2)
      AEV=ETT(K)*(S2**2)+EHA*(S1**2)
      IF(QQX-YQQ(K))83,83,75
   83 QQX=YQQ(K)
      KA=K
      PFA=YFCA(K)
      PFC=YFC2M(K)
      GOTO 75
   77 IF(LC-LB)84,84,75
   84 WB=WF
      WF=WB+YH/S1
      DDX(K)=AL-WB*S2
      VFXX(K)=VFX*WB*T*S2/1000.
      KP=K-1
      IF(LC-2)900,900,901
  900 HDX(KP)=.5*YH+ZZ
      GOTO 902
  901 HDX(KP)=YH
  902 ALZ=AL-ALRZ*S2
      IF(DDX(K)-ALZ)712,712,713
  713 ETT(K)=WB*(E1T-E1Z)/ALRZ+E1Z
      GOTO 714
  712 ETT(K)=(E1T-E1B)*(ALR-WB)/(ALR-ALRZ)+E1B
  714 VY(K)=VT+VFXX(K)-XB1
      IF(DDX(K)-ALLA)812,812,813
  812 AREA2=(DDX(K)-HF)*T+.5*(WE+T)*HF
      GOTO 814
  813 X3=DDX(K)-ALLA
      WE2=T+2.*X3
      IF(WE2-BF)611,611,612
  612 WE2=BF
  611 AREA2=(AL-2.*HF)*T+.5*(WE+T)*HF+.5*(WE2+T)*X3
  814 IF(ETT(K)-.0000666)85,86,86
   86 FT1(K)=0.315*SQRT(FCPX1)
      GOTO 87
   85 FT1(K)=ETT(K)*EC
```

FILE: WALLS FORTRAN *

```
 87 QM=FT1(K)*(S5**2)
    XB1=XB1+FSH(K)
    YFCA(K)=-(2500.*VY(K)*S5/(AREA2)-QM)
    IF(YFCA(K))194,194,7500
194 YFC2M(K)=FCPX/(0.8-0.34*ETT(K)/E0)
    IF(ABS(YFC2M(K))-ABS(FCPX))88,88,89
 89 YFC2M(K)=FCPX
 88 YQQ(K)=YFCA(K)/YFC2M(K)
    IF(YQQ(K)-1.)106,106,41
106 E2H(KP)=E0*(1.-SQRT(1.-YQQ(K)))
    GXY(KP)=2.*S1*S2*(ETT(K)-E2H(KP))
    DEL(KP)=GXY(KP)*HDX(KP)
    DSHX=DSHX+DEL(KP)
    GA=GA+GXY(KP)
    AEE(KP)=ETT(K)*(S1**2)+E2H(KP)*(S2**2)
    AED(KP)=ETT(K)*(S2**2)+E2H(KP)*(S1**2)
    DO 535 I=1,N
    IF(D(I)-DDX(K))535,536,536
536 IF(D(I)-DDX(KP))537,535,535
537 E2V(I)=E0*(1.-SQRT(1.-YQQ(K)))
535 CONTINUE
    IF(QQX-YQQ(K))90,90,75
 90 QQX=YQQ(K)
    KA=K
    PFA=YFCA(K)
    PFC=YFC2M(K)
 75 CONTINUE
    ETTY=E1B
    IF(ETTY-.0000666)282,283,283
283 FT1Y=.315*SQRT(FCPX1)
    GOTO 284
282 FT1Y=ETTY*EC
284 QM=FT1Y*(S5**2)
    IF(C-HF)815,815,816
815 AREA4=AF1
    GOTO 817
816 AREA4=AF
817 FCAB=-2500.*VSL*S5/AREA4+QM
    IF(FCAB)195,195,1671
1671 DEL2=0.0
    DSHX=DSHX+DEL2
    GOTO 9971
 195 FC2MB=FPC/(.8-.34*E1B/E01)
    IF(ABS(FC2MB)-ABS(FPC))285,285,286
 286 FC2MB=FPC
 285 QQB=FCAB/FC2MB
    IF(QQB-1.)107,107,41
 107 RFC2=FDIA4/FCPX
    E2H(K)=E0*(1.-SQRT(1.-QQB))
    HDX2=.5*YH+HCOV
    GXY2=2.*S1*S2*(E1B-E2H(K))
    DEL2=GXY2*HDX2
    DSHX=DSHX+DEL2
    GA=GA+GXY2
    AEX1=E1B*(S1**2)+E2H(K)*(S2**2)
```

```
FILE: WALLS    FORTRAN  *


      AEV1=E1B*(S2**2)+E2H(K)*(S1**2)
      E1B=-E0*(1.-SQRT(1.-QQB))*(S5**2)
      DO 557 I=1,N
      IF(D(I)-C)557,538,538
  538 IF(D(I)-DDX(K))539,557,557
  539 E2V(I)=E0*(1.-SQRT(1.-QQB))
  557 CONTINUE
      IF(QQX-QQB)94,94,95
   94 QQX=QQB
      PFA=FCAB
      PFC=FC2MB
C     CHECK FOR DIAGONAL COMPRESSION FAILURE
      IF(QQX-1.)9971,41,41
   95 IF(QQX-1.)9971,41,41
 9971 WRITE(6,2223)ECC,VT,DSHX,VSL,RV,TE
 2223 FORMAT(F9.6,2X,F7.2,2X,F7.3,2X,F7.2,2X,F5.2,2X,F5.2)
C9971 WRITE(6,2223)ECC,VT,DSHX
C2223 FORMAT(3X,F9.6,3X,F7.2,3X,F6.3)
C9971 WRITE(6,2225)DSHX,VT
C2225 FORMAT(3X,F6.3,3X,F7.2)
  167 KX=0
      KY=0
      ECC=ECC-.00001
      GOTO 14
   45 WRITE(6,1166)DIF,BMT,BMH,BMY
 1166 FORMAT(/3X,'DIF =',F7.2,3X,'BMT =',F7.2,3X,'BMH =',F7.2,3X,'BMY ='
     1,F7.2/)
      WRITE(6,166)ECC,E1T
  166 FORMAT(/3X,'ECC =',F8.5,3X,'E1T =',F4.2,2X,'EXCEEDS THE LIMIT'/)
      GOTO 167
   16 WRITE(6,158)ERR1,VMAX,EMAX
  158 FORMAT(/2X,'FINAL SPEC. ERROR IS',F7.2/2X,'MAX LOAD = VT =',F8.2,2
     1X,'FOR ECC =',F8.5/2X,'PROGRAM IS ENDED'/1X,'----------------'///)
      GOTO 41
 1646 ID=ID+1
      IF(ID-1)1647,1647,16
 1647 WRITE(6,1618)
 1618 FORMAT(/3X,'FLEXURAL FAILURE'/2X,'----------------'/)
      WRITE(6,131)ECC,C,VT,BM
  131 FORMAT(2X,'ECC =',F9.6,2X,'C =',F7.2,2X,'V =',F7.2,2X,'M =',F7.2)
   41 STOP
      END
```